Role of Neuroligin-2 and its Interacting Inhibitory Synapse Organizers in the Circuits of Fear Learning and Anxiety

Dissertation
for the award of the degree
"Doctor rerum naturalium"
of the Georg-August-Universität Göttingen

within the doctoral program *(IMPRS Neuroscience)*
of the Georg-August University School of Science (GAUSS)

submitted by

Heba Ali

Born in
Latakia, Syria

Göttingen, 2022

Thesis Committee

Prof. Dr. Dilja Krüger-Burg
Cell and Neurobiology group, Institute for Microscopic Anatomy and Neurobiology, Mainz
Dept. of Molecular Neurobiology, Max Planck Institute for Multidisciplinary Sciences, Göttingen

Prof. Dr. Thomas Dresbach
Dept. of Anatomy and Embryology, University Medical Center, Göttingen

Prof. Dr. Dr. Hannelore Ehrenreich
Dept. of Clinical Neuroscience, Max Planck Institute for Multidisciplinary Sciences, Göttingen

Members of the Examination Board

1st Referee: Prof. Dr. Dilja Krüger-Burg
Cell and Neurobiology group, Institute for Microscopic Anatomy and Neurobiology, Mainz
Dept. of Molecular Neurobiology, Max Planck Institute for Multidisciplinary Sciences, Göttingen

2nd Referee: Prof. Dr. Thomas Dresbach
Dept. of Anatomy and Embryology, University Medical Center, Göttingen

Further members of the Examination Board

Prof. Dr. Nils Brose
Dept. of Molecular Neurobiology, Max Planck Institute for Multidisciplinary Sciences, Göttingen

Dr. Camin Dean
Synaptic Dysfunction group, German Center for Neurodegenerative Diseases, Berlin

Dr. Katrin Willig
Optical Nanoscopy in Neuroscience group, Max Planck Institute for Multidisciplinary Sciences, Göttingen

Date of oral examination: May 11th, 2022

Table of Contents

List of Figures

List of tables

List of abbreviations

5-CSRTT	Five-choice serial reaction time task

5HT2A	Serotonin receptor 2a
AAV	Adenoassociated virus
AB	Antibody
ACBC	Nucleus accumbens, core
ACSF	Artificial cerebrospinal fluid
ANOVA	Analysis of variance
AP	Anterio-posterior
ASR	Acoustic startle response
Au1	Primary auditory cortex
AuC	Auditory cortex
AuD	Secondary auditory cortex- dorsal area
AUs	Arbitrary units
AUs	Arbitrary units
AuV	Secondary auditory cortex-ventral area
BA	Basal amygdala
BLA	Basolateral amygdala
bp	base pairs
BST	Bed nucleus of the stria terminalis
BSTMA	bed nucleus of stria terminalis, medial division, anterior part
C°	Degree Celsius
CA1-CA3	Cornu ammonis fields
CaIr	Calretinin
CAMKII	CA^{+2}/calmodulin-dependent protein kinase II
CB	Calbindin
Cb	Collybistin
CB1-R	Endocannabinoid receptor-1
CCK_L	Large cholecystokinin cells
CCK_S	Small cholecystokinin cells
CeA	Central amygdala
CeL	Contralateral amygdala
CeL ON	Centrolateral amygdala-ON cells
CeL-OFF	Centrolateral amygdala- OFF cells
CeM	Centromedial amygdala
ChR2	Channel rhodopsin 2

Cl^-	Chloride ions
cm	Centimeter
CP	Cross point
CPU	Caudate putamen
CREB	cAMP response element-binding protein
CRF/CRH	Corticotropin releasing hormone/corticotropin releasing factor
CS	Conditioned stimulus
DAPI	4′,6-diamidino-2-phenylindole
dB	Decibel
DG	Dentate gyrus
DGL-α	Diacylglycerol lipase-α
dlPAG	Dorsolateral periaqueductal gray
DNA	Deoxyribonucleotide
DV	Dorso-ventral
E/I	Excitatory/inhibitory
EC	Entorhinal cortex
eEPSCs	Evoked excitatory post synaptic currents
EGFP	Enhanced green fluorescent protein
EPM	Elevated plus-maze
EYFP	Enhanced yellow fluorescent protein
FC	Fear conditioning
fEPSCs	Field excitatory postsynaptic currents
FISH	Fluorescent In Situ Hybridization
fl	Flox
FRIL	Freeze-fracture replica immunolabeling
g	Gravitational force
GABA	Gamma-aminobutyric acid
$GABA_AR$	Gamma aminobutyric acid A receptors
GAD	Glutamic acid decarboxylases
GAD65	Glutamate acid decarboxylase isoform 65 kDa
GAD76	Glutamate acid decarboxylase isoform 67 kDa
GC	Granule cell
GFP	Green fluorescent protein
GPe	Globus pallidus external

GPI	Glycosylphosphatidylinositol
GTP/GDP	Guanosine triphosphate/Guanosine diphosphate
h	Hour
HPC	Hippocampus
HyD	Hybrid detectors
i.p.	Intraperitoneal injection
IgSF9b	Immunoglobulin superfamily member 9b
IHC	Immunohistochemistry
IL	Infralimbic
INs	Interneurons
IPSCs	Inhibitory post synaptic currents
iPSCs	Induced pluripotent stem cells
IQR	Interquartile range method
ITR	Inverted terminal repeat region
KCL	Potassium Chloride
KD	Knockdown
kDA	Kilodalton
kg	Kilogram
kHz	Kilohertz
KO	Knockout
LA	Lateral amygdala
LDB	Light-dark box
LDDM	Laterodorsal thalamic nucleus, medial part
LFP	Local field potentials
LHB	Lateral habenular nucleus
LS	Lateral septum
LSN	Lateral septal nucleus
LTP	Long-term potentiation
mA	Milliampere
MDGA1	MAM Domain Containing Glycosylphosphatidylinositol Anchor 1
mEPSCs	Miniature excitatory post synaptic currents
MGB	Medial geniculate body
MHB	Medial habenular nucleus
mIPSCs	Miniature inhibitory post synaptic currents

MKN	Milliknots
ML	Medio-lateral
mPFC	Medial prefrontal cortex
ms	millisecond
MSN	Medial septal nucleus
NDNF	Neuron-derived neurotrophic factor
NIR	Near-infrared
Nlgn2	Neuroligin2
Nlgns	Neuoroligins
nm	Nanometer
nl	Nanoliter
NR	Nucleus reuniens
Nrxns	Neurexins
Nts	Neurotensin
OFT	Open field test
PAG	Periaqueductal gray
PB	Parabrachial nucleus
PBS	Phosphate buffered saline
PCR	Polymerase chain reaction
PFA	Paraformaldehyde
PFC	Prefrontal cortex
PIL	Posterior interlaminar nucleus
PKCδ	Protein kinase C- δ
PML	Polymorph layer of the dentate gyrus
PN	Pyramidal neuron
PrL	Prelimbic cortex
PTSD	Post-traumatic stress disorder
PV	Parvalbumin
PVT	Paraventricular nucleus of the thalamus
qPCR	Qualitative Polymerase Chain Reaction
ROIs	Regions of interest
RT	Room temperature
S-SCAM	Synaptic scaffolding molecule
sec	Second

SEM	Standard error of the mean
SG	Supragenicula te nucleus
SLM	stratum laconosum moleculare
SLM	stratum-Lacunosum Moleculare
SO	stratum Oriens
SOM	Somatostatin
SP	stratum Pyramidale
SR	stratum radiatum (hippocampus)
SR	stratum Radiatum
SST	Somatostatin
STED	Stimulated Emission Depletion
Tac2	Tachykinin 2
US	Unconditioned stimulus
VDB	Diagonal band nucleus
vGAT	vesicular GABA transporter
vGlut1	Cesicular glutamate transporter-1
vHPC	Ventral hippocampus
VIP	Vasoactive intestinal peptide
vlPAG	Ventrolateral periaqueductal gray
WLL	White light laser
WT	Wild type

Abstract

Neuroligin-2 (Nlgn2) is a synaptic adhesion molecule that promotes the maturation and function of inhibitory synapses. Lack of Nlgn2 in mice produced a reduction in inhibitory synaptic transmission in many brain regions. However, at the level of behavioral circuits, Nlgn2 knockout mice (Nlgn2 KO) exhibited phenotypes that were specifically related to the function of emotional circuits, such as anxiety-like behavior and cognitive impairments involving aversive emotional valence. Aiming to understand how Nlgn2 regulates the function and plasticity of emotional circuits, I characterized its role in fear learning using the Pavlovian fear conditioning (FC) paradigm. I observed a behavioral impairment measured at the level of short and long-term fear memory retrieval in Nlgn2 KO mice that was specific to auditory, but not contextual FC. Using immediate-early gene expression assay to probe neuronal activation during FC retrieval, I detected dysregulated activation in Nlgn2 KO mice in brain regions that are involved in fear memory processing such as the lateral amygdala (LA), the medial prefrontal cortex (mPFC) and the auditory cortex (AuC). In these regions, a lack of activation in response to FC was detected in Nlgn2 KO compared to WT mice, in line with impaired plasticity required for fear memory formation. Using cell-type specific gene knockout approach, I found that the FC deficit in Nlgn2 KO was caused by lack of Nlgn2 from specific inhibitory neurons subtypes rather than excitatory neurons. Particularly, deletion of Nlgn2 from vasoactive intestinal peptide (VIP) expressing inhibitory neurons, but not from Ca^{+2}/Calmodulin-dependent protein kinase-II (CAMKII) expressing excitatory neurons, recapitulated the FC deficit in Nlgn2 KO. This result was also supported by learning-dependent overactivation of VIP interneurons (INs) in the LA during FC retrieval. While the reduction in fear learning in a mouse model with increased anxiety-like behavior is intriguing, I found that these two behaviors are controlled by effects of Nlgn2 on different cell types. Unlike what I observed in fear learning, deletion of Nlgn2 from excitatory CAMKII neurons fully recapitulated the anxiety-like behavior of Nlgn2 KO mice in the open field test. In contrast, mice lacking Nlgn2 from specific inhibitory neurons showed normal exploratory behavior using the same test. Moreover, the modulation of Nlgn2 function by its interaction partner IgSF9b was also distinct between fear learning and anxiety. Particularly, Nlgn2-IgSF9b double deletion exacerbated the fear learning deficit in Nlgn2 KO mice, in contrast to the normalization of anxiety-like behavior reported previously in the double KO mice. Taken together, my data reveals the complexity by which inhibitory synapse organizers regulate brain function in a circuit specific and a cell-type specific manner.

1. Introduction

Defining the neural correlates of emotions has been a long-standing quest in neuroscience. Particularly of interest, is how the brain encodes and stores emotional experiences and how impaired emotional processing leads to psychiatric disorders such as anxiety and depression. Like any other brain function, processes that underlie the generation and processing of emotions are encoded within highly organized neuronal circuits that transmit and integrate neural signals between different brain regions. As the fundamental computational units of neuronal circuits, synapses can largely define and control information processing within the circuit, based on whether they are inhibitory or excitatory, stable or versatile (Sudhof, 2021). Of special interest are inhibitory synapses that bear an exquisite level of complexity in terms of their presynaptic and postsynaptic sites. Presynaptically, inhibitory synapses are formed by inhibitory neurons, which represent a highly diverse population of neurons in terms of their function, connectivity, and contribution to the regulation of emotional circuits. Postsynaptically, the inhibitory synapse comprises complex machinery of proteins that work together to regulate the function of neurotransmitter receptors and other aspects of signal transmission across the inhibitory synapse. Among inhibitory synapse proteins, the synaptic adhesion molecule Nlgn2 was shown to be a central organizer of inhibitory synapse function and a key regulator of anxiety-like behaviors in mice (Ali et al., 2020). In line with this notion, Nlgn2 KO mice showed a robust anxiety-like behavior associated with a dysregulation in the brain circuits controlling anxiety (Babaev et al., 2016; Blundell et al., 2009; Cruces-Solis et al., 2021) . However, it is not known whether this anxiety-like phenotype is associated with an impairment in the processing of aversive memories, a process that has been linked to the etiology of anxiety disorders in humans (Duits et al., 2015; Lissek et al., 2005). Aversive memories are formed, stored, and retrieved in response to threat-predicting cues to promote the individual's survival and the circuits that underlie these processes are highly evolutionary conserved across species (Ledoux, 2000). Most of the knowledge about the brain circuits and synaptic processes that mediate the formation of aversive memories was obtained from rodent studies investigating fear learning. Therefore, understanding how fear learning is regulated by Nlgn2 and how this behavior is related to the anxiety-like phenotype on the circuit level are key steps towards understanding how Nlgn2-mediated synaptic inhibition regulates emotional circuits in the brain.

1.1. Fear, fear learning, and anxiety

While the three terms share a component of negative emotional valence, it is important to distinguish between innate fear, learned fear, and anxiety. Fear is an emotional response triggered by stimuli that are innately threatening or fearful. In contrast, fear learning describes a process by which a neutral stimulus becomes fearful or predictive of threat through association with an aversive stimulus (Tovote et al., 2015). Therefore, fear learning describes mainly an emotional memory process that leads to the expression of fear as a behavioral response. Experimentally, fear learning can be characterized using the fear conditioning (FC) paradigm, in which the subject is exposed to a neutral sensory stimulus, such as a tone or light, that is presented contingently with a noxious stimulus such as a foot shock, called the unconditioned stimulus (US). Due to the formation of an associative memory between both stimuli, re-exposure of the subject to the sensory cue alone, then called the conditioned stimulus (CS), elicits motor, autonomic and endocrine responses indicative of fear.

Anxiety, on the other hand, represents a state of high vigilance and apprehension that is, in pathological conditions, elicited in response to ambiguous stimuli which do not necessarily pose or predict threat (Calhoon and Tye, 2015). In mice, anxiety-like behavior is assessed by approach-avoidance paradigms that characterize exploration in a novel environment, such as the open field test (OFT) and the elevated plus-maze (EPM). In these paradigms, avoiding exposed areas, such as the center of the OFT or the open arms of the EPM, is used as a measure of anxiety.

The brain circuits underlying fear learning and anxiety are thought to be overlapping, specifically in the pathways mediating the behavioral output (Tovote et al., 2015). However, the extent of this overlap is not entirely known, especially since most of the knowledge about the processing in aversive circuits is obtained from studies investigating fear learning.

1.2. Neural circuits of fear learning

1.2.1. The amygdala; function, anatomy, and role in fear learning

At the core of the circuit involved in fear memory formation lies the amygdala (figure 1), a highly complex structure embedded in the medial temporal lobe. Early evidence implicated the amygdala in mediating innate and learned fear responses to aversive external stimuli. Its bilateral lesions in rhesus monkeys lead to reduced avoidance of aversive stimuli and shock-predictive cues (Weiskrantz, 1956). Similar findings were obtained later using the

fear conditioning paradigm in rodents (Blanchard and Blanchard, 1972) and in humans, as reported in the case of patient SM (Bechara et al., 1995), indicating that the role of the amygdala in fear processing is highly evolutionary conserved. Beyond fear, the amygdala is also implicated in reward-based learning (Cador et al., 1989), leading to the emerging picture that it meditates adaptive behavioral responses to external stimuli based on their valence (Beyeler et al., 2018; Calhoon and Tye, 2015). Furthermore, impaired amygdala function has been strongly linked to anxiety disorders. Functional neuroimaging studies

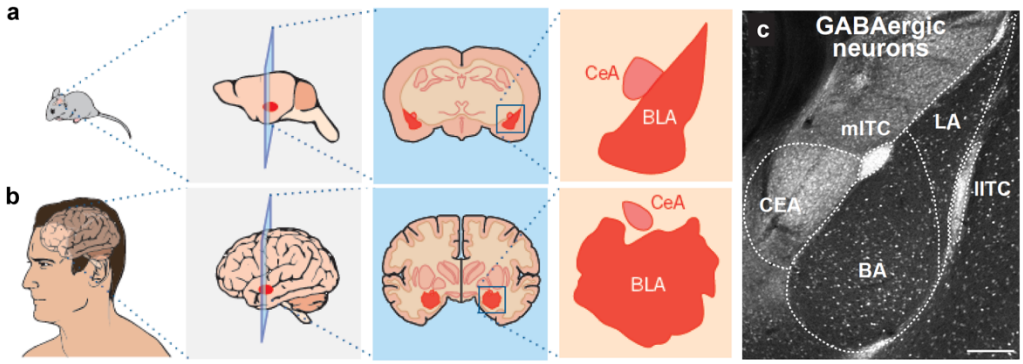

Figure 1 The amygdala in mice and humans. a, b.
Schematics showing the anatomical location, the shape and size of the amygdala in mice (**a**) and humans (**b**). **c**. A micrograph showing a coronal section of the amygdala in mice expressing enhanced green fluorescent protein (EGFP) in GABAergic neurons (GAD76-EGFP) to reveal their distribution among different amygdala nuclei. Reprinted from (Janak and Tye, 2015) by permission from Copyright Clearance Center (license number 5320110429559) and from (Krabbe et al., 2018).
.

reported amygdala hyperexcitability in patients with generalized anxiety (Nitschke et al., 2009) and post-traumatic stress disorder PTSD (Shin LM, 2004). In this context, the amygdala has been shown to be a central node in processing anxiety using approach-avoidance paradigms (Babaev et al., 2018b; Calhoon and Tye, 2015). However, since most of the knowledge about amygdala connectivity is obtained from studies investigating fear learning, it is not clear whether the amygdala processes fear learning and anxiety through shared or distinct circuits.

Anatomically, the amygdala comprises approximately 20 subnuclei and exhibits high diversity in its neuronal composition (Marek and Sah, 2018). However, functional analyses investigating fear learning highlighted the role of four main subnuclei in this circuit. These subnuclei included the lateral (LA) and the basal (BA) amygdala, which form together the basolateral amygdala (BLA), and the central amygdala (CeA) comprising the contralateral (CeL) and centromedial amygdala (CeM) (Sah et al., 2003) (figure 1 and 2). The amygdala shows high anatomical heterogeneity. For example, the BLA was shown to be a cortical-like structure comprising mainly excitatory neurons and a minor fraction of inhibitory

interneurons (20%). The CeA, on the other hand, is a striatal-like structure that is formed entirely by inhibitory neurons that include interneurons and projection neurons (Marek and Sah, 2018; Sah et al., 2003).

As elucidated by the auditory fear conditioning paradigm, sensory information, including CS and US signals converge onto LA neurons during fear memory acquisition (Romanski et al., 1993). This conversion leads to the potentiation of sensory input synapses via associative plasticity mechanisms, which renders these neurons more excitable in response to CS presentation during fear memory retrieval (Johansen et al., 2011a). Consistent with this notion, interfering with the molecular mechanisms mediating LA plasticity, modeled using the long-term potentiation paradigm (LTP), prevented fear learning (Johansen *et al.*, 2011a; Ledoux, 2000).

From the LA, the potentiated CS signal during FC retrieval is relayed to the BA (figure 2), which is the main recipient for LA output projections based on anatomical studies (Pitkanen et al., 1997) and its activity is required for fear expression as shown by inactivation after fear acquisition (Anglada-Figueroa and Quirk, 2005). Also, the BA represent an interface for the communication between the amygdala and other brain regions involved in modulating fear memory such as the mPFC (Krabbe et al., 2018; Senn et al., 2014). The BA transmits the CS potentiated signal to CeA where fear responses are generated (Ciocchi et al., 2010). However, a direct projection between the LA and the CeL, bypassing the BA, was also described, and shown with optogenetics to be crucial for fear memory formation (Li et al., 2013). In the CeA, the CeL was found to be a site for learning-dependent plasticity (Ciocchi et al., 2010; Haubensak et al., 2010). Additionally, it is a source of projections to downstream regions such as the ventrolateral periaqueductal gray (vlPAG), the paraventricular nucleus of the thalamus (PVT) (Li et al., 2013; Penzo et al., 2014) (figure 2) and to the CeM (Ciocchi et al., 2010). The CeM is known to be the main output nucleus of the amygdala that controls fear responses, including freezing that was shown to be mediated by projections to the vlPAG (Ciocchi et al., 2010; Tovote et al., 2016; Viviani et al., 2011) (figure 2).

1.2.2. The distributed network of fear learning

In addition to the central role played by the amygdala, several other brain regions contribute to the formation, expression, and modulation of fear memory within a widespread network of distal and local projections (Herry and Johansen, 2014). An overview of the main nodes that are involved in fear memory processing is provided below.

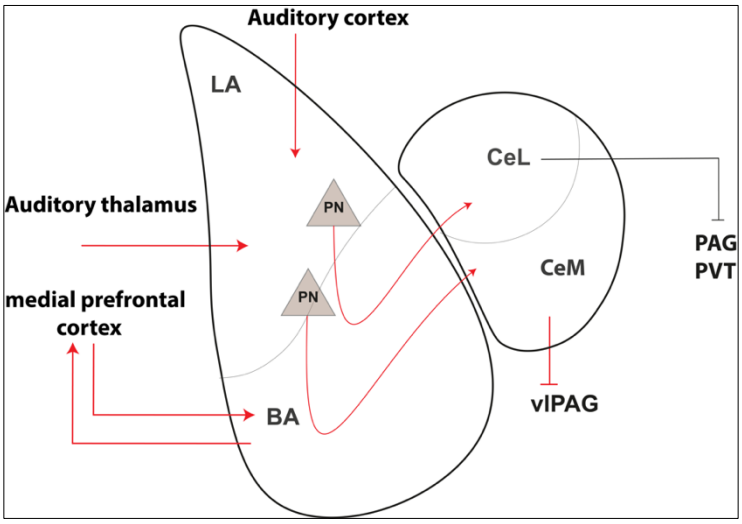

Figure 2 Amygdala fear conditioning circuit.
A simplified schematic showing main intra-amygdala projections in addition to the main input and output projections between the amygdala and other brain regions within the distributed FC network.

1.2.2.1. CS pathways to the amygdala

The most studied form of fear conditioning is the auditory or cued fear conditioning where the CS is an auditory cue. Accordingly, CS information is transmitted through the ascending auditory pathway from the cochlea to the cochlear nucleus of the medulla, then to the superior olivary nucleus in the pons, and from there to the inferior colliculus of the midbrain (Felix et al., 2018; Kandel, 2013). From the inferior colliculus, CS information is relayed to the auditory thalamus and then to the LA directly or via the auditory cortex (figure 2). An early view of the differential role for thalamic and cortical auditory input to the amygdala in fear learning described that the thalamus provides rapid but 'crude' sound representations to the amygdala while the cortex encodes slower but more detailed CS features (Ledoux, 2000). However, recent studies demonstrated that the role of each of the auditory thalamus and cortex extends beyond sensory encoding as both of them showed to be sites for CS-US convergence and fear memory formation and storage.

a. The auditory thalamus

As the source of auditory input to the amygdala and the auditory cortex, the auditory thalamus comprises a group of nuclei including the medial geniculate body (MGB), the posterior interlaminar nucleus (PIL), and the suprageniculate nucleus (SG) (Barsy et al., 2020; Romanski and LeDoux, 1992b; Taylor et al., 2021). Of these nuclei, the medial division of the MGB and the associated PIL and SG showed responses to both auditory and somatosensory stimuli (Barsy et al., 2020; Bordi and LeDoux, 1994; Grundemann, 2021; Taylor et al., 2021*)*. In line with their role in plasticity, potentiated CS responses and tuning shifts towards the CS frequency were measured in the auditory thalamus neurons (Edeline and Weinberger, 1991; Ryugo and Weinberger, 1978). Furthermore, increased levels of

phosphorylated cAMP response element-binding protein (CREB), as a marker of neuronal plasticity, were measured in auditory thalamus neurons after auditory but not contextual FC (Han et al., 2008). While lesioning the thalamic projections to the amygdala yielded controversial effects on FC (Campeau and Davis, 1995; Romanski and LeDoux, 1992a), optogenetic inhibition of MGB neural populations projecting to the BLA impaired fear acquisition (Barsy et al., 2020) and retrieval (Barsy et al., 2020; Taylor et al., 2021). To elucidate how the single-cell plasticity of auditory thalamus neurons contributes to sensory coding by large populations of neurons, Taylor et al (Taylor et al., 2021) used in vivo calcium imaging to follow the activity of BLA-projecting MGB neuronal populations across FC days. They found that CS sensory representation by these populations of neurons during FC becomes similar to US representation. However, this representation shift is not consolidated after training in order to allow for stable sensory representation of the CS. The observed single-cell and population-level plasticity in MGB neurons during FC was thus predicted to be important for driving plasticity in downstream targets such as the BLA (Grundemann, 2021; Taylor et al., 2021). Taken together, plasticity of auditory thalamus neurons during fear learning was found to be necessary for fear acquisition and retrieval.

b. The auditory cortex

The canonical role of the AuC in auditory processing involves the detailed processing and encoding of the physical attributes of sound stimuli (Concina et al., 2019). However, the sensory representation of sounds in the AuC was shown to be modulated by experience to encode the behavior salience and the emotional valence of sounds (Concina et al., 2019). An example of the AuC adaptive sound encoding is manifested by its role in fear conditioning where it showed to host associate plasticity. Early evidence of AuC plasticity arose from single-unit electrophysiological recordings in the auditory association cortex areas (Te1v-Te3) showing potentiated CS responses after FC (Quirk et al., 1997). Interestingly, learning-evoked changes in the AuC took more trials to develop compared to ones measured in the LA and the CS responses appeared at a higher latency from CS onset, indicating that they predicted US delivery (Quirk et al., 1997). In line with this role, increased immediate early-gene expression was detected in these higher-order auditory associative cortices after fear learning (Grosso et al., 2017). The requirement of AuC in fear learning was investigated using lesion studies but yielded contrasting results (Boatman and Kim, 2006; Campeau and Davis, 1995; Romanski and LeDoux, 1992b). However, a causal role for AuC activity in fear acquisition and expression was confirmed with several reversible inactivation studies (Dalmay et al., 2019; Letzkus et al., 2011; Wigestrand et al., 2017). Based on these studies, the AuC showed to be required specifically in fear conditioning paradigms involving complex sounds as the CS, such as the frequency-modulated sweeps

(Dalmay et al., 2019) or paradigms where discrimination between two CSs is required (Dalmay et al., 2019; Wigestrand et al., 2017). Although the AuC itself has shown to be a potential site for CS-US convergence by exhibiting responses to US presentation (Letzkus et al., 2011), a recent study demonstrated that input to the AuC originating from higher-order auditory thalamic nuclei conveys experience-dependent information (Pardi et al., 2020). Using projection-specific in vivo calcium imaging, increased calcium influx in the boutons of axonal projections originating in higher-order auditory thalamus and terminating in layer 1 AuC neurons was measured in response to the CS after FC training. Consistently, specific inactivation of these projections impaired fear acquisition without affecting basic auditory processing (Pardi et al., 2020). Based on this, top-down regulation of AuC function by the higher-order thalamus shows to be a crucial determinant for its role in FC in addition to its previously established role as a site of CS-US plasticity.

1.2.2.2. US pathways to the amygdala

As an instructive aversive signal, the most commonly used unconditioned stimulus (US) in FC paradigms is a mild electric shock delivered to the floor of the conditioning chamber. The discriminative sensory component of such noxious stimulus is transmitted via the spinothalamic pathway for pain and temperature starting from sensory neurons in the dorsal root ganglia that synapse onto the dorsal horn neurons of the spinal cord. The neural signal is then relayed to the thalamic ventral posterior nucleus and then to somatosensory cortices that register the physical aspects of the stimulus (Kandel, 2013). The affective component of the US noxious signal is, however, encoded via separate pathways that are shown to involve projections of dorsal horn neurons to the pontine parabrachial nucleus (PB) and to the dorsolateral periaqueductal gray (dlPAG) in the midbrain (Kandel, 2013; Yeh et al., 2018). Both dlPAG and the PB were shown to be crucial sites for mediating US signal to the LA and to the CeA respectively during fear learning (Han et al., 2015; Johansen et al., 2010; Sato et al., 2015; Watabe et al., 2013). However, more recent studies demonstrated that these regions do not carry sensory information directly to the amygdala. Instead, the PB conveys nociceptive information from the spinal cord to the interlaminar thalamic nucleus (Deng et al., 2020) while the dlPAG, similarly, mediates the US signal during FC by projections to the anterior paraventricular (PVT) nucleus of the thalamus (Yeh et al., 2021). Furthermore, monosynaptic rabies tracing performed in a population of US responsive neurons in the thalamic PIL and SG nuclei revealed that they receive direct projections from the PB, the PAG, and the principle trigeminal sensory nucleus. While the same population of neurons was found in this study to be a major source of input to the LA, these neurons were proposed to mediate US input to the LA (Barsy et al., 2020).

Another important source of aversive information to the LA is mediated by neuromodulatory systems that were shown to regulate plasticity in the LA via effects on PNs or GABAergic neurons (Yeh et al., 2018). In line with this, blocking β adrenergic receptors in the LA impaired fear learning induced by moderate training conditions (Herry and Johansen, 2014; Johansen et al., 2014). Moreover, inhibition of cholinergic projections from the basal nucleus to the BLA during fear learning reduced conditioned freezing (Jiang et al., 2016) and a similar effect on FC was observed by blocking cholinergic receptors in the AuC (Letzkus et al., 2011). Taken together, current findings highlighted the thalamic input and neuromodulatory signaling to be the main sources of US input to the amygdala.

1.2.2.3. The medial prefrontal cortex

The prefrontal cortex is a neocortical area located in the frontal lobe. It is a major hub that integrates, processes, and stores information about the environment and the internal states of the individual. Accordingly, the PFC provides top-down control of brain output that guides behavior towards survival and maintains behavior flexibility in response to a changing environment (Chini and Hanganu-Opatz, 2021). Based on this, the PFC regulates several cognitive functions such as working memory, decision making, and attention in addition to its role in emotional learning (Chini and Hanganu-Opatz, 2021; Courtin et al., 2013). Although these functions are more highly developed in humans, functional homology between the human PFC and the medial PFC (mPFC) in rodents exists and is strongly manifested in the control of fear learning behavior (Courtin 2015). In rodents, two main areas of the mPFC are mostly investigated in terms of their role in fear learning, namely the prelimbic (PrL) and infralimbic (IL) areas of the ventromedial PFC. These two areas showed functional dichotomy in regulating expression versus extinction of learned fear (Giustino and Maren, 2015). Although lesions and manipulation of the mPFC function yielded controversial effects on fear learning (Courtin et al., 2013), the most consistent finding supports a correlation between PrL neuronal activity and fear expression. For example, inactivation of the PrL after fear acquisition reduced conditioned freezing (Corcoran and Quirk, 2007; Sierra-Mercado et al., 2011). Also, sustained firing was measured in PrL neurons during the presentation of conditioned CS using in vivo single-unit recordings (Burgos-Robles et al., 2009). Such a role of the mPFC in fear expression was shown to be mediated by reciprocal connectivity between the mPFC and the BLA. In line with this role, optogenetic activation of PrL CA/calmodulin-dependent protein kinase II (CAMKII) neurons produced robust evoked excitatory responses (eEPSCs) in the BLA, which were much larger in the BA compared to the LA and were potentiated in FC-trained compared to naïve mice (Arruda-Carvalho and Clem, 2014). On the other hand, combining retrograde tracing

in the BA with cFos assay revealed increased neuronal activation of BA neurons projecting to the PrL during fear acquisition and retrieval (Senn et al., 2014). Furthermore, retrogradely labeled PrL projecting BA neurons showed an increase using in vivo single-unit responses during freezing to a conditioned CS, and optogenetic inhibition of these neurons reduced conditioned freezing (Senn et al., 2014). Taken together, the mPFC is shown to play a main role in modulating fear expression through its reciprocal interaction with the BA.

1.2.2.4. The hippocampus

The hippocampus (HPC) is located in the medial temporal lobe in an adjacent position to the amygdala (Marek and Sah 2018). In addition to its established role in the formation of spatial and episodic memories, its role in emotional processing has been early recognized being the key component of the limbic system (Marek and Sah, 2018). The HPC comprises several sub-regions; the dentate gyrus (DG), the cornu ammonis fields (CA1-CA3), and the subiculum. Neural signal is transmitted through the HPC by a series of connections known as the trisynaptic circuit (McDonald 2016), where sensory input enters the HPC from the adjacent entorhinal cortex (EC) through what is known as the 'perforant path'. The signal is then relayed to the DG and from there it is passed to the CA3 through the mossy fibers and then to the CA1 through the Schäffer collaterals (McDonald and Mott, 2017). Following information processing through this circuit, the neural signals exit the HPC through a projection from the subiculum to the EC and then to other brain areas (McDonald and Mott, 2017). The HPC circuit is involved in multimodal processing that integrates different sensory information into complex representations known as contexts. Based on this role, the HPC has been implicated in the formation of aversive memories that involves associations with contexts, modeled experimentally by the contextual fear conditioning paradigm (Maren et al., 2013). In contrast to cued FC where US presentation is coupled to a discrete auditory cue as the CS, contextual FC involves presenting the US within a certain delay after exposure to the training context. The latter is encoded by the integration of several temporal, olfactory and spatial information. Contextual memory retrieval is then tested by exposing the subject to the same context where it received the US, as opposed to cued FC, where CS memory retrieval is conducted in a different context (Marek and Sah, 2018). Interfering with HPC function by lesions or inactivation have shown to impair contextual FC acquisition (Phillips and LeDoux, 1992), consolidation (Sacchetti et al., 1999) and retrieval (Frankland et al., 1998; Kim and Fanselow, 1992). A prominent view of the HPC role in FC is that it encodes contextual information and relays it to the amygdala where context-US associations are formed (Fanselow, 2010; Maren et al., 2013). However, substantial evidence demonstrates a role for the HPC plasticity in contextual fear memory formation and consolidation. In line with this notion, learning-dependent changes such as expression

of immediate early genes and glutamate receptors and increases in spine density were observed in the HPC after contextual FC (Chaaya et al., 2018). Interestingly, chemogenetic inactivation of HPC CAMKII neurons after contextual FC acquisition impaired retrieval (Zhu et al., 2014), which confirmed previous findings from lesion studies regarding HPC implication in fear memory consolidation.

1.2.2.5. The ventrolateral periaqueductal gray

The periaqueductal gray (PAG) is a cell dense region that surrounds the aqueduct in the midbrain. In addition to its role in regulating several autonomic functions such as breathing, heart rate and analgesia, it represents an exit relay for mediating different forms of defensive behaviors (Keay and Bandler, 2015). Based on its connectivity and function, the PAG displays a columnar organization where the dorsolateral column dlPAG controls active defensive responses such as escape behavior, while the ventrolateral column vlPAG regulates passive defensive responses such as freezing (Fanselow, 1991; Keay and Bandler, 2015). In the context of fear learning, early evidence highlighted the role of the vlPAG in the expression of conditioned freezing responses that was reduced after vlPAG lesions (LeDoux et al., 1988). Also, conditioned freezing was associated with increased cFos expression in the vlPAG that was reduced by CeA inactivation by lidocaine (Carrive, 2000; Carrive et al., 1997). Monosynaptic retrograde tracing performed in the vlPAG produced dense labeling in the CeM confirming previous results (Viviani et al., 2011). A more recent finding using in vivo optogenetics revealed that the activity of excitatory neurons of the vlPAG is necessary and sufficient for the display of conditioned freezing (Tovot*e* et al., 2016). This effect was shown to be mediated by a disinhibitory projection from the CeA to the vlPAG that is further relayed to motor centers in the medulla (Tovote et al., 2016). Based on this, the vlPAG represents a crucial node that drives conditioned freezing responses downstream of the amygdala.

1.3. Inhibitory regulation of fear learning

Most of the circuits described above involved mainly glutamatergic transmission driven by excitatory neurons, specifically CAMKII neurons, being the most abundant in the forebrain and the most studied with regards to plasticity and cellular mechanisms of learning. However, inhibitory neurons, despite representing a minor population in the brain, were found to be critical components for the regulation of fear learning (Ehrlich et al., 2009). Early evidence about the role of inhibition in fear learning arose from studies revealing a negative effect of benzodiazepines, a group of $GABA_A$ receptor ($GABA_A$-R) agonist drugs, on the acquisition and/or expression of fear (Fanselow and Helmstetter, 1988; Harris and

Westbrook, 1995). Subsequently, in vitro electrophysiological studies highlighted the role of inhibition in amygdala plasticity required for fear learning. In this context, feed-forward and feedback inhibition, mediated by $GABA_A$ or $GABA_B$ receptors, respectively, were found to gate the induction of LTP in synapses formed by cortical and thalamic afferents to the BLA (Bissiere et al., 2003; Shaban et al., 2006). In line with this role, deletion of the gene encoding GABA synthesizing enzyme glutamate acid decarboxylase isoform 65 kDa (GAD65) lead to fear generalization (Bergado-Acosta et al., 2008; Sangha et al., 2009). Recently, detailed analyses of the inhibitory regulation of fear learning arose from cell-specific circuit mapping studies that helped to elucidate the contribution of inhibitory neurons in fear learning and provided grounds for investigating inhibitory transmission in a synapse-specific manner.

1.3.1. Inhibitory neurons in fear learning

Inhibitory neurons represent a highly heterogeneous group of neurons that can largely regulate brain function. They are classified based on their morphology, expression of cytosolic markers, electrophysiological properties, and synaptic targeting (Cummings et al., 2021). Accordingly, their contribution to brain circuits is highly diverse and includes mechanisms such as providing gain control, producing rhythmic oscillations, or mediating disinhibition, by which they can control the output of brain circuits and thereby control behavior (Cummings et al., 2021). The advent of genetic tools, optogenetic manipulations, and methods assessing in vivo single-cell responses allowed detailed characterization for inhibitory neurons activity during FC.

1.3.1.1. Inhibitory neuron networks in the basolateral amygdala

In the BLA, inhibitory interneurons (INs) comprise 20% of the neuronal population (Krabbe et al., 2018; Marek and Sah, 2018). Based on their expression of the calcium-binding proteins, BLA INs can be divided into calbindin positive (CB) and calretinin positive (Calr) INs (Krabbe et al., 2018). CB INs are further divided into parvalbumin (PV), somatostatin (SOM), neuropeptide Y and large cholecystokinin (CCK_L) positive INs. While Calr INs include vasoactive intestinal peptide (VIP) positive INs and small CCK positive cells (CCK_S) (Krabbe et al., 2018).

During FC, the transmission and plasticity of CS signal through BLA PNs are controlled by soma-targeting PV INs and distal dendrites-targeting SOM INs (Krabbe et al., 2018; Perumal and Sah, 2021; Wolff et al., 2014) (figure 3). Using in vivo single-unit recordings, Wolff et al showed that CS presentation during FC training leads to the activation of PV INs and inhibition of SOM INs (Wolff *et* al., 2014). This was explained by a disinhibitory

projection from PV onto SOM INs revealed with slice electrophysiology leading to ultimate disinhibition of BLA PNs in response to the CS. US presentation during FC training, on the other hand, inhibited both PV and SOM INs and the inhibition of PV INs during US was shown to be required for fear learning (Wolff et al., 2014). Such inhibition of both subtypes during US was thought to provide a teaching signal that would allow for depolarization of PN via disinhibition during CS-US pairing and induce CS plasticity. A recent study explored the source of this inhibition onto PV and SOM INs during US presentation using in vivo calcium imaging and revealed that it is mediated by the activation of VIP INs (Krabbe et al., 2019) (figure 3). Intriguingly, VIP INs showed increased spike-triggered calcium transients during the US presentation and were shown in vitro to inhibit both SOM and PV INs leading to PN disinhibition (Krabbe et al., 2019). Using in vivo optogenetics, this disinhibitory circuit motif by VIP INs onto PNs was shown to provide the necessary instructive signal for fear memory acquisition (Krabbe et al., 2019).

In line with the reported changes in BLA INs activity during fear acquisition, structural plasticity was observed in GABAergic synapses formed onto PN in the BA after FC (Kasugai et al., 2019) .Using the detergent-solubilized freeze-fracture replica immunolabeling (FRIL) method, increased somatic and dendritic GABAergic postsynaptic areas was detected in BA PNs in mice that underwent FC. This effect was associated with a decrease in the density of $GABA_A$-γ2 receptor subunit and an increase in the density of α2 subunit in these synapses (Kasugai et al., 2019). While this structural remodeling was proposed to alter the gating kinetics of $GABA_A$-R in response to FC, the functional implication of this effect in fear learning was not further explored.

In addition to regulating signal propagation within the amygdala projecting PNs, BLA INs were shown to control the long-range connectivity of PNs in a pathway-specific manner. In a study by Vogel et al (Vogel et al., 2016), CCK_L INs expressing the endocannabinoid receptor-1 (CB1-R) in the BA showed to mediate differential levels of inhibition onto IL projecting versus Prl projecting PNs. This effect was associated with higher expression of the endocannabinoid synthesizing enzyme diacylglycerol lipase α (DGL-α) by CCK_L INs inhibiting IL-projecting PNs that mediate reduction of fear responses (Vogel 2016). Based on this differential CB1-R mediated signaling, CCK_L INs were proposed in this study to regulate the switch between high and low fear states determined by the long-range projection from BA PNs to the mPFC (Vogel et al., 2016).

Taken together, it is evident that the distinct patterns of activity and plasticity displayed by different IN subtypes within the BLA can largely influence fear learning by modulating the plasticity of local and long-range PN.

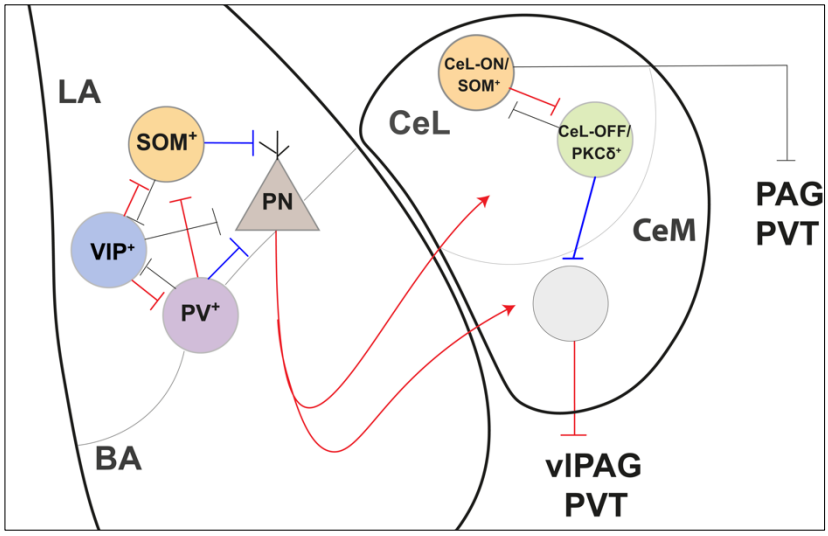

Figure 3 Inhibitory neuron networks in the amygdala.
A simplified schematic depicting the connectivity patterns between major amygdala inhibitory neuron subtypes. Red colored projections represent projections promoting fear memory acquisition/expression. Blue colored projections represent projections gating fear memory acquisition/expression. Red and blue projections are functionally validated using in vivo electrophysiology/ calcium imaging during FC. Gray projections are described based on neuroanatomical tracing or in vitro electrophysiology experiments.

1.3.1.2. Inhibitory neuron networks in the central amygdala

In the CeL, which is made entirely of GABAergic neurons, two major populations of these neurons are identified based on their expression of the markers SOM and protein kinase C - δ (PKCδ). Additionally, minor populations of inhibitory neurons expressing the markers: corticosterone releasing factor/hormone (CRF/CRH), tachykinin 2 (Tac2), neurotensin (Nts), and serotonin receptor 2a ($5HT_{2A}$) were also identified (Babaev et al., 2018b). CeL inhibitory neurons were classified based on the increase or decrease of their CS evoked responses during FC retrieval measured with single-unit recordings. Accordingly, CeL ON, INs were the ones showing increased CS-evoked firing after FC and CeL-OFF cells are the ones showing depression (Ciocchi et al., 2010) (figure 3). Using in vitro recordings combined with optogenetic stimulation, both cell types were shown to be reciprocally connected via inhibitory projections. In a parallel study, the CeL-OFF cells were shown to share functional overlap with a population of (PKCδ) INs (Haubensak et al., 2010). Interestingly, optogenetic activation of PKCδ INs silenced the CeM output and their silencing during FC training and testing lead to increased CS freezing. Hence, data provided by these studies unveiled a disinhibitory circuit from the CeL to the CeM that is recruited by learning-

dependent plasticity to mediate fear acquisition (Ciocchi et al., 2010; Haubensak et al., 2010) (figure 3), While the identity of CeL-ON cells in these studies was not explored, and neither the source of their activation in response to the CS, it was indicated that they likely represent SOM neurons being the other major subtype residing in the CeL. Using slice electrophysiology combined with optogenetic stimulation, SOM neurons of the CeA were shown to receive potentiated synaptic input from the LA and increased frequency and amplitude of mEPSCs after FC (Li et al., 2013). Interestingly, chemogenetic silencing of SOM neurons in this region during acquisition interfered with fear learning, a function that was supported by the tracing of direct long-range projections from CeL SOM neurons to the vlPAG and the PVT (Li et al., 2013; Penzo et al., 2014).

Taken together, CeA inhibitory neurons contribute substantially to the plasticity required for fear acquisition. Also, disinhibition appears to be a dominant motif for the inhibitory regulation of fear learning in the amygdala.

1.3.1.3. Inhibitory neuron networks in the auditory cortex

The three major inhibitory INs in the AuC include PV, SOM, and ionotropic serotonin receptor 5HT3a-R expressing INs that are subdivided into VIP and neurogliaform cells expressing neuron-derived neurotrophic factor (NDNF)(Studer and Barkat, 2022). In addition to regulating different aspects of sound processing within AuC PNs, specific IN subtypes were causally implicated in mediating associative fear memories to sound stimuli by controlling PN plasticity. In this context, a pioneering study implementing in vivo calcium imaging in anesthetized mice revealed a prominent role for layer 1 INs that showed strong activation in response to the US presentation during FC training (Letzkus et al., 2011). The activation of L1 INs, in turn, produced inhibition of layer 2/3 PV INs and ultimate disinhibition of PNs (figure 4). While the US-induced activation of L1 INs was shown to be mediated by acetylcholine release from the basal forebrain, blocking nicotinic acetylcholine receptors in the AuC during FC training reduced fear memory retrieval. These findings identified the AuC as a site for CS-US convergence and demonstrated a causal role for L1 INs mediated disinhibitory circuit in memory formation (Letzkus et al., 2011).

In addition to enabling PN plasticity via disinhibition, L1 INs were shown to be themselves subject to fear learning-dependent plasticity. A study by Abs et al (Abs et al., 2018) showed that $NDNF^{+}$ L1 INs exhibit increased calcium responses to the CS after FC. However, their responses decreased in responses to repeated, unpunished tones, indicating that their plasticity serves to encode the behavior relevance of sounds (Abs et al., 2018). Interestingly, this plasticity pattern of L1 NDNF INs was found to be reversed in SOM INs which were

shown by different studies to exhibit increased responses to repeated tones and decreased responses to sounds associated with behavioral outcomes (Hartung and Letzkus, 2021). While NDNF and SOM INs represented the major source of inhibition onto PN distal dendrites in L1 of the AuC, these contrasting plasticity patterns by each of these IN subtypes were proposed to modulate the dendritic sound processing within PN based on the afferent source. However, it is still unclear how the potentiation of CS responses in NDNF INs contributes to fear memory recall in the context of this inhibitory projection to PNs.

Another IN subtype in the AuC, namely VIP INs, was shown to regulate associative aversive and appetitive learning (Pi et al., 2013). In fact, the disinhibitory circuit motif by VIP INs described in the BLA was first described in cortical areas, namely the AuC and the mPFC. In the study by Pi et al 2013, VIP INs in the AuC were shown to be strongly activated in response to a reinforcing aversive and appetitive stimulus in head-fixed mice performing an auditory go/no-go task. Although the outcome of this activation on memory was not directly tested in this study, the authors could show that optogenetic activation of VIP IN in vivo leads to the disinhibition of PNs. They also demonstrated with in vitro electrophysiology that the PN disinhibition is likely mediated by inhibition of SOM and to a lesser extent, PV INs.

Based on these studies, AUC INs were found to undergo plastic changes in response to fear learning, as seen in L1 INs. Also, L1 INs and VIP INs were shown to play a key role in mediating US instructive signals that enabled the PN plasticity via disinhibition.

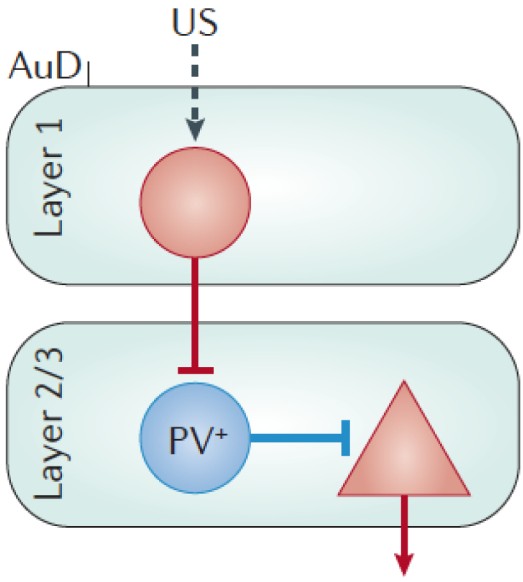

Figure 4 A disinhibitory network in the auditory cortex mediates fear learning.
A schematic showing a disinhibitory network in the AuC that is recruited by US presentation via cholinergic signaling. Reprinted from (Tovote et al., 2015*)* by permission from Copyright Clearance Center (license number 5320121472056).

1.3.1.4. Inhibitory neuron networks in the medial prefrontal cortex

As described earlier, PN of the mPFC were shown to modulate fear expression by means of reciprocal connectivity with the BLA. Interestingly, this role was largely controlled by local inhibitory INs of the mPFC. One example was shown in a study by Courtin et al (Courtin et al., 2014), which investigated the activity of different mPFC neuron types during FC using in vivo single-unit recordings. After FC, CS presentation elicited potentiated responses in PNs that correlated positively with conditioned freezing. Contrastingly, PV INs were shown to be inhibited and their activity correlated negatively with fear expression during CS presentation. In line with this, optogenetic inhibition and activation of PV INs during CS presentation increased and reduced fear expression and PN activity, respectively (Courtin et al., 2014). This disinhibitory circuit was found thereby to be necessary and sufficient for the expression of fear memory. The source of PV inhibition during CS presentation remained, however, unexplored. Recently, another study investigated the relevance of this disinhibitory circuit in fear memory acquisition and expression and identified SOM INs to be the source of inhibition onto PV INs (Cummings and Clem, 2020) (figure 5). Using a combination of in vitro electrophysiological recordings and in vivo calcium imaging, Cummings et al showed that SOM INs in the PrL layer 2/3 exhibit potentiated synaptic transmission and increased CS-induced calcium transients after FC. Using in vivo optogenetics, the activity of SOM INs during CS presentation was shown to be required for the acquisition and expression of fear and was sufficient to induce freezing in mice. To explain this effect, a cell-type-specific circuit analysis revealed an inhibitory projection from

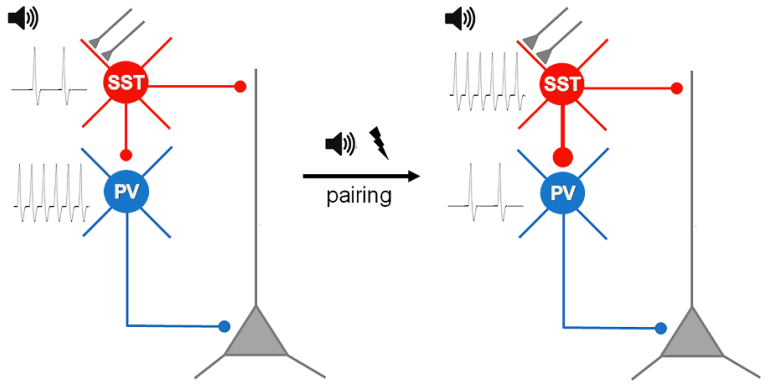

Figure 5 A disinhibitory network in the mPFC promotes fear memory acquisition and retrieval.
A schematic showing a disinhibitory network onto mPFC PNs that is recruited by CS presentation. FC potentiates excitatory synaptic input onto somatostatin INs (SST) leading to disinhibition of PNs by inhibition of PV INs. Reprinted from (Cummings et al., 2021) by permission from Copyright Clearance Center (license number 5320140089388).

SOM INs onto PV INs that lead to the disinhibition of PNs in the PrL (Cummings and Clem, 2020). These two studies implicated mPFC INs causally in fear learning and confirmed that disinhibition is a prominent circuit motif for driving PN activity during fear learning.
In summary, Inhibitory neurons were demonstrated to be key players in the regulation of fear learning by showing dynamic responses to the CS and/or US and hosting plastic changes that promoted the plasticity of projection neurons.

1.4. Nlgn2 is a central regulator of synaptic inhibition

1.4.1. Functional organization of the inhibitory synapse

Inhibitory regulation of brain circuits depends on inhibitory synapses, known also as Gray type II or symmetric synapses. In the brain, the majority of inhibitory synapses rely on the release of the neurotransmitter gamma-aminobutyric acid (GABA), in contrast to glycine that is released predominantly in the brainstem and spinal cord inhibitory synapses (Fishell and Rudy, 2011). GABA is synthesized in the presynaptic terminal by decarboxylation of glutamic acid through the activity of glutamic acid decarboxylases (GAD), which exists in two isoforms with different molecular weights: 65 kDa and 67 kDa. GABA is then transported into the presynaptic vesicles via the activity of the vesicular GABA transporter (vGAT) (Rowley et al., 2012). The release of GABA from the presynaptic terminal is shown to be governed by the same basic molecular machinery that controls glutamate release from excitatory presynapses (Krueger et al., 2012).

After its release, GABA binds to ionotropic $GABA_A$ receptors (GABA-$_A$R) that are ligand-gated chloride channels. Activation of $GABA_A$ receptors and the resulting influx of extracellular chloride ions Cl^- leads to the inhibition of the postsynaptic neuron mainly by hyperpolarization that leads to reduced neuronal excitability (Fishell and Rudy, 2011). $GABA_A$ receptors show a pentameric structure that results from the assembly of 5 subunits around a central ion pore. This subunit composition is selected from 19 different isoforms that could be arranged into different configurations to form the receptor, giving rise to high structural and functional heterogeneity (Fritschy et al., 2012; Sigel and Steinmann, 2012).
In addition to GABA receptors, the inhibitory postsynapse includes scaffolding proteins, intracellular signaling proteins, and synaptic adhesion molecules that were shown to be critical for its differentiation, structural integrity, and functions. Known as inhibitory synapse organizers, these molecules are highly distinct from the ones present at excitatory postsynapses and their functions at the synapses are mediated through complex interactions (Krueger-Burg et al., 2017). One of the most established inhibitory synapse organizers is the synaptic adhesion molecule Nlgn2 (figure 6). Nlgn2 is a member of the

Neuoroligins (Nlgns) family of synaptic adhesion molecules that bind with presynaptic Neurexins (Nrxns). This interaction is crucial for the maturation of the synapse as each of Nrxns and Nlgns were shown to mediate the recruitment of different synaptic components on their respective side of the synapse (Krueger et al., 2012). Nlgns include five protein members in humans (Nlgn1, 2, 3, 4X and 4Y) and 4 in mice (Nlgn1, 2, 3 and 4). Nlgn1 was the first Nlgn member to be identified and was associated specifically with excitatory synapses structure and functions. In contrast, Nlgn2 showed specificity for inhibitory synapses and Nlgn3 was validated at both inhibitory and excitatory synapses. Interestingly, Nlgn4 was linked to inhibitory synapses in rodents and excitatory synapses in humans (Nguyen et al., 2020).

1.4.2. Nlgn2 Identification, localization, and structure

Nlgn2 was first identified using polymerase chain reaction assay (PCR) based on primers from the Nlgn1 gene. The resulting DNA products were sequenced to reveal two novel *Nlgn* genes, namely *Nlgn2* and *Nlgn3* (Ichtchenko et al., 1996). Early analyses of Nlgn2 expression using Northern Blot, Fluorescent *In Situ* Hybridization (FISH) and Western Blot assays revealed enrichment of Nlgn2 expression in brain tissue (Ichtchenko et al., 1996; Scheiffele et al., 2000; Varoqueaux et al., 2004). Its localization in the rat brain slices and dissociated hippocampal cultures exhibited a highly preferential expression at inhibitory synapses as it appeared opposite to vGAT, but not to vesicular glutamate transporter 1 (vGlut1) labeled structures (Varoqueaux et al., 2004). Therefore, Nlgn2 was the only member of Nlgn family found to be specific to inhibitory synapses across species. This notion was further strengthened with many following gain of function and loss of function-based studies, in vitro and in vivo, that reported synaptic function alterations that were specific to inhibitory synapses (Ali et al., 2020).

Similar to Nlgn1, Nlgn2 was shown to bind presynaptically to Neurexin (Ichtchenko et al., 1996; Tsetsenis et al., 2014) (figure 6, A). This interaction with Nrxns is proposed to define Nlgns localization to inhibitory versus excitatory synapses (Südhof, 2017). The Nlgn2 protein comprises three domains, an extracellular N terminal domain, a single pass alpha-helical transmembrane domain, and an intracellular C terminal domain (Ichtchenko et al., 1996). The extracellular domain shows homology with acetylcholine esterase enzymes and contains a site that mediates the binding with presynaptic Neurexins. The binding of Nlgn2 with Nrxns, and thereby its localization to inhibitory synapses, is controlled by alternative splicing. Accordingly, the lack of the splice site B in the Nlgn2 gene and the presence of the splice site 4 in the α-neurexin gene underlies the specific localization of Nlgn2 at inhibitory synapses (Graf et al., 2006; Kang et al., 2008). The C terminal intracellular domain of Nlgn2

protein bears several binding sites that mediate Nlgn2 known interactions with other inhibitory postsynapse proteins such as Collybistin, Gephyrin, and S-SCAM (Krueger-Burg et al., 2017) (figure 6, A).

1.4.3. Nlgn2 function at inhibitory synapses

Early investigation of a potential role of Nlgn2 in synapse formation included in vitro synaptogenesis assays. In this system, exogenous expression of Nlgn2 by non-neuronal cells induced the assembly of presynaptic proteins in opposing presynaptic terminals of co-cultured neurons (Scheiffele et al., 2000). Intriguingly, despite its ability to initiate synapse formation in vitro, studies investigating the effect of Nlgn2 deletion in vivo did not support such a role. In most brain regions investigated, the inhibitory synapse density, quantified by the expression of inhibitory presynaptic marker vGAT, was unaltered in Nlgn2 KO mice (Ali et al., 2020). These findings demonstrated that Nlgn2 is dispensable for initial synapse formation. Instead, constitutive and conditional Nlgn2 deletion prominently affected the efficiency of inhibitory synaptic transmission and lead to altered composition of inhibitory postsynapse in many brain regions. Parameters such as the frequency and/or amplitude of miniature inhibitory postsynaptic currents mIPSCs were frequently reported to be reduced, as well as the density of postsynaptic markers such as the scaffold protein Gypherin and GABA receptor subunits (Ali et al., 2020). Based on these findings, Nlgn2 was shown to be crucial for the maturation and function of inhibitory postsynapses.

A mechanism by which Nlgn2 mediates this role in synapse maturation was proposed by Poulopoulos et al, who investigated the interactions of the Nlgn2 intracellular domain using a series of in vitro two-hybrid screen, membrane recruitment, and immunoprecipitation assays (Poulopoulos et al., 2009). Based on the model proposed by this study, Nlgn2 binds to the scaffold protein Gephyrin and the GTP/GDP exchange factor Collybistin through distinct sites on the intracellular domain of Nlgn2 (figure 6, A). The binding with Nlgn2 activates Collybistin to mediate the tethering of Gephyrin to the postsynaptic membrane and the assembly of Gephyrin scaffold, leading ultimately to the recruitment of GABA receptors to the postsynaptic membrane (Poulopoulos et al., 2009) (figure 6, A). Supporting this model in vivo, an increased level of intracellular Gephyrin aggregates was quantified in the pyramidal layer of the hippocampal CA1 in Nlgn2 KO mice, indicating a failure of Gephyrin recruitment to the membrane in the absence of Nlgn2 (Poulopoulos et al., 2009). Also, this model explains the reduction in GABA receptor subunits detected in Nlgn2 KO mice across several brain regions (Babaev et al., 2016; Hoon et al., 2009; Jedlicka et al., 2011; Poulopoulos et al., 2009). In line with its role in regulating inhibitory synapse maturation and function, deletion of Nlgn2 largely affected network excitability in vivo. Using

electrophysiological field recordings in anesthetized mice, one study revealed increased excitability in dentate gyrus granule cells upon perforant path stimulation and a reduced threshold to generate epileptiform discharges (Jedlicka et al., 2011). This finding highlights the key role played by Nlgn2 in regulating excitatory/inhibitory balance at the neuronal network level.

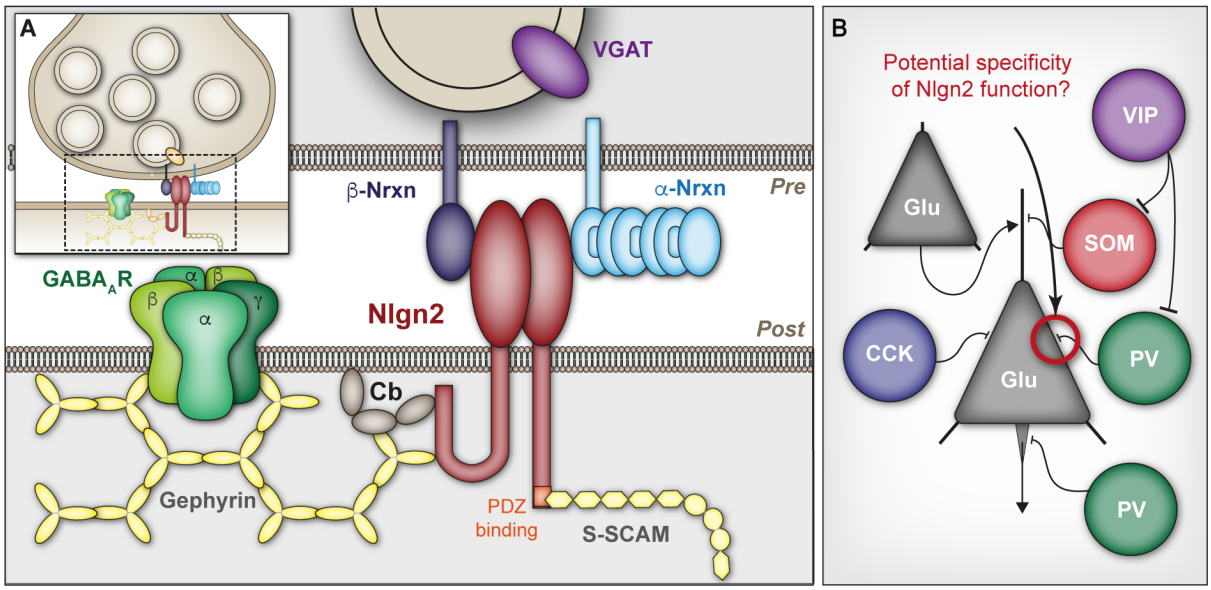

Figure 6 Nlgn2 is a central organizer of inhibitory synapse maturation and function.
A. A schematic showing different components of the inhibitory synapse including Nlgn2 and its pre and postsynaptic interaction partners. The interaction of Nlgn2 with presynaptic Nrxns determines Nlgn2 localization at inhibitory synapses. The postsynaptic interaction with collybistin (Cb) and Gephyrin mediates the recruitment of $GABA_AR$s to the postsynaptic membrane. **B**. A cartoon depicting the proposed synapse specificity of Nlgn2 function in brain circuits. Nlgn2 deletion in vivo preferentially affected perisomatic inhibitory synapses formed by PV INs onto PNs. Adapted from (Ali et al., 2020), figure credit: Prof. Dr. Dilja Krüger-Burg.

1.4.4. Synapse specificity of Nlgn2

Studies addressing Nlgn2 localization in vivo indicated a global pattern of expression (Poulopoulos et al., 2009; Varoqueaux et al., 2004). However, the function of Nlgn2 in postsynapse maturation was reported to be relevant specifically for inhibitory synapses formed at the perisomatic region of pyramidal neurons (figure 6, B). This notion arose from studies demonstrating a decrease in the density in perisomatic, but not total, Gephyrin puncta in Nlgn2 KO mice quantified in regions such as the CA1 in the hippocampus and the BA in the amygdala (Babaev et al., 2016; Poulopoulos et al., 2009). Furthermore, paired electrophysiological recordings performed in the somatosensory cortex revealed a decrease in the amplitude of unitary IPSCs originating from fast-spiking PV INs onto PNs in Nlgn2 KO mice compared to WT mice. This decrease was, however, not detected for unitary IPSCs originating from SOM INs (Gibson et al., 2009). Taken together, this body of data

supports a synapse-specific role for Nlgn2 in perisomatic synapses originating from fast-spiking INs such as PV INs. However, a role for Nlgn2 in synapses made by other IN subtypes onto PNs or synapses made between inhibitory neurons has never been systematically addressed. Also, whether this effect on the perisomatic synapses is global across brain regions or specific to the ones mentioned above, is also unclear.

1.4.5. Nlgn2 and synaptic plasticity

Being key organizers of synapse maturation, Nlgns were investigated for their potential roles in regulating different aspects of synapse function including synaptic plasticity. While many reports implicated Nlgn1 in excitatory synapse plasticity, modeled by the long-term potentiation paradigm (Jiang et al., 2017; Kim et al., 2008; Wu et al., 2019), the role of Nlgn2 in this process was not fully understood. In vitro, the synaptogenic ability observed by Nlgn2 overexpression was shown to be highly activity dependent (Chubykin et al., 2007). In vivo, one study investigating plasticity of perforant path synapses onto granule cells (GC) cells in the dentate gyrus (DG) reported unchanged LTP in Nlgn2 KO compared to WT mice (Jedlicka et al., 2011). In another report, increased short-term depression was measured in Nlgn2 KO mice using paired recordings in synapses made by SOM INs onto pyramidal neurons in the somatosensory cortex (Gibson et al., 2009). However, the potential role of Nlgn2 in regulating synapse plasticity still requires more investigation.

1.4.6. Interaction partners of Nlgn2

1.4.6.1. IgSF9b

The most established role for Nlgn2 function in inhibitory synapse differentiation relies on its interaction with Nrxns presynaptically and with Gephyrin and Collybistin postsynaptically. However, several other postsynaptic interaction partners of Nlgn2 have been identified and were shown to modulate this role (Ali et al., 2020). One of these interaction partners is the Immunoglobulin superfamily member 9b (IgSF9b), a synaptic adhesion molecule that was shown to colocalize with Nlgn2 in dissociated HPC cultures (Woo et al., 2013) (figure 7, a). IgSF9b was found to mediate hemophilic adhesion using in vitro assays, but its overexpression in HEK293T cells was not sufficient to induce synapse formation in co-cultured neurons. Yet, knockdown of IgSF9b produced a reduction in inhibitory synapses puncta from cultured INs and impaired inhibitory synaptic transmission assessed with reduced mIPSCs frequency, indicating a role in inhibitory synapse maturation (Woo et al., 2013). The interaction between IgSF9b and Nlgn2 was described based on their binding to the synaptic scaffolding molecule (S-SCAM) that was shown to bridge the two molecules in vitro (figure 7, a). However, evidence for this molecular complex in vivo is still lacking. In

fact, the one study investigating a functional interaction between Nlgn2 and IgSF9b in vivo using Nlgn2, IgSF9b and double KO mice reported independent effects on inhibitory transmission in the amygdala (Babaev et al., 2018a). In this study, Nlgn2 KO mice showed reduced IPSCs amplitude in the BA, while IgSF9b KO mice showed increased mIPSCs frequency in the CeA, and both of these effects were maintained in the double KO. Showing a contrasting region specificity and opposing effects on the inhibitory transmission by Nlgn2 and IgSF9b in the amygdala, this study argues against a molecular complex mediating their functions in this region (Babaev et al., 2018a). However, it is not known whether these findings apply to other brain regions, which would be important to fully assess their potential interaction.

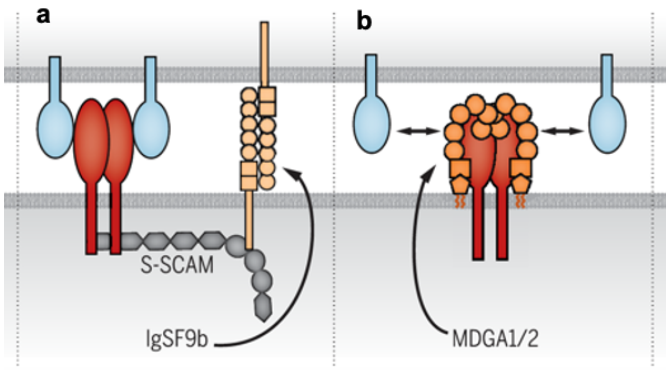

Figure 7 IgSF9b and MDGA1 are interaction partners of Nlgn2.
a, b. A schematic illustrating the interaction between Nlgn2 and each of IgSF9b (**a**) and MDGA1 (**b**). **a**. Nlgn2 and IgSF9b bind at different sites of the scaffold protein S-SCAM. **b**. MDGA1 binds to Nlgn2 and impede its interaction with Nrxns (Nlgn2 is depicted in dark red). Reprinted from (Ali et al., 2020), figure credit: Prof. Dr. Dilja Krüger-Burg.

1.4.6.2. MDGAs

The MAM domain-containing glycosylphosphatidylinositol anchor proteins (MDGAs) are a family of immunoglobulin superfamily proteins that are tethered to the membrane through GPI anchor. Two members of this family namely MDGA1 and MDGA2 were proposed to inhibit the effect of Nlgns in synapse maturation by interfering with the latter's interaction with the presynaptic Nrxns (Connor et al., 2019; Pettem et al., 2013). MDGA1 was shown to inhibit specifically the function of Nlgn2 in vitro and its overexpression and knockdown in non-neuronal cells selectively reduced and increased the numbers of inhibitory synapses, respectively (Pettem et al., 2013). Such negative regulation of inhibitory synapse numbers by MDGA1 was also reproduced in cultured cortical neurons with a reduction in mIPSCs frequency upon MDGA1 overexpression (Lee et al., 2013). In vivo, assessment of inhibitory synapse numbers in the pyramidal layer of the hippocampal CA1 revealed an increase in MDGA1 KO mice, supporting an inhibitory effect of MDGA1 on perisomatic synapse formation (Connor et al., 2017). Consistently, electrophysiological recordings in slices revealed increased mIPSCs in CA1 pyramidal neurons, increased resistance to

overexcitation, and impaired LTP (Connor et al., 2017) . While these findings demonstrate suppression of inhibitory synapse formation and function by MDGA1, an in vivo characterization of Nlgn2 and MDGA1 interaction, however, is still lacking.

1.4.7. Nlgn2 function in brain circuits

1.4.7.1. Role of Nlgn2 in the regulation of anxiety-like behavior

The function of brain circuits relies on a calibrated ratio of excitation and inhibition each neuron receives within the network, a feature known as the excitatory/inhibitory (E/I) balance. Considering its role in the maturation and function of inhibitory synapses, Nlgn2 was expected to influence the E/I balance within brain circuits. Therefore, many studies using constitutive and conditional Nlgn2 deletion and overexpression aimed at characterizing its function in behavioral circuits (Ali et al., 2020). One of the most prominent behavioral phenotypes detected in Nlgn2 KO mice was the increased anxiety-like behavior characterized using approach-avoidance paradigms like the open field test (OFT), the elevated plus maze (EPM), and the light-dark box (LDB). Using these paradigms, different studies reported increased avoidance of exposed areas by Nlgn2 KO mice indicative of anxiety (Babaev et al., 2016; Blundell et al., 2009; Cruces-Solis et al., 2021). This anxiety-like phenotype was found to be associated with a dysregulation in the amygdala anxiety circuit. Particularly, assessment of the expression of the immediate-early gene *cfos*, used as a proxy for neural activation during open-field exploration, revealed increased cFos levels in the BA and CeM nuclei of the amygdala (Babaev et al., 2016). Consistent with the increased activation in the BA, structural and electrophysiological findings indicative of impaired inhibitory transmission were also detected in this region. Precisely, a reduction in mIPSC frequency and in the density of perisomatic Gephyrin puncta were measured in the BA (Babaev et al., 2016). In the CeM, however, the increased activation was found to be due to an overactivated projection from the BA to the CeM and not to a local deficit in synaptic inhibition (Babaev et al., 2018a). Furthermore, the anxiety-like behavior of Nlgn2 KO mice was accompanied by changes at the level of long-range connections that extended beyond the local amygdala anxiety circuit. Recording of local field potentials in Nlgn2 KO versus WT mice while exploring the open field revealed exaggerated LFP power in the ventral hippocampus (vHPC), another region involved in anxiety processing (Cruces-Solis et al., 2021). Also, altered synchrony in the theta frequency range in the vHPC-mPFC-BLA anxiety network was measured in Nlgn2 KO, reflecting disruption of long-range connectivity between these regions.

Supporting a causal role for the BLA and vHPC in mediating the anxiety-like behavior in Nlgn2 KO mice, conditional deletion of Nlgn2 using adenoassociated (AAV) viral vectors recapitulated distinct aspects of this behavior (Cruces-Solis et al., 2021). Intriguingly, deletion of Nlgn2 from the mPFC and the lateral septum (LS) produced anxiolytic effects, indicating a region-specific effect of Nlgn2 in the regulation of anxiety (Liang et al., 2015; Troyano-Rodriguez et al., 2019).

1.4.7.2. Interaction of Nlgn2 and IgSF9b in the regulation of anxiety

While deletion of Nlgn2 produced a robust anxiety-like behavior, this effect was modulated by its proposed interaction partner IgSF9b. Behavioral characterization of Nlgn2 KO, IgSF9b and Nlgn2-IgSF9b double KO mice using the OFT revealed normalized anxiety-like behavior in the double KO mice indicating antagonistic effect by these two proteins on anxiety-like behavior (Babaev et al., 2018a). Circuit activation analysis and assessment of inhibitory synapse density and function revealed that this normalization in behavior results from opposing effects on inhibition by these proteins in different amygdala nuclei. While Nlgn2 deletion impaired inhibitory transmission in the BA, IgSF9b deletion enhanced inhibition in the CeM, leading to normalized amygdala anxiety output. This effect was confirmed by performing local deletion of IgSF9b in the CeM in Nlgn2KO mice, which rescued anxiety-like behavior similar to double KO mice. While these two proteins clearly do not interact on the same synapse to regulate anxiety, it would be interesting to know whether their reported interaction in vitro could be shown in vivo in another circuit.

1.4.7.3. Role of Nlgn2 in cognitive functions

While the role of Nlgn2 in cognitive function is still not fully understood, studies from constitutive and local conditional KO mice reported impairments or improvements in certain cognitive functions. For example, impaired emotional learning assessed using the cued and contextual FC was described in mPFC local Nlgn2 KO mice (Liang et al., 2015). This phenotype was associated with reduced immediate-early genes expression in the mPFC after FC training, which was interpreted as a deficit in mPFC recruitment in the processing of salient events (Liang et al., 2015). Interestingly, however, mPFC cNlgn2 KO mice displayed normal spatial memory assessed with the Y maze test (Liang et al., 2015). Another study implicated Nlgn2 in the context generalization aspect of fear learning. Particularly, improved context discrimination was measured after viral-mediated knockdown (KD) of Nlgn2 in the nucleus reuniens (NR) of the thalamus (Xu and Sudhof, 2013). While the activity of NR was shown by the authors to correlate with context discrimination, impaired inhibitory transmission assessed in this region after Nlgn2 KD likely mediated the

behavioral improvement by increasing its activation (Xu and Sudhof, 2013). Beyond aversive learning circuits, Nlgn2 in the mPFC showed positive regulation of attention assessed using the five-choice serial reaction time task (5-CSRTT) (Tzanoulinou et al., 2016). In this study, exposure to prepubertal stress correlated with reduced Nlgn2 expression in the mPFC and produced attention deficit in adult rats. Interestingly, this deficit was rescued by viral-mediated expression of Nlgn2 in the mPFC (Tzanoulinou et al., 2016). Furthermore, a more recent report demonstrated a deficit in Nlgn2 KO mice in a memory-based frequency discrimination task (Chen et al., 2019). In this task performed in the Audiobox setup, Nlgn2 KO mice exhibited reduced avoidance of a compartment where tones were presented in association with aversive air puffs. As Nlgn2 KO showed normal frequency discrimination, the authors interpreted this phenotype as impairment in valence encoding (Chen et al., 2019).

Taken together, these studies implicated Nlgn2 in cognitive functions, however, its role in cognition shows to involve predominantly learning tasks that involve aversive emotional valence. However, the mechanisms by which these behaviors are regulated by Nlgn2 were not explored.

1.4.8. Nlgn2 as a disease model

1.4.8.1. Nlgn2 mutations in psychiatric disorders

Being a key regulator of the E/I balance, mutations of Nlgn2 and its interaction partners were detected in many psychiatric disorders characterized by disruption in this balance (Ali et al., 2020). First reports came from patients with schizophrenia where six rare mutations in the Nlgn2 gene were detected (Sun et al., 2011). One of these mutations, namely the R215H point mutation, was shown in vitro to result in loss of function due to failure in protein maturation and glycosylation and subsequently deficient trafficking to the synaptic membrane (Sun et al., 2011). Consistently, another study reported several mutations in the non-coding regions of the *Nlgn2* gene detected in the genome of schizophrenia patients (Curtis, 2016; Curtis and Consortium, 2016). Another evidence linking Nlgn2 to schizophrenia in humans arose from a study showing reduced Nlgn2 protein levels and concomitant synaptic deficits in induced pluripotent stem cells (iPSCs) derived cortical interneurons obtained from patients with schizophrenia (Kathuria et al., 2019). Supporting a link of Nlgn2 with anxiety disorders in humans, a study reported the presence of *de novo* nonsense mutation in the site Y147 of the *Nlgn2* gene in a patient with a set of psychiatric conditions including anxiety, autism spectrum disorder, and obsessive-compulsive disorder (Parente et al., 2017). In addition, Nlgn2 levels were shown to be reduced in the nucleus

accumbens of patients with major depressive disorder (Heshmati et al., 2018). Although further work is required to validate the role of Nlgn2 in the etiology of such psychiatric conditions, these reports highlight the clinical relevance for understanding Nlgn2 function in health and disease.

1.4.8.2. The R215H variant-derived mouse model of schizophrenia

Among the different Nlgn2 mutations identified in human patients, the R215H variant detected in schizophrenia patients was characterized using a knock-in mouse model containing the same variant (Chen et al., 2017; Chen et al., 2020; Jiang et al., 2018). Interestingly, behavioral assessment of R215H knock-in mice revealed an impairment in auditory and contextual fear conditioning associated with reduction in inhibitory synaptic transmission in regions such as the hippocampal DG and the mPFC. While this indicates that impaired E/I balance in these regions might have contributed to this phenotype, the circuits and/or mechanisms underlying these deficits were not investigated in the R215H mouse model.

1.5. Aim of the study

Previous work demonstrated a role for the inhibitory synapse organizer Nlgn2 in the regulation of emotional brain functions. Particularly, Nlgn2 KO mice exhibited anxiety-like defensive behaviors associated with impaired processing of anxiety (Babaev et al., 2016; Blundell et al., 2009; Cruces-Solis et al., 2021; Wohr et al., 2013) and showed deficits in cognitive functions involving aversive emotional valence (Chen et al., 2019). To further understand how Nlgn2 regulates emotional processing, I sought in my doctoral work to address the following questions:

1) Does Nlgn2 regulate the formation of aversive memories in mice?

To answer this question, I characterized auditory and contextual fear conditioning (FC) in Nlgn2 KO versus WT mice and performed control behavioral assessments of sensory and motor functions.

2) Does Nlgn2 regulate the activation of brain regions involved in the processing of fear memory?

This question was addressed using cFos as a marker for neuronal activation. *cfos* is an immediate-early gene that is expressed in neurons 60-90 min after depolarization and is used widely to map the activation of brain circuits during behavior (Guzowski et al., 2005). Accordingly, to explore circuit activation during fear memory processing, Nlgn2 KO and WT mice that underwent FC testing were subjected to perfusion fixation and cFos immunohistochemistry 90 min after behavior. Consequently, cFos expression was

visualized and assessed in the brain regions involved in fear learning using confocal microscopy.

3) Which brain region mediate Nlgn2 effects on fear learning and do these regions also mediate Nlgn2 effects on anxiety-like behavior?

To explore a causal role between the FC impairment and the circuit alteration observed in Nlgn2 KO mice, local deletion of Nlgn2 was performed in the regions showing cFos dysregulation in Nlgn2 KO mice. This manipulation was followed by a behavioral assessment of auditory fear conditioning and anxiety-like behavior to elucidate region-specific regulation of these two circuits by Nlgn2.

4) Which neuron subtypes mediate Nlgn2 effects on fear learning and do these neurons also mediate Nlgn2 effects on anxiety-like behavior?

While previous findings demonstrated a role of Nlgn2 in synapses made onto excitatory neurons, the circuit underlying fear learning were shown to be regulated by both excitatory and inhibitory neurons. To pinpoint which neuron types are affected by Nlgn2 in the fear learning circuit, I implemented two approaches: a) inhibitory neuron-specific cFos assay in the amygdala after fear memory retrieval. b) Behavioral assessment of fear learning and anxiety-like behavior of cell-type specific conditional cNlgn2 KO mice lacking Nlgn2 in specific inhibitory neuron subtypes and in CAMKII neurons as a control.

5) How is the role of Nlgn2 in fear learning modulated by its interaction partner IgSF9b?

To investigate a potential interaction between IgSF9b and Nlgn2 in the regulation of fear learning, I characterized FC behavior in Nlgn2 KO, IgSF9b KO and Nlgn2-IgSF9b double KO mice. Since information about IgSF9b localization and function in vivo is still lacking, I performed immunohistochemical characterization of its expression in the mouse brain and conducted preliminary inspection of hippocampal LTP in adult IgSF9b versus WT mice.

6) Does Nlgn2 colocalize with its interaction partner MDGA1 in vivo?

As part of a study analyzing the interaction between Nlgn2 and MDGA1 in anxiety-like behavior in vivo, I analyzed the colocalization between these proteins in different layers of the hippocampal CA1using immunohistochemistry and confocal microscopy.

Taken together, my doctoral work provided novel insights into how Nlgn2 regulate emotional brain circuits and addressed open questions related to its region and synapse specificity and modulation by interaction partners.

2. Materials and methods

2.1. Animals

All experimental animals were maintained on a C57BL/6J background and only male mice between 8 and 14 weeks of age were used for experiments. Mice were kept on a 12h light/dark cycle (7:00 to 19:00 light period) with food and water *ad libitum*. All behavior experiments were conducted during the light cycle except for the recording of homecage activity. The experimenters were blind to genotype during data acquisition and analysis of all experiments unless stated otherwise. All experimental procedures were approved by the state of Niedersachsen and were conducted in agreement with animal welfare regulations issued by the Federal Government of Germany and the Max Planck Society under the following license numbers: 16/2366, 18/2957 and 20/3368.

Table 1 Mouse lines used in the experiments

Mouse line	Genetic background	Reference
Nlgn2 KO	C57BL/6J	(Varoqueaux et al., 2006)
IgSF9b KO	C57BL/6J	(Babaev et al., 2018a)
Nlgn2-IgSF9b double KO	C57BL/6J	(Babaev et al., 2018a)
Nlgn2-MDGA1-double KO	C57BL/6J	(Ishikawa et al., 2011)
Nlgn2-fl/fl	C57BL/6J	(Cruces-Solis et al., 2021)
CAMKII-Cre	C57BL/6J	(Minichiello et al., 1999)
PV-Cre	C57BL/6J	(Hippenmeyer et al., 2005)
VIP-IRES-Cre	C57BL/6J	(Taniguchi et al., 2011)
SOM-IRES-Cre	C57BL/6J	(Taniguchi *et al.*, 2011)
CaMKII-Cre: Nlgn2- fl/fl	C57BL/6J	This Study
PV-Cre: Nlgn2-fl/fl	C57BL/6J	This Study
VIP-IRES-Cre: Nlgn2-fl/fl	C57BL/6J	This Study
SOM-IRES-Cre: Nlgn2-fl/fl	C57BL/6J	This Study
ChR2-EYFP (Ai32)	C57BL/6J	(Madisen et al., 2012)
PV-Cre: ChR2-EYFP	C57BL/6J	This Study
VIP-IRES-Cre: ChR2-EYFP	C57BL/6J	This Study
SOM-IRES-Cre: ChR2-EYFP	C57BL/6J	This Study

Genotyping of mice was performed by the AGCT lab (Molecular Neurobiology department, Max-Planck Institute of Experimental Medicine) using genomic DNA from tail biopsies from three-week-old mice.

2.2. Behavioral experiments

2.2.1. Cued fear conditioning

2.2.1.1. Cued FC protocol intended for behavioral characterization

This protocol was conducted to assess fear conditioning behavior in the following experimental groups:

- Nlgn2 KO, IgSF9b KO, Nlgn2-IgSF9b double KO versus WT mice.
- cNlgn2 KO versus WT mice exposed to AAV-mediated local Nlgn2 deletion experiments.
- Cell-type specific cNlgn2 KO mice versus WT mice (PV-Cre:Nlgn2 fl/fl verus PV-Cre:Nlgn2 WT, VIP-IRES-Cre:Nlgn2 fl/fl versus VIP-IRES-Cre:Nlgn2 WT, SOM-IRES:Cre-Nlgn2 fl/fl versus SOM-IRES-Cre:Nlgn2 WT and CAMKII-Cre:Nlgn2 fl/fl versus CAMKII-Cre:Nlgn2 WT mice).

Cued FC training was conducted according to the protocol from Netrakanti et al (Netrakanti et al., 2015) with modifications, using the near infrared (NIR) video fear conditioning set up. Mice were placed individually in the training chamber (59.69 x 71.12 x 31.75 cm) and were left to explore the chamber for 2 min during which freezing levels were scored as a measure of anxiety in a novel environment and were denoted as ‘training baseline’ freezing. After 2 min, the conditioned stimulus (CS) comprising a tone (80 dB, 5 kHz, 30 sec) was played by an internal loudspeaker and it co-terminated with a mild foot-shock (2 sec, 0.5 mA) delivered through the stainless-steel grid floor and served as the unconditioned stimulus (US). After 60 sec, a second CS-US pairing was introduced, then the mouse was placed back in its homecage 30 sec after the last shock presentation (to minimize agitation during handling). Fear memory retrieval was assessed for each mouse twenty-four hours (or two hours) after FC training. Accordingly, each mouse was picked up from its homecage and placed in the testing chamber (59.69 x 71.12 x 31.75 cm) and exposed to same protocol used on the training day with the exclusion of the foot-shock presentation. Freezing levels during the first 2 min of the testing protocol was measured to assess context generalization between the training and testing contexts and was denoted as ‘testing baseline’ freezing. Conditioned freezing was assessed during the presentation of the first CS and was denoted as ‘CS freezing’. Mouse behavior during training and testing was recorded using a video camera

at sampling rate of 15 frames per second and the freezing duration was automatically registered using the Video Fear software. Using a motion threshold of 60 arbitrary units (AUs), a freezing bout was defined as 7 frames of absence of movement excluding respiratory movements. Experimenters were blind to genotype during all experiments and mice from different genotypes/conditions were organized in counterbalanced experimental sets. When performing behavioral analysis on several mice belonging to the same homecage, mice that were trained/tested first were not placed back directly into the homecage. Instead, they were placed in a fresh cage until the remaining cagemates were trained/tested. This is also to avoid stressful reactivity from the tested mice that might influence the behavior of their cagemates to be tested.

To reduce context generalization between training and testing days the following measures were taken:

- Mice were handled by the experimenters using white latex gloves on the training day and blue nitrile gloves on the testing day.
- Whenever possible, training and testing were done by a different experimenter (testing was done by Prof. Dr. Dilja Krüger-Burg).
- The training chamber was lit with bright and NIR lights and cleaned with distilled water, while the testing chamber was lit with only NIR light and cleaned with 70 % ethanol. Additionally, the metal grid in the testing chamber, used to deliver the shock, was replaced with plastic flooring and the walls were covered with sheet protectors and decorated with different patterns.
- On the training day, mice were placed in a quiet area for 15 min before they were picked up for training using a fresh cage as a transfer box. On the testing day, mice were picked directly from the mouse hotel using an opaque transfer box cleaned with 70 % ethanol.

2.2.1.2. Cued FC protocol intended for cFos assay

In this experiment cued fear conditioning was conducted to compare cFos protein levels, as a marker for neural activation, between Nlgn2 KO and WT mice during fear retrieval. For this purpose, four experimental groups were used, including two groups of Nlgn2 KO and WT mice that received paired training (Nlgn2 KO- FC and WT-FC) and two groups of Nlgn2 KO and WT mice that received training with only tone presentation (Nlgn2 KO-Ctrl and WT-Ctrl, the same protocol was used for the FC group, but footshock presentation was omitted). The “Ctrl” groups were added to control for the neural activation resulting from receiving the CS and distinguish it from activation related to CS memory retrieval across the two

genotypes. Training and testing parameters inside the respective chambers were applied according to section (2.2.1.1), but specific additional measures were used during mouse handling as follows:

- Mice were organized in counterbalanced experimental sets, each containing one mouse from each of the groups (WT-FC, Nlgn2 KO- FC, WT-Ctrl and Nlgn2 KO-Ctrl) that were subjected to behavioral analysis within the same time window (in randomized order) and were later processed together for cFos IHC.
- Before the beginning of training, mice were single-housed and kept in a quiet area for two hours, at least, before the beginning of training. The single housing was necessary to maintain minimal baseline cFos levels by avoiding stimulation due to interaction with cagemates. Although this is only relevant on the testing day, but it was applied starting from the training day to avoid introducing new additional stress during testing. The habituation time applied after single housing and before training was to allow the mouse to accommodate to the new housing conditions before the training started.
- A time interval of 30 min was used between mice during training (and testing) with matching the training and testing times for each mouse to be exactly 24 hours apart. The 30 min interval was used to allow time for performing perfusion fixation on consecutively tested mice.
- After training, mice were placed back into the habituation area until all mice were trained, to minimize interfering with memory consolidation after training that may result from repetitive opening of the mouse hotel. Two hours after the last mouse was trained, all mice were returned to the mouse hotel to reduce differences in the conditions for memory consolidation between mice tested at early and late time points.
- After testing, each mouse was transferred back immediately to the mouse hotel and kept for 90 min before it was anesthetized using avertin (250 mg/kg) then subjected to perfusion fixation for cFos (IHC).

2.2.2. Contextual fear conditioning

Contextual FC was assessed to compare between Nlgn2 KO, IgSF9b KO, Nlgn2-IgSF9b double KO and their littermate WT mice. Mice were arranged in counterbalanced, randomized sets of four mice. The training was conducted by placing the mouse in the training context and recording 2 min of baseline behavior. Afterwards, a foot-shock (0.5 mA, 2 sec) was introduced. After 60 sec of intertrial interval, another foot-shock was introduced and 30 sec later the mouse was placed back in its homecage. After twenty-four hours,

individual mice were tested by being placed in the same training context again for 2 min and the duration of freezing behavior was recorded during this period by the Video Fear software using the same acquisition parameters as in the cued fear conditioning. Contextual FC chamber was cleaned with distilled water on both training and testing days and both of NIR and bright lights were used during training and testing sessions.

2.2.3. Homecage activity

Homecage activity for Nlgn2 KO, IgSF9b KO, double KO and their littermate WT mice was assessed using the LABORAS system. Mice were single housed and habituated in in the experimental room overnight for two consecutive days (16-17 h per day) to mimic the LABOAS setting, then they were placed back into their homecages during the day. On the third day, individual mice were placed in the LABORAS housing cages (22 × 16 × 14 cm) using their bedding from the habituation cages. Homecage activity was recorded for 16 hours (from 17:00 to 9:00 o'clock). Different behaviors were extracted using the LABORAS software including locomotor activity duration, locomotor velocity, immobility duration, total distance travelled and the duration of behaviors such as eating, climbing, rearing and circling.

2.2.4. Acoustic startle response (hearing assessment)

To assess hearing ability in Nlgn2 KO, IgSF9b KO, double KO in comparison to their littermate WT mice, the acoustic startle response (ASR) test was applied using the TSE system. In this test the startle response of the mouse in response to a sudden sound stimulus was measured. The experiment protocol was adapted from Dere and colleagues (Dere et al., 2014) and was conducted as follows: mice were placed individually in a sound attenuated chamber inside an animal holder (82 × 40 × 40 mm) equipped with a force sensitive platform which is attached to a sensor that detects its vertical movement. Inside the chamber, acoustic stimuli were played by a loudspeaker suspended above the animal holder. The session started with a habituation period of 2min in which a white noise stimulus of 65dB was played and continued as a background throughout the session. A baseline recording of 1min in the presence of the background noise followed the habituation period. Afterwards, sound stimuli with different intensities (65-120 dB, 40 ms) were applied in a pseudorandom order with an inter-stimulus interval of 8-22 sec, so that 10 stimuli for every sound intensity were presented during the session. The startle amplitude in response to a given stimulus intensity was recorded and calculated by the software provided with the system. The startle amplitude was defined as the difference between the maximum force detected during the recording window (100 ms after stimulus onset) and the force measured

prior to the onset of the stimulus. Startle amplitudes measured by arbitrary units for every intensity were averaged across the session for every animal and a hearing threshold was calculated as the sound intensity that elicits a startle amplitude that is two times above baseline amplitude. The baseline amplitude was calculated as the average startle amplitude elicited in in response to stimuli between 56 and 77 dB).

2.2.5. The visual placing test

To test for lack of vision in Nlgn2 KO, IgSF9b KO, double KO mice and their littermate WT mice, the visual placing test was applied as described by Pinto and colleagues (Pinto and Enroth-Cugell, 2000) and the SHIRPA protocol for phenotype assessment (Rogers et al., 1997). The mouse was lifted by the base of the tail to 15 cm above a mesh grid and lowered slowly towards the grid. The behavior of extending the forelimbs to reach out to the grid was observed and scored as 1 when it was observed at approximately 5 cm or higher from the grid. Alternatively, a score of 0 was given when the paw extension was not observed at all or only observed within 5 cm of height from the grid. Since in the latter case, the mouse could use the whiskers to sense the grid. The test was conducted in 3 trials per mouse and the scores were averaged across trials.

2.2.6. The open field test (OFT)

Assessment of anxiety-like behavior using the open field test was performed on the following experimental groups:

- Nlgn2 fl/fl versus WT mice exposed to AAV-mediated local Nlgn2 deletion experiments.
- Cell- type specific cNlgn2 KO mice versus WT mice (PV-Cre:Nlgn2 fl/fl versus PV-Cre:Nlgn2 WT, VIP-IRES-Cre:Nlgn2 fl/fl versus VIP-IRES-Cre:Nlgn2 WT, SOM-IRES-Cre:Nlgn2 fl/fl versus SOM-IRES-Cre:Nlgn2 WT and CAMKII-Cre:Nlgn2 fl/fl versus CAMKII-Cre:Nlgn2 WT mice).

The open field test was performed according to the protocol described previously by our group (Babaev et al., 2016). As the open field, a square chamber made of white plastic with 50 × 50 × 50 cm dimensions was used. The open field was illuminated during the recording with indirect white light of 40 lux intensity and cleaned with 70% ethanol and double distilled water after the testing of each mouse. Each mouse was taking from its homecage and placed in the corner of the open field (OF) and recorded while exploring it for 10 min using a video camera. Different parameters such as time, distance, speed and number of entries during the exploration of the open field were extracted from the recording using the Viewer3

software. Each of the above-mentioned parameters was registered automatically with the software for every area of interest. Areas of interest were predefined within the total area of the open field as follows: OFT periphery: 50 ×50 cm, OFT intermediate zone: 27.5 × 27.5 cm and OFT center: 25 × 25 cm. After 10 min open field exploration, the mouse was placed in a separate cage until its cage mates were tested, then it was placed back in the homecage.

2.3. cFos assay

To assess neural activation during cued FC retrieval, mice were anesthetized 90 min after retrieval testing and subjected to perfusion fixation. Next, the brains were dissected and processed according to the steps described in section 2.4. Mice were arranged in sets of 4 mice including one of each of the groups (Nlgn2 KO-Ctrl, Nlgn2-KO-FC, WT-Ctrl and WT-FC mice). Brain samples from mice belonging to the same experimental set were processed simultaneously for IHC, image acquisition and image analysis. cFos labelled nuclei were quantified within different brain regions irrespective of cell-type to assess general neural activation (general cFos analysis). Also, cFos expression by specific inhibitory neuron subtypes was performed by colocalizing cFos labelled nuclei with different inhibitory neuron markers (inhibitory neuron-specific cFos analysis). Details of the IHC, image acquisition and image analysis for cFos analysis are described in sections 2.4.1, 2.5.1 and 2.6.1.

2.4. Immunohistochemistry

2.4.1. IHC for the labeling of cellular markers

2.4.1.1. PFA perfusion fixation and free-floating sections

This method used for immunolabelling of cellular proteins for the following experiments:

- cFos assay on slices obtained from Nlgn2 KO-Ctrl, Nlgn2-KO-FC, WT-Ctrl and WT-FC mice
- GFP immunolabelling for validation of viral placement after local Nlgn2 deletion experiments.

Mice were anesthetized with avertin (250 mg/kg, see solutions) delivered by intraperitoneal injection **(**i.p.). When fully anesthetized, mice were subjected to transcardial perfusion with 0.9% sodium chloride solution for one minute followed by perfusion of 4% paraformaldehyde (PFA) fixative solution for 8min. After perfusion, brains were collected and stored in the PFA fixative solution at 4 °C for 24 h. On the following day, brains were

cryoprotected by replacing the fixative solution with 30% sucrose solution and stored at 4 °C for 24- 48 h. For immunostaining, coronal brain slices were cut at 40 µm thickness using the cryostat. Slices were obtained from Bregma levels between -0.82 and -1.94 and collected into the wells of 24-well plates (free floating sections) containing phosphate buffered saline (PBS). Sections were washed 3 times for 10 min in PBS on a shaker then incubated with the blocking buffer for one and a half hours at room temperature (RT). After blocking, sections were incubated with primary antibodies solutions in blocking buffer at 4° C, overnight. Afterwards, slices were washed 3 times in PBS and incubated with secondary antibodies raised in goat, against the corresponding primary antibody species for 2 h at RT. Following three times washing in PBS, slices were stained with 4′,6-diamidino-2-phenylindole (DAPI) to label cell nuclei and washed 3 more times before they were mounted on glass microscope slides. Slides were stored overnight at 4 °C to dry. One the next day, slides were coverslipped using mounting medium (aqua polymount) and stored at 4 °C for one day at least before they were used for imaging.

2.4.2. IHC for the labeling of synaptic markers

2.4.2.1. Methanol fixation of fresh frozen brain sections

This method was applied for immunolabelling of synaptic proteins for the following experiments:

- Qualitative assessment of Nlgn2 localization at inhibitory neuron synapses using mice with the following genotypes: PV-Cre:ChR2-EYEP, SOM-IRES-Cre:ChR2-EYEFP and VIP-IRES-Cre:ChR2-EYEFP.
- Validation of Nlgn2 local deletion after AAV-Cre injections
- Quantification of IgSF9b in the mouse brain using IgSF9b KO mice and their littermate WT mice.
- Analysis of Nlgn2 and MDGA1 colocalization in the hippocampus using Nlgn2-MDGA1 double KO mouse versus littermate WT.

Mice were anesthetized using isoflurane and their brains were rapidly dissected and immersed in isopentane at -35 to -38 °C for approximately 30 sec. Brains were stored in the cryostat for 30 min at -18 °C to get acclimated to the cryostat temperature. Coronal (or sagittal) brain sections were prepared at 18 µm thickness and mounted on glass slides so that sections with matching anatomical locations from each WT and KO mice were mounted on the same slide to unify the labeling conditions between compared genotypes. The brain

sections were dried at RT for 30 min and then fixed by immersion in methanol pre-cooled to -20 °C for 5 min, followed by three washing steps with phosphate buffered saline (PBS) for 10 min each. Sections were incubated for one hour in blocking buffer at RT. Afterwards, they were incubated over night with primary antibody solution in blocking buffer at 4 °C. On the next day, sections were washed three times with PBS and were incubated for 2 h with the secondary antibody solution in blocking buffer at RT (goat anti rabbit Alexa Fluor 555, 1:600) followed by 3 washing steps with PBS. Next, nuclei were labeled using DAPI (0.1 µg/ml) in PBS for 10 min at RT to help anatomically identifying the relevant brain regions, followed by 3 additional washing steps after which the sections were stored overnight at 4 °C to dry. On the next day, the sections were coverslipped using aqua poly mount mounting medium and imaged within two weeks after immunostaining.

One variation from the normal protocol was applied when processing samples prepared for STED imaging to determine Nlgn2 colocalization in inhibitory neuron synapses. In this experiment, brain slices were mounted on the coverslip during IHC processing instead of being mounting on the microscopic slide. Before imaging, the coverslip carrying the brain slices was mounted on the microscopic slide using the same mounting medium mentioned above. This was done to avoid excess mounting medium accumulating between the slice and the coverslip which would reduce the resolution due to differences in the refractive indices between the objective and the mounting medium.

A summary of IHC experiments including primary/secondary antibody combinations is described in table (2). Information about antibodies (species, dilution and purchase information are available in table (6).

Table 2 Summary of IHC methods

Experiment	IHC method	Brain areas	Primary AB	Species	Secondary AB
cFos assay	PFA perfusion fixation and free-floating sections	Amygdala	cFos	Guinea pig	Goat anti guinea pig AF-633
		mPFC	SOM	Mouse	Goat anti mouse-AF-555
		vlPAG	PV	Rabbit	Goat anti rabbit - AF-488
		AuC	VIP	Rabbit	Goat anti rabbit - AF-488
			PKCδ	Mouse	GAM- AF-555
Validation of virus placement		LA	GFP	Rabbit	Goat anti rabbit - AF-488

Nlgn2 localization in inhibitory neuron synapses	Fresh frozen sections with methanol fixation	LA AuC	Nlgn2	Guinea pig	Goat anti guinea pig -AF- 594
			vGAT	Rabbit	Goat anti rabbit - STAR-635p
			GFP	Chicken	Goat anti Chicken AF488
Validation of AAV-mediated Nlgn2 deletion		BLA	GFP	Rabbit	Goat anti rabbit - AF-488
			Nlgn2	Guinea pig	Goat anti guinea pig AF-555
IgSF9b quantification		Various	IgSF9b	Rabbit	Goat anti rabbit- AF-555
MDGA1-Nlgn2 colocalization		CA1	MDGA1	Rabbit	Goat anti rabbit- AF-488
			Nlgn2	Guinea pig	Goat anti guinea pig AF-555

2.5. Image acquisition

2.5.1. Image acquisition for cFos assay

For general and cell type-specific cFos analysis, brain slices were obtained from Nlgn2 KO-Ctrl, Nlgn2-KO-FC, WT-Ctrl and WT-FC mice and processed for IHC using the protocol described in section 2.4.1. Images were acquired using the 20X oil immersion objective (numerical aperture 0.75) the Leica TCS-SP8 laser scanning microscope. Tiled images with spatial resolution of 512× 512 pixel covering the amygdaloid complex were acquired and stitched using the navigator function of the LAS X software associated with the SP8 system. Acquisition parameters such as laser power, offset and gain of the detectors (when using photomultiplier tubes as detectors) were kept constant across brain samples belonging to one behavioral set. In addition, samples from the same set were imaged in one microscopy session to allow for comparison. For quantification of general cFos, 8 amygdala slices per animal were obtained and analyzed. For inhibitory neuron- specific cFos quantification, four slices per animal were obtained.

2.5.2. Image acquisition for Nlgn2 localization in inhibitory neuron synapses

2.5.2.1. Stimulated Emission Depletion (STED) microscopy

Brain slices obtained from VIP-IRES-Cre:ChR2-EYFP, PV-Cre:ChR2-EYFP and SOM-IRES-Cre:ChR2-EYFP mice were processed for IHC according to the protocol described in

section 2.4.2. Brain samples from Nlgn2 KO mice were obtained as negative control for Nlgn2 labelling and were mounted on the same coverslips as brain slices obtained from the above-mentioned mice.

Image acquisition was performed using custom-built STED microscope developed in the lab of Dr. Katrin Willig for 2-color STED imaging and was assisted by the Impspector software obtained from Abberior Instruments. 1.5 µm thick image stacks were acquired using a 63x oil immersion objective of 1.4 numerical aperture at 500 µm step size and 20 nm pixel spacing. Fluorophores labeling Nlgn2 (AF-594) and vGAT (STAR 635p) puncta were excited using orange (586 nm, 16.6 µW) and red lasers (630 nm,12.3 µW), respectively and were subjected to depletion using a STED laser beam (775 nm, 178 mW). ChR2-EYFP fluorescence was excited with blue laser (480 nm, 8µW) and imaged with the confocal mode of the microscope. Laser power was kept constant during all imaging experiments and WT/KO pairs were imaged in the same session. 10 image stacks per region were collected from 2 different brain slices obtained from each mouse.

2.5.3. Image acquisition for validation of virus placement

Brain slices obtained from Nlgn2 fl/fl and WT mice injected with AAV-Cre-GFP virus in the LA were processed for IHC according to the protocol described in section 2.4.2. Tiled images covering the whole brain slice were acquired using the 10x objective of the Leica TCS-SP8 laser scanning microscope at spatial resolution of 256 × 256 pixel from brain slices spanning the region of interest. Mice with misplaced, unilateral, or insufficient GFP expression (based on an empirically determined fluorescence intensity value) were excluded from the analysis.

2.5.4. Image acquisition for validation of Nlgn2 local deletion

Brain slices obtained from Nlgn2 fl/fl mice injected with AAV-Cre-GFP or AAV-GFP viruses were processed for IHC as described in section 2.4.1. Images were collected using the 63X objectives of the Leica SP8 laser scanning microscope at spatial resolution of 512× 512pixel. Nlgn2 expression at the site of injection where GFP expression was observed, was quantified using Fiji's 'analyze particles' function after binarization of images using a threshold of $3 \times$ background intensity.

2.5.5. Image acquisition for IgSF9b quantification

Overview images of brain sections were acquired using the stitching mode of the Zeiss axio imager2 fluorescent microscope with the 10x objective. For quantifying IgSF9b puncta,

images were acquired using the 63x objective of the Leica SP2 confocal microscope. Gain and offset conditions were kept constant during the imaging of all brain regions for each IgSF9b WT/KO mouse pair. Three Z-stacks comprising three optical sections at 1 µm step size were obtained from 20 brain regions in WT and IgSf9b KO mice.

2.5.6. Image acquisition for MDGA1-Nlgn2 colocalization

Image acquisition for analysis of Nlgn2 and MDGA1 colocalization was conducted using the Leica TCS- SP8 laser scanning confocal microscope (Leica microsystems, Germany) equipped with white light laser (WLL) and hybrid detectors (HyD). 63X oil immersion objective with a numerical aperture of 1.4 was used to obtain single plane micrographs at 1024×1024 spatial resolution and pixel spacing of xy= 45.09 nm. Laser power was optimized to ensure that the detected fluorescence intensity is within the dynamic range of detection. All imaging parameters were kept constant for images acquired from WT and KO mouse brain sections and also for images acquired from different HPC layers. Images were then subjected to deconvolution using the Lightning function of the Leica LAS X software (global mode).

Tiled overview images of the hippocampus were acquired using the 20x oil immersion objective of the Leica SP8 (numerical aperture 0.75) where the navigator function of the LAS-X software was used to acquire and stitch the tiles. Tiled overview images of the CA1 were acquired using the 63x objective.

2.6. Image analysis

2.6.1. Image analysis for cFos assay

Images were pre-processed and binarized using macros written in Image J macro language. To determine a threshold intensity value for binarization, two regions of interest (ROIs) from the background were manually selected from each image using the freehand tool and the mean gray value was measured for each of them. A background value per image was calculated as follows:

$$\text{Background intenity} = \frac{\text{Mean gray value (ROI1)} + \text{Mean gray value (ROI2)}}{2}$$

A threshold value above background intensity was selected empirically for every labelling depending on the signal to noise ratio as follows:

Threshold value for cFos and PV staining = 3 × background

Threshold value for SOM staining = 2.5 × background

Threshold value for VIP staining = 2 × background

Threshold value for PKCδ staining = 1.5 × background

After binarizing the images, the 'noise despeckle' function was used to reduce background noise. Binary images were saved into 'tiff' format and loaded into IMARIS software where cFos nuclei and cells positive to each of PV, SOM, VIP and PKCδ were counted using the 'spots' algorithm. Colocalization between cFos and the cellular markers was determined using the 'colocalize spots' function in IMARIS. For quantification of general cFos, the average number of total cFos positive nuclei was calculated per region for each mouse within an experimental set. A set comprised four animals: Nlgn2 KO-Ctrl, Nlgn2-KO-FC, WT-Ctrl and WT-FC which underwent FC consecutively in the same time slot and were processed in one session for IHC and also imaged within one session. Afterwards, each average value of cFos positive nuclei per mouse was normalized to the average number of cFos positive nuclei obtained across the 4 different mice within the set to reduce variation between experimental sets. The resulting normalized count of cFos-positive nuclei for every animal within the set was calculated as a percentage of the WT-Ctrl cFos count. For inhibitory neuron-specific cFos expression analysis, number of cFos- labeled nuclei colocalized with each interneuron subtype (PV, SOM, VIP or PKCδ) per region was calculated as a percentage of the total number of the respective labelled interneuron in that region. For example, percentage of VIP -cFos co-labelled cells was calculated from total VIP positive cells detected within LA borders. Similar to general cFos analysis, the resulting percentage values from each animal per experimental set were then normalized to the average percentage across different mice in that set. Subsequently, the final inhibitory neuron/cFos percentage value for each mouse was calculated as a percentage of the WT-Ctrl mouse.

2.6.2. Image analysis for Nlgn2 localization in inhibitory neuron synapses

Images were subjected to minimal processing to enhance brightness and contrast for the each of Nlgn2, vGAT and ChR2-EYFP labeling using the Fiji software. To standardize Nlgn2 brightness enhancement, the same enhancement was applied to images obtained from WT and KO mice (mounted on the same slide). Due to high background in some Nlgn2 labelled samples obtained from Nlgn2 KO mice, only images were Nlgn2 fluorescence was 10 times brighter in the WT slice compared to the corresponding KO slice were selected for qualitative analysis. Selected images were visually inspected to find synapses containing

Nlgn2 and vGAT labelled structures that share colocalization with the ChR-EYFP labelled processes. Synapses where the overlap between the 3 fluorophores was 100% were excluded, as in this case, the relative positions between them in the synapse could not be determined. In selected example synapses, a line profile analysis for each fluorophore using the Fiji (plot profile) function was conducted using multi-channel images saved as z-stacks. This was done to confirm that the synapse configuration was determined correctly based on the relative position of vGAT, Nlgn2 and YFP labelled structures.

2.6.3. Image analysis for IgSF9b puncta quantification

Images were binarized manually using the same threshold value for all images acquired from the same IgSF9b WT/KO pair. The resulting binary images were then processed by the 'noise despeckle' algorithm followed by watershed correction to improve puncta segmentation. Each binary image was then used as a mask to quantify IgSF9b puncta number, size and fluorescence intensity in the original image using the 'analyze particles' algorithm. The number of puncta per region counted in the images obtained from the KO mouse was subtracted from the number of puncta counted in this region in the WT mouse of the same set. The minimum threshold value for binarizing images from the WT and KO mice of one set was defined as 5 times the mean average intensity measured from all KO images of this set.

2.6.4. Image analysis for MDGA1-Nlgn2 colocalization

Composite two-channel images of Nlgn2 and MDGA1 labelling acquired from different hippocampus layers were splitted and further processed using the Fiji software. Images of Nlgn2 channel were binarized and subjected to noise despeckle and watershed segmentation in Fiji to retain clearly defined Nlgn2 puncta. The threshold value used for binarization of Nlgn2 images was calculated as follows: Threshold = 20 $\times$ average intensity of images acquired from the KO sample mounted on the same slide as the WT sample used in the analysis. Binary images were then subjected to segmentation using the 'analyze particles' algorithm of FIJI using a size filter of 0.3-1.5 µm and were added to the ROI manager where the average intensity for every Nlgn2 punctum was measured inside the MDGA1 channel by using the 'Measure' command while redirecting the measurement settings to the MDGA1 image. Frequency distribution histograms of the MDGA1 intensity inside Nlgn2 puncta across all images acquired (8 images per layer) were then plotted using Graphpad Prism. Total area imaged per layer was17060.74 μm^2.

Representative images included in figures were processed by being subjected to contrast enhancement and smoothing (1 time). The same minimum and maximum brightness range

for every channel was used for all images taken from WT and KO samples and for all images across hippocampus layers to allow for comparison.

2.7. Production of Adeno-associated viral (AAV) particles

AAV viruses were prepared by Sally Wenger (Molecular Neurobiology department, Max-Planck Institute of Experimental Medicine) according to the protocol described by Cruces-Solis and colleagues (Cruces-Solis et al., 2021). For production of AAV, a plasmid encoding the viral DNA construct (AAV-Cre-EGFP) and a packaging plasmid encoding the virus capsid (serotype AAV5, pDP5rs) were used. Both plasmids were introduced into HEK293T cells using the calcium chloride transfection method and the viral particles were then isolated from the cells after 3 days using enzymatic cell lysis. Virus solution in PBS was then purified using iodixanol gradient.

2.8. Qualitative Polymerase Chain Reaction (qPCR) titration of AAV particles

To measure the concentration of AAV virus particles in the purified solution, qPCR assay was performed using primers based on the virus inverted terminal repeat region (ITR, (Aurnhammer et al., 2012) that were made by the AGCT lab (Molecular Biology department, Max Planck Institute for Experimental Medicine). Virus DNA plasmid (concentration =3.3 µg/µl, size = 8002bp) was diluted to give a solution with a concentration that equals 2×10^9 molecule/µl. A serial dilution was then prepared from this solution used to set the standard curve for the assay. Viral samples were incubated with DNaseI (0.21 Unit/µl) for 30 min at RT to digest DNA remaining from virus production then the DNAse was heat inactivated by incubating the samples for 10 min at 75 °C before they were also serially diluted. 6 µl of every viral sample or plasmid dilution were pipetted in triplicates into the wells of a 384-well qPCR plate (light cycler 480, 384 well plates, Roche) as a part of the following reaction mix: Syber green (7.5 µl), forward ITR primer (10 pmol/µl, 0.75 µl), reverse ITR primer (10 pmol/µl, 0.75 µl) on ice. A reaction mix containing double distilled water instead of virus or DNA sample was used as a negative control for the qPCR and a reaction mix containing plasmid DNA treated with DNAse was used as negative control to confirm the efficacy of DNase treatment. The qPCR plate was then sealed with the sealing foil and centrifuged for 2 min at 1500g to remove air bubbles and then placed into the plate holder of the real-time PCR system where it was subjected to incubation program described in table (3). Data were analyzed using the light cycler 480 software where the resulting cross point (C_P) values measured by the system for each of the diluted virus samples, plasmid DNA samples

Table 3 qPCR program for AAV titration

Process	Temperature	Duration
Pre-incubation (1X)	50°	2 min
	95°	3min
Amplification (45X)	95°	15sec
	60° → acquisition (single)	30sec
Cooling (1X)	40°	30sec

and negative controls were used to calculate the titer based on the known concentration of plasmid DNA samples. The titer of the original virus sample was then back calculated from each dilution and an average of the concentration calculated from different dilutions was used as a final titer of the virus. The final titer for of AAV5-Cre-GFP batches used for local deletion of Nlgn2 measured between 1.04 and 3.77×10^{11} viral particles/ml.

2.9. Stereotaxic surgery for virus delivery

Stereotactic surgeries were performed according to the protocol described by Cruces-Solis et al (Cruces-Solis et al., 2021). Prior to the start of the surgery, glass capillaries were pulled to have a tip opening of approximately 20 µm and filled with paraffin oil. Afterwards, the pipette was attached to the microinjector and front-filled with AAV1/2-Cre-GFP virus solution. Nlgn2 fl/fl or their littermate WT male mice of 6-7 weeks old were weighted and placed in the gas anesthesia induction chamber. 4% isoflurane in O_2 (1 L/min) was then delivered to the chamber through a tubing connected to the gas anesthesia system. After loss of movement and reduced breathing rate, the mouse was placed on heating pad mounted on the stereotaxic frame and set to 37 °C. Isoflurane was delivered at 1.5-2% in O_2 through a mask covering the mouse's snout and the depth of anesthesia was monitored by observing the breathing rate and maintained by adjusting the percentage of isoflurane. Next, carprofen was injected intraperitoneally (i.p.) to reduce post-surgery pain symptoms (5 mg/kg**)** and eye ointment was applied on the eyes to prevent dehydration (Bepanthen)**.** After ensuring deep anesthesia, the mouse head was mounted into the stereotaxic frame so that the teeth are tethered into the mouthpiece. The head was then stabilized in this initial position by gently tightening the snout clamp. Fixation of the mouse head was then started by sliding the ear bars into the ear canals and fixing them in a symmetrical position against the skull. An incision of approximately 1 cm was made in the skin covering the skull surface and 150 µl of local anesthetic (Lidocaine) was applied on the incision location for 1 min then removed using pre-autoclaved cotton swabs before proceeding with the injection. After identifying bregma and lambda on the mouse skull using an attached microscope camera,

the heights of the ear bars and the mouthpiece were adjusted to achieve horizontal head position in both mediolateral (ML) and anteroposterior (AP) planes. This was confirmed by obtaining an equal depth of the skull surface at two symmetrical points that are 2 mm lateral to bregma (for the mediolateral plane) and obtaining an equal depth of the skull surface at both of bregma and lambda (for the anteroposterior plane). Afterwards, 2 holes of maximum 1mm diameter were made in the skull surface at the injection coordinates (calculated in relation to bregma) using a microdrill mounted on the stereotaxic frame. After the holes were made, the pipette (attached to the microinjector) was brought to a position matching the injection ML and AP coordinates. The pipette was then lowered manually into the hole at a speed of 1 mm/min until the injection dorsoventral (DV) coordinate was reached (calculated from the skull surface in the periphery of the hole). Then, the virus injection was initiated using a micropump controlling the injector (at a rate of 100 MKN (approximately 0.5 mm/sec). After the injection was completed, the pipette was left in place for 5 min to prevent virus backflow before it was lifted. The pipette was initially lifted by 0.1mm and left again in place for 3 additional minutes to allow for restricted virus spread in the injection site before being completely withdrawn from the brain at a speed of 1 mm/min. After completion of the injections bilaterally, the skin was sutured using surgical sutures and 300 µl of saline was injected i.p. for hydration. The mouse was then removed from the stereotaxic frame and returned to the homecage that was placed partially on a heating pad where a pain killer (metamizol) was mixed in the drinking water at a concentration of 1.6 mg/ml, for three days post-surgery. The recovery of the mouse was monitored daily for 7 days after the surgery and then after 2 weeks post- surgery. For monitoring mice health, a detailed scoring was given based on the mouse's weight, wound condition, activity, posture, and fur condition. Mice not showing full recovery (based on the previous scores) until 48 hours post-surgery were sacrificed. Six weeks after surgery, mice were used for behavioral analysis after being allowed to habituate to the testing facility for 1-2 weeks.

For the lateral amygdala injections, 150 nl or 300 nl of AAV-Cre-GFP virus were injected bilaterally using the following coordinates: ML: -/+3.55 mm, AP: -1 mm, and DV: -3.65 mm which were optimized based on the coordinates obtained from the mouse brain atlas (Paxinos and Franklin, 1997).

For auditory cortex injections, 800 nl of AAV-Cre-GFP virus were injected bilaterally using the following coordinates: ML: -/+4.5 mm, AP: -2.46 mm, and DV: -0.9 mm (Letzkus et al., 2011).

2.10. Field recordings in acute hippocampal slices

Eight to -twelve-old WT and IgSF9b KO mice were anesthetized with 4% isoflurane, decapitated and brains were rapidly dissected and placed in ice-cold sucrose-based slicing solution (1X) infused with carbogen (95% O2 and 5% CO2 to maintain pH at 7.4). Next, the dorsal hippocampi were isolated from the brain by microdissection in the same slicing solution. Hippocampal slices were prepared using a tissue chopper at 300 µm thickness and allowed to recover in carbogenated artificial cerebrospinal fluid (ACSF,) solution (1X) for 25-30 min at 31-34 °C. Afterwards, slices were transferred to the recording chamber and were continuously superfused with carbogenated ACSF at 27-29 ° C. Electrical stimulation was performed with an isolated stimulator and delivered through a stainless-steel bipolar electrode to the Schäffer collaterals in the CA3 region. Recording pipettes were pulled from borosilicate glass capillaries with a tip resistance of approximately 1-3 MΩ and filled with ACSF. Recording micropipette was placed in the stratum radiatum in the CA1. Field excitatory post synaptic potentials fEPSPs were recorded in current clamp mode of the commander software associated with the multiamp amplifier digitized using the 1440A Digidata system and displayed using the Clampex software. First, input/output curves were generated by introducing single-pulse stimuli with increasing intensity between 0 and 150 µA with a step size of 2 µA and at 30 sec intervals. The stimulus intensity that evoked a fEPSP of an amplitude equal to 50% of the maximum obtained fEPSP amplitude was used for the subsequent baseline and long-term potentiation (LTP) recordings. After obtaining 20min of stable baseline fEPSPs recording, one train of high frequency stimulation at 100 Hz was introduced at same intensity used for baseline recording. Next, evoked fEPSPs were recorded in response to single pulse stimulation at 30 sec intervals for 1 h after train stimulation. Increase in amplitude, calculated as the percentage of baseline amplitude, was plotted along the recording duration from WT and IgSf9b KO mice. fEPSP traces were processed and analyzed using the Axograph software and plotted using Graphpad Prism.

2.11. Statistical analysis

Data were collected, organized, and stored using Microsoft Excel. Data plotting and statistical analyses were performed using Graphpad Prism 9. All data were first tested for normal distribution using Shapiro-Wilk test. Normally distributed datasets were subjected to Rout's outlier analysis and analyzed using two-tailed t-test (when 2 datasets were compared) or two-way analysis of variance (ANOVA) followed by Tukey's post-hoc analysis (when 4 datasets with 2 variables were compared). Data that were non-normally distributed were subjected to 1.5 interquartile range method (1.5 IQR) of outlier analysis and then

analyzed using Mann-Whitney test (when 2 datasets were compared) or with two-way ANOVA followed by Tukey's post-hoc analysis (when 4 datasets with 2 variables were compared). The threshold for statistical significance was set at $p < 0.05$. Data represented in bar graphs show the mean ± standard error of the mean (SEM) in addition to individual data points.

2.12. Chemicals and reagents

Table 4 List of chemicals and reagents

Reagent	Company	Cat. No.
2-Methyl Butane (Isopentane)	Merck	78-78-4
2,2,2-Tribromethanol (Avertin)	Sigma-Aldrich	75-80-9
4′,6-diamidino-2-phenylindole (DAPI)	Thermofisher Scientific	D1306
Aqua poly mount	Polysciences	18606
AAV-Cre-GFP plasmid	Addgene	49056
Bovine serum albumin (BSA)	Sigma-Aldrich	A4503
Bepanthen- Augen und Nasensalbe	Bayer	
Carprofen (Rycarfa 50 mg/ml)	TAD Phrama	796-828
Calcium chloride dihydrate ($CaCl_2.2H_2O$)	Sigma-Aldrich	C3881-500G
DNase I (1.5 U/µl)	Thermofisher Scientific	E1011-A
Ethanol	Honeywell	K115032205
Goat serum	Gibco	PCN 5000
D-(+)-Glucose monohydrate	Fluka	49159
Isoflurane (IsoFlo)	Abbot	TU061220
Lidocaine (Lidor 20 mg/ml)	Fendigo	140060
Magnesium chloride hexahydrate ($MgCl_2.6H_2O$)	Merck	A748033012
Metamizol (Novaminsulfon)	Ratiopharm	V157138
Methanol	J. T. Baker	8404.25
Paraffin oil	Applichem	A2135
Paraformaldehyde (PFA)	Serva	UN2213
Potassium Chloride (KCL)	Merck	1.049.361.000
Potassium dihydrogen phosphate) KH_2PO_4	Merck	1.04.873.1000

Power Syber green master mix	Thermofisher Scientific	4367659
pDP5rs packaging plasmid (for AAV production)	PlasmidFactory	PF405
Sodium Chloride	Merck	1.06404.1000
Sodium hydrogen phosphate dihydrate $Na_2HPO_4.2H_2O$	Merck	10028-24-7
Sodium hydrogen carbonate ($NAHCO_3$)	Merck	1.06329
Sodium dihydrogen phosphate monohydrate $NaH_2PO_4.H_2O$	Merck	1.06346.1000
Sucrose	Merck	1.07651.1000
Tissue-Tek OCT compound	Labtech	16004004
Triton-X 100	Roche	

2.13. Equipment

Table 5 . List of equipment

Product	Company	Cat. No.
Isoflurane anesthesia system (UniVet Porta-T5)	Groppler	UV17001-T5
Mclwain slice chopper	Campden instruments	TC752
Micro drill (micro4)	WPI	SYS-MICRO4
Hydrophobic pen (DAKO)	Agilent	S2002
Micropipette puller	Sutter Instruments	P-97
Anesthesia mask	WPI	OC-SEM-KIT
Microinjection system	WPI	NANOLITER2010
Fear conditioning system	MED Associates	MED-VFC-USB-M
Cryostat	Leica	Leica CM3050S
Isolated stimulator (IsoStim-01D)	Scientific instruments	ISO-01D
Glass Capillaries	Science products	GB150F-8P
Microscope (Dino-lite digital microscope)	Dino-Lite	AM4113TL
Sutures	Implantis	8697H
Coverslips (confocal imaging)	VWR	630-1845
Glass capillaries	WPI	504949
Microdrill (micro4)	WPI	503589

Mouse adaptor	WPI	502600
Probe holder	WPI	502244
Ear bars	WPI	502235
Bipolar electrode	FHC	30200
Replacement O-Rings kit	WPI	3000521
Adhesive glass slides for microscopy (SuperFrost Plus)	Fisher Scientific	11950657
Precision cover glass 1.5 H (STED imaging)	Marienfeld	0107052
Axio imager 2	Zeiss	-
Leica TCS SP2 laser scanning confocal microscope	Leica	-
Leica TCS SP8 laser scanning confocal microscope	Leica	-
Acoustic startle response system	TSE Systems	-
LABORAS system	Metris B.V	-
Viewer system (OFT)	Biobserve	-
Heating pad	Thermolux	-
Light Cycler 480 system	Roche diagnostics	-
Perfusion pump	IKA	-
Multiclamp amplifier 700B	Axon instruments	-
Digitizer (Digidata 1440A)	Molecular devices	-

2.14. Antibodies

Table 6 List of antibodies

Antibody	Species	Company	Cat. No.	Dilution
cFos	Guinea pig	Synaptic systems	226005	1:2000
SOM	Mouse	Santa Cruz	SC-55565	1:500
PV	Rabbit	Swant	PV235	1:5000
VIP	Rabbit	Immunostar	20077	1:500
PKCδ	Mouse	BD transduction laboratories	610398	1:2000

GFP	rabbit	Synaptic systems	132003	1:1000
GFP	Chicken	Aves Labs	GFP-120	1:3000
Nlgn2	Guinea pig	Synaptic systems	129205	1:500
vGAT	Rabbit	Synaptic systems	131003	1:1000
IgSF9b	Rabbit	Merck	HPA010802	1:1000
MDGA1	Rabbit	Synaptic systems	421002	1:1000
Anti-rabbit AF-488	Goat	Thermofisher Scientific	A-11008	1:600
Anti-guinea pig AF-555	Goat	Thermofisher Scientific	A-21435	1:600
Anti-mouse AF-555	Goat	Thermofisher Scientific	A28180	1:600
Anti-guinea pig AF-633	Goat	Thermofisher Scientific	A-21105	1:600
Anti-guinea pig AF-594	Goat	Thermofisher Scientific	A-11076	1:100
Anti-rabbit STAR-635p	Goat	Abberior	ST635P	1:50

2.15. Solutions

Phosphate buffered saline (10X): pH 6.8

Ingredient	Molecular weight (g/M)	Final concentration (in ddH_2O)
NaCl	58.44	1.37 M
KCl	74.55	27 mM
$Na_2HPO_4.2H_2O$	177.99	100 mM
KH_2PO_4	136.09	18 mM

Phosphate buffer (0.2M), pH=7.4:

Ingredient	Molecular weight (g/M)	Final concentration (in ddH_2O)
$NaH_2PO_4.H_2O$	137.99	45.14 mM
$Na_2HPO_4.2H_2O$	177.99	154.82 mM

Sucrose cryoprotectant solution: 30% (w/v) sucrose in PB buffer (0.1 M)

4%PFA fixative solution: 4% (w/v) in 0.1 PB buffer (0.1 M).

PFA was weighted and added to a solvent solution comprising PB (0.2 M, 50% of the total volume) and ddH_2O (25% of the total volume). The solution was warmed on a hotplate while being continuously stirred until its temperature reached 60 °C maximum. The solution was then left to cool down while being stirred until PFA was completely dissolved (solution turned transparent). Next, ddH_2O was added (25% of total volume) in addition to 20 µl of NAOH 1 M. The PFA solution was filtered using filtering units with 0.22 µm pore size and stored at 4 °C until it was used. The PFA solution was prepared freshly on the day it was intended to be used.

Blocking buffer: 10% (v/v) goat serum, 0.3% (v/v) Titon-X-100, 3% (w/v) BSA in 1X PBS

Saline solution: 0.9% NaCl (w/v) in ddH_2O

Avertin solution (20mg/ml): 100 µl avertin solution (1 g/ml TBE), 400 µl ethanol, 4500 µl saline

ACSF solution (10X): D-(+)-Glucose monohydrate (100 mM), NaCl (1200 mM), KCl (20 mM), KH_2PO_4 (10 mM), $NAHCO_3$ (260 mM) in ddH_2O, pH= 8. $MgCl_2$ (1 mM), $CaCl_2$ (2 mM) were added freshly to the 1X ACSF prior to use.

Sucrose- based slicing solution (5X): Sucrose (1150 mM), KCL (10mM), KH_2PO_4 (5 mM), D-(+)-Glucose monohydrate (50 mM), $NAHCO_3$ (130 mM) in ddH_2O. $MgCl_2$ (3mM) and $CaCl_2$ (0.5 mM) were added freshly to 1X slicing solution before use.

3. Results

3.1. Chapter 1: Role of Nlgn2 in regulating fear learning behavior and circuit

Being a key regulator of the maturation and function of inhibitory synapses (Ali et al 2020), Nlgn2 has been implicated in many psychiatric pathologies in humans that share a common pathophysiology of disrupted E/I balance and impaired affective processing such as schizophrenia, anxiety and autism (Parente et al., 2017; Sun et al., 2011). Furthermore, Nlgn2 KO mice show a robust anxiety-like behavior that was linked to synaptic and network-level deficits in the regions that regulate anxiety and emotional processing in general (Babaev et al., 2016; Cruces-Solis et al., 2021). However, the role of Nlgn2 in the formation of emotional memories and how that is related to the anxiety-like behavior has not been investigated in detail. Therefore, I sought to investigate aversive emotional learning in Nlgn2 KO mice using the fear conditioning paradigm by characterizing this behavior and its underlying circuit activation in Nlgn2 KO versus WT mice.

3.1.1. Cued fear memory retrieval is reduced in constitutive Nlgn2 KO mice

As described in section (1.1), the Pavlovian FC paradigm is one of the most robust and frequently used paradigms to assess fear memory formation in rodents (Tovote et al., 2015). This paradigm is based on measuring the animal's defensive response to a sensory cue or a context (conditioned stimulus, CS) that has been previously associated with an aversive experience (unconditioned stimulus, US). Preliminary work from my group conducted by Dr. Olga Babaev (Department of Molecular Neurobiology, Max Planck institute for Experimental Medicine), demonstrated a mild deficit in fear memory retrieval in Nlgn2 KO mice using a discriminative FC protocol (data not shown). To confirm and further investigate this observation, I characterized FC behavior of Nlgn2 KO mice in comparison with their littermate WT mice using a simple, non-discriminative protocol (see methods, section 2.2.1). In the paradigm I implemented, the mouse was placed in the training context and exposed to a tone (80 dB, 5 KH), which serves as the CS, for 30 sec. The CS co-terminated in the last two seconds with a mild footshock (0.5 mA) that served as the US (figure 8, a). Either 2 h or 24 h after training, the mouse was placed in a different context and exposed to the CS presentation alone two times. The percentage of time when the mouse showed freezing behavior, defined as the absence of movement except for respiratory movements, was measured during the first CS presentation as a readout of the magnitude of fear memory

retrieval. I observed a significant reduction in %CS freezing in Nlgn2 KO mice compared to their littermate controls 24 hours later (figure 8, b, CS freezing). This reduction was also detected when testing was conducted 2 h after training (figure 8, c) indicating that Nlgn2 KO mice have a deficit in both short- and long-term fear memory measured at the level of retrieval.

Being a well-established model for anxiety-like behavior (Babaev et al., 2016; Blundell et al., 2009), it was interesting to test whether Nlgn2 KO mice also exhibit higher freezing levels in a novel context. Therefore, baseline freezing in the first two min after placement in the training context was measured. As expected and demonstrated in earlier reports (Babaev et al., 2016), Nlgn2 KO mice showed higher baseline freezing to the novel context than their littermate WT mice. This increase was statistically significant in the mice cohort exposed to the short-term memory retrieval test (figure 8, c, training: baseline freezing).
To confirm that CS freezing in WT mice was specific to the tone and not due to context generalization (Fanselow, 1990) baseline freezing in the testing context was measured (figure 8, b and c, testing: baseline freezing) and showed to be minimal in WT mice compared to CS freezing. This confirmed that most of the freezing detected during CS presentation was induced by the CS. Freezing levels due to context generalization were, however, comparable between Nlgn2 KO and WT mice.

Having observed a deficit in auditory FC retrieval where the CS used is an auditory cue, I aimed to further investigate potential brain origins for this deficit by assessing contextual FC in Nlgn2 KO mice. While auditory FC is shown to be mainly dependent on associative plasticity mechanisms occurring in the amygdala (Ledoux, 2000; LeDoux, 2000), contextual FC involves the hippocampus for context encoding where learning-dependent plasticity is also shown to occur (Chaaya et al., 2018). To assess contextual FC in Nlgn2 KO versus WT mice, the mice were placed in the training context and exposed to two US presentations (figure 8, d). 24 hours later, the mice were placed again in the same context where they received the training. The freezing was then measured during the 2 min of context exposure.

Surprisingly, Nlgn2 KO mice showed no significant change in CS freezing in comparison with WT mice (figure 8, e) but they rather showed a trend toward increased contextual freezing. This strongly suggests that the deficit in fear retrieval is specific to the auditory FC and likely involves impaired amygdala-dependent plasticity. Similar to previous observations, baseline freezing in the novel context on the training day was significantly increased in Nlgn2 KO compared to WT mice (figure 8, e, baseline freezing), in line with the known anxiety-like behavioral phenotype of Nlgn2 KO mice.

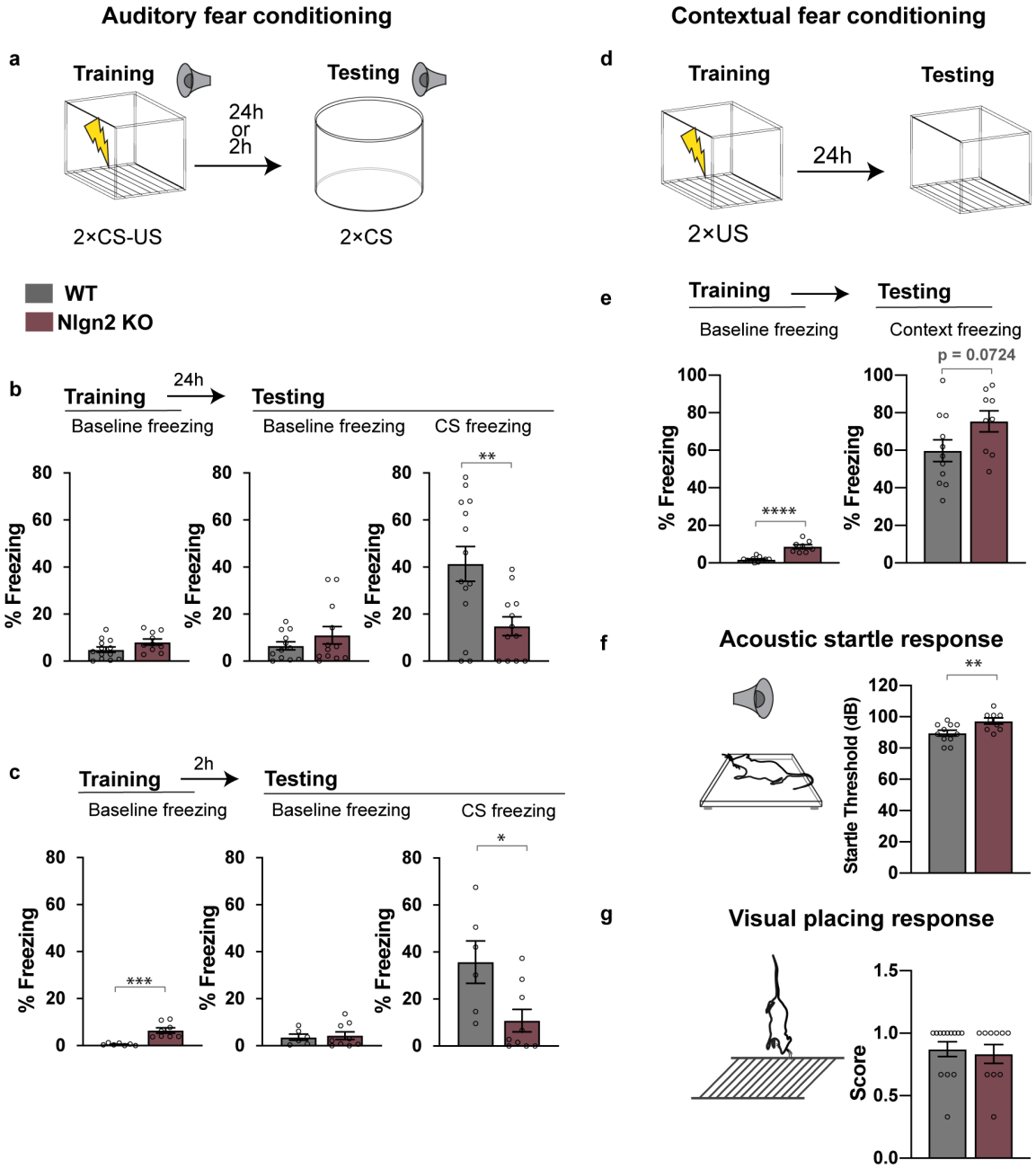

Figure 8 Auditory, but not contextual, fear memory retrieval is reduced in Nlgn2 KO mice. **a**. Schematic of the auditory FC paradigm. **b**, **c**. Percentages of time spent freezing at baseline or in response to the CS in the auditory FC paradigm in Nlgn2 KO and WT mice tested after 24h (**b**, training baseline: two tailed t-test p = 0.0750, testing baseline: N = 12 mice, Mann-Whitney test p = 0.6011, CS freezing: N = 12-14 mice, two-tailed t-test p = 0.0061) or 2h (**c**, training baseline: N = 7-8 mice, Mann-Whitney test p = 0.0003, testing baseline: N = 6-9, Mann-Whitney test p = 0.8861, CS freezing: N = 6-9 mice, Mann-Whitney test p = 0.0172).**d**. Schematic of the contextual FC paradigm. **e**. Percentage of time spent freezing at baseline or in response to the training context, training baseline: N = 8-11 mice, two-tailed t-test p < 0.0001, context freezing: N = 9-11 mice, two tailed t-test p = 0.0724. **f**. Schematic of the acoustic startle response test with the measured startle threshold in decibel, N = 9-11 mice, two tailed t -test p = 0.0095. **g**. A schematic of the visual placing response test (left) and the scores in the visual placing test plotted between Nlgn2 KO and WT mice, N = 10-13 mice, Mann-Whitney test p = 0.7319.

In light of the observed deficit in auditory FC, it was important to rule out the possibility that the constitutive deletion of Nlgn2 might cause disrupted hearing ability in Nlgn2 KO mice. Hearing has been assessed before in Nlgn2 KO mice using the acoustic startle response test (ASR) and mice showed comparable startle responses to WT mice **(**Wohr et al., 2013)**.** Moreover, Nlgn2 KO mice exhibited normal auditory acuity and frequency discrimination in a memory-based auditory task (Chen et al., 2019). To confirm these findings in my experimental mice, I characterized their behavior using the ASR paradigm. To this end, Nlgn2 KO and their WT littermates were placed in a sound attenuated chamber (see methods, section 2.2.4) and their startle amplitude, which is measured as the force detected by a force-sensitive platform on which the mouse is placed, in response to sound stimuli of increasing intensity. By comparing the startle threshold, which is the sound pressure level at which the mouse shows a certain startle amplitude above baseline (defined empirically), I saw that Nlgn2 KO showed a slight but significant increase in startle threshold compared to WT mice (figure 8, f). However, the magnitude of this increase was too small to reflect a potential lack of hearing in Nlgn2 KO mice and might rather represent a motor impairment.

Since contextual fear learning relies in part on the mouse ability to visually perceive the context, it was also necessary to ensure that constitutive Nlgn2 KO mice don't suffer from absence of vision. That is why I performed the visual placing response test used to detect blindness in rodents (Pinto and Enroth-Cugell, 2000). In the test the mouse is held aloft at approximately 15 cm from a cage grid and lowered slowly toward the grid (see methods, section 2.2.5). When the mouse extends its forelimbs to reach out to the grid at a distance where it cannot sense the grid by the whiskers (approximately 5 cm), its visual ability is scored as 1, otherwise it is scored as 0. By performing three trials per mouse for Nlgn2 KO and WT mice, I observed no difference in the visual placing score, indicating that Nlgn2 can see comparably to WT mice (figure 8, g).

Taken together, these findings show that Nlgn2 KO mice have a deficit in fear memory retrieval that is detected specifically in the auditory form of fear conditioning, but not in the contextual form. This deficit cannot, however, be explained by lack of hearing in these mice. Also, Nlgn2 KO mice do not show to suffer from blindness as indicated by the visual placing test.

3.1.2. Nlgn2 KO mice show increased locomotion in the homecage.

To gain more insights on the effect of Nlgn2 deletion on mice behavior in a less stressful experimental conditions, I characterized homecage activity of Nlgn2 KO mice versus WT using the LABORAS system. This paradigm allows for automated detection and

quantification of different mouse behaviors in the homecage such as locomotion, eating, drinking, grooming, etc. During the recording, the mice were single-housed and their behavior was recorded between 17:00 and 9:00 o'clock after 2 days of habituation (see methods, section 2.2.3). As reported previously by our group (Babaev et al., 2016), Nlgn2 KO mice showed increased locomotion in the homecage with parameters such as locomotion duration (figure 9, b), locomotion speed (figure 9, c) and total distance travelled (figure 9, d) being significantly increased in Nlgn2 KO mice compared to WT mice while the immobility duration (figure 9, e) was significantly reduced in these mice. Furthermore, climbing and rearing durations (figure 9, i, j) were also significantly increased in Nlgn2 KO mice. Other homecage behaviors such as eating, drinking, grooming, and circling were not altered in Nlgn2 KO mice compared to WT mice (figure 9, f, g, h and k). Despite the observed increase in locomotion in the homecage, the freezing deficit in auditory FC cannot be confound by a motor problem, since Nlgn2 KO mice showed normal freezing levels in contextual FC (figure 8, e, CS freezing). Also, the reduced locomotion reported in these mice in anxiogenic conditions argues against this possibility (Babaev et al., 2016).

3.1.3. Neural circuits underlying auditory FC deficit in Nlgn2 KO

Having produced such a prominent reduction in auditory FC retrieval, Nlgn2 deletion is expected to affect the activation of neural circuits controlling this behavior. To explore the changes in circuit activation during fear memory retrieval, analysis of the immediate early gene *cfos* expression was conducted after FC testing and quantified in different brain regions that are crucial for the formation and/or retrieval of fear memories. These regions included the amygdala, the medial prefrontal cortex, the ventrolateral periaqueductal gray and the auditory cortex.

3.1.3.1. The amygdala

The amygdala is one of the most well-established components in the neural circuitry underlying fear memory acquisition, consolidation, and retrieval (Duvarci and Pare, 2014; Ledoux, 2000; Sun et al., 2020). Therefore, I hypothesized that the reduction in fear memory retrieval in Nlgn2 KO mice would be associated with an alteration in the amygdala circuit activation. To test this hypothesis, cFos assay was performed in amygdala subregions 90 min after FC testing (figure 10, a). cFos immunohistochemistry and image and data analysis for this experiment was co-performed with Lena Marth (Department of Molecular Biology, Max Planck for Experimental Medicine) under my supervision. Lena contributed to this project as part of her medical doctoral thesis and the results obtained from cFos assay experiments are published in her medical thesis.

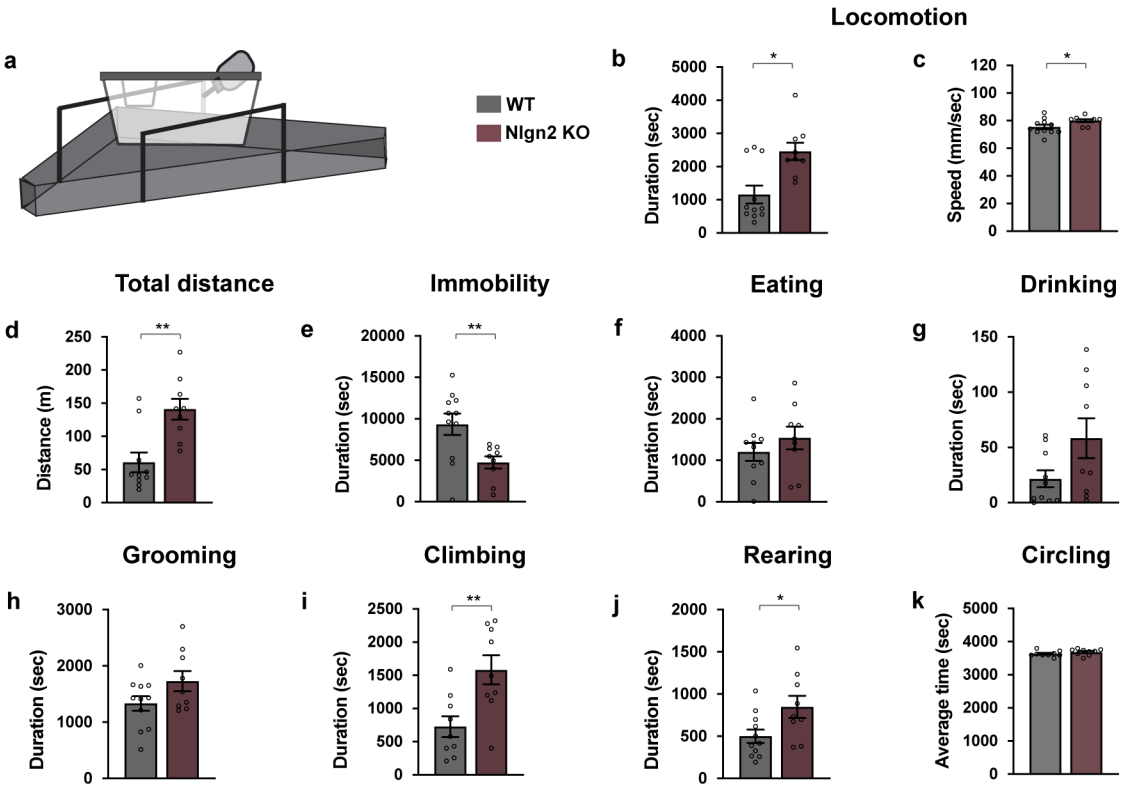

Figure 9 Characterization of homecage activity in Nlgn2 KO mice.
a A schematic of the LABORAS system. **b**. Average locomotor duration, N = 9-11 mice, Mann-Whitney test p = 0.0159. **c**. Average locomotion speed, N = 9-11 mice, Two-tailed t-test p = 0.0475. **d**. Total distance travelled, N = 9-10 mice, Mann-Whitney test p = 0.0030. **e**. Immobility duration, N = 9-11 mice, Two-tailed t-test p = 0.0097. **f**. Eating duration. N = 9-10 mice, Two-tailed t-test p = 0.3420. **g**. Drinking duration, N = 9-10 mice, Mann-Whitney test p = 0.0789. **h**. Grooming duration, N = 9-11 mice, two-tailed t-test p = 0.0879. **i**. Climbing duration, N = 9 mice, two-tailed t-test p = 0.0059. **j**. Rearing duration, N = 9-11, two -tailed t-test p = 0.0283. **k**. Circling duration, N = 9, Two-tailed t-test p = 0.2139.

To distinguish changes in cFos expression that reflect CS-US associations from the ones elicited solely by CS exposure, mice of each genotype were split into two experimental groups based on the training protocol they received on the first day. These groups included WT and Nlgn2 KO mice that received paired training (WT-FC and Nlgn2 KO- FC), and WT and Nlgn2 KO mice that received only CS training with no US introduction (WT-Ctrl and Nlgn2 KO- Ctrl). By comparing freezing levels on the testing day between mice from the four experimental groups, I again observed a significant deficit in CS freezing in Nlgn2 KO mice that received paired training (Nlgn2 KO-FC) compared to WT mice (WT-FC). However, mice that received only CS training (WT-Ctrl and Nlgn2 KO Ctrl) showed minimal freezing levels in both genotypes (figure 10, CS-freezing). Two-way analysis of variance (two-way ANOVA) showed a significant main effect of genotype, training, and interaction in CS freezing responses. This means that while mice that received paired training from both genotypes show increased CS freezing compared to their control condition, the magnitude of this increase is significantly reduced in Nlgn2 KO mice (figure 10, b, CS freezing). Again,

Nlgn2 KO mice showed increased baseline freezing in the novel training context with the genotype being a significant main factor with two-way ANOVA (figure 10, b, training: baseline freezing) and with Nlgn2 mice from the FC and Ctrl conditions showing significant increase in training baseline freezing compared to WT mice using Tukey's post-hoc analysis for pairwise comparisons. On the other hand, testing baseline freezing, reflecting context generalization, was not different between genotypes although it showed to be dependent on training as a main factor with two-way ANOVA. Also, both genotypes showed a comparable increase in the FC compared to Ctrl conditions using Tukey's analysis (figure 10, b, testing: baseline freezing). This phenotype replicated the previous behavioral findings of Nlgn2 KO mice showing reduced conditioned CS freezing, but increased innate, novelty-induced freezing.

Analysis of cFos expression in different amygdala subregions in WT mice showed distinct patterns of cFos expression during FC testing. For example, the lateral amygdala (LA) showed significantly increased cFos expression in WT-FC mice compared to WT-Ctrl mice (figure 10, d). This observation is in line with the literature regarding the role of the LA as a site for associative plasticity that leads to potentiated CS responses after FC (Ledoux, 2000). In contrast to the LA, other amygdala subregions such BA, CeL and CeM did not seem to be differentially activated in WT -FC mice compared to WT-Ctrl (figure 10, e, f, g), although that in the CeL and CeM a trend toward increased activation in FC-WT mice was observed but was not found significant using two-way ANOVA.

Interestingly, cFos expression in the LA of Nlgn2 KO-FC mice was not increased compared to Nlgn2 KO-Ctrl mice, which was demonstrated by a significant genotype- training interaction in the LA using two-way ANOVA. This finding indicates that the exposure to FC training leads to differential effect on LA activation during FC retrieval in Nlgn2 KO compared to WT mice. Unlike WT mice, no significant difference was detected in the pairwise comparison between Nlgn2-KO- Ctrl and Nlgn2-KO-FC groups. This indicates that the LA amygdala neurons in Nlgn2 KO mice show reduced learning-induced activation during retrieval compared to WT mice.

In contrast to the LA, BA neurons showed a different pattern of activation during FC retrieval, being differentially activated in a genotype dependent manner and showing an increase in Nlgn2 KO mice regardless of training. This increase between the Nlgn2-KO-FC and the WT-FC was significant using Tukey's pairwise comparisons and it likely reflects an anxiety phenotype as demonstrated previously in this region (Babaev et al., 2016).

Although they were showing a trend toward reduced cFos expression, CeL and CeM neurons were not significantly differentially activated in Nlgn2 KO mice compared to WT mice (figure 10, f and g). This indicates that the CeA does not contribute substantially to the Nlgn2 KO phenotype, or its potential changes are not detected using our methods.

3.1.3.2. The medial prefrontal cortex (mPFC)

The mPFC modulates fear memory through reciprocal connections with the amygdala (see introduction, section 1.2.2.3). Two areas of the mPFC, namely the PrL and the IL were shown to regulate fear expression and extinction, respectively (Senn et al., 2014). Using the same paradigm for cFos assay after FC retrieval testing (figure 11, a), Lena Marth performed IHC and analysis of cFos expression in the PrL (figure 11, c and f) and IL (figure 11, d and g) areas of the mPFC.

While in the PrL, both genotype and training were found to be significant main factors using two-way ANOVA, interaction between both factors was not significant (figure 11, f). Additionally, Tukey's post-hoc comparisons showed a significant increase in cFos expression of PrL neurons in the WT-FC compared to the WT-Ctrl group. Similar to the LA, this increase was not significant between the comparable groups in Nlgn2 KO mice (Nlgn2 KO-Ctrl and Nlgn2 KO- FC). However, PrL neurons in Nlgn2 KO seemed to have higher activation that was found to be significantly different at the basal level (between Nlgn2 KO Ctrl and WT-Ctrl groups, figure 11, f). This increased baseline activation in PrL neurons of Nlgn2 KO mice might explain the lack of significant difference in activation between the Nlgn2 KO-FC compared to the Nlgn2 KO- Ctrl group. It is unclear, however, how this dysregulation might contribute to the FC deficit in Nlgn2 KO mice, knowing that PrL activation correlates with fear expression.

In contrast to PrL, activation of IL neurons did not show to be dependent on genotype, instead, training was a significant main effect of variation in cFos expression by these neurons as found using two-way ANOVA (figure 11, d and g). This indicates that neurons in this region become activated during retrieval in mice that received FC training, but in a comparable way between Nlgn2 KO and WT mice. Therefore, the IL is unlikely a site for Nlgn2-mediated FC deficit.

3.1.3.3. The ventrolateral periaqueductal gray (vlPAG)

The vlPAG has been identified as a crucial component in the FC circuit that is specifically important for the expression of conditioned freezing. It receives projections from the CeA

and projects to the motor centers that elicits freezing (see introduction, section 1.2.2.5). To test whether the vlPAG is dysregulated in Nlgn2 KO mice, Lena Marth performed IHC and analysis of cFos expression in this region after FC testing.

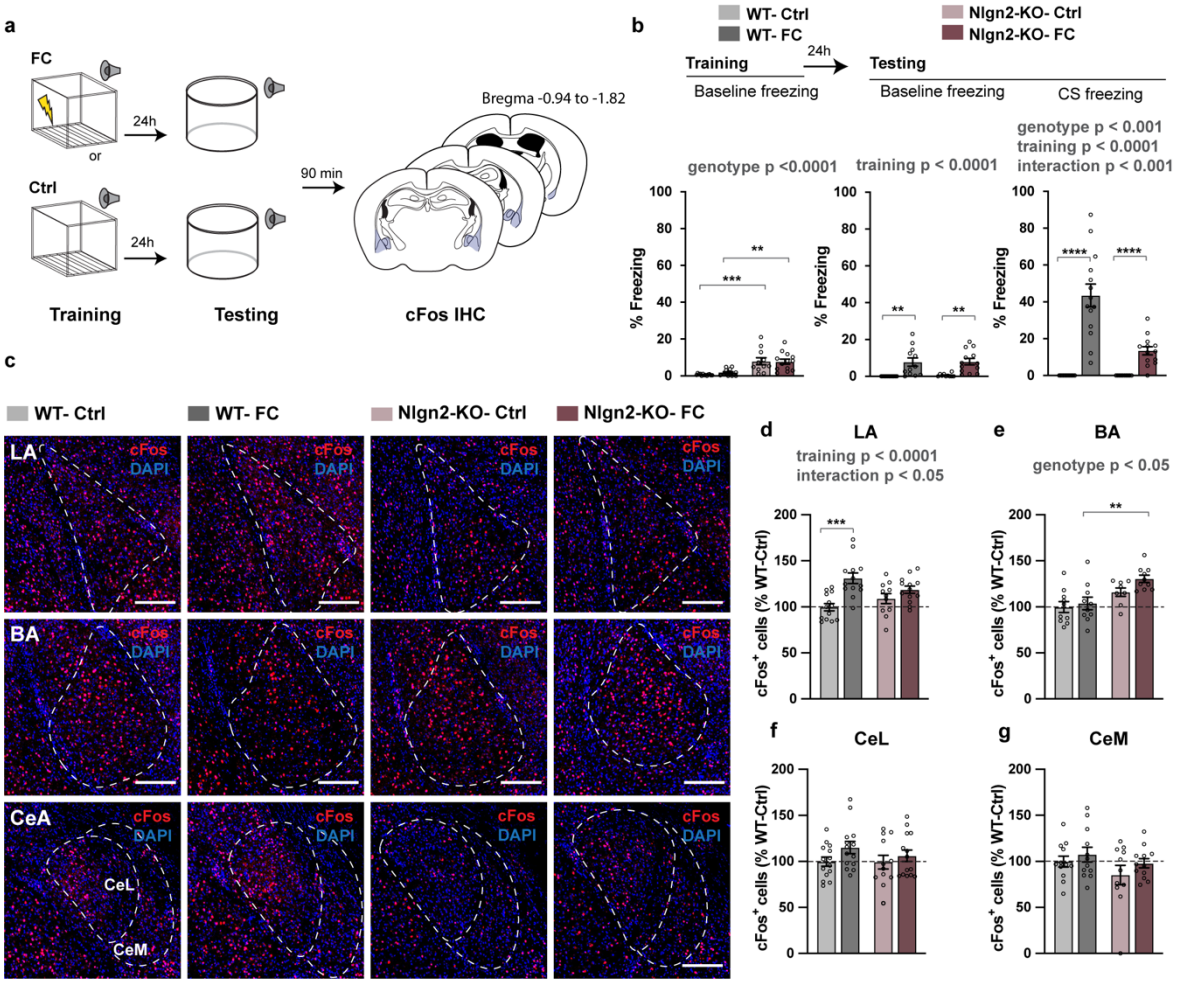

Figure 10 Amygdala circuit is dysregulated in Nlgn2 KO during fear memory retrieval.
a. Schematic of the experimental paradigm used for cFos expression analysis after FC testing. **b**. percentage of time spent freezing during CS presentation (CS freezing, N = 12-14 mice, two-way ANOVA; Genotype: F (1,45) = 15.62, p = 0.0003. Training: F (1, 45) = 56.35, p < 0.000. Interaction: F (1, 45) = 15,62,p = 0.0003) or at baseline during training (training baseline, N = 11-14 mice, two-way ANOVA; Genotype: F(1, 47) = 35.36, p<0.0001; Training: F(1, 47) = 0.1691, p = 0.6828; Interaction: F(1, 47) = 0.3630, p = 0.5497) and testing (testing baseline; N = 10-13 mice; two-way ANOVA; Genotype: F (1, 45) = 0.06270, p = 0.8034; Training: F(1, 45) = 28.06, p < 0.0001; Interaction: F(1, 45) = 0.01838, p = 0.8928) in Nlgn2 KO and WT mice exposed to CS-US (FC) or only CS during training (Ctrl). **c**. 20x confocal micrographs of brain slices labelled with antibody against cFos (red) and DAPI for nuclei (blue). Images show amygdala subregions (top to bottom LA, BA and CeA) in Nlgn2 KO and WT mice subjected on day 1 to paired training (FC) or only CS training (Ctrl), dashed lines indicate region borders according to Paxinos mouse brain Atlas(Paxinos and Franklin, 1997), scale bar 200 µm. **d-g** Normalized number of cFos expressing cells calculated as a percentage of the WT-Ctrl group in the LA (**d**, N = 11-13 mice, two-way ANOVA; Genotype: F (1, 46) = 0.1163, p = 0.7346; Training: F (1, 46) = 18.45, p < 0.000; Interaction: F (1, 46) = 5.176. p = 0.0276), BA (**e**, N=8-10 mice, two-way ANOVA; Genotype: F (1, 34) = 14.80, p = 0.0005; Training: F (1, 34) = 2.767, p = 0.1054; Interaction: F (1, 34) = 0.8671, p = 0.3585), CeL (**f**, N = 12-14 mice, two-way ANOVA; Genotype: F(1, 50) = 0.5663, p = 0.4553; Training: F(1, 50) = 3.145, p = 0.0822, Interaction: F(1, 50) = 0.4508, p = 0.5050) and CeM (**g**, N = 11-12 mice, two-way ANOVA; Genotype: F (1, 43) = 2.634, p = 0.1119; Training: F (1, 43) = 1.844, p = 0.1816; Interaction: F (1, 43) = 0.1262, p =

0.7242). Significant Tukey's pairwise comparisons between marked groups are indicated with * $p < 0.05$, ** $p < 0.01$, *** $p < 0.001$ and **** $p < 0.0001$.

Interestingly, despite the robust deficit in CS freezing in Nlgn2 KO mice, analysis of cFos expression in vlPAG neurons showed no effect of the genotype on cFos levels with two-way ANOVA (figure 11, e and h). Instead, vlPAG neurons were differentially activated during retrieval in both Nlgn2 KO and WT mice that received FC training, and the training was found to be a main factor of variance with two-way ANOVA. Based on this result, cFos levels in the vlPAG reflected increased activation after FC training that was not significantly different between Nlgn2 KO and WT mice. This finding was, however, in discrepancy with the role of the vlPAG as a main center where freezing responses are elicited, possibly due to technical limitations of the cFos assay.

3.1.3.4. The auditory cortex (AuC)

Other than being a crucial relay station for CS information to the lateral amygdala through the thalamocortical pathway (Ledoux, 2000), increasing evidence implicates the AuC in the encoding and storage of fear memory (see introduction, section 1.2.2.1.b) (Campeau and Davis, 1995; Grosso et al., 2017; Letzkus et al., 2011; Quirk et al., 1997). To test whether the AuC could be a site for altered neural activation in Nlgn2 KO mice, Lena Marth performed IHC and analysis of cFos expression in this region 90 min after FC retrieval. To this end, three divisions of the AuC were included in the analysis, namely the primary auditory cortex (Au1), the dorsal area of the secondary auditory cortex (AuD) and the ventral area of the secondary auditory cortex (AuV).

Interestingly, a significant increase in cFos expression after FC retrieval was detected in the Au1 of WT-FC mice that underwent paired training compared to WT-Ctrl mice. This increase, however, was absent in Nlgn2 KO mice (figure 12, a and d) and a significant difference was detected between WT-FC and Nlgn2 KO-FC groups using Tukey's multiple comparisons analysis (figure 12, d). Additionally, two-way ANOVA showed significant interaction between genotype and training in the Au1 and AuD cortices (figure 12, c and d). In the AuV, although a similar trend in activation change was observed, but was not statistically significant using ANOVA (figure 12, e). These findings are in line with the previously reported fear learning induced changes in the AuC in WT mice, and they strongly implicate the AuC as a potential site for the behavioral FC retrieval deficit observed in Nlgn2 KO mice.

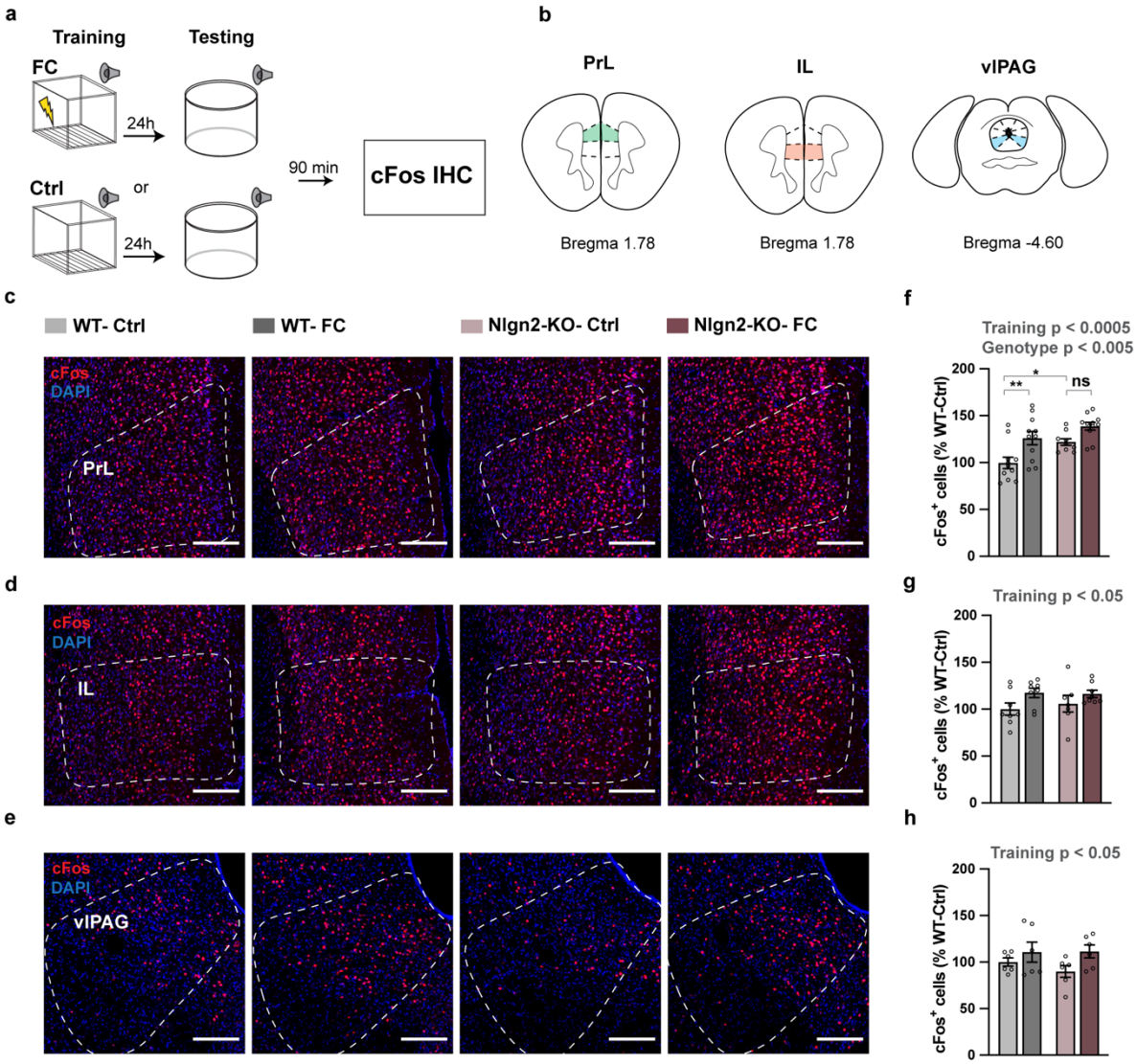

Figure 11 cFos activation in the mPFC and vlPAG during FC retrieval in Nlgn2 KO and WT mice.

a. A schematic of the experimental paradigm for cFos assay after FC testing. **b**. Diagrams of mouse brain sections containing the PrL, the IL and the vlPAG (left to right) with the corresponding bregma levels, adapted from the Paxinos mouse brain atlas(Paxinos and Franklin, 1997) . **c**, **d** and **e**, 20x confocal micrographs of brain slices labelled with antibody against cFos (red) and DAPI for nuclei (blue). Images show the prelimbic area PrL (**c**) and the infralimbic area IL (**d**) of mPFC and the vlPAG (**e**) and are obtained from Nlgn2 KO and WT mice subjected on day1 to paired training (FC) or only CS (Ctrl). Dashed lines indicate region borders according to Paxinos mouse brain Atlas, scale bar 200µm. **f**, **g** and h. Normalized number of cFos expressing cells calculated as a percentage of the WT-Ctrl group in the PrL (**f**, N = 9-11, two-way ANOVA; Genotype: F (1, 38) = 9.781, p = 0.0034; Training: F (1, 38) = 14.92, p = 0.0004; Interaction: F (1, 38) = 0.7314, p = 0.3978), the IL (**g**, N=7-8 mice, two-way ANOVA; Genotype: F (1, 27) = 0.1407, p = 0.7105; Training: F (1, 27) = 5.141, p = 0.0316; Interaction: F (1, 27) = 0.3145, p = 0.5795) and the vlPAG (**h**, N= 6 mice, two-way ANOVA; Genotype: F (1, 20) = 0.3888, p = 0.5400; Training: F (1, 20) = 4.536, p = 0.0458; Interaction: F (1, 20) = 0.5066, p = 0.4848).

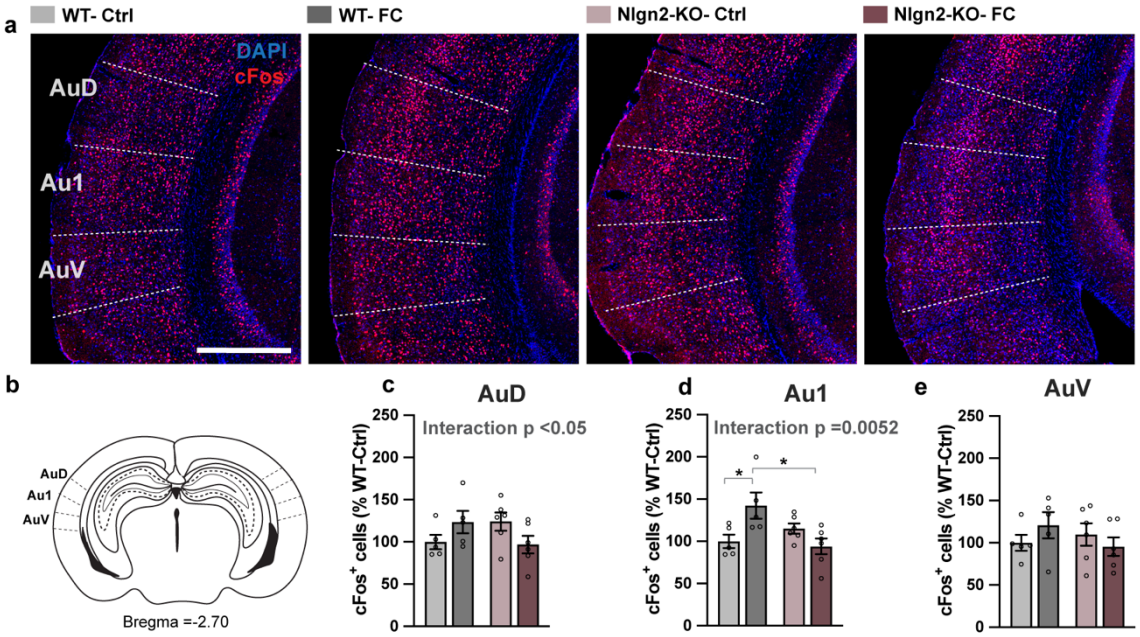

Figure 12 Dysregulated cFos activation in the auditory cortex in line with FC retrieval deficit. **a**. 20x confocal micrographs of brain slices labelled with antibody against cFos (red) and with DAPI (blue). Images show the auditory cortex in Nlgn2 KO and WT mice subjected on day 1 to paired training (FC) or only CS training (Ctrl), dashed lines indicate region borders according to Paxinos mouse brain Atlas (Paxinos and Franklin, 1997), scale bar 500µm. **b**. A diagram of a mouse brain section containing the auditory cortex with its different areas, adapted from Paxinos mouse brain atlas (Paxinos and Franklin, 1997). **c**, **d** and **e**. Normalized number of cFos expressing cells calculated as a percentage of the average number obtained from the WT-Ctrl group in the dorsal area of the secondary auditory cortex AuD (**c**, N=5-6, two-way ANOVA; Genotype: F (1, 18) = 0.01198, p = 0.9141; Training: F (1, 18) = 0.03258, p = 0.08588; Interaction: F (1, 18) = 5.442, p = 0.0315), the primary auditory cortex Au1 (**d**, N=5-6, two-way ANOVA; Genotype: F (1, 18) = 2.720, p = 0.1164; Training: F (1, 18) = 1.125, p = 0.3028; Interaction: F (1, 18) = 10.08, p = 0.0052) and ventral area of the secondary auditory cortex AuV (**e**, N=5-6, two-way ANOVA; Genotype: F (1, 18) = 0.3756, p = 0.5476; Training: F (1, 18) = 0.06659, p = 0.7993; Interaction: F (1, 18) = 1.948, p = 0.1798).

3.1.4. Region specificity of Nlgn2 function in regulating fear learning versus anxiety like behavior

Being a crucial site for the plasticity underlying fear memory encoding, the lack of activation in the LA neurons after FC was highly reflective of the fear memory deficit observed in Nlgn2 KO mice. However, it remained unclear whether the LA is causally implicated in mediating this deficit. To address this possibility, I aimed to test the outcome of local Nlgn2 deletion in the LA on FC behavior. One way to achieve local deletion is by delivering an AAV virus expressing the Cre recombinase enzyme combined with a GFP tag (AAV-Cre-GFP) to the LA of conditional Nlgn2 KO mice (Nlgn2- fl/fl). In these mice, the exon 2 of the *Nlgn2* gene, which contains the start codon, is flanked by two lox-p sites. Therefore, subsequent introduction of Cre recombinase targeting these sites would lead to the excision of exon 2 so that the *Nlgn2* gene would be no longer transcribed in transduced cells. Following a

period of 6 weeks to allow for the expression of the viral construct, the Cre-mediated recombination and the degradation of the existing Nlgn2 protein, a local deletion of Nlgn2 could be achieved in the site of the injection (Liang et al., 2015). Using this method, a recent publication by our group revealed that local deletion of Nlgn2 in the BLA and ventral hippocampus (vHPC) recapitulated certain aspects of the anxiety-like phenotype observed in Nlgn2 KO mice (figure 13) (Cruces-Solis et al., 2021). As part of my contribution to this work, I validated the efficiency of the local deletion method in vitro and in vivo. To this end, I transduced cultured hippocampal neurons with one of the following viruses: AAV-Cre-GFP or AAV-GFP as a control. After two weeks, I quantified Nlgn2 protein levels in the transduced cells using western blot assay. I observed approximately 90% reduction in Nlgn2 levels in neurons transduced with AAV-Cre-GFP virus compared to AAV-GFP-transduced neurons (figure 14, a, b and c). To confirm this finding in vivo, I performed stereotaxic surgeries to deliver the AAV-Cre-GFP or the AAV- GFP viruses to the BLA of Nlgn2 fl/fl mice. After 6 weeks from the injection, which is the same time point for performing the behavioral analysis, I quantified Nlgn2 protein expression by IHC in the BLA, identified by GFP expression. Consistently with findings from the in vitro analysis, I observed 80% reduction in Nlgn2 levels at the injection site in mice injected with AAV-Cre-GFP virus compared to mice injected with control AAV-GFP virus (figure 14, d, e and f).

To exclude the possibility of potential effects of lox-P sequences on the behavior of Nlgn2-fl/fl mice, Dr. Olga Babaev previously assessed anxiety-like behavior in mice that are heterozygous (fl/WT) or homozygous (fl/fl) for the floxed *Nlgn2* allele and found no indication of anxiety-like behavior during OFT exploration with all center parameters, as well as total distance travelled, being comparable between genotypes (figure 14, j-k). Similarly, by assessing FC in Nlgn2 fl/fl mice, I observed no significant difference in CS freezing or testing baseline freezing between Nlgn2-fl/fl and Nlgn2-WT mice (figure 14, l and m). However, a small increase in training baseline freezing was measured in Nlgn2 fl/fl mice compared to WT mice (figure 14, m, training: baseline freezing).

Having validated that fear learning is not affected in Nlgn2 fl/fl mice in the absence of Cre-recombinase, I proceeded by investigating the effect of Nlgn2 local deletion in the LA on FC behavior. Surprisingly, despite testing two different doses of AAV-Cre-GFP injected in the LA: 150 nl (figure 15) or 300 nl (figure 16), deletion of Nlgn2 in this region did not seem to affect FC in mice. This indicates that the LA does not mediate the FC deficit observed in Nlgn2 KO mice despite the dysregulated activation observed in this region during FC retrieval.

In light of the effects on anxiety-like behavior we observed by locally deleting Nlgn2 in the BLA (Cruces-Solis et al., 2021), I sought to analyze anxiety-like behavior in LA-cNlgn2 KO mice to gain more insights on the role of Nlgn2 in regulating FC versus anxiety through the amygdala. To this end, I performed OFT analysis in mice that underwent LA-cNlgn2 deletion, before the mice were subjected to FC. Similarly, I observed no significant difference in the number of entries, duration or distance travelled in the center of the open field in Nlgn2 fl/fl mice compared to WT mice injected with the Cre expressing virus (figures 15 and 16, c, d and e).

Taken together, my current data showed no effect of Nlgn2 local deletion on fear learning or anxiety like behavior in mice. Since cFos analysis revealed changes in several other regions like the AuC and the mPFC, these regions can be alternative potential sites for the FC deficit.

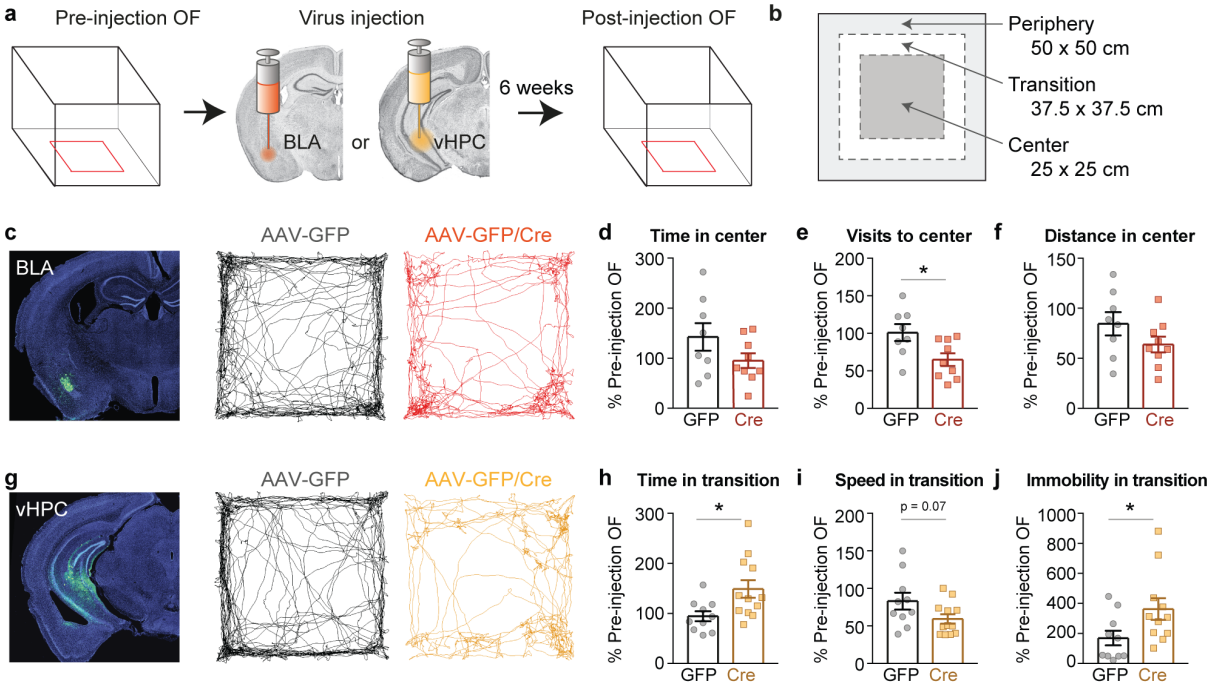

Figure 13 local deletion of Nlgn2 in the BLA and vHPC recapitulates different aspects of anxiety-like behavior in Nlgn2 KO mice.
a. A schematic of the experimental procedure where mice were tested in the OFT before they were subjected to stereotaxic injection of AAV-Cre-GFP or AAV-GFP viruses in the BLA and the vHPC of cNlgn2 KO mice. 6 weeks later, mice were tested again in the OFT. **b**. Dimensions and designations of different areas in the OF. **c**, **g**. micrographs of coronal sections showing GFP expression in the BLA (**c**) and the vHPC (g) after viral-mediated delivery along with example tracks of mice injected with either AAV-Cre-GFP or AAV-GFP in these regions while exploring the OF. **d**, **e**, and **f**. Time in the center. (**d**), visits to the center (**e**) and distance in the center (**f** in mice injected in the BLA with AAV-Cre-GFP or AAV-GFP viruses after the stereotaxic surgery expressed as percentage of values of the same parameters measured before the surgery. **h**, **i**, and **j**. Time (**h**), speed (**i**) and immobility (**j**) in the transition zone of the OFT in Nlgn2 fl/fl injected with AAV-Cre-GFP or AAV-GFP in the vHPC, expressed as a percentage of values of the same parameters before the injection. Figure

adapted from (Cruces-Solis et al., 2021). Stereotaxic injections were co-performed with Dr. Olga Babaev, OFT was performed by Sally Wenger.

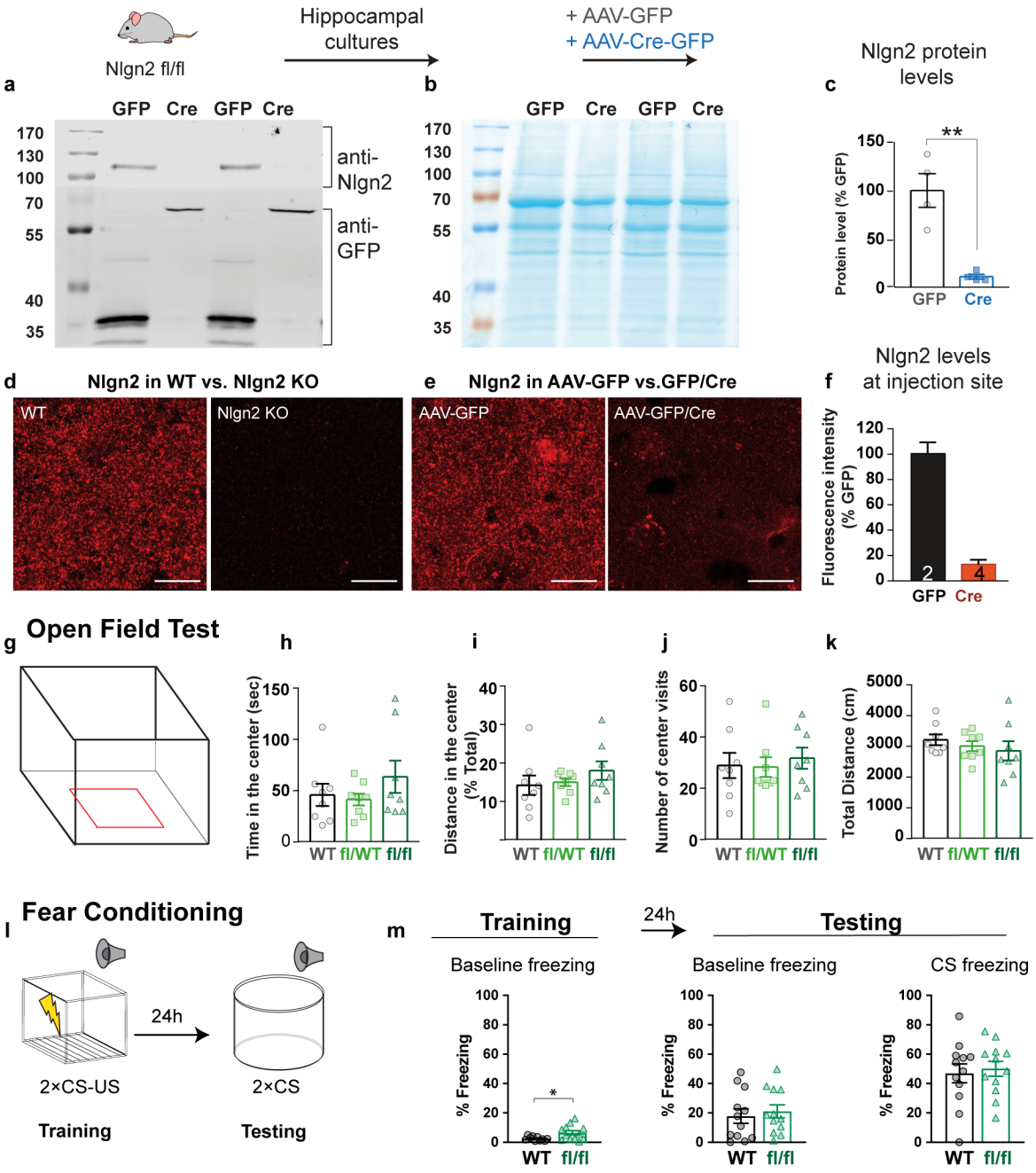

Figure 14 Validation of AAV-Cre mediated deletion of Nlgn2 and Nlgn2 fl/fl mice.
a-c Cultured HPC neurons isolated form Nlgn2 fl/fl mice were infected with AAV-Cre-GFP or AAV-GFP viruses and then lysed for western blot analysis after 14 days. **a**. A western blot showing lack of Nlgn2 immunolabelled bands in neurons infected with AAV-Cre-GFP but not with AAV-GFP virus. **b**. Total protein stain obtained from the membrane used for Nlgn2 immunoblotting. **c**. Quantification of the WB analysis. **d-f**. Immunohistochemical analysis of Nlgn2 protein expression in the BLA following stereotaxic delivery of AAV-Cre-GFP or AAV-GFP viruses. **d**. Confocal micrographs showing Nlgn2 immunolabelling in the BLA of WT (left) and Nlgn2 KO mice (right). **e**. Confocal micrographs showing Nlgn2 immunolabelling in the BLA of AAV-GFP (left) and AAV-Cre-GFP (right) injected mice. **f**. Quantification of Nlgn2 protein levels at the injection site of AAV-GFP and AAV-Cre-GFP injected mice. **g-k**. Behavioral assessment of mice that are homozygous (Nlgn2 fl/fl) or heterozygous (fl/WT) for the floxed Nlgn2 allele in using the OFT. **g**. A schematic of the OFT (center is outlined in red). **h**. Time spent exploring the center of the OFT. **i**. Distance travelled in the center

in the OFT. **j**. Number of visits to the center of the OFT. **k**. Total distance travelled during OFT exploration. **l-m**. Assessment of auditory FC in Nlgn2 fl/fl mice. **l**. A schematic of the FC paradigm. m. Percentage of time spent freezing during training baseline (left), testing baseline (middle) and CS presentation (right) in Nlgn2 fl/fl mice versus WT littermates: Training baseline freezing (left, N = 10-12, two tailed t-test p = 0.0270), Testing baseline freezing (middle, N = 12, two-tailed t-test p = 0.6374) and CS freezing (right, N = 12, two-tailed t-test p = 0.7056). Data in graphs **a**- **k** are adapted from (Cruces-Solis et al., 2021).

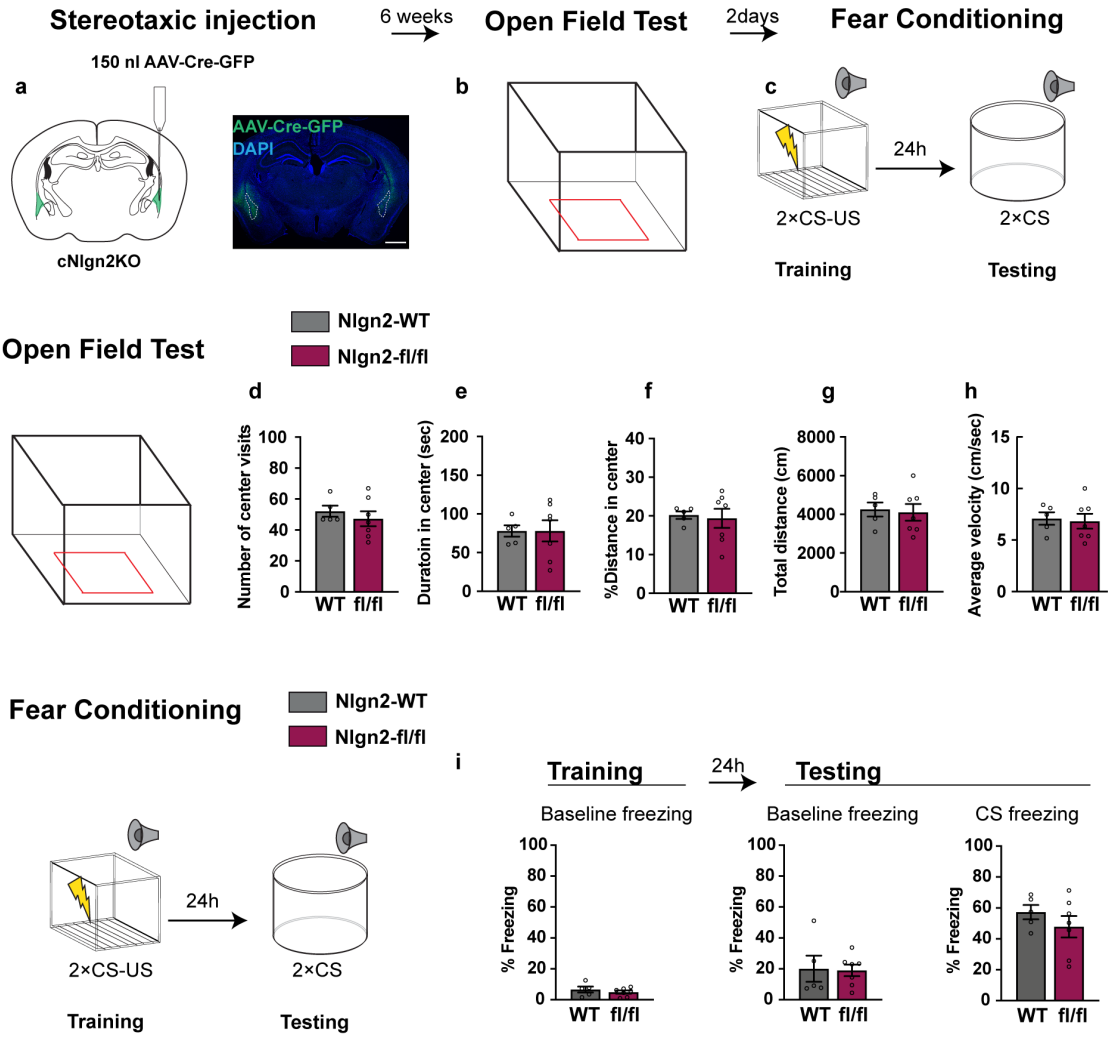

Figure 15 local deletion of Nlgn2 in the LA using a virus dose of 150 nl does not alter OFT and FC behaviors.

a. A schematic of the experimental procedure where 150 nl of AAV-Cre-GFP virus is injected in the LA of Nlgn2 fl/fl and WT mice (left) and a micrograph showing a coronal brain section obtained from an injected mouse labelled with antibody against GFP (green) and DAPI for nuclei (blue) to show placement of virus, scale bar 500 µm. **b**. A schematic of the open field (left) performed 6 weeks after injection along with example tracks obtained from WT and Nlgn2 fl/fl mice while exploring the open field (right). **c**. Number of visits to the center (N=5-7 mice, Mann-Whitney test p = 0.4293). **d**. Duration of time spent in the center (N = 5-7 mice, two-tailed t-test p = 0.9867). **e**. Percentage of distance travelled in the center from the total distance travelled (N = 5-7 mice, two tailed t-test p = 0.7967). **f**. Total distance travelled (N = 5-7, two-tailed t-test p = 0.8037). Average velocity (N = 5-7 two-tailed t-test p = 0.8039). **h**. A schematic of the FC paradigm performed 6 weeks+ 2 days after the stereotaxic injection in Nlgn2 fl/fl and WT mice. **i**. Percentage of time spend freezing by Nlgn2 fl/fl and WT mice injected with AAV-Cre-GFP virus: Training baseline freezing (left, N = 5-7, two-tailed t-test p = 0.4455), testing baseline freezing (middle, N = 5-7, two-tailed t-test p = 0.8954) and CS freezing

(right, N = 5-7, two-tailed p = 0.3318) measured during FC.

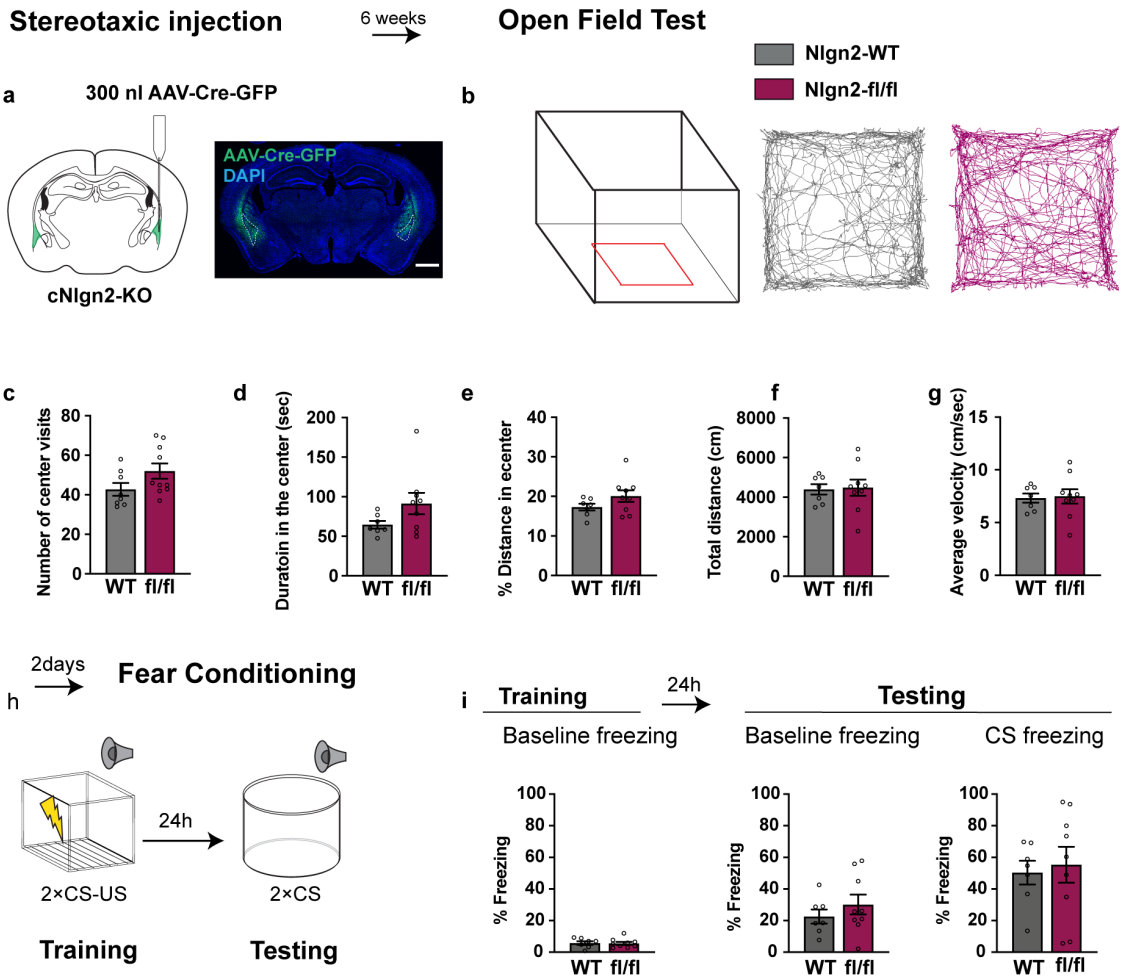

Figure 16 local deletion of Nlgn2 in the LA using a virus dose of 300 nl does not alter OFT and FC behaviors.
a. A schematic of the experimental procedure where 300 nl of AAV-Cre-GFP virus is injected in the LA of Nlgn2 fl/fl and WT mice (left) and a micrograph showing a coronal brain section obtained from an injected mouse labelled with antibody against GFP (green) and DAPI for nuclei (blue) to show placement of virus, scale bar 500 µm. **b**. A schematic of the OFT arena (left) along with example tracks obtained from WT and Nlgn2 fl/fl mice while exploring the open field (right) 6 weeks after injection. **c**. Number of visits to the center (N = 7-9 mice, two-tailed t-test p = 0.1080). **d**. Duration of time spent in the center (N = 7-9 mice, two-tailed t-test p = 0.1131). **e**. Percentage of distance travelled in the center from the total distance travelled (N = 7-9 mice, two tailed t-test p = 0.1561). f. Total distance travelled (N = 7-9, two-tailed t-test p = 0.8588). **g**. Average velocity (N = 7-9 two-tailed t-test p = 0.8595). **h**. A schematic of the FC paradigm performed 6 weeks+ 2 days after the stereotaxic injection in Nlgn2 fl/fl and WT mice. **i**. Percentage of time spend freezing by Nlgn2 fl/fl and WT mice injected with AAV-Cre-GFP virus: Training baseline freezing (left, N = 7-9, two-tailed t-test p = 0.9013), testing baseline freezing (middle, N = 7-9, two-tailed t-test p = 0.3674) and CS freezing (right, N = 7-9, two-tailed p = 0.7312) measured during FC.

3.2. Chapter 2: Cell specificity of Nlgn2 function

Being one of the first identified synaptic adhesion molecules that is specific to inhibitory synapses, Nlgn2 function in regulating inhibitory synaptic transmission has been a major research focus for years (Ali et al., 2020). A prominent finding from these studies demonstrated that Nlgn2 affects primarily perisomatic synapses made onto excitatory neurons such as pyramidal neurons in the CA1 (Poulopoulos et al., 2009) or the basal amygdala (Babaev et al., 2016). Furthermore, these studies suggested that Nlgn2 selectively functions at synapses made by fast-spiking PV INs onto PNs (Babaev et al., 2016; Gibson et al., 2009; Poulopoulos et al., 2009). However, to my knowledge, the questions of whether Nlgn2 functions at synapses formed onto inhibitory neurons or at synapses made by other inhibitory neuron subtypes other than PV INs were never systematically addressed.

To gain more insights onto the role of Nlgn2 in inhibitory neurons, I investigated the potential contribution of these neurons to the FC deficit and the circuit dysregulation observed in Nlgn2 KO mice. To achieve this, I followed 3 different approaches: 1) I investigated the activation of different amygdala IN subtypes during fear memory retrieval using cFos assay (co-performed with Lena Marth who contributed to the data collection and analysis). 2) I characterized FC in conditional Nlgn2 KO mice that lack Nlgn2 in specific inhibitory neuron subtypes and contrasted the outcome of Nlgn2 deletion on FC versus anxiety-like behaviors. 3) I explored the localization of Nlgn2 in inhibitory neuron synapses in two brain regions that are relevant for FC, namely the LA and the AuC using STED microscopy.

3.2.1. Amygdala inhibitory neurons are dysregulated in Nlgn2 KO mice during FC retrieval.

Amygdala inhibitory neurons were shown to largely control fear memory acquisition and expression by regulating the activity and plasticity of PNs in the BLA and by affecting other inhibitory neurons activity in the CeA (Ciocchi et al., 2010; Haubensak et al., 2010; Krabbe et al., 2019; Wolff et al., 2014). Having observed changes in cFos expression in the amygdala during FC retrieval in Nlgn2 KO mice, I aimed to analyze the contribution of major amygdala IN subtypes to these changes. To do this, amygdala slices were labeled using antibodies against different inhibitory neuron markers including PV, SOM, VIP and PKCδ in addition to cFos antibody. Subsequently, cFos expression by each of these neurons was quantified in the amygdala subregions where they are reported to be expressed using colocalization analysis. In this way, cFos expression by PV and VIP INs was quantified in

the LA and the BA, cFos expression by PKCδ INs was quantified in CeL, and cFos expression by SOM neurons was quantified in the four amygdala subregions.

In the LA, analysis of cFos expression by PV INs revealed a genotype dependent difference in cFos activation using two-way ANOVA (figure 17, a and b) with no significant change in the total number of detected PV INs (figure 17, c). This indicated that PV INs were differentially activated in the LA of Nlgn2 KO mice during FC retrieval irrespective of training. SOM neurons, however, did not show a change in activation due to genotype or training during FC retrieval and neither did their total number detected in this region (figure 17, d-f). Intriguingly, analysis of cFos expression by VIP INs revealed a significant interaction between genotype and training using two-way ANOVA, indicating that exposure to FC training affects activation of LA-VIP INs during FC retrieval in Nlgn2 KO mice differently to WT mice (figure 17, g and h). Although Tukey's pairwise comparisons analysis did not show a significant increase in cFos activation in LA-VIP INs between the WT-FC and Nlgn2 KO-FC groups, a trend towards increased activation in the latter group was present (figure 17, h). The total number of detected VIP IN cell bodies in the LA was not significantly different across experimental groups (figure 17, i).

In the BA, cFos activation of PV, SOM and VIP neurons did not vary significantly based on genotype or training as revealed by two-way ANOVA (figure 18). However, it was interesting to see a distinct pattern of activation in BA-VIP INs than the one observed in the LA. Where in the LA, VIP INs showed a trend towards reduced activation in WT-FC compared to WT-Ctrl mice, LA-VIP INs in Nlgn2 KO-Ctrl showed lower activation than in WT-Ctrl mice at basal level but their activation in the Nlgn2-KO-FC group was increased (figure 17, h). In contrast, the activity of BA-VIP INs was upregulated in the FC group of WT but not Nlgn2 KO mice (figure 18, h). Similarly to the LA, the number of detected cells of each of PV, SOM and VIP INs was not significantly different in the BA between genotypes or conditions (figure 18, c, f and i).

In the CeA, where cFos expression was analyzed for SOM and PKCδ neurons, the only observed difference was a significant main effect of genotype in the activation of SOM neurons in the CeM with no change in the number of these cells in Nlgn2 KO mice (figure 19, g- i).

3.2.2. Cell-type specific and circuit specific effects of Nlgn2 in regulating emotional circuits

The detected changes in the activation of amygdala inhibitory neurons in Nlgn2 KO mice during FC retrieval indicated an effect of Nlgn2 on the function of inhibitory neurons taking part in controlling this circuit and potentially mediating the observed deficit. To test whether Nlgn2 effect on inhibitory neurons plays a causal role in the FC deficit in a cell-autonomous manner, we generated cell-specific cNlgn2 KO mice by crossing Nlgn2 fl/fl mice with cell-specific Cre driver lines including PV-Cre, SOM-IRES-Cre, VIP-IRES-Cre and CAMKII-Cre where the expression of the Cre recombinase enzyme is under the control of cell-specific promoters. Subsequently, I characterized FC behavior in offspring mice with the following genotypes: PV-Cre:Nlgn2-fl/fl versus PV-Cre:Nlgn2-WT, SOM-IRES-Cre:Nlgn2-fl/fl versus SOM-IRES-Cre:Nlgn2-WT, VIP-IRES-Cre:Nlgn2-fl/fl versus VIP-IRES-Cre:Nlgn2-WT and CAMKII-Cre:Nlgn2-fl/fl versus CAMKII-Cre:Nlgn2-WT.

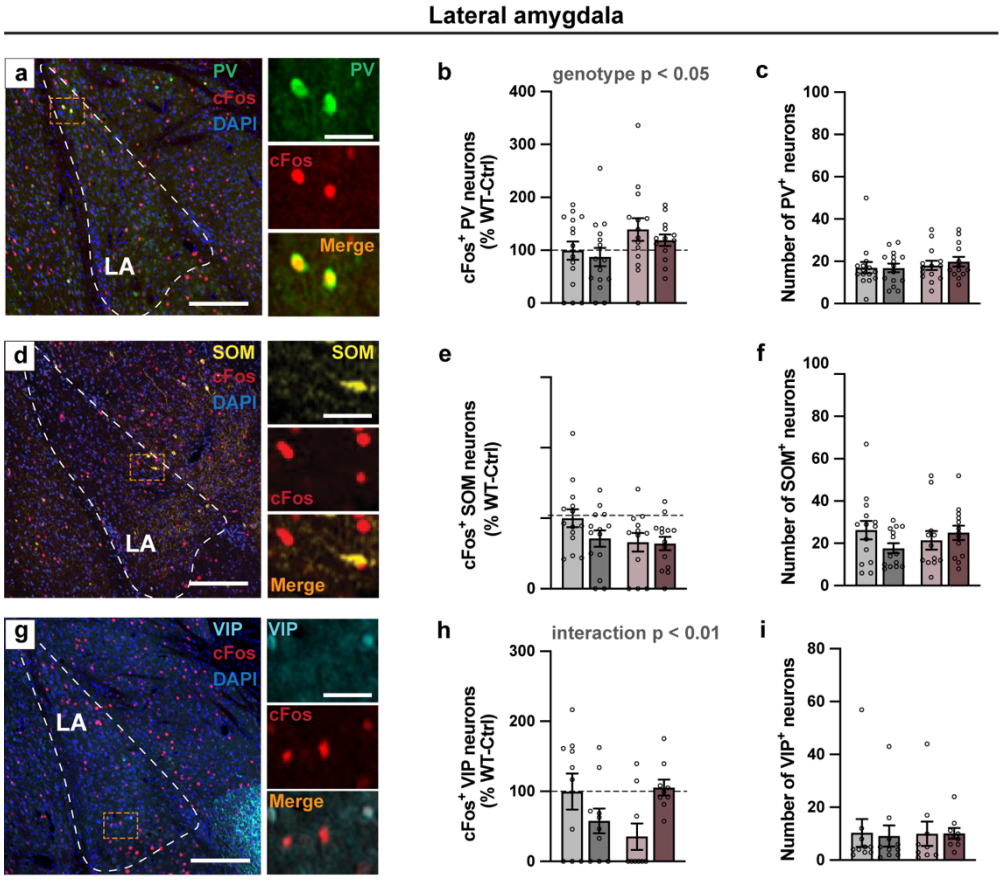

Figure 17 cFos expression by PV and VIP INs is altered in the LA of Nlgn2 KO mice during FC retrieval.
a, **d** and **g**. 20x confocal micrographs showing overview of the LA in brain slices immunolabelled with antibodies against PV (**a**), SOM (**d**) and VIP (**g**) in addition to cFos and DAPI labelling (left), scalebar 200 µm. The region outlined with an orange dashed box is shown on the right with higher magnification to show individual co-labelled cells across different channels (top to bottom) scalebar 40µm. **b**, **e** and **h**. Normalized percentage of cells that express PV(**b**), SOM (**e**) or VIP (**h**) and are

co-labelled with cFos among the total number of cells expressing each of these markers. The resulting percentage value was calculated as a percentage of the average percentage value obtained from the WT-Ctrl group. **b**. Normalized percentage of PV^+ cells co-labelled with cFos among total number of detected PV^+ cells (N = 13-15, two-way ANOVA; Genotype: F (1, 53) = 4.158, p = 0.0464; Training: F (1, 53) = 0.8561, p = 0.3590; Interaction: F (1, 53) = 0.05163, p = 0.8211). **c**. Total number of detected PV^+ cells per each experimental group (N = 13-15, two-way ANOVA; Genotype: F (1, 53) = 0.7524, p = 0.3896; Training: F (1, 53) = 0.1165, p = 0.7342; Interaction: F (1, 53) = 0.1595, p = 0.6912). **e**. Normalized percentage of SOM^+ cells co-labelled with cFos among total number of detected SOM^+ cells (N = 12-14, two-way ANOVA; Genotype: F (1, 50) = 3.004, p = 0.0892; Training: F (1, 50) = 1.654, p = 0.2044; Interaction: F (1, 50) = 1.295, p = 0.2605). **f**. Total number of detected SOM^+ cells per each experimental group (N = 12-14, two-way ANOVA; Genotype: F (1, 50) = 0.1480, p = 0.7021; Training: F (1, 50) = 0.4317, p = 0.5142; Interaction: F (1, 50) = 2.923, p = 0.0935). **h**. Normalized percentage of VIP^+ cells co-labelled with cFos among total number of detected VIP^+ cells (N = 9-10, two-way ANOVA; Genotype: F (1, 34) = 0.1834, p = 0.6711; Training: F (1, 34) = 0.5277, p = 0.4725; Interaction: F (1, 34) = 8.260, p = 0.0069). **i**. Total number of detected VIP^+ cells per each experimental group (N = 9-10, two-way ANOVA; Genotype: F (1, 34) = 0.007536, p = 0.9313; Training: F (1, 34) = 0.01594, p = 0.9003; Interaction: F (1, 34) = 0.02491, p = 0.8755).

Another question I wanted to address with this experiment is whether Nlgn2 regulates FC and anxiety-like behaviors through effects on the same neuron types. Therefore, analysis of anxiety-like behavior using the OFT in cell-type specific cNlgn2 KO mice was performed prior to FC.

Interestingly, deletion of Nlgn2 from PV neurons did not affect anxiety-like behavior with all parameters in the open field center in PV-Cre:Nlgn2-fl/fl mice being comparable to PV-Cre-Nlgn2-WT mice, including number of visits, duration, and distance in the center (figure 20, c, d and e). Additionally, locomotor activity parameters in the OFT were also comparable between genotypes including the total distance traveled and the average velocity (figure 20, f and g). Similarly, FC retrieval also remained unchanged in PV-Cre:Nlgn2-fl/fl mice as shown by measuring % CS freezing after FC (figure 20, i, CS freezing). Baseline freezing during training and testing were also not different between genotypes (figure 20, i, training and testing baseline freezing). These findings exclude a role of Nlgn2 mediated synaptic inhibition onto PV neurons in controlling these behaviors and thereby the relevant deficits observed in constitutive Nlgn2 KO mice.

By characterizing OFT and FC behaviors in SOM-IRES-Cre:Nlgn2-fl/fl mice, interesting changes were observed. In the OFT, SOM-IRES-Cre:Nlgn2-fl/fl mice showed a small, but significant increase in the number of visits to the open field center compared to SOM-IRES-Cre:Nlgn2-WT mice (figure 21, c). However, duration and percentage of distance spent in the center were not changed (figure 21, d and e). In addition, the change in center visits was accompanied by a significant increase in the total distance travelled and the average velocity (figure 21, f and g). This reflects hyperactivity in the OFT that might be indicative of

a locomotor or exploratory phenotype rather than an alteration in anxiety-like behavior, since the duration and distance in the center were not significantly increased.

In line with the observed hyperactivity in the OFT, SOM-IRES-Cre:Nlgn2-fl/fl mice showed significant reduction in conditioned and unconditioned freezing during FC (figure 21, i), with CS freezing on the testing day in addition to baseline freezing on training and testing days being significantly reduced. However, it is not possible to distinguish whether this lack of freezing results from altered fear learning, locomotion and /or exploratory behavior.

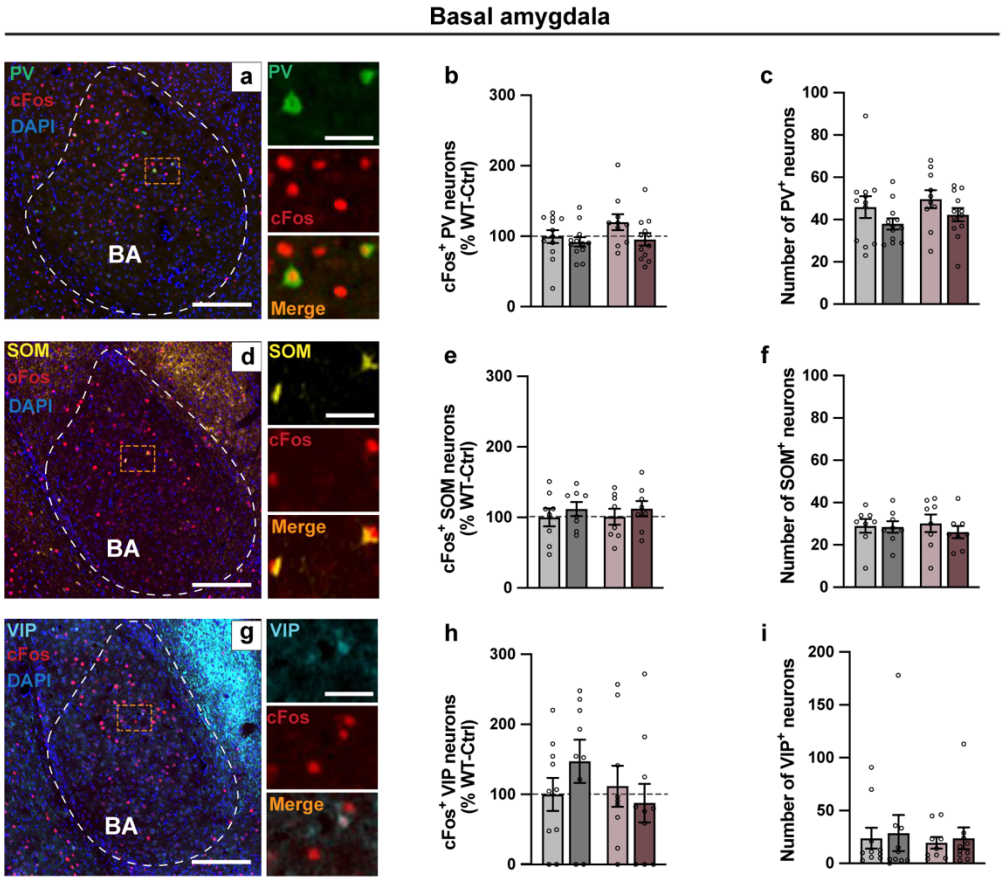

Figure 18 No significant changes of inhibitory neuron activity in the BA during FC retrieval. **a**, **d** and g. 20x confocal micrographs showing overview of the BA in brain slices immunolabelled with antibodies against PV (**a**), SOM (**b**) and VIP (**c**) in addition to cFos and DAPI labelling (left), scalebar 200 µm. The region outlined with an orange dashed box is shown on the right with higher magnification to show individual co-labelled cells across different channels (top to bottom), scalebar 40µm. **b**. Normalized percentage of PV^+ cells co-labelled with cFos among total number of detected PV^+ cells (N = 10-12, two-way ANOVA; Genotype: F (1, 42) = 1.762, p = 0.1915; Training: F (1, 42) = 3.130, p = 0.0841; Interaction: F (1, 42) = 0.8861, p = 0.3573). **c**. Total number of detected PV^+ cells per each experimental group (N=10-12, two-way ANOVA; Genotype: F (1, 34) = 1.066, p = 0.3077; Training: F (1, 34) = 3.838, p = 0.0568; Interaction: F (1, 34) = 0.005690, p = 0.9402). **e**. Normalized percentage of SOM^+ cells co-labelled with cFos among total number of detected SOM^+ cells (N = 8, two-way ANOVA; Genotype: F (1, 28) = 0.004685, p = 0.9459; Training: F (1, 28) = 1.049, p = 0.3146; Interaction: F (1, 28) = 0.0005851, p = 0.9809). **f**. Total number of detected SOM^+ cells per each experimental group (N = 8, two-way ANOVA; Genotype: F (1, 28) = 0.02923, p = 0.8655; Training: F (1, 28) = 0.4931, p = 0.4883; Interaction: F (1, 28) = 0.3030, p = 0.5864). **h**. Normalized percentage of VIP^+ cells co-labelled with cFos among total number of detected VIP^+ cells

(N = 9-10, two-way ANOVA; Genotype: F (1, 34) = 0.7382, p = 0.3963; Training: F (1, 34) = 0.1752, p = 0.6782; Interaction: F (1, 34) = 1.633, p = 0.2099). **i**. Total number of detected VIP$^+$ cells per each experimental group (N = 9-10, two-way ANOVA; Genotype: F (1, 34) = 0.1583, p = 0.6932; Training: F (1, 34) = 0.1516, p = 0.6994; Interaction: F (1, 34) = 0.0006419, p = 0.9799).

In VIP-IRES-Cre:Nlgn2-fl/fl mice, the behavior in the OFT was comparable to WT littermates, as the number of visits, duration and distance were unchanged, as were the total distance and average velocity (figure 22, c-g). This indicated that Nlgn2 mediated inhibition in VIP neurons, similar to PV neurons, was not required for the exploratory behavior of the mice under anxiogenic conditions, and that the anxiety-like behavior in

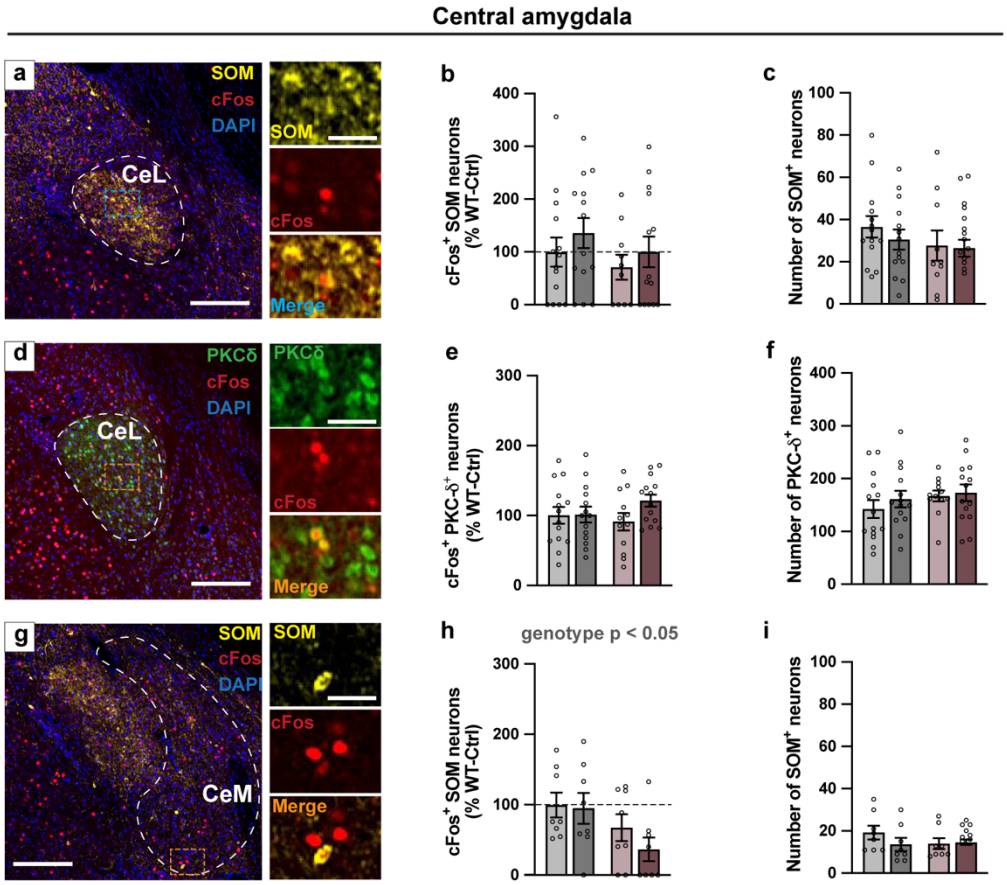

Figure 19 Dysregulated activation of SOM neurons in the CeM of Nlgn2 KO mice during FC retrieval.
a, **d** and g. 20x confocal micrographs showing overview of the CeA in brain slices immunolabelled with antibodies against SOM (**a** in CeL and **g** in CeM) or PKCδ (**d**) in addition to cFos and DAPI labelling (left) scalebar 200 µm. The region outlined with an orange dashed box is shown on the right with higher magnification to show individual co-labelled cells across different channels (top to bottom) scalebar 40µm. **b**. Normalized percentage of SOM$^+$ cells co-labelled with cFos among total number of detected SOM$^+$ cells in the CeL (N = 10-14, two-way ANOVA; Genotype: F (1, 48) = 1.315, p = 0.2571; Training: F (1, 48) = 1.347, p = 0.2515; Interaction: F (1, 48) = 0.01446, p = 0.9048). **c**. Total number of detected SOM$^+$ cells per each experimental group in the CeL (N = 10-14, two-way ANOVA; Genotype: F (1, 48) = 1.562, p = 0.2174; Training: F (1, 48) = 0.4844, p = 0.4898; Interaction: F (1, 48) = 0.2125, p = 6469). **e**. Normalized percentage of PKCδ $^+$ cells co-labelled with cFos among total number of detected PKCδ cells (N = 12-14, two-way ANOVA; Genotype: F (1, 50) = 0.2366, p = 0.6288; Training: F (1, 50) = 1.928, p = 0.1712; Interaction: F (1, 50) = 1.667, p = 0.2026). **f**. Total number of detected PKCδ$^+$ cells per each experimental group in the CeL (N = 12-14, two-way ANOVA; Genotype: F (1, 50) = 1.494, p = 0.2273; Training: F (1, 50) = 0.6793, p = 0.1437; Interaction:

F (1, 50) = 0.1716, p = 0.6805). **h**. Normalized percentage of SOM$^+$ cells co-labelled with cFos among total number of detected SOM$^+$ cells in the CeM (N = 8, two-way ANOVA; Genotype: F (1, 28) = 5.706, p = 0.0239; Training: F (1, 28) = 0.8874, p = 0.3542; Interaction: F (1, 28) = 0.4734, p = 0.4971). **h**. Total number of detected SOM$^+$ cells per each experimental group in the CeM (N = 8, two-way ANOVA; Genotype: F (1, 28) = 0.6391, p = 0.4308; Training: F (1, 28) = 0.8836, p = 0.3553; Interaction: F (1, 28) = 1.382, p = 0.2497).

constitutive KO mice did not result from lack of Nlgn2 in these neurons. However, the picture was different when the FC behavior was assessed in VIP-IRES-Cre:Nlgn2-fl/fl mice, since they showed a significant reduction in CS freezing compared to VIP-IRES-Cre:Nlgn2-WT mice (figure 22, I, CS freezing). In contrast, their baseline freezing during testing and training

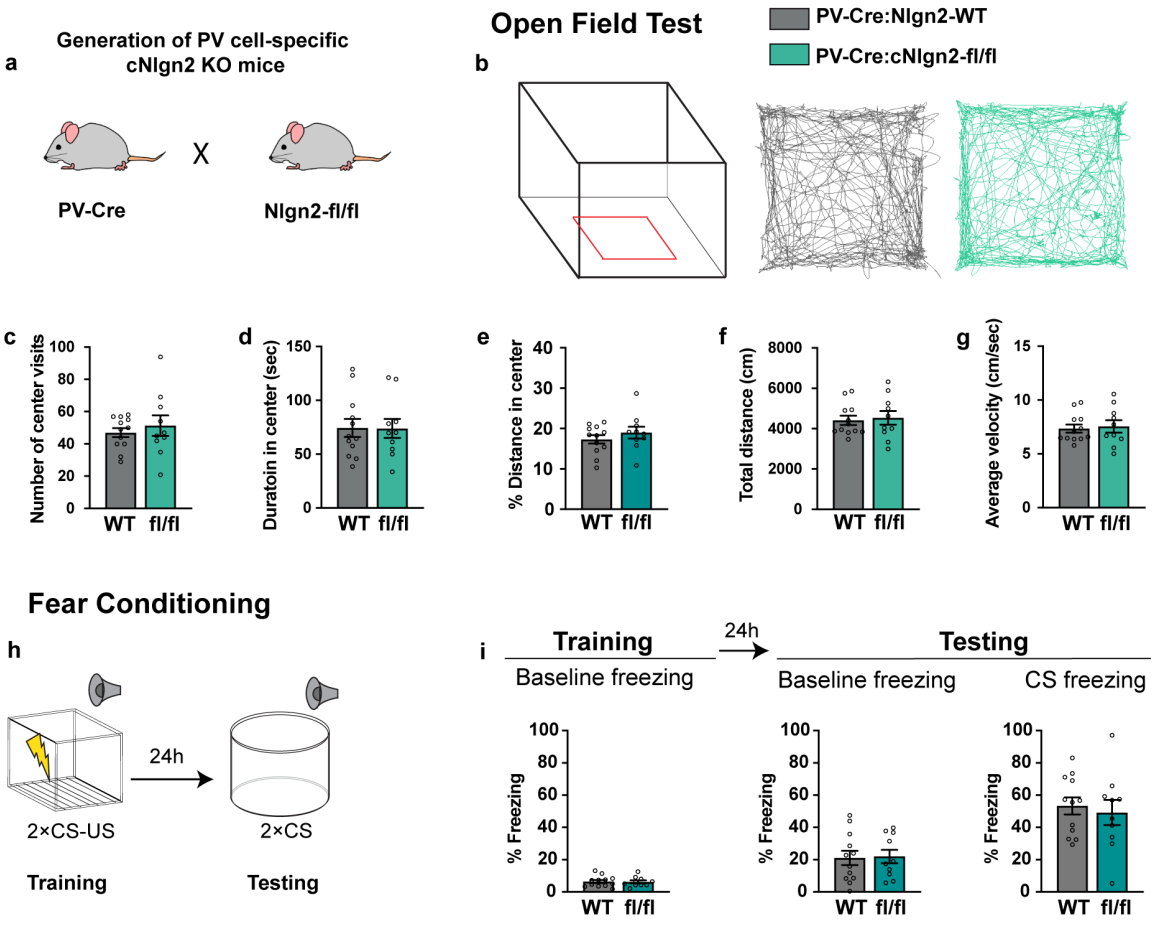

Figure 20 Normal exploratory behavior and FC in mice lacking Nlgn2 from PV neurons .
a. A schematic showing the breeding scheme used to generate PV neuron-specific cNlgn2 KO mice. **b**. a schematic of the OFT arena with the center outlined with a red rectangle (left) along with example tracks obtained from PV-Cre:Nlgn2 WT and PV-Cre:Nlgn2 fl/fl mice while exploring the OFT arena. **c** Number of visits to the center, N = 10-12, two-tailed t-test p = 0.5126. **d**. Duration in the center, N = 10-12, p = 0.9668. **d**. Percentage of distance in the center from the total distance travelled, N = 10-12, two-tailed t-test p = 0.3412. **e**. Total distance travelled in the OFT, N = 10-12, two-tailed t-test p = 0.7633. **f**. Average velocity during OFT, N = 10-12, two-tailed t-test p = 0.7628. **g**. A schematic of the FC paradigm. **h**. Percentage of time spent freezing during 2 min baseline on training day (left, N = 10-12, two tailed t-test p = 0.8960), baseline freezing on the testing day (middle, N = 10-12, two tailed t-test p = 0.8929) and CS freezing on testing day (right, N = 10-12, Two-tailed t-test p = 0.6567).

remained unchanged. Interestingly, the reduction in CS freezing in VIP-IRES-Cre:Nlgn2-fl/fl mice did not fully recapitulate the deficit observed in Nlgn2 KO mice which was stronger. However, these results showed that lack of Nlgn2 from VIP neurons is causally implicated in the FC deficit observed in Nlgn2 KO mice.

Finally, to compare the results I obtained by deleting Nlgn2 from INs with the previously reported effect on excitatory neurons, I also characterized the OFT and FC behaviors in mice lacking Nlgn2 from CAMKII excitatory neurons (CAMKII-Cre:Nlgn2-fl/fl versus WT littermates. In complete overlap with the observation made form constitutive Nlgn2 KO mice, CAMKII-Cre:Nlgn2-fl/fl mice showed also significant reduction in all OFT parameters (figure 23, c-g) compared to CAMKII-Cre:Nlgn2-WT littermates. This shows that the anxiety-like

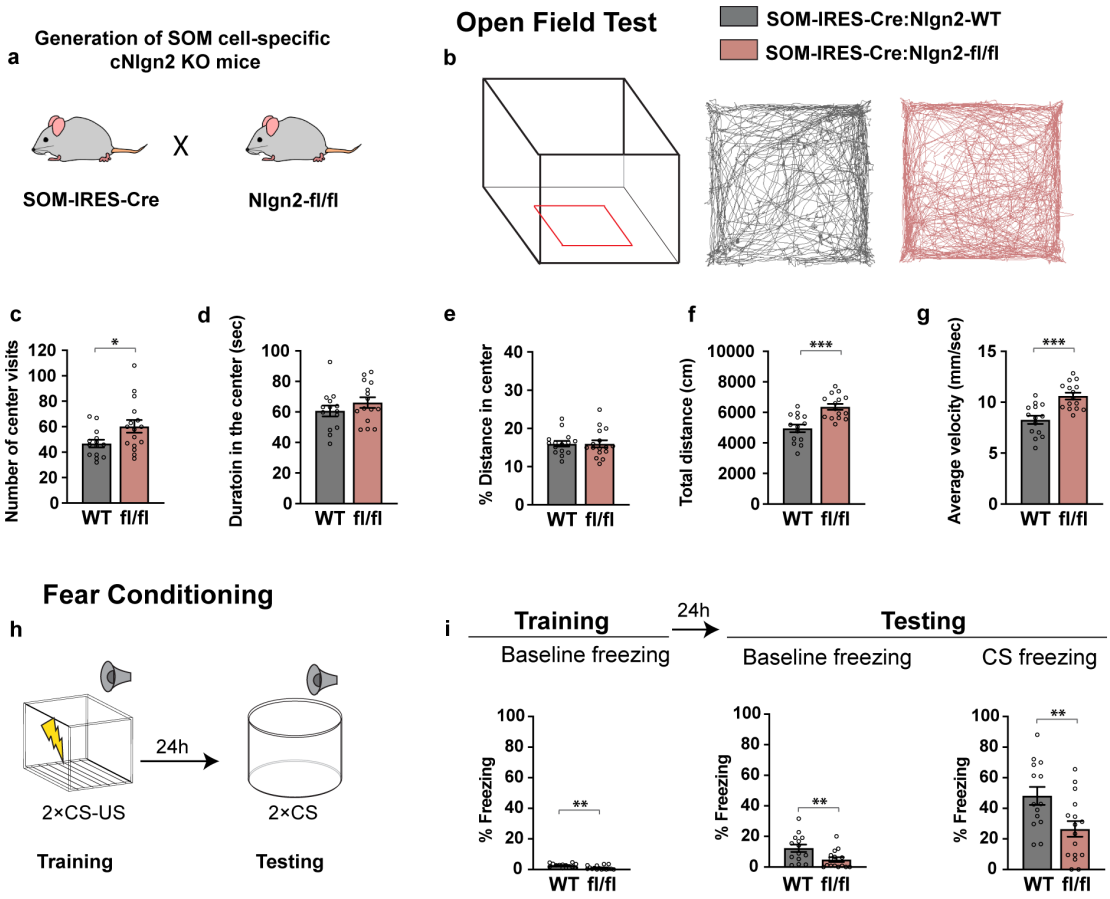

Figure 21 Hyperactivity and reduced freezing in mice lacking Nlgn2 from SOM neurons. **a**. A schematic showing the breeding scheme used to generate SOM neuron-specific cNlgn2 KO mice. **b**. A schematic of the OFT arena with the center outlined with a red rectangle (left) along with example tracks obtained from SOM-IRES-Cre:Nlgn2 WT and SOM-IRES-Cre:Nlgn2 fl/fl mice while exploring the OFT arena. **c** Number of visits to the center, N = 14-16, two-tailed t-test p = 0.0317. **d**. Duration in the center, N = 14-15, p = 0.2726. **d**. Percentage of distance in the center from the total distance travelled, N = 14-16, two-tailed t-test p = 0.9956. **e**. Total distance travelled in the OFT, N = 14-15, two-tailed t-test p = 0.0001. **f**. Average velocity during OFT, N = 14-15, two-tailed t-test p = 0.0001. **g**. A schematic of the FC paradigm. **h**. Percentage of time spent freezing during 2 min

baseline on training day (left, 13-16, Mann Whitney test p = 0.0017), baseline freezing on the testing day (N = 14-15, two tailed t-test p = 0.0056) and CS freezing on testing day (N = 14-16, Two-tailed t-test p = 0.0098).

behavior observed in the Nlgn2 KO mice is largely driven by the lack of Nlgn2 from CAMKII neurons selectively. In contrast, FC did not seem to be significantly altered in these mice as CS freezing levels in CAMKII-Cre:Nlgn2-fl/fl mice were comparable to that of CAMKII-Cre:Nlgn2-WT mice (figure 23, i, CS freezing). Surprisingly, these results revealed a lack of effect of Nlgn2 in CAMKII neurons in regulating the FC circuit. Another interesting finding obtained from this experiment, was that CAMKII-Cre:Nlgn2-fl/fl mice showed significantly increased training baseline (figure 23, I, training: baseline freezing) compared to WT littermates, which is in line with the observation made earlier in Nlgn2 KO mice (figure 8).

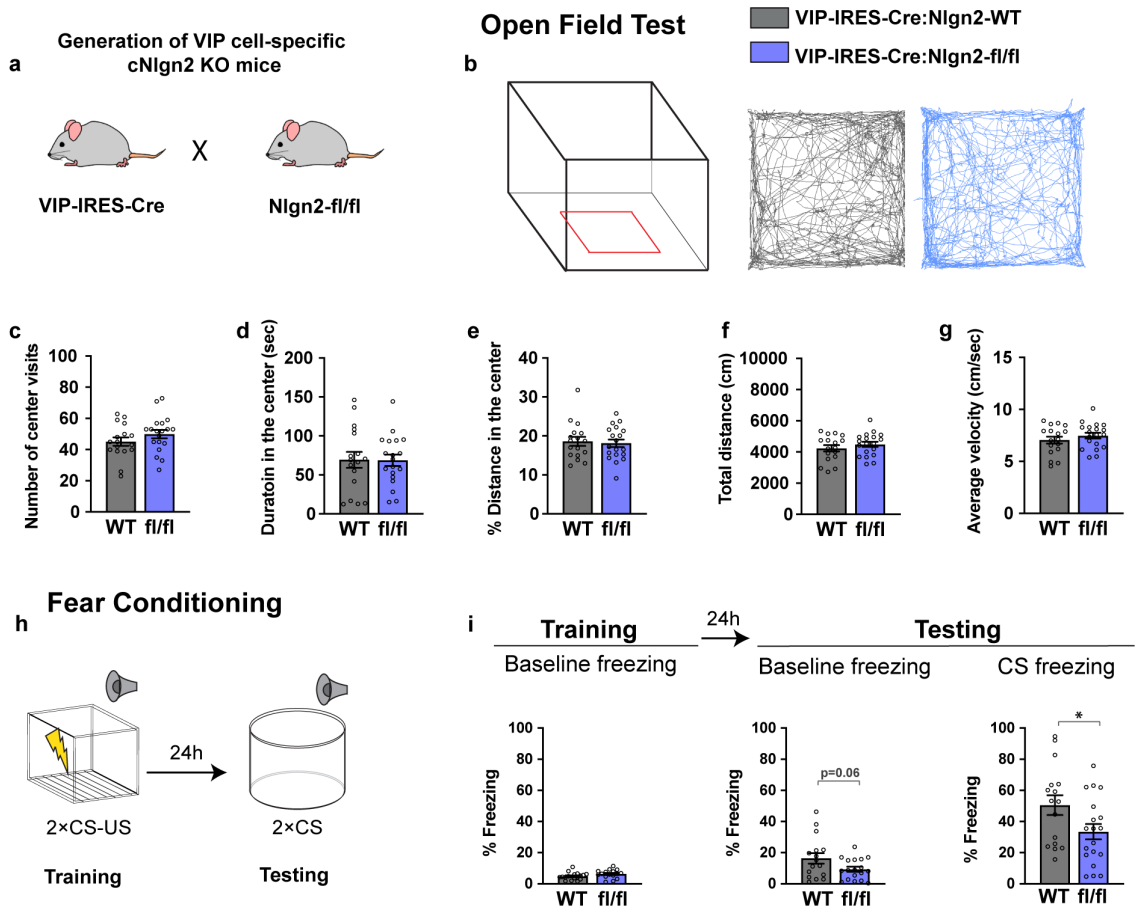

Figure 22 Normal exploratory behavior and reduced FC retrieval in mice lacking Nlgn2 from VIP neurons.
a. A schematic showing the breeding scheme used to generate VIP neuron-specific cNlgn2 KO mice. **b**. a schematic of the OFT arena with the center outlined with a red rectangle (left) along with example tracks obtained from VIP-IRES-Cre:Nlgn2 WT and VIP-IRES-Cre:Nlgn2 fl/fl mice while exploring the OFT arena. **c** Number of visits to the center, N= 17-19, two-tailed t-test p = 0.2118. **d**. Duration in the center, N = 17-19, p = 0.9600. **d**. Percentage of distance in the center from the total distance travelled, N = 17-19, two-tailed t-test p = 0.7549. **e**. Total distance travelled in the OFT, N = 17-19, two-tailed t-test p = 0.3365. f. Average velocity during OFT, N = 17-19, two-tailed t-test p = 0.3375. **g**. a schematic of the FC paradigm. **h**. Percentage of time spent freezing during 2 min baseline on

training day (left, N = 16-19, two-tailed t-test p = 0.0403), baseline freezing on the testing day (N = 16-17, two tailed t-test p = 0.1115) and CS freezing on testing day (N = 16-18, two-tailed t-test p = 0.0600).

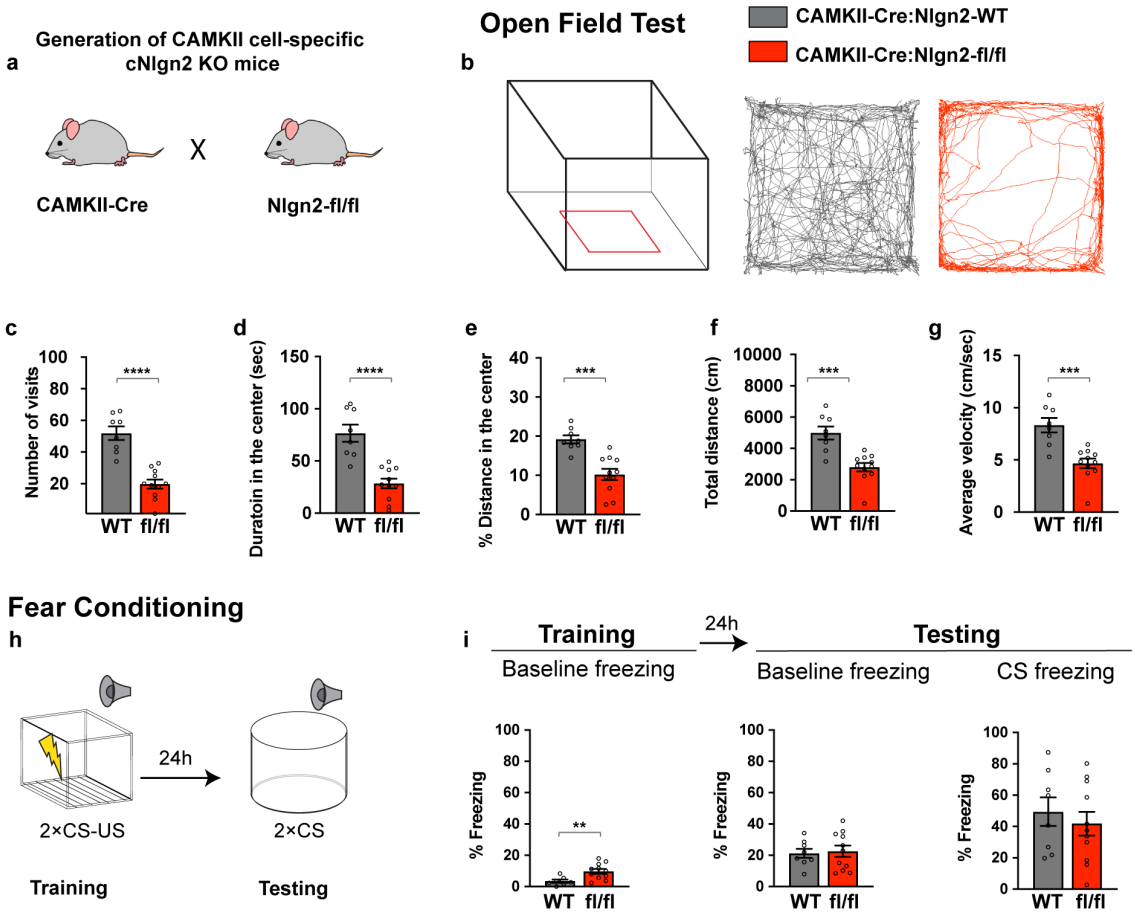

Figure 23 Robust anxiety-like behavior and normal FC in mice lacking Nlgn2 from CAMKII neurons.
a schematic showing the breeding scheme used to generate CAMKII neuron-specific cNlgn2 KO mice. **b**. a schematic of the OFT arena with the center outlined with a red rectangle (left) along with example tracks obtained from WT and cNlgn2 KO mice while exploring the OFT. **c**. Number of visits to the center, N= 8-10, two-tailed t-test p < 0.0001. **d**. Duration in the center, N = 8-11, two-tailed t-test p < 0.0001. **d**. Percentage of distance in the center from the total distance travelled, N = 8-11, two-tailed t-test p = 0.0002. **e**. Total distance travelled in the OFT, N = 8-11, two-tailed t-test p = 0.0003. **f**. Average velocity during OFT, N = 8-11, two-tailed t-test p = 0.0003. **g**. a schematic of the FC paradigm. **h**. Percentage of time spent freezing during 2 min baseline on training day (left, 7-11, two-tailed t-test p = 0.0085), baseline freezing on the testing day (N = 8-11, two tailed t-test p = 0.7951) and CS freezing on testing day (N = 8-11, two-tailed t-test p = 0.5266).

3.2.3. Nlgn2 is present on GABAergic synapses formed by and onto inhibitory neurons.

The results obtained so far from cell specific Nlgn2 KO mice indicate that Nlgn2 is expressed by inhibitory neurons, specifically SOM and VIP neurons, and is involved in regulating FC and OFT behaviors. However, to my knowledge, the protein expression of Nlgn2 by

inhibitory neurons has not been investigated before. Furthermore, the current knowledge about Nlgn2 highlights its role in synapses made by fast spiking PV IN onto PNs, but whether synapses made by other inhibitory neurons subtypes could contain Nlgn2 is also a question that was never directly addressed. To further understand the role of Nlgn2 expressed by inhibitory neurons in the context of the FC circuit, I investigated the localization of Nlgn2 in synapses made onto or from SOM, PV and VIP neurons in the LA and AuC, being the regions in the FC circuit where I observed robust learning specific changes during FC retrieval. For the purpose of this experiment, we crossed inhibitory neuron- specific Cre driver lines, namely, PV-Cre, SOM-IRES-Cre and VIP-IRES-Cre with Ai32 mice that express the fusion protein comprising channelrhodopsin2 and enhanced yellow fluorescent protein (ChR2-EYFP) following exposure to Cre recombinase. The resulting progeny of mice that carry the Cre recombinase and the Ai32 alleles therefore would show inhibitory neuron-specific expression of Chr2-EYFP. These mice were next used for qualitative IHC analysis of Nlgn2 localization in inhibitory neuron synapses using stimulated emission depletion (STED) that provided the ability to visualize synapses with superresolution. This experiment was done through a collaboration with the lab of Dr. Katrin Willig in the Max Planck Institute for Multidisciplinary Sciences, Göttingen. To this end, methanol-fixed slices obtained from PV-Cre:ChR2-EYFP, SOM-IRES-Cre:ChR2-EYFP and VIP-IRES-Cre: ChR2-EYFP mice were immunolabelled for Nlgn2, which is localized to the inhibitory postsynapse, and vGAT that localizes to the presynaptic site of the inhibitory synapse (McIntire et al., 1997). Taking advantage of the nanoscale resolution provided by the 2 color STED method, I detected Nlgn2$^+$ synapses onto the EYFP$^+$ processes (the latter visualized with the confocal mode) in all of the three mouse lines in the LA and the AuC (figure 24, 26 and 28). Since the EYFP encoding gene is fused in the ai32 mouse with ChR2, EYFP expression thereby is expected to localize to the cellular membrane, but with no selective localization to dendrites versus axon terminals. This was also shown by overview images taken from the LA and AuC in PV-Cre:ChR2-EYFP, SOM-IRES-Cre:ChR2-EYFP and VIP-IRES-Cre: ChR2-EYFP mice that showed dense EYFP labelling of cell bodies and processes of the respective cell types (a and d in figures 24, 26 and 28). Since using classical markers to label axons versus dendrites was not compatible with the fixation method used for Nlgn2 staining, I relied on the relative positions of Nlgn2 puncta and vGAT clusters to the EYFP$^+$ processes to infer the configuration of the synapse, i.e., whether it is formed by or onto the EYFP$^+$ processes. Using this method, I detected putative synapses where Nlgn2 puncta where more distal in relation to EYFP$^+$ processes than vGAT$^+$ structures (b, c, g and h in figures 25, 27 and 29), indicating that these synapses are likely made by EYFP$^+$ synaptic terminals belonging to each of PV, SOM and VIP neurons and contain Nlgn2 on their post synaptic site. This implies that Nlgn2 is potentially present in

synapses made by all three inhibitory neuron subtypes, and not just on synapses made by fast spiking PV INs, at least in the LA and the AuC.

On the other hand, synapses where Nlgn2 puncta were in closer proximity to EYFP$^+$ processes than vGAT were also detected (d, e, i and j in figures 25, 27 and 29), indicating that these synapses are likely formed onto PV, SOM and VIP inhibitory neurons and they contain Nlgn2 on their postsynapses.

Having detected Nlgn2 at GABAergic synapses formed onto SOM and VIP inhibitory neurons in the LA and AuC along with the behavioral phenotypes observed in mice lacking Nlgn2 in these neurons support the notion that Nlgn2 is expressed by these neurons and is relevant for their function in regulating behavioral circuits.

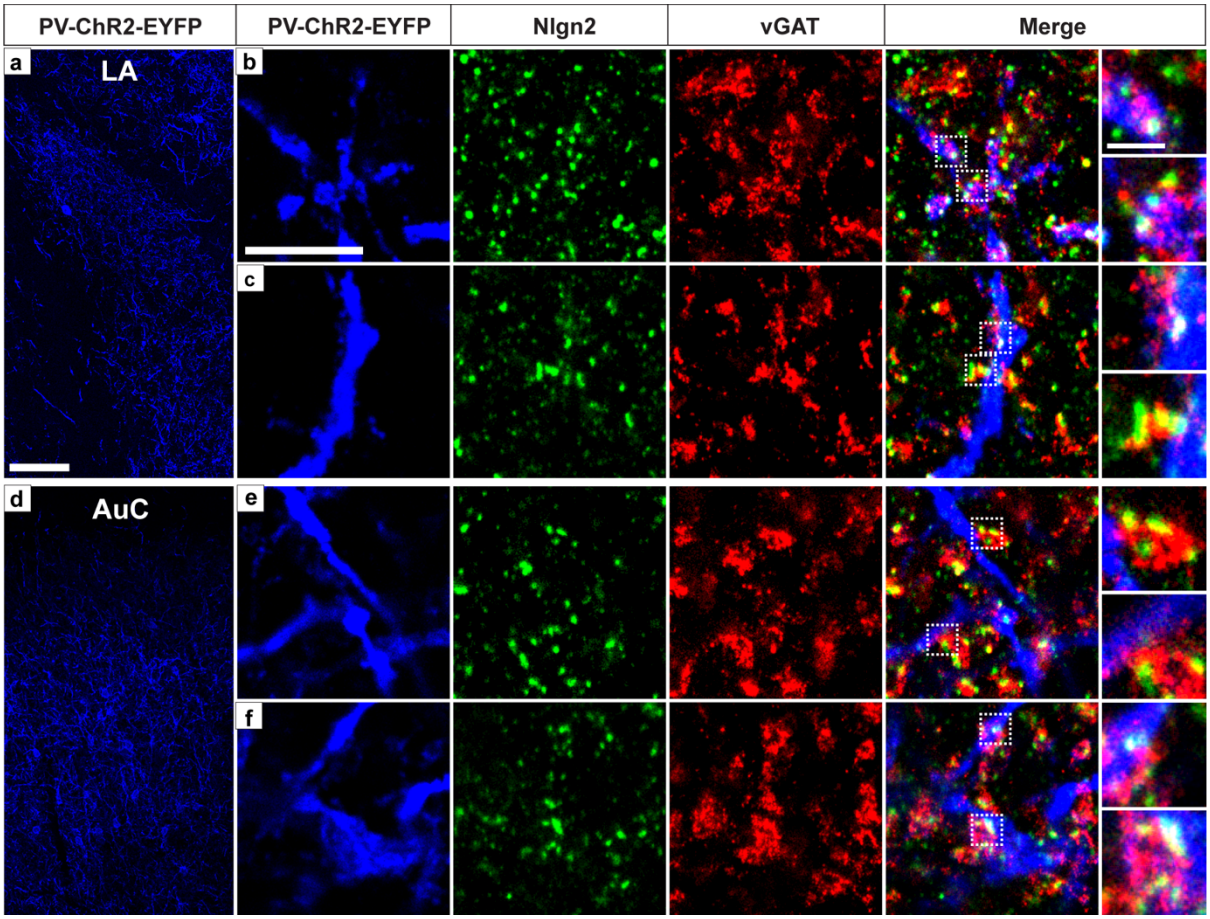

Figure 24 Nlgn2 is present on synapses formed by and onto PV INs.
a and **d**. Confocal micrograph showing EYFP fluorescence by PV INs in the LA (**a**) and the AuC (d) in methanol-fixed brain slices obtained from PV:Cre- ChR-EYFP mouse, scale bar 100 µm. **b**, **c**, **e** and **f**. confocal and STED micrographs taken from the LA (**b** and **c**) and the AuC (**e** and **f**) and are showing EYFP$^+$ PV IN processes (blue, confocal), Nlgn2 (green, STED) and vGAT (red, STED) immunolabelling, scale bar 5 µm. Dotted rectangles in the merge image are shown in higher detail on the right and they outline putative Nlgn2$^+$ synapses from or onto PV INs, scale bar 1 µm. The images presented in **b** and **e** show Nlgn2$^+$ synapses made from PV INs inferred by vGAT clusters being in closer proximity to EYFP$^+$ processes than their colocalized Nlgn2 puncta. The images

presented in **c** and **f** show Nlgn2^{+} synapses made onto PV INs inferred by Nlgn2 puncta being in closer proximity to EYFP^{+} processes than their colocalized vGAT clusters.

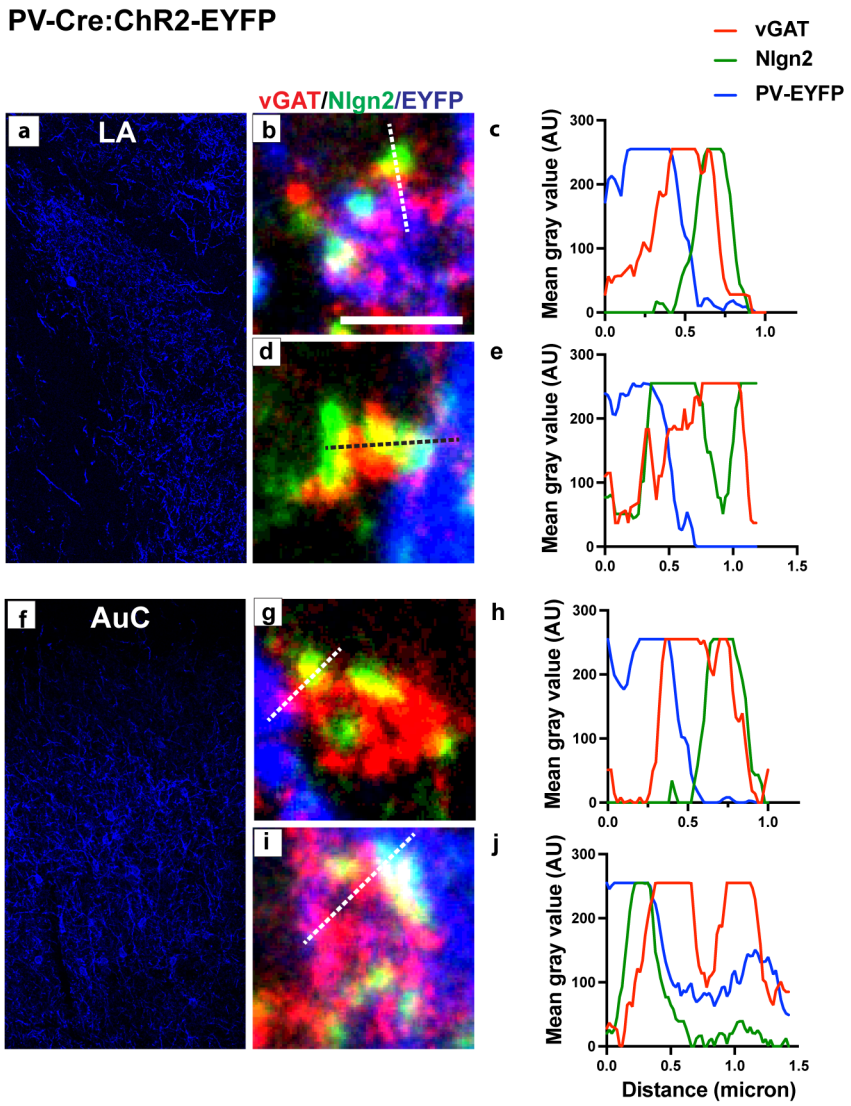

Figure 25 Qualitative assessment for the relative positions of Nlgn2, vGAT and EYFP labelled structures in selected synapses from PV-Cre:ChR-EYFP mice.
a and **f**. Confocal micrographs showing EYFP fluorescence by PV INs in the LA (**a**) and the AuC (**f**), scale bar 100μm (duplicated from figure 24). **b**, **d**, **g** and **i.** Merged multichannel confocal/STED micrographs showing individual inhibitory synapses, identified by colocalized vGAT (red, STED) and Nlgn2 (green, STED) labellings, that are potentially formed from EYFP^{+} processes (blue, confocal, putative synaptic terminals, (**b**,**g**) or onto EYFP^{+} processes (blue, confocal, putative dendritic shafts, **d**, **i**), scale bar 1 μm, (duplicated from figure 24). **c**,**e**,**h** and **j**. Line profile analysis depicting relative distances between vGAT, Nlgn2 and EYFP labeled structures. Plots are generated by plotting mean gray value for each labeling against distance across a line passing through the synapse (dashed line **b**, **d**, **g** and **i**).

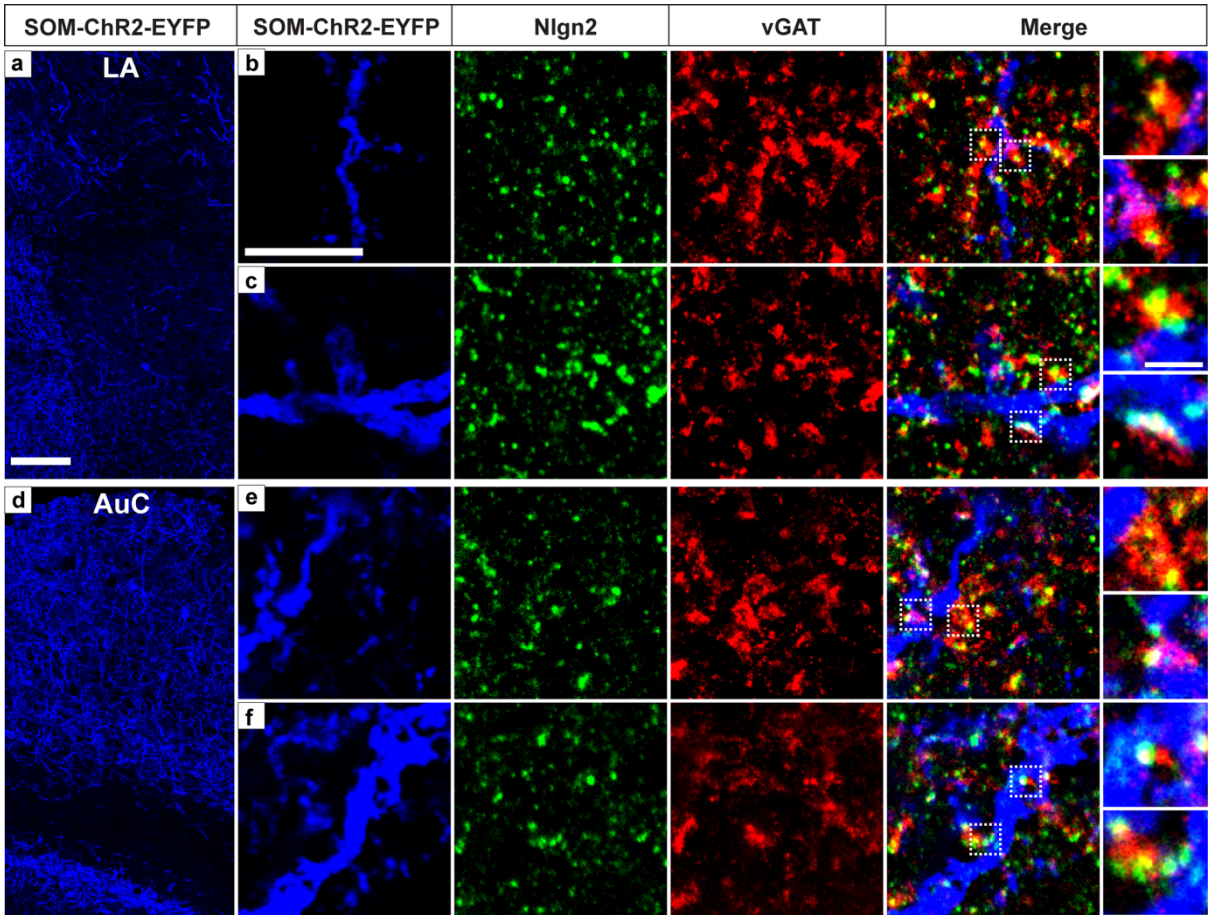

Figure 26 Nlgn2 is present on synapses formed by and onto SOM neurons.
a and **d**. Confocal micrograph showing EYFP fluorescence by SOM neurons in the LA (**a**) and the AuC (d) in methanol-fixed brain slices obtained from SOM-IRES-Cre:ChR-EYFP mouse, scale bar 100 µm**. b**, **c**, **e** and **f**. Confocal and STED micrographs taken from the LA (**b** and **c**) and the AuC (**e** and **f**) and are showing EYFP$^+$ SOM neuron processes (blue, confocal), Nlgn2 (green, STED) and vGAT (red, STED) immunolabelling, scale bar 5 µm. Dotted rectangles in the merge image are shown in higher detail on the right and they outline putative Nlgn2$^+$ synapses from or onto SOM neurons, scale bar 1 µm. The images presented in **b** and **e** show Nlgn2$^+$ synapses from SOM neurons inferred by vGAT clusters being in closer proximity to EYFP$^+$ processes than their colocalized Nlgn2 puncta. The images presented in **c** and **f** show Nlgn2$^+$ synapses onto SOM neurons inferred by Nlgn2 puncta being in closer proximity to EYFP$^+$ processes than their colocalized vGAT clusters.

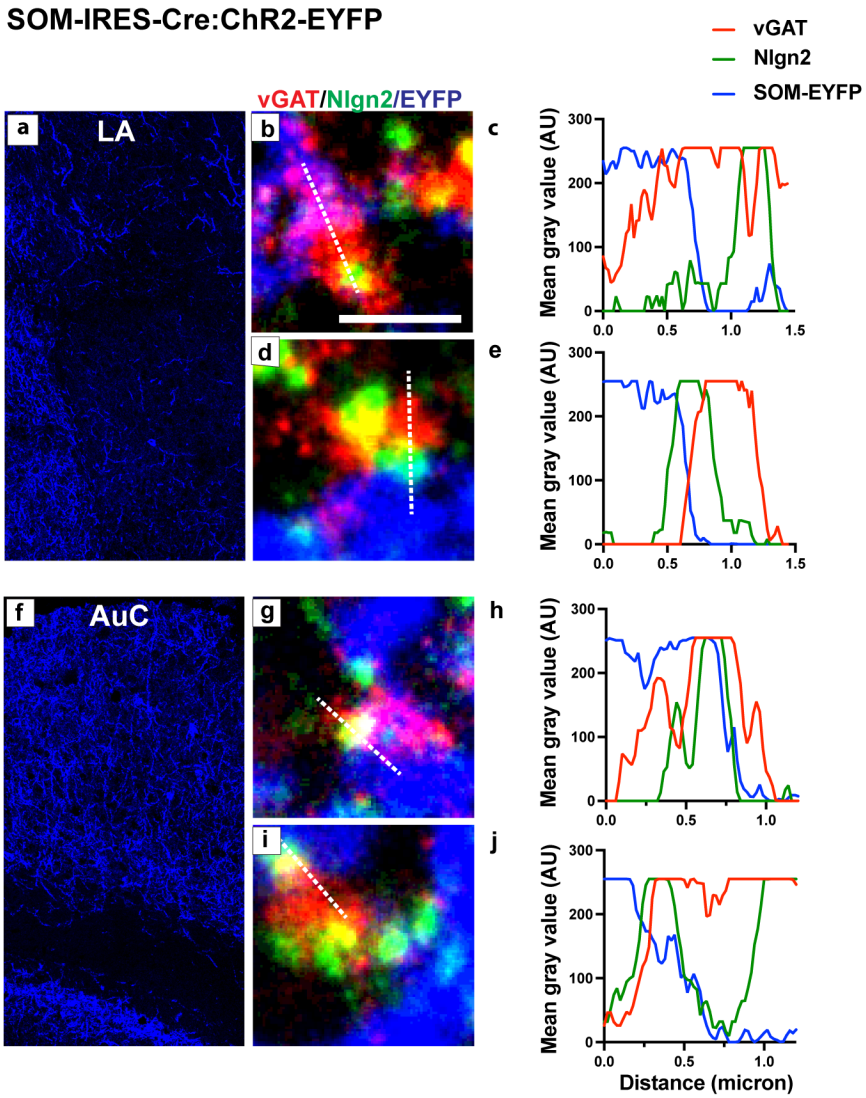

Figure 27 Qualitative assessment for the relative positions of Nlgn2, vGAT and EYFP labelled structures in selected synapses from SOM-IRES-Cre:ChR-EYFP mice.
a, **f**. Confocal micrographs showing EYFP fluorescence by SOM neurons in the LA (**a**) and the AuC (**f**), scale bar 100 µm (duplicated from figure 26). **b**, **d**, **g** and **i**. Merged multichannel confocal/STED micrographs showing individual inhibitory synapses, identified by colocalized vGAT (red, STED) and Nlgn2 (green, STED) labeling, that are potentially formed from $EYFP^+$ processes (blue, confocal, putative synaptic terminals, (**b**,**g**) or onto $EYFP^+$ processes (blue, confocal, putative dendritic shafts, **d**, **i**), scale bar 1 µm, (duplicated from figure 26). **c**, **e**, **h** and **j**. Line profile analysis depicting relative distances between vGAT, Nlgn2 and EYFP labeled structures. Plots are generated by plotting mean gray value for each labeling against distance across a line passing through the synapse (dashed line **b**, **d**, **g** and **i**).

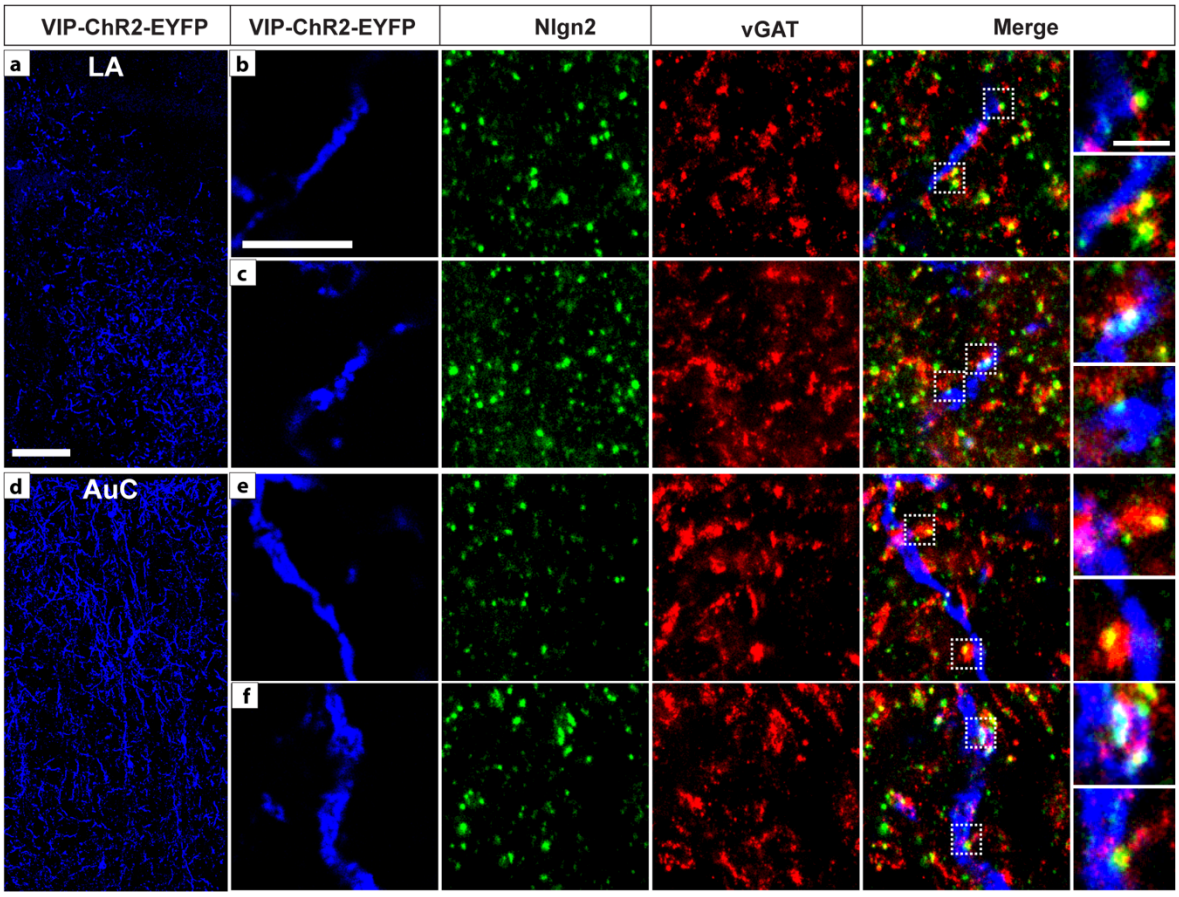

Figure 28 Nlgn2 is present on synapses formed by and onto VIP INs.
a and **d**. Confocal micrograph showing EYFP fluorescence by VIP INs in the LA (**a**) and the AuC (**d**) in methanol fixed brain slices obtained from VIP-IRES-Cre:ChR2-EYFP mouse, scale bar 100 µm. **b**, **c**, **e** and **f**. Confocal and STED micrographs taken from the LA (b and c) and the AuC (**e** and **f**) and are showing EYFP$^+$ VIP IN processes (confocal, blue), Nlgn2 (green, STED) and vGAT immunolabelling (red, STED), scale bar 5 µm. Dotted rectangles in the merge image are shown in higher detail on the right and they outline putative Nlgn2$^+$ synapses onto or from VIP interneurons, scale bar 1 µm. The images presented in **b** and **e** show Nlgn2$^+$ synapses from VIP INs inferred by vGAT clusters being in closer proximity to EYFP labelled processes than their colocalized Nlgn2 puncta. The images presented in c and **f** show Nlgn2$^+$ synapses onto VIP INs inferred by Nlgn2 puncta being in closer proximity to EYFP labelled processes than their colocalized vGAT clusters.

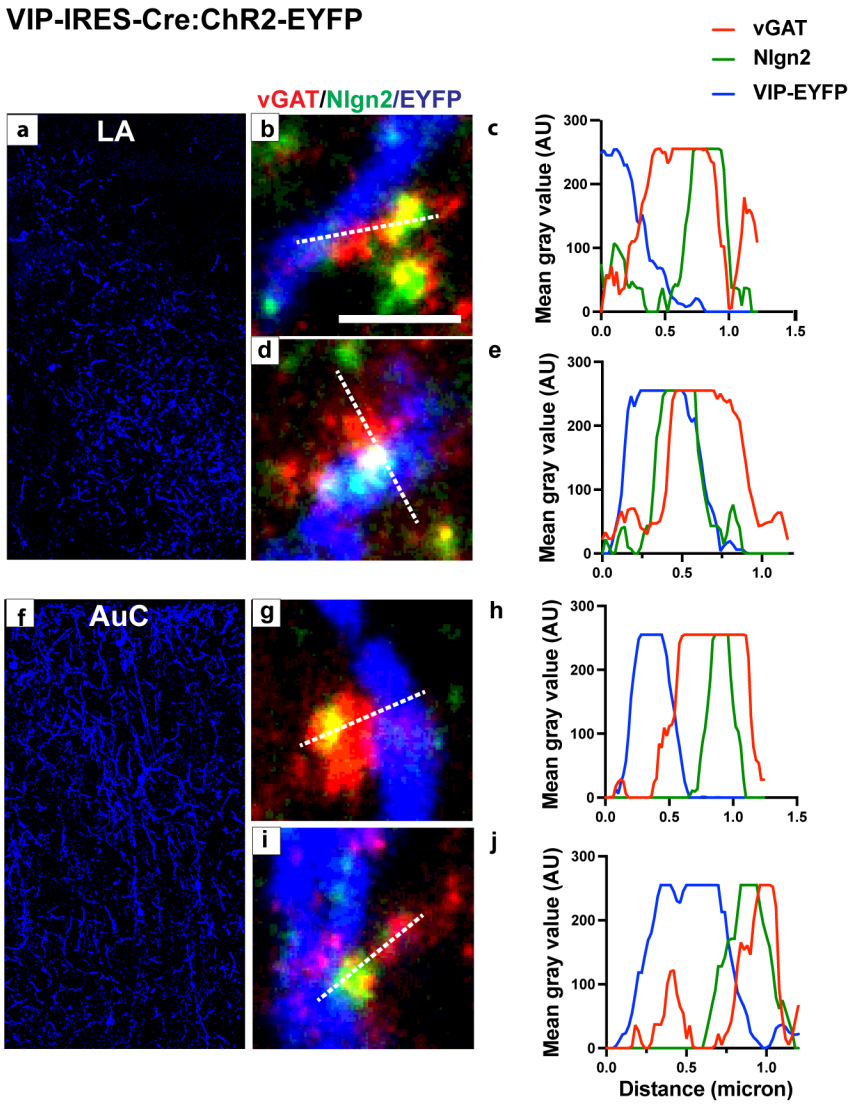

Figure 29 Qualitative assessment for the relative positions of Nlgn2, vGAT and EYFP labelled structures in selected synapses from VIP-IRES-Cre:ChR-EYFP mice.
a, **f**. Confocal micrographs showing EYFP fluorescence by VIP INs in the LA (**a**) and the AuC (**f**), scale bar 100µm (duplicated from figure 28). **b**, **d**, **g** and **i**. Merged multichannel confocal/STED micrographs showing individual inhibitory synapses, identified by colocalized vGAT (red, STED) and Nlgn2 (green, STED) labeling, that are potentially formed from $EYFP^+$ processes (blue, confocal, putative synaptic terminals, (**b**, **g**) or onto $EYFP^+$ processes (blue, confocal, putative dendritic shafts, **d**, **i**), scale bar 1 µm, (duplicated from figure 28). **c**, **e**, **h** and **j**. Line profile analysis depicting relative distances between vGAT, Nlgn2 and EYFP labeled structures. Plots are generated by plotting mean gray value for each labeling against distance across a line passing through the synapse (dashed line **b**, **d**, **g** and **i**).

3.3. Chapter 3: Interactions of Nlgn2 in the inhibitory synapse

In addition to the well-known interaction of Nlgn2 with the presynaptic Neurexins, which is shown to mediate the maturation of the inhibitory synapse (Südhof, 2017), several interactions of Nlgn2 on the postsynaptic level have been identified and shown to modulate its effect in regulating synapse function (Ali et al., 2020). To understand how Nlgn2 function is modulated by its post-synaptic partners, I investigated in this chapter aspects of two postsynaptic Nlgn2 interactions. One is the interaction with IgSF9b, which I investigated in terms of its potential effect on fear learning behavior. The second is the interaction with MDGA1, which I addressed in terms of colocalization of both proteins in the mouse brain.

3.3.1. The Interaction between Nlgn2 and IgSF9b in regulating FC behavior

IgSF9b is a synaptic adhesion molecule that was shown to be preferentially localized to inhibitory synapses and to function in molecular complex with Nlgn2 using in vitro assays (Woo et al., 2013). However, previous work from our group investigating their interaction in vivo demonstrated that they antagonistically regulate anxiety-like behavior via effects on different amygdala nuclei (Babaev et al., 2018a). To gain more insights on how Nlgn2 and IgSF9b interact to regulate emotional circuits, I characterized the FC behavior in mice lacking each of *Nlgn2* and *IgSF9b*, or both genes versus their littermate WT mice.

3.3.1.1. Deletion of IgSF9b exacerbates auditory FC deficit observed in Nlgn2 KO mice.

To test whether Nlgn2 and IgSF9b interact in regulating fear learning, I characterized FC behavior, using the same paradigm described in section (2.2.1) in mice with the following genotypes: Nlgn2 KO, IgSF9b KO and Nlgn2-IgSF9b double KO mice versus their WT littermates. The Nlgn2 KO and WT groups used for this analysis are displayed separately in (section 3.1.1., figure 8) and were presented again in this section (figure 30) after they were statistically analyzed in comparison to IgSF9b KO and double KO mice. By assessing auditory FC, I measured comparable conditioned freezing levels between IgSF9b KO and WT mice during FC retrieval testing done 24 h after training, with a mild trend towards reduced CS freezing in IgSF9b KO mice. Strikingly, double KO mice showed completely abolished CS freezing (figure 30, b, CS freezing). This indicated that deletion of IgSF9b exacerbates the deficit in FC retrieval observed in Nlgn2 KO mice. Two -way ANOVA analysis revealed a significant main effect of Nlgn2 on CS freezing levels, but no significant interaction between Nlgn2 and IgSF9b. Nlgn2 was also a main factor of variation in the levels of training baseline freezing, that showed a trend toward an increase in Nlgn2 KO

and double KO mice (figure 30, training baseline). By measuring testing baseline freezing, IgSF9b was shown to be a main factor using ANOVA, suggesting that its deletion underlies a trend towards reduced context generalization in IgSF9b KO and double KO mice (figure 30, testing: baseline freezing). By testing FC retrieval after 2 h of training, the same profile was observed with exacerbated deficit in freezing in double KO mice. However, IgSF9b KO mice showed significant reduction in CS freezing and IgSF9b appeared as a significant main factor with ANOVA (figure 30, c, CS freezing). This effect of reduction in CS freezing in IgSF9b KO mice is likely due to agitation and hyperactivity observed in these mice after US exposure, since retrieval testing was done shortly (2 h) after the training. Also, the fact that they did not show such a deficit when their CS freezing was measured after 24 h of training supports intact auditory FC acquisition and retrieval (figure 30, b). Similar to what was observed in the 24 h cohort, Nlgn2 was a main factor for the variance in the training baseline freezing using ANOVA and IgSF9b was a main factor for testing baseline freezing (figure 30, c, training: baseline freezing).

These findings indicate that Nlgn2 and IgSF9b play a synergistic role in regulating auditory FC circuit, in contrast to the antagonistic interaction reported in the context of anxiety-like behavior (Babaev et al., 2018a).

3.3.1.2. Contextual FC is reduced in IgSF9b KO mice and rescued in Nlgn2-IgSF9b double KO mice

To test whether Nlgn2 and IgSF9b interact in a similar way in regulating the contextual FC to the one observed in auditory FC, I assessed contextual FC behavior in Nlgn2 KO, IgSF9b KO and double KO versus WT mice. In this paradigm IgSF9b showed a robust deficit in conditioned context freezing during FC retrieval that was normalized in the double KO (figure 30, e). Two-way ANOVA showed a significant main effect of both of IgSF9b and Nlgn2 on context freezing that is possibly due to the trend towards increased context freezing in Nlgn2 KO mice. Together, these results reflect an antagonistic pattern of interaction in contextual FC similar to the one reported for the anxiety-like behavior. As shown in (section 3.1.1, figure 8), Nlgn2 was again determined as a main factor for training baseline freezing.

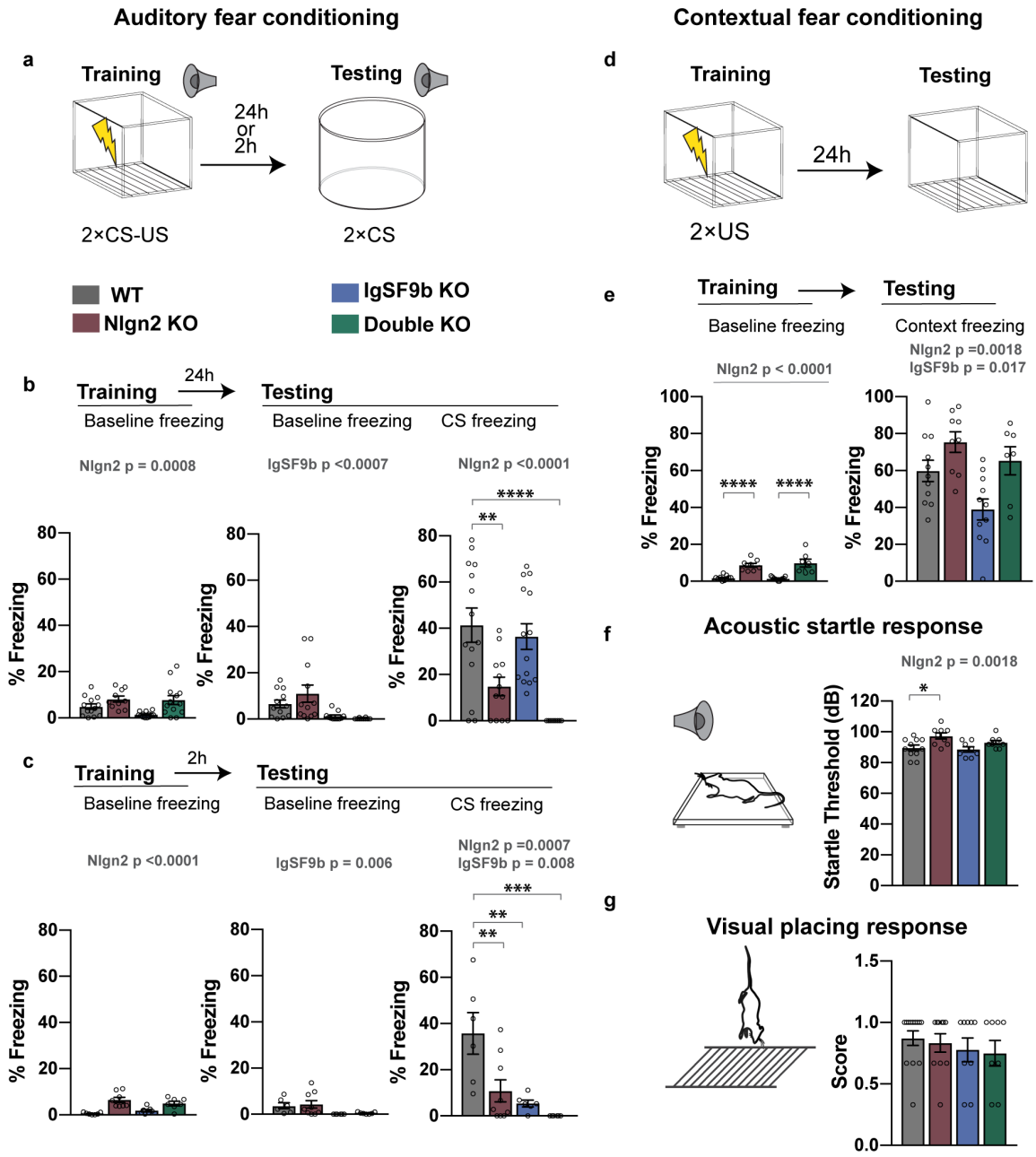

Figure 30 Nlgn2-IgSF9b interaction in auditory versus contextual FC.
a. Schematic of the auditory FC paradigm. **b**, **c**. percentages of time spent freezing at baseline or in response to the CS in the auditory FC paradigm in Nlgn2 KO, IgSF9b KO, double KO and WT mice tested after 24 h (**b**, training baseline: N = 10-13 two-way ANOVA Nlgn2 F(1, 45) = 13.07, p = 0.0008, IgSF9b F(1, 45) = 2.107, p = 0.1535, Interaction F(1, 45) = 1.349, p = 0.2516), testing baseline: N = 10-12 mice, two-way ANOVA Nlgn2 F (1, 41) = 0.6011, p = 0.4426, IgSF9b F (1, 41) = 13.34, p = 0.0007, Interaction F (1, 41) = 1.619, p = 0.2104), CS freezing: N = 10-14 mice, Two-way ANOVA; Nlgn2 F (1, 46) = 31.76, p < 0.0001, IgSF9b F (1, 46) = 3.117, p = 0.0841, Interaction F (1, 46) = 0.7900, p = 0.3787) or 2 h (**c**, training baseline: N = 7-8 mice, Two-way ANOVA; Nlgn2 F (1, 25) = 30.23, p <0.0001, IgSF9b F (1, 25) = 0.01925, p = 0.8908, Interaction F (1, 25) = 3.057, p = 0.0927) testing baseline: N = 6-9, Two-way ANOVA; Nlgn2 F (1, 24) = 30.23, p = 0.6564, IgSF9b F (1, 24) = 8.985, p = 0.0062, Interaction F (1, 24) = 0.003409, p = 0.9539) CS freezing: N = 6-9 mice, Two-way ANOVA; Nlgn2 F (1, 23) = 8.433, p = 0.0080, IgSF9b F (1, 23) = 15.48, p = 0.0007, Interaction F (1, 23) = 3.47, p = 0.0750) **d**. Schematic of the contextual FC paradigm. **e**. Percentage of time spent freezing at baseline or in response to the CS, training baseline: N = 7-11 mice, Two-way ANOVA; Nlgn2 F (1, 33) = 61.83, p < 0.0001, IgSF9b F (1, 33) = 0.1733, p = 0.6799, Interaction F (1, 33) = 0.6951, p = 0.4104), CS freezing: N = 7-11 mice, Two-way ANOVA; Nlgn2 F (1, 34) = 11.46, p =

0.0018, IgSF9b F (1, 34) = 6.259, p = 0.0018, Interaction F (1, 34) = 0.7675, p = 0.3871) **f**. A schematic of the acoustic startle response test with the measured startle threshold in decibel. N = 8-11 mice, Two-way ANOVA; Nlgn2 F (1, 32) = 11.65, p = 0.0018, IgSF9b F (1, 32) = 2.030, p = 0.1639, Interaction F (1, 32) = 0.8341, p = 0.3679). **g**. A schematic of the visual placing response test. N = 10-13 mice, Two-way ANOVA; Nlgn2 F (1, 36) = 1.182, p = 0.2842, IgSF9b F (1, 36) = 0.1620, p = 0.6897, Interaction F (1, 24) = 0.004112, p = 0.9492). Significant Tukey's pairwise comparisons between marked groups are indicated with * p < 0.05, ** p < 0.01, *** p < 0.001 and **** p < 0.0001. Nlgn2 KO and WT datasets here are the same as the ones included in figure 1.

To investigate whether auditory and visual functions are affected in IgSF9b and double KO mice, I assessed their behavior using the acoustic startle response and visual placing tests. In these tests, no changes were observed in IgSF9b KO and double KO mice compared to WT mice (figure 30, f and g respectively). These results confirm that the reduced context freezing during FC retrieval in IgSF9b is not due to loss of vision. Nlgn2, however, was found to be a main factor for the variance in the startle threshold as shown by two-way ANOVA, indicating that lack of Nlgn2 could mildly affect the hearing threshold in Nlgn2 KO and double KO mice. Alternatively, Nlgn2 deletion might be producing this slightly altered startle threshold by effects on motor coordination (Blundell et al., 2009), however, these findings exclude a potential lack of hearing in these mice.

In summary, the resulting contrasting outcomes of Nlgn-IgSF9b double deletion on auditory versus contextual FC suggest a circuit-specific interaction between these molecules. Therefore, further work to elucidate how Nlgn2 affect auditory FC and how IgSF9b affect contextual FC, individually, is necessary to interpret the behavior data obtained from double KO mice.

3.3.1.3. Further increase in locomotion parameters in Nlgn2-IgSF9b double KO mice

Since the lack of CS freezing could also result from a motor phenotype or a change in basal activity, assessment of homecage behavior in IgSF9b KO and double KO mice in addition to Nlgn2 KO and WT mice was conducted using LABORAS (see methods. Section 2.2.3). Data from Nlgn2 and WT groups here were duplicated from section 3.1.2 (figure 9) and were reanalyzed with the inclusion of IgSF9b KO and double KO groups.

Interestingly, the increase in locomotion parameters such as locomotor duration, speed and total distance observed in Nlgn2 KO mice was even higher in double KO mice (figure 31, b, c and d). Both Nlgn2 and IgSF9b were found to be significant main factors by two-way ANOVA. The immobility duration thereby was strongly reduced in the double KO with both of Nlgn2 and IgSF9b being identified as main factors. Additionally, a significant interaction was detected, beyond the main effect of each of Nlgn2 and IgSF9b, in the locomotion speed

(figure 31, c), total distance (figure 31, d) and the climbing duration with the latter being interestingly increased significantly in IgSF9b KO and normalized in the double KO (figure 31, i). By measuring grooming and rearing durations, a main effect of Nlgn2 was detected in these behaviors with the duration of both being increased in Nlgn2 KO and double KO mice (figure 31, h and j respectively). Other behaviors such as eating, drinking, and circling were not changed between genotypes (figure 31, f, j and k respectively).

These results obtained from analyzing homecage behavior suggest a role of Nlgn2 and IgSF9b in regulating locomotion where they also function in synergism as the double KO showed hyperactivity beyond the one observed in the single KO of each of Nlgn2 KO and IgSF9b KO. One exception for this pattern among locomotion parameters was the climbing duration where the double KO had normalized effect in relation to the one observed in single IgSF9b KO. Importantly, the locomotor hyperactivity observed in the double KO does not confound the conditioned freezing deficit observed in auditory FC as these mice showed, similar to Nlgn2 KO mice, normal context freezing (figure 30, e).

3.3.2. Further insights on the localization and function of IgSF9b

3.3.2.1. Abundant but region-specific IgSF9b expression in the mouse brain

IgSF9b is shown in vitro to function in a molecular complex with Nlgn2, but not much information is available about its localization and function in vivo. To gain more insights about the function of IgSF9b and how it could regulate behaviors such as contextual FC, it is crucial to know first in which brain regions it is expressed. Therefore, I sought to characterize the expression of IgSF9b in the mouse brain using IHC analysis in methanol fixed slices. IgSF9b showed to be widely expressed in the brain, but with a specific pattern where it was selectively increased in certain regions or subregions (figure 32, a and b). High expression levels were observed in the cortex, the amygdala, the habenula, thalamic and hypothalamic nuclei in addition to a specific strong band of expression in stratum lacunosum moleculare layer (SLM) of the hippocampus (figure 32, a and b).

By quantifying the number, size and total intensity of IgSF9b puncta detected with confocal imaging at a high magnification (figure 32, d, e and f), the region that had the most and brightest puncta was the SLM layer of the hippocampus CA1, implying a role for IgSF9b in this region (figure 32, a, b, c, d and e). Among the regions also that showed the high number and intensity of puncta was also the lateral and medial habenular nuclei, the BA and the CeM amygdala nuclei, the dentate gyrus polymorph layer and the CeL (figure 32, c, d and

e). Average IgSF9b puncta size was shown to be between 1 and 3 µm and the largest puncta were found in habenular regions (figure 32, f).

3.3.2.2. A trend toward reduced LTP in IgSF9b KO mice

Synaptic plasticity is a prevalent mechanism that is thought to underlie learning and memory formation (Takeuchi et al., 2014). One of the most powerful experimental models to assess synaptic plasticity in the hippocampus is the long-term potentiation (LTP) paradigm described at Schäffer collateral synapses between CA3 and CA1 regions of the hippocampus (Bliss and Lomo, 1973). Based on the impairment observed in IgSF9b KO mice in contextual fear memory retrieval, it was interesting to test whether hippocampal LTP is affected in these mice which would explain the observed deficit (Levenson et al., 2002b; Penn et al., 2017; Tang et al., 1999). To test this, acute hippocampal slices from adult IgSF9b KO and WT mice were prepared. Subsequently, high frequency stimulation was introduced to the Schaffer collateral in the CA3 region of the HPC and the resulting field excitatory post synaptic currents (fEPSCs) were recorded in the stratum Radiatum of the CA1 of IgSF9b and WT mice. Using this method, LTP was induced in these synapses in WT hippocampal slices characterized by an increase in the amplitude of the fEPSPs after introducing the stimulus train that persisted for 1 h. Interestingly, the magnitude of this increase showed a trend towards reduction in IgSF9b KO (figure 33). Although this result is preliminary and requires more experimental animals to confirm a statistically significant difference, it implies a role for IgSF9b in hippocampal plasticity that may underlie the observed deficit in contextual FC.

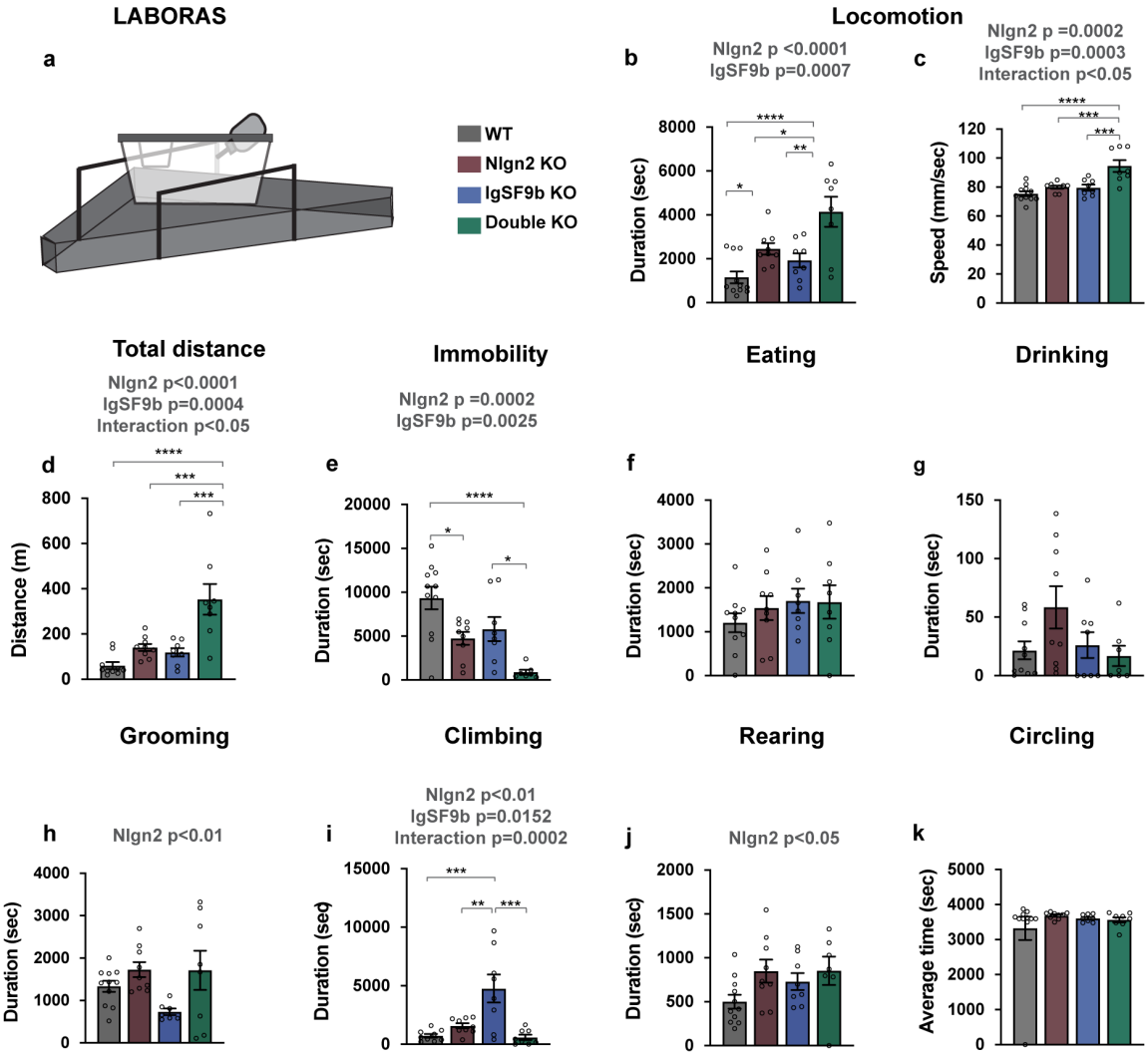

Figure 31 . Characterization of homecage activity in Nlgn2 KO, IgSF9b and double KO mice. **a** schematic of the Laboras system. **b**. Average locomotor duration, N = 8-11 mice, two-way ANOVA Nlgn2 F (1, 29) = 26.07, p < 0.0001, IgSF9b F (1, 29) = 14.28, p = 0.0007, Interaction F (1, 29) = 0.2550, p = 0.6174), **c**. Average locomotion speed, N = 8-11 mice, , two-way ANOVA Nlgn2 F (1, 32) = 17.53, p = 0.0002, IgSF9b F (1, 32) = 16.20, p = 0.0003, Interaction F (1, 32) = 5.151, p = 0.0301). **d**. Total distance travelled, N = 8-10 mice, two-way ANOVA Nlgn2 F (1, 31) = 21.17, p < 0.0001, IgSF9b F (1, 31) = 15.60, p = 0.0004, Interaction F (1, 31) = 5.096, p = 0.0312). **e**. Immobility duration, N = 8-11 mice, two-way ANOVA Nlgn2 F (1, 31) = 17.98, p = 0.0002, IgSF9b F (1, 31) = 10.86, p = 0.0025, Interaction F (1, 31) = 0.02010, p = 0.8882). f. Eating duration. N = 8-11 mice, two-way ANOVA Nlgn2 F (1, 31) = 0.2933, p = 0.5920, IgSF9b F (1, 31) = 1.243, p = 0.2734, Interaction F (1, 31) = 0.4073, p = 0.5280). **g**. Drinking duration, N = 7-10 mice, two-way ANOVA Nlgn2 F (1, 30) = 1.231, p = 0.2760, IgSF9b F (1, 30) = 2.237, p = 0.1452, Interaction F (1, 30) = 3.440, p = 0.0735). **h**. Grooming duration, N=7-11 mice, two-way ANOVA Nlgn2 F (1, 31) = 7.566, p = 0.0098, IgSF9b F (1, 31) = 1.509, p = 0.2285, Interaction F (1, 31) = 1.375, p = 0.2499). **i**. Climbing duration, N = 8-9 mice, two-way ANOVA Nlgn2 F (1, 30) = 7.819, p = 0.0089, IgSF9b F (1, 30) = 6.625, p = 0.0152, Interaction F (1, 30) = 18.01, p = 0.0002). **j**. Rearing duration, N = 7-11, two-way ANOVA Nlgn2 F (1, 31) = 4.187, p = 0.0493, IgSF9b F (1, 31) = 1.015, p = 0.3215, Interaction F (1, 31) = 0.9275, p = 0.3430). **k**. Circling duration, N = 8-9, two-way ANOVA Nlgn2 F (1, 30) = 0.01125, p = 0.9162, IgSF9b F (1, 30) = 2.553, p = 0.1206, Interaction F (1, 30) = 1.263, p = 0.2700).

3.3.3. The interaction between Nlgn2 and MDGA1 in the hippocampal CA1- a colocalization analysis

MDGA1 (MAM-domain GPi anchored protein 1) is a synaptic adhesion molecule that has been shown in vitro to bind to Nlgn2 and impede its ability to mediate the establishment of inhibitory synapses by interfering with its binding to presynaptic neurexins (Kim et al., 2017; Lee et al., 2013). In line with this, deletion of MDGA1 in mice produced an increase in synaptic inhibition reflected by increase in number of inhibitory synapses and increase in the frequency of mIPSC in the PNs of the hippocampal CA1 region that was suggested to be due to an increase in Nlgn2 semantogenic function (Connor et al., 2019). However, since an antibody that detects endogenous MDGA1 has only been recently developed (Toledo et al., 2021), an investigation of Nlgn2-MDGA1 colocalization in the CA1 to support their functional interaction in this region has not yet been done. In this project, as part of a manuscript that investigates the behavioral and synaptic interaction between MDGA proteins 1 and 2 and Nlgn2, I characterized the colocalization between Nlgn2 and MDGA1 in the CA1 of the adult mouse hippocampus. To this end, methanol fixed brain slices were prepared from a WT and a Nlgn2-MDGA1 double KO mouse and immunolabelled with Nlgn2 and MDGA1 antibodies. Nlgn2 immunofluorescence showed to span all layers of the hippocampus across the CA1, CA2, CA3 and DG regions with a brighter band of expression in the SLM layer of the CA1 (figure 34, a, upper panel, red channel). Such labeling pattern was absent in slices from the double KO mouse despite the presence of a slight background in the Nlgn2 channel (figure 34, a, lower panel, red channel). At higher resolution, Nlgn2 showed punctate labelling that was similar across different CA1 layers and comparable with the labelling described previously in this region (figure 34, c, red channel, (Poulopoulos et al., 2009). As to MDGA1, it showed a dense, diffuse labelling that was present in the CA1, CA2, CA3 and DG regions but seemed to be strongly reduced in specific layers such as the stratum Pyramidale of the CA regions (figure 34, a-c, green channel), and the molecular layer of the DG where it showed a line of expression that outlines the granule cell layer (figure 34, a, green channel).

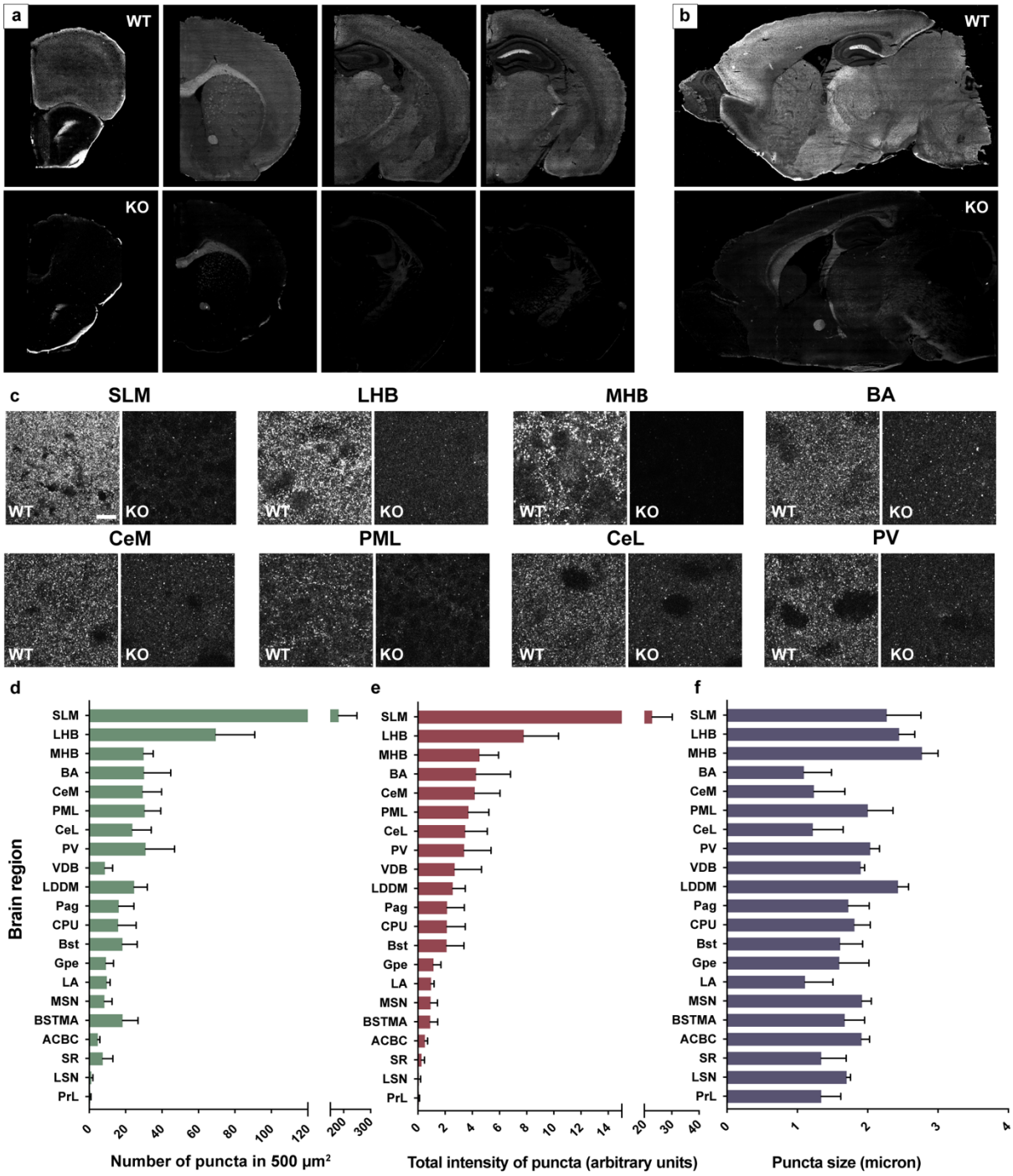

Figure 32 IgSF9b is widely expressed in the mouse brain but in a region-specific manner.
a and **b** Coronal (**a**) and sagittal (**b**) brain sections obtained from WT (top) and IgSF9b KO mice (bottom) immunolabelled with IgSF9b antibody. **c**. 63x confocal micrographs showing IgSF9b punctate labelling in several brain regions where the highest expression was observed in WT (left image) and IgSF9b KO mice (right image), scale bar 5 µm. **d**. Number of detected IgSF9b puncta in 500 µm^2 plotted across different brain regions. Values from different regions are ordered from the highest (top) to the lowest (bottom) puncta density. N= 3-7 mice. **e**. Total fluorescence intensity of detected IgSF9b puncta plotted across different brain regions and ordered according to the order in d, N= 3-7 mice. **f**. average puncta size plotted across different regions and ordered according to the order in **d**, N = 6-7 mice. **SLM**: stratum-Lacunosum Moleculare (hippocampus), **LHB**: lateral habenular nucleus, **MHB**: medial habenular nucleus, **BA**: basal amygdala. **CeM**: centromedial amygdala, **PML**: polymorph layer of the dentate gyrus. **PV**: paraventricular thalamic nucleus. **VDB**: nucleus of the vertical limb of the diagonal band of Broca (basal forebrain). **LDDM**: laterodorsal

thalamic nucleus, medial part. **PAG**: Periaqueductal gray. **CPU**: caudate putamen (striatum). **Bst**: Bed nucleus of the stria terminalis. **GPe**: Globus pallidus external (striatum). **LA**: lateral amygdala. **MSN**: medial septal nucleus. **BSTMA**: bed nucleus of stria terminalis, medial division, anterior part. **ACBC** Nucleus accumbens, core. **SR**: stratum radiatum (hippocampus). **LSN**: lateral septal nucleus. **PrI**: prelimbic area of the medial prefrontal cortex.

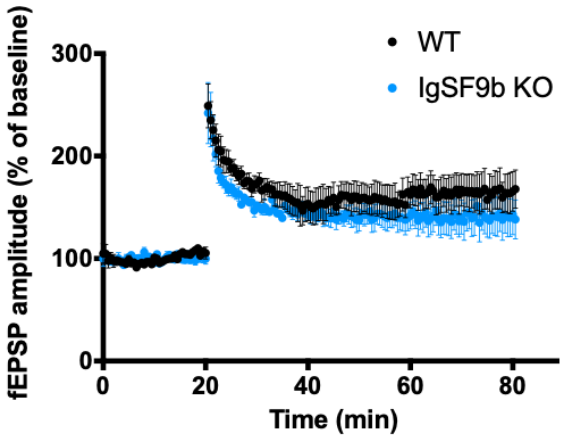

Figure 33 A trend towards reduced long-term potentiation in CA3-CA1 synapses in IgSF9b KO mice.

Time course of field excitatory post-synaptic potentials recorded in the CA1 stratum Radiatum while stimulating the Schäffer collaterals between CA3-CA1 from adult WT and IgSF9b KO mice. 100 Hz stimulation train introduced after 20 min.

The labelling of MDGA1 was highly specific and showed to be completely absent in the double KO mouse (figure 34, lower panel, green channel). By plotting frequency distributions of Nlgn2 puncta according to the intensity of their colocalizing MDGA1 fluorescence values, colocalization of Nlgn2 with MDGA1 in the CA1 was assessed across different layers (figure 34, d-g). High level of colocalization was observed in the stratum Oriens (SO), stratum Radiatum (SR) and stratum Lacunosum Moleculare (SLM) of the CA1 with the majority of Nlgn2 puncta showing MDGA1 intensity that is equal or higher than 500 AU (figure 34, d, f and j). This was not true in the stratum Pyramidale (SP), where the majority of Nlgn2 puncta accumulated around low MDGA1 intensities (figure 34, e). Interestingly, the colocalization levels in the SO and SR were very comparable as the puncta intensity was centered around 500 AU in both regions. In the SLM, higher number of Nlgn2 puncta showed a peak at this intensity indicating that this region has the highest level of colocalization (figure 34, g). However, more Nlgn2 puncta in the SO and SR showed intensities higher than 1000 AU compared to SLM, suggesting that colocalizing MDGA1 puncta are brighter in the SO and SR than in the SLM. Taken together, these findings nominate the SLM, SR and SO as sites for potential interaction between MDGA1 and Nlgn2 in the CA1 and likely excludes the pyramidal layer, since very low expression of MDGA1 was detected in this region which was also reflected by low colocalization with Nlgn2.

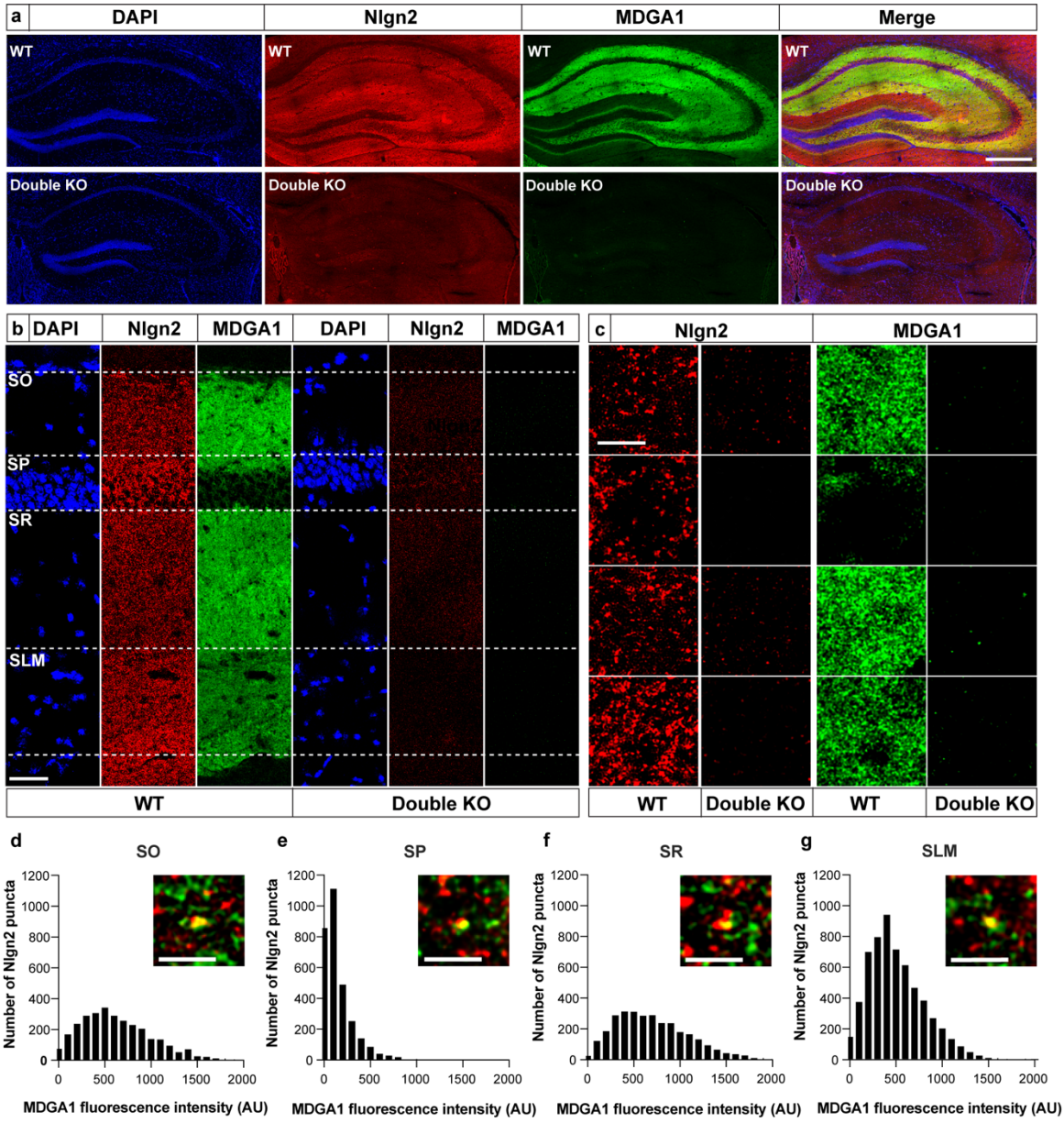

Figure 34 Nlgn2-MDGA1 colocalization in the CA1 region of the HPC.
a. 20x micrographs showing an overview of the dorsal hippocampus in WT mouse (upper panel) versus Nlgn2-MDGA1 double KO mouse (lower panel) labelled with DAPI and antibodies against Nlgn2 (red) and MDGA1 (green), scale bar 500 µm. **b**. 63x confocal micrographs showing an overview of DAPI, Nlgn2 and MDGA1 labelling across different layers in the CA1 region of WT and Nlgn2-MDGA1 double KO mice. Stratum oriens (SO), Stratum Pyramidale (SP), Stratum radiatum (SR) and Stratum lacunosum- moleculare (SLM). **c.** 63x confocal micrographs showing an overview of the CA1 with its different layers labelled with DAPI (left), Nlgn2 (middle) and MDGA1 (right) in WT and Nlgn2-MDGA1 double KO mice, scale bar 5 µm. **d-g**. Histograms showing the frequency distribution of MDGA1 average fluorescence intensity measured within a mask of Nlgn2 labelled puncta within each layer (from left to right: SO, SP, SR and SLM) along with high resolution micrographs showing example of MDGA1 colocalized Nlgn2 puncta for each hippocampal layer, scale bar 2 µm.

4. Discussion

Nlgn2 is a synaptic adhesion molecule that is required for the maturation and function of inhibitory synapses (Ichtchenko et al., 1996; Poulopoulos et al., 2009; Varoqueaux et al., 2004) and was implicated in the pathophysiology of psychiatric disorders such as schizophrenia and anxiety (Parente et al., 2017; Sun et al., 2011). Additionally, deletion of Nlgn2 in mice produced a robust anxiety-behavior that was associated with synapse and circuit level dysregulation in brain regions involved in emotional processing (Babaev et al., 2016; Blundell et al., 2009; Cruces-Solis et al., 2021). Aiming to advance the knowledge of how Nlgn2 regulates emotional brain function, I asked whether Nlgn2 is involved in the formation of aversive memories. To answer this question, I characterized the behavior of Nlgn2 KO mice using the fear conditioning paradigm and found a deficit in conditioned freezing in Nlgn2 KO mice compared to WT mice. To pinpoint the brain regions and cell types underlying this deficit in Nlgn2 KO mice, I conducted a detailed behavioral assessment combined with neural activation assay and region and cell specific gene manipulations. The results I obtained from these analyses supported the following findings:

1) Nlgn2 is required for auditory FC and its deletion produces a reduction in FC retrieval in Nlgn2 KO mice that is reflective of a memory impairment rather than a sensory or a motor deficit.

2) The reduced FC retrieval in Nlgn2 KO mice was associated with dysregulated neuronal activation in several brain regions that are involved in fear memory formation and storage. However, the site where the deficit in fear learning is originating, is still to be determined.

3) The fear learning deficit in Nlgn2 KO mice was caused mainly by its loss from inhibitory neurons. Particularly, VIP INs that exhibited learning-dependent dysregulation during FC retrieval in Nlgn2 KO mice and their lack of Nlgn2 produced a significant reduction in FC retrieval. Intriguingly, lack of Nlgn2 from excitatory CAMKII neurons did not significantly alter fear learning, indicating that the proposed synapse specificity of Nlgn2 onto PN is not the one underlying the fear learning deficit in Nlgn2 KO mice.

4) Showing opposing effects on anxiety-like behavior versus fear learning, Nlgn2 was found to regulate these circuits by effects on different regions and different cell types. Intriguingly, deletion of Nlgn2 from excitatory CAMKII neurons recapitulated the anxiety-like phenotype in Nlgn2 KO mice, indicating that, unlike in fear learning, Nlgn2 onto PN is a key player in anxiety-like behavior.

5) While Nlgn2 and its proposed interaction partner IgSF9b were shown to antagonistically regulate anxiety-like behavior, their interaction in auditory FC revealed a synergistic effect, indicating that the interaction between these proteins is highly circuit specific.

4.1. Nlgn2 is a key regulator of emotional brain circuits

4.1.1. Nlgn2 KO mice show impaired auditory fear learning

By promoting the establishment of inhibitory synapses within defined brain circuits, Nlgn2 mediates stable E/I balance within these circuits and thereby contributes to their ultimate behavioral outcome. Such a function implies a global role for Nlgn2 in maintaining inhibition within brain circuits and predicts a severe outcome for its constitutive deletion. Interestingly, however, behavioral assessment of Nlgn2 KO mice revealed that its deletion affects mainly circuits involved in emotional functions as shown by the robust anxiety-like behavior (Blundell 2009, Babaev 2016). In line with previous unpublished data from the thesis work of Dr. Olga Babaev (Department of Molecular Neurobiology, Max Planck institute for Experimental Medicine), I characterized a short and long-term deficit in aversive learning using the auditory FC paradigm. The deficit was assessed by reduced conditioned freezing during FC retrieval despite showing increased novelty induced freezing compared to WT littermates. This finding confirms a key role for Nlgn2 in emotional processing, but it also highlights a compelling function of Nlgn2 in regulating fear learning versus anxiety. Although increased anxiety is often associated in animal models with increased fear learning (Bárez-López et al., 2017), the synaptic deficit produced by Nlgn2 deletion helped to stratify these behaviors and the neuronal circuits controlling them. Remarkably, Nlgn2 KO mice represent an animal model in which increased generalized anxiety is associated with a cognitive deficit leading to impaired emotional learning. Such an intriguing behavioral phenotype highlights that anxiety and fear learning are mediated by separate circuits/mechanisms. One aspect in this distinction is the related to the role of synaptic inhibition, mediated by synaptic organizers, such as Nlgn2.

Interestingly, the deficit in conditioned freezing in Nlgn2 KO mice was already present after 2 h from FC training, indicating an impairment in memory formation rather than consolidation, since an impairment in only consolidation would leave short-term memory intact. Also, Nlgn2 KO mice exhibited normal freezing in contextual FC, indicating that their reduced freezing in auditory FC is not due to a motor problem blocking fear expression. However, addressing, in detail, how Nlgn2 regulates each of these stages requires an approach that allows transient loss of Nlgn2 function that could be applied during specific

days of the protocol. For example, during training only, after training and during testing only. In this context, manipulation such as Nlgn2 conditional knockout, knockdown or functional blocking using synthetic peptides could be, in principle, used specifically after training and its effect on testing could be assessed to address the Nlgn2 role in consolidation. However, this is not experimentally feasible using the same FC protocol we implemented as testing was conducted 24 h after training, which is not enough time to allow for such manipulations to have effect. To address this, long-term FC protocols could be validated and applied for this purpose. The role of Nlgn2 on auditory fear expression, could be indirectly assessed by implementing optogentic/chemogentic manipulations targeting cell types affected in Nlgn2 KO, i. e. VIP neurons that could be applied during FC testing to test whether it rescues the FC deficit.

Another point of significance for the FC deficit I characterized in Nlgn2 KO mice is that it strengthens the face validity of Nlgn2 KO mice as a disease model for schizophrenia, where cognitive deficits, including impaired fear learning, were found in patients and animal models (Brzózka et al., 2010; Tuominen et al., 2022). Interestingly, mice bearing the Nlgn2 single point mutation R215H derived from schizophrenia patients, showed a similar behavioral phenotype (Jiang et al., 2018). While this mutation is shown to impede Nlgn2 function in inhibitory postsynape assembly (Sun et al., 2011) my data were consistent with the behavioral finding reported in this R215H mutant mice and confirms the relevance of Nlgn2 KO mice as a schizophrenia disease model.

4.1.2. Impaired auditory fear learning in Nlgn2 KO mice is not due to sensory or motor deficits

Intact sensory and motor functions are crucial for the generation of measurable conditioned freezing responses to the CS during auditory FC. Earlier studies reported no changes in sensory and motor functions in Nlgn2 KO (Wohr et al., 2013). However, to confirm these findings and validate the impaired FC phenotype in Nlgn2 KO mice, sensory and motor functions were assessed in this study. Interestingly, a mild increase in startle threshold in Nlgn2 KO mice was detected in an approach to indirectly assess auditory function. This is surprising since a similar behavior analysis was conducted by Wohr et al and revealed no change compared to WT mice (Wohr et al., 2013). Since the startle threshold does not directly reflect the hearing threshold in mice but rather the loudness required to generate a motor startle response, such a change might result from a change in motor coordination. Also, the small magnitude of the change in startle threshold in Nlgn2 KO mice compared to WT mice excludes a potential lack of hearing. Furthermore, a recent study investigating the effect of the anxiety state in Nlgn2 KO mice on a memory-based frequency discrimination

task revealed a comparable discrimination threshold in Nlgn2 KO to WT mice (Chen et al., 2019). While the task in the study by Chen et al involved sound stimuli of sound pressure level range between 67 to 73 dB, which is lower than the stimulus intensity used for FC in this study (80 dB), the reduction in CS freezing observed in Nlgn2 KO mice cannot be explained by impaired CS detection.

A mildly reduced pain sensitivity has been previously reported in Nlgn2 KO mice using a hotplate test (Blundell et al., 2009). However, when I assessed contextual FC using the same footshock intensity used for auditory FC (0.5 mA), Nlgn2 KO mice showed normal conditioned freezing levels. Therefore, a potential reduction in pain sensitivity could not confound the reduction in auditory CS freezing.

By assessing the locomotion of Nlgn2 KO mice in a homecage setting, increased locomotion parameters were measured in these mice, indicative of hyperactivity. However, this observation is in contrast to the hypoactivity phenotype assessed in a novel, anxiogenic, environment such as the OFT (Babaev et al., 2016). While the FC chambers resemble more in their features the OFT than the homecage settings, it is unlikely that the potential hyperactivity measured in the homecage is also present during FC. Importantly, contextual FC freezing levels in Nlgn2 KO mice (and in Nlgn2-IgSF9b double KO mice) were comparable to WT mice, which excluded a potential effect of this hyperactivity phenotype observed in the homecage on the ability to show conditioned freezing.

Taken together, despite detecting some mild sensory and motor abnormalities in Nlgn2 KO mice, none of these observations could potentially confound the robust deficit in auditory CS freezing. Along with their increased anxiety-like behavior, this deficit in fear learning in Nlgn2 KO mice places Nlgn2 as a key regulator of emotional brain circuits.

4.1.3. Differential effects of Nlgn2 deletion on auditory versus contextual fear learning

Interestingly, Nlgn2 deletion had contrasting effects on auditory versus contextual FC, with the deficit being restricted to auditory FC. In the auditory FC paradigm, acquisition of fear memory is strongly correlated with synaptic plasticity in the amygdala (Duvarci and Pare, 2014; Ledoux, 2000) and in upstream regions involved in CS processing, like the auditory thalamus and cortex (Barsy et al., 2020; Letzkus et al., 2011; Taylor et al., 2021). Contextual FC, on the other hand, requires the hippocampus for context encoding and for mediating plasticity mechanisms required for learning (Chaaya et al., 2018; Levenson et al., 2002a; Penn et al., 2017). Interestingly, a deficit in spatial memory was reported using the Morris

water maze test upon AAV mediated overexpression of Nlgn2 in the hippocampus (Van Zandt et al., 2019). This implies a negative regulation by Nlgn2 of hippocampal dependent memory. In line with this, a trend towards increased contextual FC was observed in Nlgn2 KO mice and the deletion of Nlgn2 lead to normalized contextual FC deficit observed in IgSF9b KO mice. Taken together, these results highlight the circuit-specific regulation of synaptic function by Nlgn2. Although the basis for this circuit specificity needs to be further investigated, a potential explanation might be that Nlgn2 mediates different roles across different brain regions, possibly through effects on different cell types.

4.2. Region specific effects of Nlgn2 KO on fear memory processing

4.2.1. Impaired fear learning in Nlgn2 KO mice is associated with circuit dysregulation in the amygdala

Studies investigating the neural circuitry of fear conditioning, starting from early lesion studies to optogenetic manipulation in behaving animals agreed on the pivotal role of the amygdala circuit in the acquisition, consolidation, and retrieval of auditory fear memory (Duvarci and Pare, 2014; Ledoux, 2000; Sun et al., 2020). Therefore, I hypothesized that amygdala FC circuit would be affected in Nlgn2 KO mice. I tested this hypothesis by analyzing cFos expression by different amygdala nuclei, as a proxy for neuronal activation, 90 min after FC retrieval. Interestingly, Nlgn2 KO mice exhibited activation changes in two amygdala nuclei, namely the LA and the BA among which changes in the LA specifically were reflective of the behavioral outcome. In line with the formation of fear memory engram, LA neurons showed increased activation during FC retrieval in WT mice that received FC training compared to Ctrl mice trained with only CS. Such an increase in LA activation in trained mice during retrieval was also found in a recent study using a similar analysis (Barsy et al., 2020). Interestingly, the size of this engram, however, was much smaller in Nlgn2 KO mice without a significant increase in cFos levels in Nlgn2 KO mice that received FC training. Early research about FC neural circuitry identified the LA as the primary site for CS and US convergence and for associative plasticity underlying fear memory acquisition (Blair et al., 2001; Ledoux, 2000; Sun et al., 2020). Potentiated CS responses in the LA are projected to the CeA where freezing responses are generated through a further projection to downstream centers (Li et al., 2013; Tovote et al., 2016; Viviani et al., 2011). Thus, the lack of upregulated neuronal activity in LA of Nlgn2 KO is tightly related to the behavioral outcome observed in these mice.

The other amygdala nucleus where we detected changes in neuronal activation was the BA. In this nucleus, higher activation was measured in Nlgn2 KO compared to WT mice

during FC retrieval irrespective of exposure to FC training. Increased BA activation has been described as hallmark for amygdala circuit activation in response to anxiogenic conditions in Nlgn2 KO mice (Babaev et al., 2016). Having detected this change during FC retrieval could be indicative of increased anxiety in Nlgn2 KO mice during the experiment, which was evident on the training day with increased baseline freezing in Nlgn2 KO mice.

While many studies investigating FC deal with the LA and BA as one functional entity, namely the BLA, we provide here more evidence to the functional distinction between these two nuclei during FC retrieval (Lucas et al., 2016). This distinction was apparent in WT mice where LA neurons showed to have increased FC related activation, but not BA neurons. Also, neuronal activation in each of these nuclei was affected differently by Nlgn2 deletion during FC retrieval. Such a functional distinction was also present at the level of IN activation during FC retrieval. For example, VIP INs showed increased activation in LA in mice that received FC training but not in BA where VIP INs showed a trend towards reduced activation. Similarly, PV INs were differentially activated in the LA during FC retrieval but not in the BA. Interestingly, such a functional distinction in PV INs between the LA and the BA was demonstrated in a study by Lucas et al (Lucas et al., 2016). In this study, PV INs in the LA, but not in the BA, provided feedforward inhibition into PNs during thalamic and cortical afferent stimulation as revealed by recording evoked IPSCs while optogenetically silencing PV INs. Also, assessment of mEPSCs after FC revealed reduction in excitatory synaptic input to the LA PV INs, but not in BA PV INs (Lucas et al., 2016). Taken together, our findings highlight the functional distinction between LA and BA in FC circuit.

Surprisingly, we could not detect consistent changes in neuronal activation in the CeA during FC retrieval in either WT or Nlgn2 KO mice. This is interesting knowing that the CeA, including CeL and CeM, is the output region of the amygdala and was expected to show changes corresponding to the final behavioral output (Ciocchi et al., 2010; Ledoux, 2000; Viviani et al., 2011), for example, an increased activation in the WT mice that received FC training but not in their Nlgn2 KO counterparts. Although a trend toward such activation pattern was apparent in both of the CeL and CeM, it was not consistent enough to reach statistical significance. Interestingly, recent analyses of cFos expression after FC retrieval yielded similar results showing no increased activation in the CeL and CeM of WT mice (Barsy et al 2020) or rats (Urien and Bauer, 2022) that received FC training. One possible explanation for this observation is that, unlike the LA and BA where the majority of neurons are excitatory and a small population (approximately 20%) consists of INs (Sah et al., 2003), the CeA is made exclusively by inhibitory neurons belonging of different subtypes that are showed opposite plasticity patterns in response to the CS (Ciocchi et al., 2010; Haubensak

et al., 2010). This cellular heterogeneity may have obscured relevant changes in individual inhibitory neuron subtype populations. Interestingly, when we analyzed activation in an inhibitory-neurons specific manner, we detected a genotype dependent reduction in the activation of SOM inhibitory neurons in the CeM of Nlgn2 KO mice, which is in line with the deficit in CS freezing. Although the function of SOM in the CeM specifically has not yet been investigated, the reduction in their activation might contribute to the deficit in fear expression in Nlgn2 KO mice in line with reduced output to downstream regions.

4.2.2. Fear learning deficit in Nlgn2 KO mice is not caused by reduced Nlgn2 in the lateral amygdala

FC retrieval in Nlgn2 KO mice was associated with a deficit in neuronal activation in the LA. This was highly indicative of a local impairment in the LA at the level of fear memory formation. Alternatively, the deficit in LA activation resulting from Nlgn2 deletion might be transmitted to the LA from an upstream region such as the auditory thalamus or the auditory cortex. I tested which of these possibilities are taking place by performing viral mediated local deletion of Nlgn2 in the LA. Strikingly, local deletion of Nlgn2 in the LA resulted in no change in FC magnitude, confirming that the observed dysregulation in neuronal activation in Nlgn2 KO mice was not originating from the LA. Using the same experimental conditions to produce local deletion in the BLA, aspects of the anxiety-like behavior in cNlgn2 KO mice (Cruces-Solis et al., 2021) were recapitulated. Furthermore, expression of the virus in site of injection was associated with a robust reduction of Nlgn2 levels (Cruces-Solis et al., 2021). Therefore, the lack of change in FC behavior in cNlgn2 KO mice following local deletion in the LA, could unlikely be explained by an experimental problem such as inefficiency of virus to produce Nlgn2 deletion. Also, expression of the viral construct was confirmed in the LA of mice included in the analysis by means of visual inspection of GFP fluorescence encoded by the viral construct (figures 15 and 16). However, a detailed placement analysis is still required to confirm this result. Also, the extent of Nlgn2 reduction achieved in the LA after the stereotaxic injection was not yet assessed. Taken these aspects into account, these findings indicate that the LA might likely not be the site where the behavioral deficit is originating in Nlgn2 KO mice. Therefore, the lack of activation in LA during FC retrieval was possibly already present at the level of an input projection to the LA from an upstream region. However, to confirm such a possibility, cFos assay could be performed in combination with retrograde tracing from the LA to explore which LA afferents are carrying this deficit in activation.

4.2.3. Impaired fear learning was associated with dysregulation in the distributed FC circuits

In addition to the amygdala, being the primary site underlying FC, several other brain regions were implicated in fear memory storage and modulation such as the mPFC, the AuC and the vlPAG (Herry and Johansen, 2014), see section (1.2.2). We tested whether deletion of Nlgn2 would lead to altered neuronal activation, assayed by cFos expression, in these regions during FC retrieval.

In the mPFC, an increase of neuronal activation was quantified in the PrL and IL divisions in WT mice that previously received FC training. Such increased activation in the PrL and IL has been previously reported when cFos assay was performed after FC training and after retrieval in response to repetitive CS exposure as a part of fear extinction training (Herry and Mons, 2004; Kim et al., 2010). Interestingly, a genotype dependent increase in activation was measured in the PrL of Nlgn2 KO compared to WT mice, which is similar to the activation profile we observed in the BA. Activated excitatory projections between the BA and the PrL, in both directions, were reported to be crucial for the expression of learned fear (Burgos-Robles et al., 2017; Senn et al., 2014). However, since the increased activation observed in these regions in Nlgn2 KO was detected at baseline, it could more likely represent a correlate of the anxiety phenotype, consistent with previous observations from our group (Babaev et al., 2016; Babaev et al., 2018a). Pharmacological activation of the PrL was shown to induce anxiety in mice by characterized by reduced time in the center of the OFT (Saitoh et al., 2014). Also, an over activated projection from PrL to BLA has been recently reported in mice that were behaviorally classified as stress-susceptible, as opposed to stress-resilient mice, while undergoing a paradigm of acute social defeat stress (Grossman et al., 2022). Interestingly, the PrL in Nlgn2 KO mice did not show significant increase in activation in FC trained mice similar to WT mice. This effect might be due to the overactivation observed at baseline rather than a failure in activation in response to training, However, we cannot rule out its involvement in the FC phenotype, especially that the activation in the PrL correlates with fear learning and expression (Burgos-Robles et al., 2017; Corcoran and Quirk, 2007; Senn et al., 2014; Sierra-Mercado et al., 2011).

Intriguingly, in a study by Liang et al (Liang et al., 2015), conditional deletion of Nlgn2 in the mPFC produced a deficit in auditory and contextual FC and lead to reduced mPFC activation during FC training in both of the PrL and IL. This indicates that intact synaptic inhibition promoted by Nlgn2 in this region is crucial for recruitment of mPFC to the FC circuit and for fear expression. However, since we observed an opposite activation pattern

in Nlgn2 KO mice, one potential explanation for this discrepancy might be due to a difference in the outcomes of constitutive versus local deletion of Nlgn2 on FC circuit regulation. For example, the increased activation we observed in the PrL might be caused by a synaptic deficit originating due to the lack of Nlgn2 elsewhere in the brain, such as the BA. Similar explanation might also underlie the discrepancy in the effect of conditional versus constitutive Nlgn2 deletion on contextual FC. Additionally, since the IL and PrL were shown to bidirectionally control fear responses (Senn et al., 2014), it is difficult to interpret the outcome of such genetic manipulation affecting both of them similarly on the FC circuit activation.

In the auditory cortex, the neuronal activation we observed in the Au1 and AuD was in line with the behavioral deficit in Nlgn2 KO mice. Precisely, in WT mice, an increase in neuronal activation after FC retrieval was measured in the Au1 of mice that received FC training compared to mice that received CS-only training. This increase, however, was not present between Nlgn2 KO-FC and Nlgn2-KO Ctrl mice. The AuC is responsible for encoding and processing CS information that is relayed to the LA as part of the cortical pathway (Ledoux, 2000). However, increasing evidence places the AuC as a crucial site for CS-US plasticity required for FC behavior (Dalmay et al., 2019; Letzkus et al., 2011). Interestingly, the involvement of AuC in fear learning has been shown to be more relevant in discriminative FC protocols that include presentation of two CS stimuli of different frequencies, namely CS^+ and CS^-, where only the CS^+ is paired with the US (Ledoux, 2000). In line with this observation, using in vivo optogenetics to inhibit the AuC during different FC protocols revealed that, in addition to discriminative protocols, the AuC is crucial for fear learning when a complex, more naturalistic CS is used such as frequency modulated sweeps (Dalmay et al., 2019). However, a recent study highlighted a role of the AuC in fear memory consolidation using a simple tone, non-discriminative FC protocol. In this study, optogenetic inhibition of AuC input to the LA after FC training impaired remote memory recall (Lee et al., 2021). Although using a FC protocol that includes a simple tone as a CS, a prominent cFos activation was detected during retrieval in the AuC of WT mice that was not observed in Nlgn2 KO mice. This is highly reflective of the behavioral impairment in Nlgn2 KO mice. Also, it indicates a strong involvement of the AuC in FC at least during retrieval. However, whether this change in activation in AuC is causal for FC deficit in Nlgn2 KO mice can only be tested by assessing the effect of local deletion of Nlgn2 in the AuC on FC behavior.

Since no significant neuronal activation changes were detected in the CeA during retrieval in mice of neither genotype, we sought to analyze the activation in the vlPAG, being a major output structure for freezing response downstream of the CeA (Ledoux, 2000; Tovote et al.,

2016). Strikingly, neuronal activation in this region did not reflect the freezing deficit observed in Nlgn2 KO mice. Instead, a mild increase in activation was detected in mice of both genotypes that received FC training. One potential explanation for the lack of correlation between neuronal activation in vlPAG and freezing is the heterogeneity of neurons in this region and their differential activation pattern during freezing. Freezing responses were shown to be elicited in the vlPAG by activation of glutamatergic neurons projecting to downstream motor centers. However, during freezing, only a subpopulation of vlPAG glutamatergic neurons were shown to be activated using in vivo single unit recordings (Tovote et al., 2016). Another identified population in the vlPAG are GABAergic INs that inhibit the glutamatergic neurons and those are shown to be inhibited during freezing (Tovote et al., 2016). These bidirectional responses of vlPAG neurons during freezing might explain the lack of consistent activation changes across these neural populations in WT and Nlgn2 KO mice.

4.2.4. Summary: potential sites for the fear learning impairment in Nlgn2 KO mice

While our circuit activation analysis revealed several potential sites for Nlgn2 mediated FC deficit, it is still unknown where this deficit is originating, and which circuit changes are causal for the behavioral phenotype in Nlgn2 KO mice. Several observations from this work, however, indicate a potential involvement for the areas responsible for processing and plasticity of the auditory cue. First, the amygdala showed to be a secondary site for the deficit by showing circuit dysregulation that reflected the FC deficit but was not causal for it based on the results from LA local deletion. Second, since contextual freezing showed to be normal in Nlgn2 KO mice, a deficit originating from the downstream circuits controlling freezing responses is also unlikely to be causal for the reduced auditory CS freezing. Also, the intact contextual fear learning provided a clear hint towards an impairment in CS processing along the auditory pathway. Regions of the auditory pathway such as the auditory thalamus and the auditory cortex, other than being relay and processing sites for CS information to the LA, are increasingly shown to be important sites for fear memory formation and storage. Recent studies showed with advanced methods that both regions are sites for CS and US convergence that host neural plasticity required for FC (Barsy et al., 2020; Dalmay et al., 2019; Letzkus et al., 2011; Taylor et al., 2021). In line with this, we detected prominent cFos activation changes in the AuC during FC retrieval that reflected a lack of increased activation in response to FC training. This finding highly nominates the AuC to be a site for Nlgn2 meditated FC deficit. Also, although we did not include the auditory thalamus in our circuit analysis, it might be a potential source for the deficit. To confirm a causal involvement for these regions, local deletion of Nlgn2 in the AuC and

auditory thalamus could be done followed by assessment fear leaning behavior in the resulting cNlgn2 KO mice.

4.3. Cell type specificity of Nlgn2 function in the regulation of fear learning

The prevalent hypothesis about Nlgn2 function highlights the role for Nlgn2 in regulating synapse differentiation preferentially around the perisomatic region of excitatory neurons (Babaev et al., 2016; Poulopoulos et al., 2009), In line with this notion, a reduction of density of Gephyrin puncta, was reported in the perisomatic region of PNs in the BA and CA1 of Nlgn2 KO mice while total Gephyrin density was unchanged. Also paired electrophysiological recordings in the somatosensory cortex of Nlgn2 KO mice revealed a reduction in the unitary IPSCs originating form fast-spiking PV INs but not from SOM INs (Gibson et al., 2009). However, it is not clear whether this synapse specificity in perisomatic PV INs to PN synapses is true in all brain regions. Also, a potential role of Nlgn2 in inhibitory synapses formed by other inhibitory neuron subtypes than PV INs, or in inhibitory-to-inhibitory neurons synapses was not systematically addressed. Since its crucial to know which cell types are affected by Nlgn2 deletion to understand its role in the circuits of fear learning, I investigated the cell specificity of Nlgn2 function in this circuit.

4.3.1. Nlgn2 in excitatory neurons

As state above, the proposed synapse specificity of Nlgn2 indicates a prominent role on perisomatic synapses between PV INs and PNs. However, established knowledge about the role of inhibition onto PN in FC argues against this synapse specificity. Particularly, plasticity of excitatory neurons in the regions such as the LA, the AuC, the mPFC and the auditory thalamus is crucial for fear memory acquisition and is negatively regulated by direct inhibition onto excitatory neurons (Cummings et al., 2021; Ehrlich et al., 2009; Letzkus et al., 2011; Taylor et al., 2021). Similarly, activity of excitatory neurons in regions such as the mPFC and vlPAG is required for fear expression and is also negatively regulated by direct inhibition (Cummings et al., 2021; Tovote et al., 2016). Based on this role of excitatory neurons in FC, it is unlikely that reduced inhibition onto excitatory neurons, produced by Nlgn2 deletion, would lead to reduced conditioned freezing. In fact, impaired inhibition onto excitatory neurons would predict the opposite outcome on auditory FC behavior to the one I observed in Nlgn2 KO mice.

To investigate a potential effect of Nlgn2 in synapses formed onto excitatory neurons, I investigated the outcome of Nlgn2 deletion from CAMKII neurons, being the most abundant

excitatory neuron subtype in the forebrain. As expected, lack of Nlgn2 from CAMKII neurons did not significantly alter FC retrieval. Instead, CAMKII-Cre:Nlgn2-fl/fl mice showed increased freezing in a novel context, reflecting increased anxiety as observed in constitutive Nlgn2 KO mice. The lack of effect of Nlgn2 deletion in CAMKII neurons, however, does not exclude a potential contribution of other excitatory neuron subtypes. A study investigating the role of the auditory thalamus calretinin neurons revealed a novel role for these neurons in mediating fear memory acquisition and retrieval via excitatory projections to the LA (Barsy et al., 2020). While it is not known whether these neurons co express CAMKII in addition to Calretinin, they might represent additional candidates for FC deficit in Nlgn2 KO mice.

In conclusion, CAMKII excitatory neurons were unlikely the primary site for the fear memory deficit in Nlgn2 KO mice.

4.3.2. Nlgn2 in PV neurons

Having detected no significant effect of Nlgn2 deletion from excitatory CAMKII neurons on FC, it was intriguing to know whether the FC deficit is mediated by effects on inhibitory neurons. To test this possibility, I implemented two separate approaches, namely assessment of inhibitory neuron activation during FC retrieval using cFos assay and characterizing of FC behavior in inhibitory-neuron specific Nlgn2 KO mice. While using these approaches, I focused on the main inhibitory neuron subtypes that are known to regulate the signal flow during the acquisition and expression of fear memory. A main source of inhibition onto PN in different brain regions involved in FC, such as the LA, the AuC and the mPFC is represented by PV INs that specifically target the perisomatic region of PNs (Cummings et al., 2021). Additionally, PV IN were shown to inhibit other inhibitory neurons subtypes, such as SOM in the BLA (Wolff et al., 2014) and were shown to be targets for inhibition by other inhibitory neuron subtypes during FC across different brain regions (Cummings and Clem, 2020; Krabbe et al., 2019; Letzkus et al., 2011; Pi et al., 2013). By assessing neural activation in amygdala PV INs during FC retrieval in Nlgn2 KO versus WT mice, a genotype dependent increase in activation was observed in these neurons irrespective of exposure to training. While this phenotype would theoretically lead to decreased activation of PNs at baseline levels, the deficit in PN activation we observed in this region, assessed by general cFos assay, did not reflect a baseline reduction in activation, but rather an altered activation specifically in response to FC training. One potential explanation, however, for such hyperactivation in LA PV INs in Nlgn2 KO mice might be a homeostatic effect produced to compensate for the reduction of functional inhibitory synapses around the perisomatic region of PNs (Babaev et al., 2016; Poulopoulos

et al., 2009). In line with lack of learning dependent changes in PV IN activation during FC retrieval, analysis of FC behavior in PV-Cre:Nlgn2 fl/fl mice that lack Nlgn2 in PV neurons, did not reveal any changes in CS freezing compared to PV-Cre- Nlgn2 WT mice.

Taken together, my results indicate that, despite their dysregulation in the LA, PV INs do not mediate the deficit in FC observed in Nlgn2 KO mice.

4.3.3. Nlgn2 in SOM neurons

Inhibitory SOM neurons include interneuron and projection neuron populations that play heterogeneous roles in FC regulation across different brain regions. For example, in the cortex and the cortical-like BLA, SOM neurons provide inhibition onto PNs targeting primarily their distal dendrites and were shown to be inhibited during FC (Cummings and Clem, 2020; Krabbe et al., 2018; Wolff et al., 2014). In the CeL, SOM INs are involved in reciprocal inhibitory connections with other IN subtypes while projection SOM neurons were shown to drive freezing responses by projections to downstream centers (Ciocchi et al., 2010; Fadok et al., 2017; Li et al., 2013). Furthermore, SOM INs in the mPFC, were found to provide disinhibition onto PNs during FC by inhibiting PV INs (Cummings and Clem, 2020). Interestingly, we detected changes in the activation of SOM neurons during FC retrieval in Nlgn2 KO mice specifically in the CeM. Particularly, reduced activation of CeM SOM neurons in Nlgn2 KO mice compared to WT mice was present irrespective of exposure to FC training. While the function of SOM neurons in the CeM is not well understood, it is known that general CeM activity correlates with fear expression via projection to downstream regions (Ciocchi et al., 2010; Ledoux, 2000; Tovote et al., 2016; Viviani et al., 2011). Therefore, this reduced activity in the CeM SOM INs might reflect partially the reduced freezing in Nlgn2 KO mice, however, this effect was independent of exposure to FC training. In line with this learning independent dysregulation, analysis of FC behavior in SOM-Cre Nlgn2 fl/fl mice also revealed a reduction in freezing that also seemed to be independent of learning and involved baseline and CS freezing on both FC training and testing days. Furthermore, parameters of locomotion such as speed and distance were increased in these mice compared to WT mice during OFT exploration. These findings indicate that deletion of Nlgn2 specifically from SOM neurons produces a hyperactivity phenotype, however, since such a phenotype was not present in constative Nlgn2 KO mice, it might be compensated by a phenotype resulting from the lack on Nlgn2 from another cell type. For example, the anxiety-related hypoactivation in a novel environment that I found to be produced by the lack of Nlgn2 from CAMKII neurons. Interestingly, a study investigating the activity of SOM neurons in the dorsolateral septum during contextual FC revealed that activity of these neurons predicts mobility states during memory recall and their activation

reduced freezing (Besnard et al., 2019). This is consistent with the reduced freezing in SOM-Cre Nlgn2 fl/fl mice that might result from decreased inhibition onto SOM neurons. In conclusion, my data show that SOM neurons represent a potential site for the FC deficit in Nlgn2 KO mice by affecting freezing in a learning-independent manner.

4.3.4. Nlgn2 in VIP neurons

VIP INs represent a primary source of disinhibition onto PNs during the US presentation that was shown to promote fear memory acquisition in the cortex and the BLA (Krabbe et al., 2019; Pi et al., 2013). Additionally, VIP INs were also found to project directly to PNs, but the functional relevance for the projection in FC was not yet investigated (Krabbe et al., 2019; Rhomberg et al., 2018). In contrast to PV INs, my data supported a key role VIP INs in mediating the FC deficit in Nlgn2 KO mice. First, neural activation of LA VIP INs during FC retrieval showed a significant interaction between genotype and training in the tested mice and a trend towards hyperactivation was present specifically in Nlgn2 KO mice that received FC training. This effect, however, is possibly mediated by increased excitatory input from another brain region, since local Nlgn2 deletion in the LA did not recapitulate the FC deficit observed Nlgn2 KO mice. Intriguingly, VIP-Cre:Nlgn2-fl/fl mice showed significantly reduced CS freezing than their littermate WT mice, confirming that Nlgn2 expressed by VIP INs mediates, at least partially, the deficit observed in Nlgn2 KO mice. If Nlgn2 plays a similar role in VIP INs to the one reported in excitatory neurons, its lack from VIP INs would lead to impaired inhibitory transmission onto these neurons during FC which renders them being overactivated when recruited to the FC circuit. The outcome of this overactivation on fear memory depends on the connectivity pattern of the affected VIP IN population with PNs. Accordingly, an overactivated disinhibitory projection from VIP INs onto PNs would lead to increased PN activity and increased CS freezing, which is the opposite phenotype to the one observed in Nlgn2 KO mice. Alternatively, an overactivated direct inhibitory projection from VIP INs onto PNs, would be in line with the FC impairment. Also, the reduced general neuronal activation we detected in the LA and AuC in FC trained Nlgn2 KO mice, which is largely contributed by PNs in these regions, favors also the second possibility. However, to know which VIP INs mediated circuit motif underlies the FC deficit in Nlgn2 KO mice, further experiments would be required. One way to address this question would be to record mEPSCs from VIP INs after FC in VIP-Cre:Nlgn2-fl/fl versus WT and to test whether VIP INs show an over potentiated synaptic responses after FC training. Based on a disrupted direct inhibitory projection from VIP IN onto PN, VIP INs should receive reduced synaptic input after FC in WT mice but not in Nlgn2 KO mice, similar to what have been observed in PV INs (Lucas et al., 2016). A disinhibitory projection from VIP INs, on the other hand, should show the opposite profile. Another experiment that could be

performed to address the effect of Nlgn2 deletion on VIP IN function in the FC circuit is measuring calcium influx in VIP INs in behaving mice using in vivo calcium imaging. In such an experiment, plasticity of VIP INs, measured with increased/decreased calcium peaks during CS presentation can be assessed during FC retrieval and compared between Nlgn2 KO and WT mice. The target brain region for such measurements is, however, still to be determined.

In conclusion, by investigation the inhibitory neuron contribution to FC deficit in Nlgn2 KO mice, it can be inferred that this deficit is likely a combinatorial effect resulting from the lack of Nlgn2 from VIP and SOM inhibitory neurons. While both neuron subtypes were shown to be key players in the FC circuit, the deficit in SOM-Cre:Nlgn2-fl/fl seemed to reflect a locomotor deficit rather than a deficit in learning. This places VIP INs to be the most relevant candidate for mediating Nlgn2 role in FC circuit.

4.3.5. Nlgn2 is present in inhibitory synapses formed by and onto inhibitory neurons

Consistent with the altered behavior resulting from lack of Nlgn2 from SOM and VIP INs, both subtypes showed to be contacted by $Nlgn2^{+}$ synapses using super resolution STED microscopy performed in the LA and AuC regions. This was confirmed by detection of Nlgn2 and vGAT labelled structures in close proximity to EYFP labelled processes belonging to each of VIP, SOM or PV neurons. Taking advantage of the STED nanoscale resolution, detected synapses were classified based on the spatial location of vGAT and Nlgn2 in relation to the cell specific EYFP labelled processes. Based on this qualitative analysis, putative $Nlgn2^{+}$ positive synapses formed by and onto each of VIP, SOM and PV INs were found in the LA and AuC regions.

Consistent with this analysis, the expression of Nlgn2 by these inhibitory neuron subtypes was confirmed using single-cell mRNA sequencing in two different studies in cortical neurons (Huntley et al., 2020; Paul et al., 2017). Interestingly, in the study by Paul et al, specifically high mRNA expression of Nlgn2 was measured in VIP INs, in line with the prominent role of Nlgn2 in these neurons.

Despite achieving a resolution of approximately 40 nm using the two-color STED method to pinpoint the relative position of Nlgn2 relative to EYFP labelled processes, acquiring quantitative data regarding the amount if Nlgn2 present in each configuration per each neuron type would be laborious and possibly inaccurate. One way to improve this analysis would be to segregate the labelling of axons and dendrites in the EYFP labelled neurons.

Using axonal and dendritic markers for this purpose was, however, not compatible with methanol fixation optimal for Nlgn2 labelling (data not shown). An alternative strategy to confirm our findings and obtain quantitative results would be to deliver into PV/VIP/SOM-Cre:Ai32 mice a fluorescent protein (of a different fluorescent wavelength than EYFP) that is expressed in a Cre-dependent manner under the control of a presynaptic protein promoter (such as Synaptophysin). Such a construct is commercially available and it would label only synaptic terminals and allow us to differentiate them from dendritic labelling.

4.4. Nlgn2 differentially regulate fear learning and anxiety

4.4.1. Nlgn2 differentially regulates fear learning and anxiety via different regions

While anxiety-like behavior is usually accompanied by increased fear learning, Nlgn2 deletion affected these two behaviors in an intriguingly contrasting manner. In addition, the circuits underlying anxiety and fear memory retrieval were shown to be also differentially affected by Nlgn2 deletion in a way that unmasked their distinct regulation at the normal level. For example, while anxiety-like behavior in Nlgn2 KO mice was associated with increased cFos activation in the BA and CeM amygdala nuclei (Babaev et al., 2018a), FC retrieval was associated with differential activation in the LA nucleus only. Interestingly, the BA also showed increased activation in Nlgn2 KO mice during retrieval, but since this activation was not affected by exposure to FC, it likely reflected an internal state of Nlgn2 KO mice that could be due to increased anxiety during the experiment. However, the CeA did not reflect changes in activation corresponding to neither FC retrieval nor potential anxiety. This could be due to a methodological limitation of the cFos assay that lacks the temporal resolution to assess transient and complex activity of the heterogeneous neuronal populations in the CeA. Furthermore, while deletion of Nlgn2 from the BLA recapitulated the anxiety like phenotype (Cruces-Solis et al., 2021), deletion of Nlgn2 in the LA did not affect fear learning despite the activation changes detected in this region in Nlgn2 KO mice. This indicates that the amygdala is likely a dispensable site for the fear learning deficit in Nlgn2 KO mice. The deficit is then probably caused by a circuit dysregulation in an upstream region such as the AuC or the auditory thalamus. Taken together, these data showed that fear learning deficit and anxiety-like behavior in Nlgn2 KO mice are associated with altered activation in distinct regions.

4.4.2. Nlgn2 differentially regulates fear learning and anxiety via different cell types

In light of the circuit specific role of Nlgn2 in regulating brain function, the differential role Nlgn2 plays in regulating fear learning and anxiety might result from differential effects of Nlgn2 on distinct cell types. Assessment of anxiety-like behavior in cell-specific Nlgn2 KO mice provided insights on the function of Nlgn2 in regulating fear learning versus anxiety. One intriguing finding was that deletion of Nlgn2 in excitatory CAMKII underlies the anxiety-like phenotype. Accordingly, the behavior of CAMKII-Cre:Nlgn2-fl/fl mice in the OFT was almost identical to the one observed in constitutive Nlgn2 KO mice (Babaev et al., 2016; Blundell et al., 2009) as well as the higher innate freezing they showed in a novel environment. In contrast to anxiety, CAMKII-Cre:Nlgn2-fl/fl mice did not show significantly reduced fear learning.

Deletion of Nlgn2 from inhibitory neurons, on the other hand, did not seem to affect anxiety-like behavior in a similar way. For example, behavior of PV-Cre-Nlgn2-fl/fl mice in the OFT did not differ from WT mice in any of the measured parameters. This confirmed that, similar to what have been observed by assessing fear learning, deletion of Nlgn2 from PV INs does not contribute to the anxiety-like phenotype in Nlgn2 KO mice. Similarly, VIP-Cre-Nlgn2 fl/fl mice did not exhibit any anxiety-like or locomotor phenotype in the OFT despite their reduced FC retrieval. Interestingly, SOM-Cre:Nlgn2-fl/fl mice showed significant increases in all the measured OFT parameters that reflected hyperactivity due to a locomotor deficit, or increased novelty-induced exploration. Together, these findings confirm that fear learning and anxiety are regulated by Nlgn2 through effects on distinct cell types. In summary, CAMKII neurons showed to be the main cell type driving anxiety-like behavior in Nlgn2 KO mice while VIP and SOM neurons mediated different aspects of the FC deficit resulting from Nlgn2 deletion.

4.4.3. Nlgn2 differentially regulate fear learning and anxiety via distinct interaction patterns with IgSF9b

Several interaction partners of Nlgn2 have been identified and shown to support or inhibit its function on the inhibitory synapse and circuit levels (Ali et al., 2020). Among these interaction partners, IgSF9b was shown to modulate anxiety-like behavior in Nlgn2 KO mice by modulating synaptic inhibition in the amygdala, but through effects on a different nucleus than the one affected by Ngn2 deletion. As a result, deletion of IgSF9b led to normalized anxiety-like behavior in Nlgn2 KO mice in line with an antagonistic effect (Babaev et al., 2018a). I sought to understand whether this interaction phenotype is also controlling fear

learning and therefore I assessed FC behavior in Nlgn2 KO, IgSF9b KO and double KO versus WT. Surprisingly, auditory FC deficit was exacerbated in IgSF9b-Nlgn2 double KO mice indicating that, in this circuit, Ngn2 and IgSF9b play synergistic roles. Remarkably, this finding highlighted another aspect of the distinct regulation between auditory fear learning and anxiety by Nlgn2. However, to understand how exactly this effect of IgSF9b deletion is exerted, further work would be still required. For example, it would be crucial to know whether the exacerbated FC deficit is mediated by effects of each protein on different brain regions, like in anxiety regulation, or by affecting specific synapses in the same region. Interestingly, measuring contextual FC revealed a similar interaction between Nlgn2 and IgSF9b as the one observed in anxiety-like behavior. In this paradigm, contextual freezing was significantly reduced in IgSF9b KO mice and the reduction was rescued by Nlgn2 deletion as double KO mice showed normal contextual freezing levels. While this observation confirmed that the lack of auditory conditioned freezing in double KO mice is not due to motor problems, it remains to be elucidated how these proteins affect contextual memory formation in the hippocampus.

4.5. Potential memory stages affected in Nlgn2 KO mice

According to the most prominent cellular model for memory, population of cells are activated and modified to store memory during acquisition and are thereby allocated to the memory trace or ‘engram’. After memory acquisition, engram cells undergo persistent changes that normally involve de novo protein synthesis, leading to memory consolidation. When the cue that elicited memory acquisition is presented again, engram cells are activated leading to the behavioral response measured as a correlate of memory (Josselyn and Tonegawa, 2020). Based on this model, the impairment in fear learning in Nlgn2 KO mice measured at the level of retrieval after 2 h and 24 h, could reflect impaired acquisition only or impaired acquisition and consolidation. The same logic applies to the lack of increased neural activation in FC trained Nlgn2 KO mice detected in the regions such as LA and AuC. Although further work is still required to elucidate how Nlgn2 deletion effects each of these memory stages, few speculations could be made based on the current knowledge about Nlgn2. At the level of memory acquisition, FC has shown to be mediated by plasticity of excitatory and inhibitory neurons in regions such as the amygdala and the cortex (Cummings and Clem, 2020; Johansen et al., 2011b; Krabbe et al., 2018; Ledoux, 2000; Letzkus et al., 2011). Studies investigating plasticity of inhibitory neurons in fear learning, showed that reduced activation of specific inhibitory neuron subtypes is required for FC (Lucas et al., 2016; Wolff et al., 2014), which might be a result of potentiated synaptic inhibition on these neurons, i.e., inhibitory plasticity. The effect of Nlgn2 on excitatory

plasticity have been assessed previously in a study measuring LTP in granule cells of the dentate gyrus while stimulating the perforant path (Jedlicka et al., 2011). As shown by this study, excitatory LTP at granule cells was not affected by Nlgn2 deletion, indicating lack of effect of Nlgn2 on this form of excitatory plasticity in this network. However, it has not been investigated before whether Nlgn2 affects inhibitory plasticity, which might be a key to understand its role in fear learning regulation.

With regard to its potential role in regulating memory consolidation, a study by Ye et al (Ye et al., 2017) investigating the role of Nlgn2 in contextual inhibitory avoidance task revealed an increase of Nlgn2 levels after training. Blocking Nlgn2 function by repetitively injecting a synthetic Nlgn2 extracellular domain peptide into the PrL cortex impaired memory consolidation required for this task. This effect was postulated by the authors to be mediated by a disinhibitory mechanism involving Nlgn2 (Katzman and Alberini, 2018). Additionally, since memory consolidation is found to be highly dependent on sleep (Stickgold, 2005), this process could be affected in Nlgn2 KO mice that were reported to have disrupted sleep cycle including increased wakefulness and reduced REM and non-REM sleep (Seok et al., 2018). The mechanisms by which Nlgn2 regulates sleep, however, are still unknown and thereby also its potential role in memory consolidation.

5. Conclusions and outlook

Using a combination of methods including behavioral analysis, neuronal activation assay and cell and region-specific genetic manipulations, I show in the present work that Nlgn2 is a key regulator for the processing of aversive memories that are acquired in association to auditory stimuli. Nlgn2 KO mice showed a robust deficit in auditory fear conditioning that was associated with dysregulation in neuronal activity within different fear memory processing nodes. Intriguingly, Nlgn2 mediated its role in FC by effects on inhibitory neurons rather than excitatory CAMKII neurons with a learning-specific effect on VIP INs. However, further work is still required to identify the brain region and the mechanism by which Nlgn2 affects VIP INs in this circuit.

Being a key regulator of anxiety-like behavior (Babaev et al., 2016; Blundell et al., 2009), the deficit in fear learning in Nlgn2 KO mice was unexpected in light of the role played by synaptic inhibition in regulating these circuits. However, analysis of cell type specificity of Nlgn2 role in these circuits unraveled the contribution of distinct cell types to the behavioral phenotype of anxiety versus fear learning. This notion reflected the complexity by which

Nlgn2 regulates brain function and confirmed that its effects extend beyond the proposed synapse specificity for its function.

The role of Nlgn2 in promoting inhibitory synapse maturation and function has shown to be critical for maintaining E/I balance within brain circuits (Ali et al., 2020). While the canonical outcome for impairment in inhibition, mediated by Nlgn2 deletion or dysfunction, would predict a shift in this balance towards increased excitation, as seen in in anxiety circuit, my data show that this simple scheme does not apply to all brain circuits regulated by Nlgn2. Instead, Nlgn2 on certain inhibitory neuron types could potentially promote overall excitation. While several other synaptic proteins were also found to be relevant for the maintenance of E/I balance (Ali et al., 2020), it is important to take this notion into account when investigating their function in brain circuits.

To better understand how the fear memory impairment is produced by Nlgn2 deletion, it would be advantageous to implement circuit analysis methods that allow for real time inspection of cell activity during behavior, as opposed to immediate early gene assays that suffer from low temporal resolution. Examples of techniques that would circumvent this limitation would include the use of in vivo single unit electrophysiological recordings or in vivo calcium imaging that could be performed in a cell-type specific manner during different stages of fear learning. Additionally, a causal link between the circuit alterations potentially detected with these methods and the behavioral deficit could be established by means of cell-type specific optogenetic or chemogenic manipulations. For example, by performing rescue experiments in which optogenetic/chemogenetic inhibition of VIP INs during fear learning could be tested for its ability to restore the FC deficit in Nlgn2 KO mice.

The cell and circuit specificity of Nlgn2 mediated regulation of inhibition, elucidated by its role in fear learning, provided novel aspects to the molecular regulation of brain function by synaptic molecules. These aspects are important to consider for the potential use of Nlgn2 and other synapse organizers as therapeutic targets for neuropsychiatric pathologies.

Acknowledgements

First, I would like to thank Prof. Dr. Dilja Krüger-Burg for giving me the chance to work on exciting research projects and for her great passion and dedication for science that were inspiring for me and all other team members. Also, thank you Dilja for your guidance and support with all aspects of my doctoral work, for giving me the chance to be part of several publications and for allowing me the freedom to have the full experience and grow towards becoming an independent researcher. I learned a lot from you and will always be grateful for that.

I am very grateful that I conducted my doctoral research as a member of the laboratory of Prof. Dr. Nils Brose. Thank you, Nils, for providing all the support for me and other colleagues, for your helpful feedback on my project and for maintaining a welcoming and motivating work environment within the Brose Lab family.

I would like to thank my current thesis committee members: Prof. Dilja Krüger-Burg, Prof. Dr. Thomas Dresbach and Prof. Dr. Hannelore Ehrenreich. Also, thanks to the previous members: Prof. Dr. Nils Brose and Dr. Camin Dean who all provided valuable feedback and a lot of support and encouragement during my TAC meetings. In addition, I would like to thank Prof. Dr. Nils Brose, Dr Camin Dean and Dr. Katrin Willig whom I will have the pleasure to have as extended committee members during my thesis defense.

I am very grateful to the collaboration with the lab of Prof. Dr. Hannelore Ehrenreich that was very essential for my doctoral work. I thank Prof. Ehrenreich for the opportunity to conduct my behavioral analyses in the behavior unit of the Clinical Neuroscience department, where I benefited from cutting-edge methodologies and optimal experimental conditions.

I would like to thank Dr. Katrin Willig for the collaboration that made a nice contribution to my findings, for guiding me through the critical concepts of superresolution and showing me how to acquire images with the mighty STED microscope. Also, thank you Katrin for being friendly and supportive and for the helpful feedback on my results.

I would like to thank Lena Marth for her hard and reliable work and for her critical thinking that all made a great contribution to my doctoral work and the publication to come.

I would like to thank the people who provided outstanding technical support for my experiments: Sally Wenger for the laborious virus preparations and the generation of cNlgn2 KO mice. I also thank Sally for being kind and supportive. Dr. Fritz Benseler and all the members of the AGCT lab in the Molecular Neurobiology department (Ivonne Thanhäuser, Dayana Warnecke and Christiane Harenberg) for the immense effort regarding mouse genotyping, generation of the cNlgn2 KO mice and production of DNA primers that were all crucial for my experiments. I would also like to thank them for their efforts with COVID- campus screen that helped maintain a safe work environment for me and all other colleagues.

I am grateful to the administration of the MPINAT animal facility (Anke Schräpler) for providing all means that facilitated my animal experiments. Also, thanks to the animal caretakers (Nadine Ilse, Christine Klaus and Bianca Nickel) for their care and maintenance of my mouse colonies and for providing me with help and support during my experiments in the animal facility despite my poor German. Also, special thanks to Dr. Ursula Fünfschilling who helped me establish optimal conditions for my experiments in the facility according to the biosafety and animal welfare guidelines and my own optimal safety. She was there every time I faced a problem and helped me deal with all technical challenges. I would like to thank Anja Ronnenberg for providing technical support, guidance and a lot of help during my experiments in the behavior unit.

I would like to thank all the people who contributed to my learning process which I value the most during the PhD experience: Prof. Dr. Dilja Krüger-Burg for the training with behavior experiments and emphasizing how critical it is to pay attention to every detail regarding mouse behavior to the level that I started to think like a mouse when handling them ☺ Also, thank you Dilja for helping me improve my skills in scientific writing, presentation and communication and for always taking the time to provide detailed and valuable feedback on all of my scientific skills. Dr. Olga Babaev for sharing her expertise and contributing to my training in several lab methodologies (imaging, stereotaxic injections) and for continuing to answer my questions even after leaving the lab. The LMF facility of the MPINAT: Dr. Miso Mitkovski and Heiko Röhse for providing training related to different aspects of confocal microscopy. Also, thank you Miso for your helpful input on my image analysis and macro design for the MDGA1-Nlgn2 colocalization project. Dr. Erinn Gideons who taught me LTP slice recordings, shared her knowledge and experience and did not mind my numerous questions despite pregnancy. Sally Wenger, again, for contributing to my laboratory training in several methods (behavior, IHC) and Carolina Pilleti Chatain for the training and help she provided when I first joined the group.

I would like to thank the people who provided help on different topics I was learning during my PhD: Dr. Carolina Thomas who introduced me to image J macro language and wrote me the first loop, Dr. Ali Shaib who gave me very helpful insights regarding microscopy, Dr. Valerie Clavet-Fournier for her useful tips and insights with STED microscopy and Dr. Francisco Lopez Murcia for sharing his knowledge with colocalization analysis.

I would like to thank the colleagues of the Brose department, who were very kind and helpful every time I approached them with a question: Dr. Hong Jun Rhee, Dr. Chungku Lee, Dr. Theofilos Papadopoulos, Dr. Benjamin Cooper, Dr James Daniel, Dr. Noa Lipstein, Dr. Holger Taschenberger, Dr. Sonja Wojcik and Dr. Fritz Benseler.

I would like to thank Mrs. Birgit Gläser for her help with paperwork and regulations in (and outside) the institute.

I would like to thank the Neuroscience Office: Dr. Michael Hörner (RIP), Dr Jonas Barth and especially Mrs. Sandra Drube who always helped me through the master's and PhD regulations.

I would like to thank the Neurasmus program family, who made it possible for me to achieve my scientific and life goals.

I would like to thank all the previous and current students in the Brose department with whom I shared a very nice journey: Sofia, Carolina, Aisha, Jutta, Lydia, Ines, Natalia, Jennifer, Öyküm, Dragana, Valentina, Kerstin, Sven, Lena, Tommaso, Valentin …

I would like to thank the friends who proofread my thesis: Dr. Anouk Meeuwissen, Dr. Sofia Elizarova, Helena Fink and Franziska Hentschel.. Thank you for the effort and support during the thesis writing.

I would like to thank my friends: Burak, Valerie, Sofia and Anouk for all the great activities we did together and for the support during stressful times. Thanks to Franzi for supporting me and cheering me up with her positivity, sense of humor and endless reservoir of boardgames. You are the best roomy ever! Thank to Labib, Hellie and Anna for being great and supportive friends.

Finally, I would like to dedicate this work to my parents Rinet and Yakoub, who encouraged me to pursue my dreams despite the war conditions they live in; To my sisters: Rasha, Lama, Rita and my brother Alaa; and to my nieces and nephews who were always able to brighten up my day every time I met or called them: Naya, Yahia, Fares, Rinet, Masha and Liana.

Bibliography

Abs, E., Poorthuis, R.B., Apelblat, D., Muhammad, K., Pardi, M.B., Enke, L., Kushinsky, D., Pu, D.L., Eizinger, M.F., Conzelmann, K.K., et al. (2018). Learning-Related Plasticity in Dendrite-Targeting Layer 1 Interneurons. Neuron *100*, 684-699 e686. 10.1016/j.neuron.2018.09.001.

Ali, H., Marth, L., and Krueger-Burg, D. (2020). Neuroligin-2 as a central organizer of inhibitory synapses in health and disease. Science Signaling *13*.

Anglada-Figueroa, D., and Quirk, G.J. (2005). Lesions of the basal amygdala block expression of conditioned fear but not extinction. J Neurosci *25*, 9680-9685. 10.1523/JNEUROSCI.2600-05.2005.

Arruda-Carvalho, M., and Clem, R.L. (2014). Pathway-selective adjustment of prefrontal-amygdala transmission during fear encoding. J Neurosci *34*, 15601-15609. 10.1523/JNEUROSCI.2664-14.2014.

Aurnhammer, C., Haase, M., Muether, N., Hausl, M., Rauschhuber, C., Huber, I., Nitschko, H., Busch, U., Sing, A., Ehrhardt, A., and Baiker, A. (2012). Universal real-time PCR for the detection and quantification of adeno-associated virus serotype 2-derived inverted terminal repeat sequences. Hum Gene Ther Methods *23*, 18-28. 10.1089/hgtb.2011.034.

Babaev, O., Botta, P., Meyer, E., Muller, C., Ehrenreich, H., Brose, N., Luthi, A., and Krueger-Burg, D. (2016). Neuroligin 2 deletion alters inhibitory synapse function and anxiety-associated neuronal activation in the amygdala. Neuropharmacology *100*, 56-65. 10.1016/j.neuropharm.2015.06.016.

Babaev, O., Cruces-Solis, H., Piletti Chatain, C., Hammer, M., Wenger, S., Ali, H., Karalis, N., de Hoz, L., Schluter, O.M., Yanagawa, Y., et al. (2018a). IgSF9b regulates anxiety behaviors through effects on centromedial amygdala inhibitory synapses. Nat Commun *9*, 5400. 10.1038/s41467-018-07762-1.

Babaev, O., Piletti Chatain, C., and Krueger-Burg, D. (2018b). Inhibition in the amygdala anxiety circuitry. Exp Mol Med *50*, 18. 10.1038/s12276-018-0063-8.

Barsy, B., Kocsis, K., Magyar, A., Babiczky, A., Szabo, M., Veres, J.M., Hillier, D., Ulbert, I., Yizhar, O., and Matyas, F. (2020). Associative and plastic thalamic signaling to the lateral amygdala controls fear behavior. Nat Neurosci *23*, 625-637. 10.1038/s41593-020-0620-z.

Bechara, A., Tranel, D., Damasio, H., Adolphs, R., Rockland, C., and Damasio, A.R. (1995). Double dissociation of conditioning and declarative knowledge relative to the amygdala and hippocampus in humans. Science *269*, 1115-1118. 10.1126/science.7652558.

Bergado-Acosta, J.R., Sangha, S., Narayanan, R.T., Obata, K., Pape, H.C., and Stork, O. (2008). Critical role of the 65-kDa isoform of glutamic acid decarboxylase in consolidation and generalization of Pavlovian fear memory. Learn Mem *15*, 163-171. 10.1101/lm.705408.

Besnard, A., Gao, Y., TaeWoo Kim, M., Twarkowski, H., Reed, A.K., Langberg, T., Feng, W., Xu, X., Saur, D., Zweifel, L.S., et al. (2019). Dorsolateral septum somatostatin interneurons gate mobility to calibrate context-specific behavioral fear responses. Nature Neuroscience *22*, 436-446. 10.1038/s41593-018-0330-y.

Beyeler, A., Chang, C.J., Silvestre, M., Lévêque, C., Namburi, P., Wildes, C.P., and Tye, K.M. (2018). Organization of Valence-Encoding and Projection-Defined Neurons in the Basolateral Amygdala. Cell Rep *22*, 905-918. 10.1016/j.celrep.2017.12.097.

Bissiere, S., Humeau, Y., and Luthi, A. (2003). Dopamine gates LTP induction in lateral amygdala by suppressing feedforward inhibition. Nat Neurosci *6*, 587-592. 10.1038/nn1058.

Blair, H.T., Schafe, G.E., Bauer, E.P., Rodrigues, S.M., and LeDoux, J.E. (2001). Synaptic plasticity in the lateral amygdala: a cellular hypothesis of fear conditioning. Learn Mem *8*, 229-242. 10.1101/lm.30901.

Blanchard, D.C., and Blanchard, R.J. (1972). Innate and conditioned reactions to threat in rats with amygdaloid lesions. J Comp Physiol Psychol *81*, 281-290. 10.1037/h0033521.

Bliss, T.V., and Lomo, T. (1973). Long-lasting potentiation of synaptic transmission in the dentate area of the anaesthetized rabbit following stimulation of the perforant path. J Physiol *232*, 331-356. 10.1113/jphysiol.1973.sp010273.

Blundell, J., Tabuchi, K., Bolliger, M.F., Blaiss, C.A., Brose, N., Liu, X., Sudhof, T.C., and Powell, C.M. (2009). Increased anxiety-like behavior in mice lacking the inhibitory synapse cell adhesion molecule neuroligin 2. Genes Brain Behav *8*, 114-126. 10.1111/j.1601-183X.2008.00455.x.

Boatman, J.A., and Kim, J.J. (2006). A thalamo-cortico-amygdala pathway mediates auditory fear conditioning in the intact brain. Eur J Neurosci *24*, 894-900. 10.1111/j.1460-9568.2006.04965.x.

Bordi, F., and LeDoux, J.E. (1994). Response properties of single units in areas of rat auditory thalamus that project to the amygdala. II. Cells receiving convergent auditory and somatosensory inputs and cells antidromically activated by amygdala stimulation. Exp Brain Res *98*, 275-286. 10.1007/BF00228415.

Brzózka, M.M., Radyushkin, K., Wichert, S.P., Ehrenreich, H., and Rossner, M.J. (2010). Cognitive and sensorimotor gating impairments in transgenic mice overexpressing the schizophrenia susceptibility gene Tcf4 in the brain. Biol Psychiatry *68*, 33-40. 10.1016/j.biopsych.2010.03.015.

Burgos-Robles, A., Kimchi, E.Y., Izadmehr, E.M., Porzenheim, M.J., Ramos-Guasp, W.A., Nieh, E.H., Felix-Ortiz, A.C., Namburi, P., Leppla, C.A., Presbrey, K.N., et al. (2017). Amygdala inputs to prefrontal cortex guide behavior amid conflicting cues of reward and punishment. Nat Neurosci *20*, 824-835. 10.1038/nn.4553.

Burgos-Robles, A., Vidal-Gonzalez, I., and Quirk, G.J. (2009). Sustained conditioned responses in prelimbic prefrontal neurons are correlated with fear expression and extinction failure. J Neurosci *29*, 8474-8482. 10.1523/JNEUROSCI.0378-09.2009.

Bárez-López, S., Montero-Pedrazuela, A., Bosch-García, D., Venero, C., and Guadaño-Ferraz, A. (2017). Increased anxiety and fear memory in adult mice lacking type 2 deiodinase. Psychoneuroendocrinology *84*, 51-60. 10.1016/j.psyneuen.2017.06.013.

Cador, M., Robbins, T.W., and Everitt, B.J. (1989). Involvement of the amygdala in stimulus-reward associations: interaction with the ventral striatum. Neuroscience *30*, 77-86. 10.1016/0306-4522(89)90354-0.

Calhoon, G.G., and Tye, K.M. (2015). Resolving the neural circuits of anxiety. Nat Neurosci *18*, 1394-1404. 10.1038/nn.4101.

Campeau, S., and Davis, M. (1995). Involvement of subcortical and cortical afferents to the lateral nucleus of the amygdala in fear conditioning measured with fear-potentiated startle in rats trained concurrently with auditory and visual conditioned stimuli. J Neurosci *15*, 2312-2327.

Carrive, P. (2000). Conditioned fear to environmental context: Cardiovascular and behavioral components in the rat. Brain Research *858*, 440-445. 10.1016/S0006-8993(00)02029-1.

Carrive, P., Leung, P., Harris, J., and Paxinos, G. (1997). Conditioned fear to context is associated with increased Fos expression in the caudal ventrolateral region of the midbrain periaqueductal gray. Neuroscience *78*, 165-177. https://doi.org/10.1016/S0306-4522(97)83047-3.

Chaaya, N., Battle, A.R., and Johnson, L.R. (2018). An update on contextual fear memory mechanisms: Transition between Amygdala and Hippocampus. Neurosci Biobehav Rev *92*, 43-54. 10.1016/j.neubiorev.2018.05.013.

Chen, C., Krueger-Burg, D., and de Hoz, L. (2019). Wide sensory filters underlie performance in memory-based discrimination and generalization. PLoS One *14*, e0214817. 10.1371/journal.pone.0214817.

Chen, C.-H., Lee, P.-W., Liao, H.-M., and Chang, P.-K. (2017). Neuroligin 2 R215H Mutant Mice Manifest Anxiety, Increased Prepulse Inhibition, and Impaired Spatial Learning and Memory. Frontiers in Psychiatry *8*. 10.3389/fpsyt.2017.00257.

Chen, J., Dong, B., Feng, X., Jiang, D., Chen, G., Long, C., and Yang, L. (2020). Aberrant mPFC GABAergic synaptic transmission and fear behavior in neuroligin-2 R215H knock-in mice. Brain Res *1730*, 146671. 10.1016/j.brainres.2020.146671.

Chini, M., and Hanganu-Opatz, I.L. (2021). Prefrontal Cortex Development in Health and Disease: Lessons from Rodents and Humans. Trends Neurosci *44*, 227-240. 10.1016/j.tins.2020.10.017.

Chubykin, A.A., Atasoy, D., Etherton, M.R., Brose, N., Kavalali, E.T., Gibson, J.R., and Sudhof, T.C. (2007). Activity-dependent validation of excitatory versus inhibitory synapses by neuroligin-1 versus neuroligin-2. Neuron *54*, 919-931. 10.1016/j.neuron.2007.05.029.

Ciocchi, S., Herry, C., Grenier, F., Wolff, S.B., Letzkus, J.J., Vlachos, I., Ehrlich, I., Sprengel, R., Deisseroth, K., Stadler, M.B., et al. (2010). Encoding of conditioned fear in central amygdala inhibitory circuits. Nature *468*, 277-282. 10.1038/nature09559.

Concina, G., Renna, A., Grosso, A., and Sacchetti, B. (2019). The auditory cortex and the emotional valence of sounds. Neurosci Biobehav Rev *98*, 256-264. 10.1016/j.neubiorev.2019.01.018.

Connor, S.A., Ammendrup-Johnsen, I., Kishimoto, Y., Karimi Tari, P., Cvetkovska, V., Harada, T., Ojima, D., Yamamoto, T., Wang, Y.T., and Craig, A.M. (2017). Loss of

Synapse Repressor MDGA1 Enhances Perisomatic Inhibition, Confers Resistance to Network Excitation, and Impairs Cognitive Function. Cell Rep *21*, 3637-3645. 10.1016/j.celrep.2017.11.109.

Connor, S.A., Elegheert, J., Xie, Y., and Craig, A.M. (2019). Pumping the brakes: suppression of synapse development by MDGA-neuroligin interactions. Curr Opin Neurobiol *57*, 71-80. 10.1016/j.conb.2019.01.002.

Corcoran, K.A., and Quirk, G.J. (2007). Activity in prelimbic cortex is necessary for the expression of learned, but not innate, fears. J Neurosci *27*, 840-844. 10.1523/JNEUROSCI.5327-06.2007.

Courtin, J., Bienvenu, T.C., Einarsson, E.O., and Herry, C. (2013). Medial prefrontal cortex neuronal circuits in fear behavior. Neuroscience *240*, 219-242. 10.1016/j.neuroscience.2013.03.001.

Courtin, J., Chaudun, F., Rozeske, R.R., Karalis, N., Gonzalez-Campo, C., Wurtz, H., Abdi, A., Baufreton, J., Bienvenu, T.C., and Herry, C. (2014). Prefrontal parvalbumin interneurons shape neuronal activity to drive fear expression. Nature *505*, 92-96. 10.1038/nature12755.

Cruces-Solis, H., Babaev, O., Ali, H., Piletti Chatain, C., Mykytiuk, V., Balekoglu, N., Wenger, S., and Krueger-Burg, D. (2021). Altered theta and beta oscillatory synchrony in a genetic mouse model of pathological anxiety. FASEB J *35*, e21585. 10.1096/fj.202002028RR.

Cummings, K.A., and Clem, R.L. (2020). Prefrontal somatostatin interneurons encode fear memory. Nat Neurosci *23*, 61-74. 10.1038/s41593-019-0552-7.

Cummings, K.A., Lacagnina, A.F., and Clem, R.L. (2021). GABAergic microcircuitry of fear memory encoding. Neurobiol Learn Mem *184*, 107504. 10.1016/j.nlm.2021.107504.

Curtis, D. (2016). Practical Experience of the Application of a Weighted Burden Test to Whole Exome Sequence Data for Obesity and Schizophrenia. Ann Hum Genet *80*, 38-49. 10.1111/ahg.12135.

Curtis, D., and Consortium, T.U.K. (2016). Practical Experience of the Application of a Weighted Burden Test to Whole Exome Sequence Data for Obesity and Schizophrenia. Annals of Human Genetics *80*, 38-49. https://doi.org/10.1111/ahg.12135.

Dalmay, T., Abs, E., Poorthuis, R.B., Hartung, J., Pu, D.L., Onasch, S., Lozano, Y.R., Signoret-Genest, J., Tovote, P., Gjorgjieva, J., and Letzkus, J.J. (2019). A Critical Role for Neocortical Processing of Threat Memory. Neuron *104*, 1180-1194 e1187. 10.1016/j.neuron.2019.09.025.

Deng, J., Zhou, H., Lin, J.K., Shen, Z.X., Chen, W.Z., Wang, L.H., Li, Q., Mu, D., Wei, Y.C., Xu, X.H., and Sun, Y.G. (2020). The Parabrachial Nucleus Directly Channels Spinal Nociceptive Signals to the Intralaminar Thalamic Nuclei, but Not the Amygdala. Neuron *107*, 909-923 e906. 10.1016/j.neuron.2020.06.017.

Dere, E., Dahm, L., Lu, D., Hammerschmidt, K., Ju, A., Tantra, M., Kastner, A., Chowdhury, K., and Ehrenreich, H. (2014). Heterozygous ambra1 deficiency in mice: a genetic trait with autism-like behavior restricted to the female gender. Front Behav Neurosci *8*, 181. 10.3389/fnbeh.2014.00181.

Duits, P., Cath, D.C., Lissek, S., Hox, J.J., Hamm, A.O., Engelhard, I.M., van den Hout, M.A., and Baas, J.M. (2015). Updated meta-analysis of classical fear conditioning in the anxiety disorders. Depress Anxiety *32*, 239-253. 10.1002/da.22353.

Duvarci, S., and Pare, D. (2014). Amygdala microcircuits controlling learned fear. Neuron *82*, 966-980. 10.1016/j.neuron.2014.04.042.

Edeline, J.M., and Weinberger, N.M. (1991). Subcortical adaptive filtering in the auditory system: associative receptive field plasticity in the dorsal medial geniculate body. Behav Neurosci *105*, 154-175. 10.1037//0735-7044.105.1.154.

Ehrlich, I., Humeau, Y., Grenier, F., Ciocchi, S., Herry, C., and Luthi, A. (2009). Amygdala inhibitory circuits and the control of fear memory. Neuron *62*, 757-771. 10.1016/j.neuron.2009.05.026.

Fadok, J.P., Krabbe, S., Markovic, M., Courtin, J., Xu, C., Massi, L., Botta, P., Bylund, K., Muller, C., Kovacevic, A., et al. (2017). A competitive inhibitory circuit for selection of active and passive fear responses. Nature *542*, 96-100. 10.1038/nature21047.

Fanselow, M.S. (1990). Factors governing one-trial contextual conditioning. Animal Learning & Behavior *18*, 264-270. 10.3758/BF03205285.

Fanselow, M.S. (1991). The midbrain periaqueductal gray as a coordinator of action in response to fear and anxiety. In The midbrain periaqueductal gray matter, (Springer), pp. 151-173.

Fanselow, M.S. (2010). From contextual fear to a dynamic view of memory systems. Trends Cogn Sci *14*, 7-15. 10.1016/j.tics.2009.10.008.

Fanselow, M.S., and Helmstetter, F.J. (1988). Conditional analgesia, defensive freezing, and benzodiazepines. Behavioral Neuroscience *102*, 233-243. 10.1037/0735-7044.102.2.233.

Felix, R.A., 2nd, Gourevitch, B., and Portfors, C.V. (2018). Subcortical pathways: Towards a better understanding of auditory disorders. Hear Res *362*, 48-60. 10.1016/j.heares.2018.01.008.

Fishell, G., and Rudy, B. (2011). Mechanisms of inhibition within the telencephalon: "where the wild things are". Annu Rev Neurosci *34*, 535-567. 10.1146/annurev-neuro-061010-113717.

Frankland, P.W., Cestari, V., Filipkowski, R.K., McDonald, R.J., and Silva, A.J. (1998). The dorsal hippocampus is essential for context discrimination but not for contextual conditioning. Behav Neurosci *112*, 863-874. 10.1037//0735-7044.112.4.863.

Fritschy, J.M., Panzanelli, P., and Tyagarajan, S.K. (2012). Molecular and functional heterogeneity of GABAergic synapses. Cell Mol Life Sci *69*, 2485-2499. 10.1007/s00018-012-0926-4.

Gibson, J.R., Huber, K.M., and Sudhof, T.C. (2009). Neuroligin-2 deletion selectively decreases inhibitory synaptic transmission originating from fast-spiking but not from somatostatin-positive interneurons. J Neurosci *29*, 13883-13897. 10.1523/JNEUROSCI.2457-09.2009.

Giustino, T.F., and Maren, S. (2015). The Role of the Medial Prefrontal Cortex in the Conditioning and Extinction of Fear. Front Behav Neurosci *9*, 298. 10.3389/fnbeh.2015.00298.

Graf, E.R., Kang, Y., Hauner, A.M., and Craig, A.M. (2006). Structure Function and Splice Site Analysis of the Synaptogenic Activity of the Neurexin-1β LNS Domain. The Journal of Neuroscience *26*, 4256-4265. 10.1523/jneurosci.1253-05.2006.

Grossman, Y.S., Fillinger, C., Manganaro, A., Voren, G., Waldman, R., Zou, T., Janssen, W.G., Kenny, P.J., and Dumitriu, D. (2022). Structure and function differences in the prelimbic cortex to basolateral amygdala circuit mediate trait vulnerability in a novel model of acute social defeat stress in male mice. Neuropsychopharmacology *47*, 788-799. 10.1038/s41386-021-01229-6.

Grosso, A., Cambiaghi, M., Milano, L., Renna, A., Sacco, T., and Sacchetti, B. (2017). Region- and Layer-Specific Activation of the Higher Order Auditory Cortex Te2 after Remote Retrieval of Fear or Appetitive Memories. Cereb Cortex *27*, 3140-3151. 10.1093/cercor/bhw159.

Grundemann, J. (2021). Distributed coding in auditory thalamus and basolateral amygdala upon associative fear learning. Curr Opin Neurobiol *67*, 183-189. 10.1016/j.conb.2020.11.014.

Guzowski, J.F., Timlin, J.A., Roysam, B., McNaughton, B.L., Worley, P.F., and Barnes, C.A. (2005). Mapping behaviorally relevant neural circuits with immediate-early gene expression. Curr Opin Neurobiol *15*, 599-606. 10.1016/j.conb.2005.08.018.

Han, J.H., Yiu, A.P., Cole, C.J., Hsiang, H.L., Neve, R.L., and Josselyn, S.A. (2008). Increasing CREB in the auditory thalamus enhances memory and generalization of auditory conditioned fear. Learn Mem *15*, 443-453. 10.1101/lm.993608.

Han, S., Soleiman, M.T., Soden, M.E., Zweifel, L.S., and Palmiter, R.D. (2015). Elucidating an Affective Pain Circuit that Creates a Threat Memory. Cell *162*, 363-374. 10.1016/j.cell.2015.05.057.

Harris, J.A., and Westbrook, R.F. (1995). Effects of benzodiazepine microinjection into the amygdala or periaqueductal gray on the expression of conditioned fear and hypoalgesia in rats. Behavioral Neuroscience *109*, 295-304. 10.1037/0735-7044.109.2.295.

Hartung, J., and Letzkus, J.J. (2021). Inhibitory plasticity in layer 1 - dynamic gatekeeper of neocortical associations. Curr Opin Neurobiol *67*, 26-33. 10.1016/j.conb.2020.06.003.

Haubensak, W., Kunwar, P.S., Cai, H., Ciocchi, S., Wall, N.R., Ponnusamy, R., Biag, J., Dong, H.W., Deisseroth, K., Callaway, E.M., et al. (2010). Genetic dissection of an amygdala microcircuit that gates conditioned fear. Nature *468*, 270-276. 10.1038/nature09553.

Herry, C., and Johansen, J.P. (2014). Encoding of fear learning and memory in distributed neuronal circuits. Nat Neurosci *17*, 1644-1654. 10.1038/nn.3869.

Herry, C., and Mons, N. (2004). Resistance to extinction is associated with impaired immediate early gene induction in medial prefrontal cortex and amygdala. Eur J Neurosci *20*, 781-790. 10.1111/j.1460-9568.2004.03542.x.

Heshmati, M., Aleyasin, H., Menard, C., Christoffel, D.J., Flanigan, M.E., Pfau, M.L., Hodes, G.E., Lepack, A.E., Bicks, L.K., Takahashi, A., et al. (2018). Cell-type-specific role for nucleus accumbens neuroligin-2 in depression and stress susceptibility. PNAS Proceedings of the National Academy of Sciences of the United States of America *115*, 1111-1116. 10.1073/pnas.1719014115.

Hippenmeyer, S., Vrieseling, E., Sigrist, M., Portmann, T., Laengle, C., Ladle, D.R., and Arber, S. (2005). A developmental switch in the response of DRG neurons to ETS transcription factor signaling. PLoS Biol *3*, e159-e159. 10.1371/journal.pbio.0030159.

Hoon, M., Bauer, G., Fritschy, J.M., Moser, T., Falkenburger, B.H., and Varoqueaux, F. (2009). Neuroligin 2 controls the maturation of GABAergic synapses and information processing in the retina. J Neurosci *29*, 8039-8050. 10.1523/JNEUROSCI.0534-09.2009.

Huntley, M.A., Srinivasan, K., Friedman, B.A., Wang, T.M., Yee, A.X., Wang, Y., Kaminker, J.S., Sheng, M., Hansen, D.V., and Hanson, J.E. (2020). Genome-Wide Analysis of Differential Gene Expression and Splicing in Excitatory Neurons and Interneuron Subtypes. J Neurosci *40*, 958-973. 10.1523/JNEUROSCI.1615-19.2019.

Ichtchenko, K., Nguyen, T., and Sudhof, T.C. (1996). Structures, alternative splicing, and neurexin binding of multiple neuroligins. J Biol Chem *271*, 2676-2682. 10.1074/jbc.271.5.2676.

Ishikawa, T., Gotoh, N., Murayama, C., Abe, T., Iwashita, M., Matsuzaki, F., Suzuki, T., and Yamamoto, T. (2011). IgSF molecule MDGA1 is involved in radial migration and positioning of a subset of cortical upper-layer neurons. Developmental Dynamics *240*, 96-107. https://doi.org/10.1002/dvdy.22496.

Janak, P.H., and Tye, K.M. (2015). From circuits to behaviour in the amygdala. Nature *517*, 284-292. 10.1038/nature14188.

Jedlicka, P., Hoon, M., Papadopoulos, T., Vlachos, A., Winkels, R., Poulopoulos, A., Betz, H., Deller, T., Brose, N., Varoqueaux, F., and Schwarzacher, S.W. (2011). Increased dentate gyrus excitability in neuroligin-2-deficient mice in vivo. Cereb Cortex *21*, 357-367. 10.1093/cercor/bhq100.

Jiang, D.Y., Wu, Z., Forsyth, C.T., Hu, Y., Yee, S.P., and Chen, G. (2018). GABAergic deficits and schizophrenia-like behaviors in a mouse model carrying patient-derived neuroligin-2 R215H mutation. Mol Brain *11*, 31. 10.1186/s13041-018-0375-6.

Jiang, L., Kundu, S., Lederman, J.D., Lopez-Hernandez, G.Y., Ballinger, E.C., Wang, S., Talmage, D.A., and Role, L.W. (2016). Cholinergic Signaling Controls Conditioned Fear Behaviors and Enhances Plasticity of Cortical-Amygdala Circuits. Neuron *90*, 1057-1070. 10.1016/j.neuron.2016.04.028.

Jiang, M., Polepalli, J., Chen, L.Y., Zhang, B., Sudhof, T.C., and Malenka, R.C. (2017). Conditional ablation of neuroligin-1 in CA1 pyramidal neurons blocks LTP by a cell-autonomous NMDA receptor-independent mechanism. Mol Psychiatry *22*, 375-383. 10.1038/mp.2016.80.

Johansen, J.P., Cain, C.K., Ostroff, L.E., and LeDoux, J.E. (2011a). Molecular mechanisms of fear learning and memory. Cell *147*, 509-524. 10.1016/j.cell.2011.10.009.

Johansen, J.P., Cain, C.K., Ostroff, L.E., and LeDoux, J.E. (2011b). Molecular mechanisms of fear learning and memory. Cell *147*, 509-524. 10.1016/j.cell.2011.10.009.

Johansen, J.P., Diaz-Mataix, L., Hamanaka, H., Ozawa, T., Ycu, E., Koivumaa, J., Kumar, A., Hou, M., Deisseroth, K., Boyden, E.S., and LeDoux, J.E. (2014). Hebbian and neuromodulatory mechanisms interact to trigger associative memory formation. Proc Natl Acad Sci U S A *111*, E5584-5592. 10.1073/pnas.1421304111.

Johansen, J.P., Tarpley, J.W., LeDoux, J.E., and Blair, H.T. (2010). Neural substrates for expectation-modulated fear learning in the amygdala and periaqueductal gray. Nat Neurosci *13*, 979-986. 10.1038/nn.2594.

Josselyn, S.A., and Tonegawa, S. (2020). Memory engrams: Recalling the past and imagining the future. Science *367*. 10.1126/science.aaw4325.

Kandel, E.R., Schwartz, J. H., Jessell, T. M., Siegelbaum, S. A., Hudspeth, A. J., & Mack, S. (2013). Principles of neural science (McGraw-Hill).

Kang, Y., Zhang, X., Dobie, F., Wu, H., and Craig, A.M. (2008). Induction of GABAergic postsynaptic differentiation by alpha-neurexins. The Journal of biological chemistry *283*, 2323-2334. 10.1074/jbc.M703957200.

Kasugai, Y., Vogel, E., Hörtnagl, H., Schönherr, S., Paradiso, E., Hauschild, M., Göbel, G., Milenkovic, I., Peterschmitt, Y., Tasan, R., et al. (2019). Structural and Functional Remodeling of Amygdala GABAergic Synapses in Associative Fear Learning. Neuron *104*, 781-794.e784. https://doi.org/10.1016/j.neuron.2019.08.013.

Kathuria, A., Lopez-Lengowski, K., Watmuff, B., McPhie, D., Cohen, B.M., and Karmacharya, R. (2019). Synaptic deficits in iPSC-derived cortical interneurons in schizophrenia are mediated by NLGN2 and rescued by N-acetylcysteine. Transl Psychiatry *9*, 321. 10.1038/s41398-019-0660-x.

Katzman, A., and Alberini, C.M. (2018). NLGN1 and NLGN2 in the prefrontal cortex: their role in memory consolidation and strengthening. Curr Opin Neurobiol *48*, 122-130. 10.1016/j.conb.2017.12.003.

Keay, K.A., and Bandler, R. (2015). Periaqueductal Gray. In The Rat Nervous System, pp. 207-221. 10.1016/b978-0-12-374245-2.00010-3.

Kim, J., Jung, S.Y., Lee, Y.K., Park, S., Choi, J.S., Lee, C.J., Kim, H.S., Choi, Y.B., Scheiffele, P., Bailey, C.H., et al. (2008). Neuroligin-1 is required for normal expression of LTP and associative fear memory in the amygdala of adult animals. Proc Natl Acad Sci U S A *105*, 9087-9092. 10.1073/pnas.0803448105.

Kim, J.A., Kim, D., Won, S.Y., Han, K.A., Park, D., Cho, E., Yun, N., An, H.J., Um, J.W., Kim, E., et al. (2017). Structural Insights into Modulation of Neurexin-Neuroligin Trans-synaptic Adhesion by MDGA1/Neuroligin-2 Complex. Neuron *94*, 1121-1131 e1126. 10.1016/j.neuron.2017.05.034.

Kim, J.J., and Fanselow, M.S. (1992). Modality-specific retrograde amnesia of fear. Science *256*, 675-677. 10.1126/science.1585183.

Kim, S.C., Jo, Y.S., Kim, I.H., Kim, H., and Choi, J.S. (2010). Lack of medial prefrontal cortex activation underlies the immediate extinction deficit. J Neurosci *30*, 832-837. 10.1523/jneurosci.4145-09.2010.

Krabbe, S., Grundemann, J., and Luthi, A. (2018). Amygdala Inhibitory Circuits Regulate Associative Fear Conditioning. Biol Psychiatry *83*, 800-809. 10.1016/j.biopsych.2017.10.006.

Krabbe, S., Paradiso, E., d'Aquin, S., Bitterman, Y., Courtin, J., Xu, C., Yonehara, K., Markovic, M., Muller, C., Eichlisberger, T., et al. (2019). Adaptive disinhibitory gating by VIP interneurons permits associative learning. Nat Neurosci *22*, 1834-1843. 10.1038/s41593-019-0508-y.

Krueger, D.D., Tuffy, L.P., Papadopoulos, T., and Brose, N. (2012). The role of neurexins and neuroligins in the formation, maturation, and function of vertebrate synapses. Curr Opin Neurobiol *22*, 412-422. 10.1016/j.conb.2012.02.012.

Krueger-Burg, D., Papadopoulos, T., and Brose, N. (2017). Organizers of inhibitory synapses come of age. Curr Opin Neurobiol *45*, 66-77. 10.1016/j.conb.2017.04.003.

LeDoux, J.E. (2000). Emotion circuits in the brain. Annu Rev Neurosci *2000*, 155-184.

Ledoux, J.E. (2000). Emotion Circuits in the Brain. Annual Review of Neuroscience *23*, 155-184. 10.1146/annurev.neuro.23.1.155.

LeDoux, J.E., Iwata, J., Cicchetti, P., and Reis, D.J. (1988). Different projections of the central amygdaloid nucleus mediate autonomic and behavioral correlates of conditioned fear. J Neurosci *8*, 2517-2529.

Lee, K., Kim, Y., Lee, S.J., Qiang, Y., Lee, D., Lee, H.W., Kim, H., Je, H.S., Sudhof, T.C., and Ko, J. (2013). MDGAs interact selectively with neuroligin-2 but not other neuroligins to regulate inhibitory synapse development. Proc Natl Acad Sci U S A *110*, 336-341. 10.1073/pnas.1219987110.

Lee, Y., Oh, J.-P., and Han, J.-H. (2021). Dissociated Role of Thalamic and Cortical Input to the Lateral Amygdala for Consolidation of Long-Term Fear Memory. The Journal of Neuroscience *41*, 9561-9570. 10.1523/jneurosci.1167-21.2021.

Letzkus, J.J., Wolff, S.B., Meyer, E.M., Tovote, P., Courtin, J., Herry, C., and Luthi, A. (2011). A disinhibitory microcircuit for associative fear learning in the auditory cortex. Nature *480*, 331-335. 10.1038/nature10674.

Levenson, J., Weeber, E., Selcher, J.C., Kategaya, L.S., Sweatt, J.D., and Eskin, A. (2002a). Long-term potentiation and contextual fear conditioning increase neuronal glutamate uptake. Nat Neurosci *5*, 155-161. 10.1038/nn791.

Levenson, J., Weeber, E., Selcher, J.C., Kategaya, L.S., Sweatt, J.D., and Eskin, A. (2002b). Long-term potentiation and contextual fear conditioning increase neuronal glutamate uptake. Nature Neuroscience *5*, 155-161. 10.1038/nn791.

Li, H., Penzo, M.A., Taniguchi, H., Kopec, C.D., Huang, Z.J., and Li, B. (2013). Experience-dependent modification of a central amygdala fear circuit. Nat Neurosci *16*, 332-339. 10.1038/nn.3322.

Liang, J., Xu, W., Hsu, Y.T., Yee, A.X., Chen, L., and Sudhof, T.C. (2015). Conditional neuroligin-2 knockout in adult medial prefrontal cortex links chronic changes in synaptic inhibition to cognitive impairments. Mol Psychiatry *20*, 850-859. 10.1038/mp.2015.31.

Lissek, S., Powers, A.S., McClure, E.B., Phelps, E.A., Woldehawariat, G., Grillon, C., and Pine, D.S. (2005). Classical fear conditioning in the anxiety disorders: a meta-analysis. Behav Res Ther *43*, 1391-1424. 10.1016/j.brat.2004.10.007.

Lucas, E.K., Jegarl, A.M., Morishita, H., and Clem, R.L. (2016). Multimodal and Site-Specific Plasticity of Amygdala Parvalbumin Interneurons after Fear Learning. Neuron *91*, 629-643. 10.1016/j.neuron.2016.06.032.

Madisen, L., Mao, T., Koch, H., Zhuo, J.-m., Berenyi, A., Fujisawa, S., Hsu, Y.-W.A., Garcia, A.J., 3rd, Gu, X., Zanella, S., et al. (2012). A toolbox of Cre-dependent optogenetic transgenic mice for light-induced activation and silencing. Nature neuroscience *15*, 793-802. 10.1038/nn.3078.

Marek, R., and Sah, P. (2018). Neural Circuits Mediating Fear Learning and Extinction. Adv Neurobiol *21*, 35-48. 10.1007/978-3-319-94593-4_2.

Maren, S., Phan, K.L., and Liberzon, I. (2013). The contextual brain: implications for fear conditioning, extinction and psychopathology. Nat Rev Neurosci *14*, 417-428. 10.1038/nrn3492.

McDonald, A.J., and Mott, D.D. (2017). Functional neuroanatomy of amygdalohippocampal interconnections and their role in learning and memory. J Neurosci Res *95*, 797-820. 10.1002/jnr.23709.

McIntire, S.L., Reimer, R.J., Schuske, K., Edwards, R.H., and Jorgensen, E.M. (1997). Identification and characterization of the vesicular GABA transporter. Nature *389*, 870-876. 10.1038/39908.

Minichiello, L., Korte, M., Wolfer, D., Kühn, R., Unsicker, K., Cestari, V., Rossi-Arnaud, C., Lipp, H.-P., Bonhoeffer, T., and Klein, R. (1999). Essential Role for TrkB Receptors in Hippocampus-Mediated Learning. Neuron *24*, 401-414. https://doi.org/10.1016/S0896-6273(00)80853-3.

Netrakanti, P.R., Cooper, B.H., Dere, E., Poggi, G., Winkler, D., Brose, N., and Ehrenreich, H. (2015). Fast cerebellar reflex circuitry requires synaptic vesicle priming by munc13-3. Cerebellum *14*, 264-283. 10.1007/s12311-015-0645-0.

Nguyen, T.A., Lehr, A.W., and Roche, K.W. (2020). Neuroligins and Neurodevelopmental Disorders: X-Linked Genetics. Frontiers in Synaptic Neuroscience *12*. 10.3389/fnsyn.2020.00033.

Nitschke, J.B., Sarinopoulos, I., Oathes, D.J., Johnstone, T., Whalen, P.J., Davidson, R.J., and Kalin, N.H. (2009). Anticipatory activation in the amygdala and anterior cingulate in generalized anxiety disorder and prediction of treatment response. Am J Psychiatry *166*, 302-310. 10.1176/appi.ajp.2008.07101682.

Pardi, M.B., Vogenstahl, J., Dalmay, T., Spano, T., Pu, D.L., Naumann, L.B., Kretschmer, F., Sprekeler, H., and Letzkus, J.J. (2020). A thalamocortical top-down circuit for associative memory. Science *370*, 844-848. 10.1126/science.abc2399.

Parente, D.J., Garriga, C., Baskin, B., Douglas, G., Cho, M.T., Araujo, G.C., and Shinawi, M. (2017). Neuroligin 2 nonsense variant associated with anxiety, autism, intellectual disability, hyperphagia, and obesity. Am J Med Genet A *173*, 213-216. 10.1002/ajmg.a.37977.

Paul, A., Crow, M., Raudales, R., He, M., Gillis, J., and Huang, Z.J. (2017). Transcriptional Architecture of Synaptic Communication Delineates GABAergic Neuron Identity. Cell *171*, 522-539.e520. 10.1016/j.cell.2017.08.032.

Paxinos, G., and Franklin, K.B.G. (1997). The mouse brain in stereotaxic coordinates.

Penn, A.C., Zhang, C.L., Georges, F., Royer, L., Breillat, C., Hosy, E., Petersen, J.D., Humeau, Y., and Choquet, D. (2017). Hippocampal LTP and contextual learning require surface diffusion of AMPA receptors. Nature *549*, 384-388. 10.1038/nature23658.

Penzo, M.A., Robert, V., and Li, B. (2014). Fear conditioning potentiates synaptic transmission onto long-range projection neurons in the lateral subdivision of central amygdala. J Neurosci *34*, 2432-2437. 10.1523/JNEUROSCI.4166-13.2014.

Perumal, M.B., and Sah, P. (2021). Inhibitory Circuits in the Basolateral Amygdala in Aversive Learning and Memory. Frontiers in Neural Circuits *15*. 10.3389/fncir.2021.633235.

Pettem, K.L., Yokomaku, D., Takahashi, H., Ge, Y., and Craig, A.M. (2013). Interaction between autism-linked MDGAs and neuroligins suppresses inhibitory synapse development. J Cell Biol *200*, 321-336. 10.1083/jcb.201206028.

Phillips, R.G., and LeDoux, J.E. (1992). Differential contribution of amygdala and hippocampus to cued and contextual fear conditioning. Behav Neurosci *106*, 274-285. 10.1037//0735-7044.106.2.274.

Pi, H.J., Hangya, B., Kvitsiani, D., Sanders, J.I., Huang, Z.J., and Kepecs, A. (2013). Cortical interneurons that specialize in disinhibitory control. Nature *503*, 521-524. 10.1038/nature12676.

Pinto, L.H., and Enroth-Cugell, C. (2000). Tests of the mouse visual system. Mamm Genome *11*, 531-536. 10.1007/s003350010102.

Pitkanen, A., Savander, V., and LeDoux, J.E. (1997). Organization of intra-amygdaloid circuitries in the rat: an emerging framework for understanding functions of the amygdala. Trends Neurosci *20*, 517-523. 10.1016/s0166-2236(97)01125-9.

Poulopoulos, A., Aramuni, G., Meyer, G., Soykan, T., Hoon, M., Papadopoulos, T., Zhang, M., Paarmann, I., Fuchs, C., Harvey, K., et al. (2009). Neuroligin 2 drives postsynaptic assembly at perisomatic inhibitory synapses through gephyrin and collybistin. Neuron *63*, 628-642. 10.1016/j.neuron.2009.08.023.

Quirk, G.J., Armony, J.L., and LeDoux, J.E. (1997). Fear conditioning enhances different temporal components of tone-evoked spike trains in auditory cortex and lateral amygdala. Neuron *19*, 613-624. 10.1016/s0896-6273(00)80375-x.

Rhomberg, T., Rovira-Esteban, L., Vikor, A., Paradiso, E., Kremser, C., Nagy-Pal, P., Papp, O.I., Tasan, R., Erdelyi, F., Szabo, G., et al. (2018). Vasoactive Intestinal Polypeptide-Immunoreactive Interneurons within Circuits of the Mouse Basolateral Amygdala. J Neurosci *38*, 6983-7003. 10.1523/JNEUROSCI.2063-17.2018.

Rogers, D.C., Fisher, E.M., Brown, S.D., Peters, J., Hunter, A.J., and Martin, J.E. (1997). Behavioral and functional analysis of mouse phenotype: SHIRPA, a proposed protocol for comprehensive phenotype assessment. Mamm Genome *8*, 711-713. 10.1007/s003359900551.

Romanski, L.M., Clugnet, M.C., Bordi, F., and LeDoux, J.E. (1993). Somatosensory and auditory convergence in the lateral nucleus of the amygdala. Behav Neurosci *107*, 444-450. 10.1037//0735-7044.107.3.444.

Romanski, L.M., and LeDoux, J.E. (1992a). Bilateral destruction of neocortical and perirhinal projection targets of the acoustic thalamus does not disrupt auditory fear conditioning. Neurosci Lett *142*, 228-232. 10.1016/0304-3940(92)90379-l.

Romanski, L.M., and LeDoux, J.E. (1992b). Equipotentiality of thalamo-amygdala and thalamo-cortico-amygdala circuits in auditory fear conditioning. J Neurosci *12*, 4501-4509.

Rowley, N.M., Madsen, K.K., Schousboe, A., and Steve White, H. (2012). Glutamate and GABA synthesis, release, transport and metabolism as targets for seizure control. Neurochem Int *61*, 546-558. 10.1016/j.neuint.2012.02.013.

Ryugo, D.K., and Weinberger, N.M. (1978). Differential plasticity of morphologically distinct neuron populations in the medical geniculate body of the cat during classical conditioning. Behav Biol *22*, 275-301. 10.1016/s0091-6773(78)92351-9.

Sacchetti, B., Lorenzini, C.A., Baldi, E., Tassoni, G., and Bucherelli, C. (1999). Auditory thalamus, dorsal hippocampus, basolateral amygdala, and perirhinal cortex role in the consolidation of conditioned freezing to context and to acoustic conditioned stimulus in the rat. J Neurosci *19*, 9570-9578.

Sah, P., Faber, E.S., Lopez De Armentia, M., and Power, J. (2003). The amygdaloid complex: anatomy and physiology. Physiol Rev *83*, 803-834. 10.1152/physrev.00002.2003.

Saitoh, A., Ohashi, M., Suzuki, S., Tsukagoshi, M., Sugiyama, A., Yamada, M., Oka, J., Inagaki, M., and Yamada, M. (2014). Activation of the prelimbic medial prefrontal cortex induces anxiety-like behaviors via N-Methyl-D-aspartate receptor-mediated glutamatergic neurotransmission in mice. J Neurosci Res *92*, 1044-1053. 10.1002/jnr.23391.

Sangha, S., Narayanan, R.T., Bergado-Acosta, J.R., Stork, O., Seidenbecher, T., and Pape, H.-C. (2009). Deficiency of the 65 kDa Isoform of Glutamic Acid Decarboxylase Impairs Extinction of Cued But Not Contextual Fear Memory. The Journal of Neuroscience *29*, 15713-15720. 10.1523/jneurosci.2620-09.2009.

Sato, M., Ito, M., Nagase, M., Sugimura, Y.K., Takahashi, Y., Watabe, A.M., and Kato, F. (2015). The lateral parabrachial nucleus is actively involved in the acquisition of fear memory in mice. Mol Brain *8*, 22. 10.1186/s13041-015-0108-z.

Scheiffele, P., Fan, J., Choih, J., Fetter, R., and Serafini, T. (2000). Neuroligin expressed in nonneuronal cells triggers presynaptic development in contacting axons. Cell *101*, 657-669. 10.1016/s0092-8674(00)80877-6.

Senn, V., Wolff, S.B., Herry, C., Grenier, F., Ehrlich, I., Grundemann, J., Fadok, J.P., Muller, C., Letzkus, J.J., and Luthi, A. (2014). Long-range connectivity defines behavioral specificity of amygdala neurons. Neuron *81*, 428-437. 10.1016/j.neuron.2013.11.006.

Seok, B.S., Cao, F., Belanger-Nelson, E., Provost, C., Gibbs, S., Jia, Z., and Mongrain, V. (2018). The effect of Neuroligin-2 absence on sleep architecture and electroencephalographic activity in mice. Mol Brain *11*, 52. 10.1186/s13041-018-0394-3.

Shaban, H., Humeau, Y., Herry, C., Cassasus, G., Shigemoto, R., Ciocchi, S., Barbieri, S., van der Putten, H., Kaupmann, K., Bettler, B., and Lüthi, A. (2006). Generalization of amygdala LTP and conditioned fear in the absence of presynaptic inhibition. Nature Neuroscience *9*, 1028-1035. 10.1038/nn1732.

Shin LM, O.S., Carson MA, Rauch SL, Macklin ML, Lasko NB, Peters PM, Metzger LJ, Dougherty DD, Cannistraro PA, Alpert NM, Fischman AJ, Pitman RK (2004). Regional cerebral blood flow in the amygdala and medial prefrontal cortex during traumatic imagery in male and female Vietnam veterans with PTSD. Arch Gen Psychiatry *2004 Feb;61(2)*, 168-176. doi: 10.1001/archpsyc.61.2.168. PMID: 14757593.

Sierra-Mercado, D., Padilla-Coreano, N., and Quirk, G.J. (2011). Dissociable roles of prelimbic and infralimbic cortices, ventral hippocampus, and basolateral amygdala in the expression and extinction of conditioned fear. Neuropsychopharmacology *36*, 529-538. 10.1038/npp.2010.184.

Sigel, E., and Steinmann, M.E. (2012). Structure, function, and modulation of GABA(A) receptors. J Biol Chem *287*, 40224-40231. 10.1074/jbc.R112.386664.

Stickgold, R. (2005). Sleep-dependent memory consolidation. Nature *437*, 1272-1278. 10.1038/nature04286.

Studer, F., and Barkat, T.R. (2022). Inhibition in the auditory cortex. Neurosci Biobehav Rev *132*, 61-75. 10.1016/j.neubiorev.2021.11.021.

Sudhof, T.C. (2021). The cell biology of synapse formation. J Cell Biol *220*. 10.1083/jcb.202103052.

Sun, C., Cheng, M.C., Qin, R., Liao, D.L., Chen, T.T., Koong, F.J., Chen, G., and Chen, C.H. (2011). Identification and functional characterization of rare mutations of the neuroligin-2 gene (NLGN2) associated with schizophrenia. Hum Mol Genet *20*, 3042-3051. 10.1093/hmg/ddr208.

Sun, Y., Gooch, H., and Sah, P. (2020). Fear conditioning and the basolateral amygdala. F1000Res *9*. 10.12688/f1000research.21201.1.

Südhof, T.C. (2017). Synaptic Neurexin Complexes: A Molecular Code for the Logic of Neural Circuits. Cell *171*, 745-769. 10.1016/j.cell.2017.10.024.

Takeuchi, T., Duszkiewicz, A.J., and Morris, R.G. (2014). The synaptic plasticity and memory hypothesis: encoding, storage and persistence. Philos Trans R Soc Lond B Biol Sci *369*, 20130288. 10.1098/rstb.2013.0288.

Tang, Y.-P., Shimizu, E., Dube, G.R., Rampon, C., Kerchner, G.A., Zhuo, M., Liu, G., and Tsien, J.Z. (1999). Genetic enhancement of learning and memory in mice. Nature *401*, 63-69. 10.1038/43432.

Taniguchi, H., He, M., Wu, P., Kim, S., Paik, R., Sugino, K., Kvitsani, D., Fu, Y., Lu, J., Lin, Y., et al. (2011). A Resource of Cre Driver Lines for Genetic Targeting of GABAergic Neurons in Cerebral Cortex. Neuron *71*, 995-1013. https://doi.org/10.1016/j.neuron.2011.07.026.

Taylor, J.A., Hasegawa, M., Benoit, C.M., Freire, J.A., Theodore, M., Ganea, D.A., Innocenti, S.M., Lu, T., and Grundemann, J. (2021). Single cell plasticity and population

coding stability in auditory thalamus upon associative learning. Nat Commun *12*, 2438. 10.1038/s41467-021-22421-8.

Toledo, A., Bimbi, G., Letellier, M., Tessier, B., Daburon, S., Favereaux, A., Chamma, I., Vennekens, K.M., Vanderlinden, J., Sainlos, M., et al. (2021). MDGAs are fast-diffusing molecules that delay excitatory synapse development by altering neuroligin behavior. 10.1101/2021.03.16.435652.

Tovote, P., Esposito, M.S., Botta, P., Chaudun, F., Fadok, J.P., Markovic, M., Wolff, S.B., Ramakrishnan, C., Fenno, L., Deisseroth, K., et al. (2016). Midbrain circuits for defensive behaviour. Nature *534*, 206-212. 10.1038/nature17996.

Tovote, P., Fadok, J.P., and Luthi, A. (2015). Neuronal circuits for fear and anxiety. Nat Rev Neurosci *16*, 317-331. 10.1038/nrn3945.

Troyano-Rodriguez, E., Wirsig-Wiechmann, C.R., and Ahmad, M. (2019). Neuroligin-2 Determines Inhibitory Synaptic Transmission in the Lateral Septum to Optimize Stress-Induced Neuronal Activation and Avoidance Behavior. Biol Psychiatry *85*, 1046-1055. 10.1016/j.biopsych.2019.01.022.

Tsetsenis, T., Boucard, A.A., Arac, D., Brunger, A.T., and Sudhof, T.C. (2014). Direct visualization of trans-synaptic neurexin-neuroligin interactions during synapse formation. J Neurosci *34*, 15083-15096. 10.1523/JNEUROSCI.0348-14.2014.

Tuominen, L., Romaniuk, L., Milad, M.R., Goff, D.C., Hall, J., and Holt, D.J. (2022). Impairment in acquisition of conditioned fear in schizophrenia. Neuropsychopharmacology *47*, 681-686. 10.1038/s41386-021-01193-1.

Tzanoulinou, S., Garcia-Mompo, C., Riccio, O., Grosse, J., Zanoletti, O., Dedousis, P., Nacher, J., and Sandi, C. (2016). Neuroligin-2 Expression in the Prefrontal Cortex is Involved in Attention Deficits Induced by Peripubertal Stress. Neuropsychopharmacology *41*, 751-761. 10.1038/npp.2015.200.

Urien, L., and Bauer, E.P. (2022). Sex Differences in BNST and Amygdala Activation by Contextual, Cued, and Unpredictable Threats. eNeuro *9*. 10.1523/ENEURO.0233-21.2021.

Van Zandt, M., Weiss, E., Almyasheva, A., Lipior, S., Maisel, S., and Naegele, J.R. (2019). Adeno-associated viral overexpression of neuroligin 2 in the mouse hippocampus enhances GABAergic synapses and impairs hippocampal-dependent behaviors. Behav Brain Res *362*, 7-20. 10.1016/j.bbr.2018.12.052.

Varoqueaux, F., Aramuni, G., Rawson, R.L., Mohrmann, R., Missler, M., Gottmann, K., Zhang, W., Sudhof, T.C., and Brose, N. (2006). Neuroligins determine synapse maturation and function. Neuron *51*, 741-754. 10.1016/j.neuron.2006.09.003.

Varoqueaux, F., Jamain, S., and Brose, N. (2004). Neuroligin 2 is exclusively localized to inhibitory synapses. Eur J Cell Biol *83*, 449-456. 10.1078/0171-9335-00410.

Viviani, D., Charlet, A., van den Burg, E., Robinet, C., Hurni, N., Abatis, M., Magara, F., and Stoop, R. (2011). Oxytocin selectively gates fear responses through distinct outputs from the central amygdala. Science *333*, 104-107. 10.1126/science.1201043.

Vogel, E., Krabbe, S., Grundemann, J., Wamsteeker Cusulin, J.I., and Luthi, A. (2016). Projection-Specific Dynamic Regulation of Inhibition in Amygdala Micro-Circuits. Neuron *91*, 644-651. 10.1016/j.neuron.2016.06.036.

Watabe, A.M., Ochiai, T., Nagase, M., Takahashi, Y., Sato, M., and Kato, F. (2013). Synaptic potentiation in the nociceptive amygdala following fear learning in mice. Mol Brain *6*, 11. 10.1186/1756-6606-6-11.

Weiskrantz, L. (1956). Behavioral changes associated with ablation of the amygdaloid complex in monkeys. J Comp Physiol Psychol *49*, 381-391. 10.1037/h0088009.

Wigestrand, M.B., Schiff, H.C., Fyhn, M., LeDoux, J.E., and Sears, R.M. (2017). Primary auditory cortex regulates threat memory specificity. Learn Mem *24*, 55-58. 10.1101/lm.044362.116.

Wohr, M., Silverman, J.L., Scattoni, M.L., Turner, S.M., Harris, M.J., Saxena, R., and Crawley, J.N. (2013). Developmental delays and reduced pup ultrasonic vocalizations but normal sociability in mice lacking the postsynaptic cell adhesion protein neuroligin2. Behav Brain Res *251*, 50-64. 10.1016/j.bbr.2012.07.024.

Wolff, S.B., Grundemann, J., Tovote, P., Krabbe, S., Jacobson, G.A., Muller, C., Herry, C., Ehrlich, I., Friedrich, R.W., Letzkus, J.J., and Luthi, A. (2014). Amygdala interneuron subtypes control fear learning through disinhibition. Nature *509*, 453-458. 10.1038/nature13258.

Woo, J., Kwon, S.K., Nam, J., Choi, S., Takahashi, H., Krueger, D., Park, J., Lee, Y., Bae, J.Y., Lee, D., et al. (2013). The adhesion protein IgSF9b is coupled to neuroligin 2 via S-SCAM to promote inhibitory synapse development. J Cell Biol *201*, 929-944. 10.1083/jcb.201209132.

Wu, X., Morishita, W.K., Riley, A.M., Hale, W.D., Sudhof, T.C., and Malenka, R.C. (2019). Neuroligin-1 Signaling Controls LTP and NMDA Receptors by Distinct Molecular Pathways. Neuron *102*, 621-635 e623. 10.1016/j.neuron.2019.02.013.

Xu, W., and Sudhof, T.C. (2013). A neural circuit for memory specificity and generalization. Science *339*, 1290-1295. 10.1126/science.1229534.

Ye, X., Kapeller-Libermann, D., Travaglia, A., Inda, M.C., and Alberini, C.M. (2017). Direct dorsal hippocampal-prelimbic cortex connections strengthen fear memories. Nat Neurosci *20*, 52-61. 10.1038/nn.4443.

Yeh, L.F., Ozawa, T., and Johansen, J.P. (2021). Functional organization of the midbrain periaqueductal gray for regulating aversive memory formation. Mol Brain *14*, 136. 10.1186/s13041-021-00844-0.

Yeh, L.F., Watanabe, M., Sulkes-Cuevas, J., and Johansen, J.P. (2018). Dysregulation of aversive signaling pathways: a novel circuit endophenotype for pain and anxiety disorders. Curr Opin Neurobiol *48*, 37-44. 10.1016/j.conb.2017.09.006.

Zhu, H., Pleil, K.E., Urban, D.J., Moy, S.S., Kash, T.L., and Roth, B.L. (2014). Chemogenetic inactivation of ventral hippocampal glutamatergic neurons disrupts consolidation of contextual fear memory. Neuropsychopharmacology *39*, 1880-1892. 10.1038/npp.2014.35.